

Intergovernmental Oceanographic Commission
technical series



70

Interdisciplinary geoscience studies of the Gulf of Cadiz and Western Mediterranean basins

Preliminary results of investigations
during the TTR- 14 cruise of
RV Professor Logachev
July-September, 2004



UNESCO 2006

Interdisciplinary geoscience studies of the Gulf of Cadiz and Western Mediterranean basins

Preliminary results of investigations during the TTR- 14 cruise of
RV Professor Logachev
July-September, 2004

Editors: N.H. Kenyon
 M.K. Ivanov
 A.M. Akhmetzhanov
 E.V. Kozlova

The designations employed and the presentation of the material in this publication do not imply the expression of any opinion whatever on the part of the Secretariats of UNESCO and IOC concerning the legal status of any country or territory, or its authorities, or concerning the delimitation of the frontiers of any country or territory.

For bibliographic purposes, this document should be cited as follows:

Interdisciplinary geoscience studies of the Gulf of Cadiz and Western Mediterranean basins.

*IOC Technical Series No. 70, UNESCO, 2006
(English)*

Cover design: A. Akhmetzhanov

Cover picture: Stromboli volcano and TTR deep-towed sidescan sonar coverage.

Printed in 2006 by the United Nations Educational, Scientific and Cultural Organisation 7, place de Fontenoy, 75352 Paris 07 SP Printed in UNESCO's Workshops

©UNESCO 2006 *Printed in France*

SC-2006/WS/15

TABLE OF CONTENTS

ABSTRACT	iii
ACKNOWLEDGEMENTS	iv
INTRODUCTION	1
LIST OF PARTICIPANTS	3
METHODS	4
I. GULF OF CADIZ (LEG 1)	8
I.1. Introduction and objectives of TTR-14 Leg 1	8
I.2. Geological setting	9
I.3. Studied areas	10
I.4. Seismic and acoustic data	10
I.4.1. Seismic data acquisition and processing	10
I.4.2. Seismic data interpretation	10
I.4.3. MAK sidescan sonar interpretation	17
I.5. Underwater video observations	24
I.6. Bottom sampling results	31
I.7. Biology	37
I.7.1. Introduction	37
I.7.2. Methods	37
I.7.3. Results	38
I.8. Gas biogeochemistry	41
1.8.1. Gas composition	42
1.8.1.1. Concentration in methane and higher hydrocarbons (ethane, propane, butane, pentane, hexane)	42
1.8.1.2. Methane stable carbon (d13C) and stable hydrogen (dD) isotopic composition	42
1.8.1.3. Carbon dioxide concentration and stable carbon (d13C) isotopic composition	43
1.8.2. Pore water volatile fatty acids (VFA), anions and cations	43
1.8.3. Sampling sites	44
II. SOUTHEASTERN IBERIAN MARGINS: THE ALBORAN BASIN AND THE PALOMARES AND CARTAGENA MARGINS (LEG 2)	44
II.1. The mud diapiric province of the West Alboran Basin	44
II.1.1. Introduction.....	44
II.1.2. Seismic interpretation and sidescan sonographs from the West Alboran Basin	46
II.2. Eastern Alboran margin: the transition between the Alboran and the Balearic-Algerian Basins	48

II.2.1. Introduction.....	48
II.2.2. The transition between the Alboran and the Balearic- Algerian Basins: seismic interpretation	49
II.3 Bottom sampling	52
II.4. The Palomares and Cartagena margins	55
II.4.1. Palomares margin: seismic interpretation	57
II.4.2. Palomares margin: sidescan sonar interpretation	57
II.4.3 The Cartagena margin: seismic interpretation	61
III. BALEARIC BASIN (LEG 3)	61
III.1. The Eivissa Channel area	61
III.1.1. Introduction	61
III.1.2. MAK-1M sidescan sonar data	64
III.2. The Mallorca Channel	67
III.2.1. Introduction	67
III.2.2. MAK-1M sidescan sonar and profiles	68
III.2.3. Bottom sampling data	71
III.3. The Rhône Neofan: A high resolution survey of a turbidite channel-lobe transition zone	72
III.3.1. Geological setting	72
III.3.2. Objectives on the Rhone fan	75
III.3.3. MAK-99MS to MAK-107MS sidescan sonar and profiles	76
III.4. The Cap de Creus Canyon system	81
III.4.1. Introduction	81
III.4.2. MAK sidescan sonar data.....	82
IV. TYRRHENIAN SEA (LEG 4)	90
IV.1. Sarrabus Canyon	90
IV.1.1. Introduction	90
IV.1.2. Lines MAK-118MS to MAK-127MS	92
IV.1.3. Bottom sampling.....	95
IV.2. History of catastrophic slope failures of Stromboli Volcano	101
IV.2.1. Introduction	101
IV.2.2. Results	103
IV.2.2.1. Underwater TV survey.....	103
IV.2.2.2. Bottom sampling	108
IV.2.3. Preliminary conclusions	110
REFERENCES	112
ANNEX I. CORE LOGS	
ANNEX II. LIST OF TTR-RELATED REPORTS	

ABSTRACT

Interdisciplinary scientific studies were conducted from the RV *Professor Logachev* on the continental margins and in the basins of the Gulf of Cadiz and Western Mediterranean Sea during the 14th Training-through-Research cruise of UNESCO -IOC.

Work in **the Gulf of Cadiz** added to the dataset collected on four earlier TTR cruises in 1999-2002. The new surveys investigated a series of landslides located in the distal part of the Portimão canyon, as well as several WNW-ESE major tectonic lineaments, believed to be strike-slip transfer zones linked to the Africa-Eurasia Plate Boundary. The southernmost known mud volcano field in the NW Moroccan margin was extended to the southwest with the discovery of the Meknes mud volcano. Additional samples of gas and gas hydrates were collected from the active Captain Arutyunov and Ginsburg mud volcanoes to complement studies already underway. New areas of carbonate crusts and chimneys near the main channel of the Mediterranean Undercurrent were covered with sidescan sonar survey and sampled by a TV-guided grab. Samples of fauna associated with fluid seepage were collected in new areas of the Gulf of Cadiz as well as from known structures for more detailed and quantitative studies. Specimens for genetic, stable isotope and ultramicroscopy analyses were also collected.

Investigations in **the Alboran basin** also continued the work started during TTR-9 and TTR-12 cruises and resulted in the discovery of the new mud volcano named Carmen, which is located between the Northern and Southern Mud Volcano Province. New high-resolution seismic lines obtained in the region allowed better understanding of basin architecture at shallower levels in the Alboran-Balearic transition. The lines were tied with ODP Leg 161 drilling results in order to provide seismostratigraphic constraints.

The Palomares and Cartagena margin is found to be a highly deformed margin, probably with active wrench tectonics which conditions sediment dispersal and mass wasting. Morphodynamic provinces include impressive turbidite systems, from incised canyons to deep sea fan lobes and with ubiquitous slides on the Cartagena margin.

Four areas were visited in **the Balearic Basin**. In the Eivissa Channel four shallow slides were covered with MAK 30 kHz sidescan sonar. The survey complemented the existing multibeam and seismic data, providing higher resolution.

Several 30 kHz sidescan sonar lines in the Mallorca Channel were aimed at studying the sedimentary processes and showed that hemipelagic sedimentation prevails over most of the area.

30 kHz sidescan sonar was used to map an extensive area (420 km²) of asymmetrical scour holes developing in the channel-to lobe transition of the Rhone neofan in the water depths of 2300-2600 m. These scours are attributed to the greater turbulence in currents from the neochannel where they reach a slope of lower gradient. Details of scour morphology and distribution pattern in relation with other seabed features will help to study the flow regime of the turbidity currents.

The study of the Cap de Creus Canyon System comprised a 30 kHz deep-towed sidescan sonar profile, running along the axis for almost 200 km from an area just below the shelf break down to the basin plain, where it connects with the Rhone Neofan survey. The profile shows changing canyon floor morphology and evolution of bedforms down the system from by-pass to depositional areas. The importance of slope breaks for formation of deep-water scour fields was confirmed.

In **the Tyrrhenian Sea** RV Professor Logachev worked in two main areas: the eastern Sardinia margin and Stromboli volcano submarine slopes. On the Sardinia margin the work comprised extensive 30 and 100 kHz deep-towed sidescan surveys and bottom sampling in the braid-like pattern found an intraslope basin situated at the water depths of 1600-1800 m and fed by Sarrabus Canyon. The study highlighted the dominance of erosional processes in the area resulting in formation of flutes and scours. The area was difficult to core with a conventional gravity corer but a spectacular sample of gravel collected by a TV-guided grab sampler indicated the presence of widespread gravels in the braided area. Integration of multibeam, sidescan sonar and sampling data showed the importance of topographic control for bedform and sediment distribution in the area.

The history of failure on the slope of Stromboli was investigated following the catastrophic tsunami and submarine slide of December 2002. On the submarine slopes and the base of the Stromboli volcano MAK sonographs showed scour marks and waves in black volcanoclastic sand related to the latest failure. The subbottom profiler showed distinct areas of erosion and deposition features including small channels, small canyons and slump scars. The debris avalanche deposits derived from the year 2002 collapse event were also imaged. Cores were taken on the far side of the Stromboli Canyon where a record of the Stromboli failures should be preserved. A significant and unexpected result was the discovery, and sampling, of an extensive pillow lava field at the base of the volcano.

ACKNOWLEDGEMENTS

The fourteenth Training-through-Research Cruise has received financial support from a variety of sources among which were: the Intergovernmental Oceanographic Commission (IOC) of UNESCO, University of Aveiro, University of Ghent, University of Granada, EUROSTRATAFORM Project of EC, University of Barcelona, the Russian Ministry of Science and Technological Policy, the Polar Marine Geosurvey Expedition (PMGRE) of the Russian Ministry of Natural Resources and Moscow State University. Logistic support was provided by the Netherlands Institute for Sea Research (NIOZ).

A number of people from different organizations supported the Training-through-Research Programme and were involved into the cruise preparation. The editors would like to express their gratitude for the contributions made by Prof. I. F. Glumov (Ministry of Natural Resources of the Russian Federation), Dr. A. Suzyumov (UNESCO), Dr. P. Bernal (Executive Secretary, IOC), and Dr. V. Zhivago (Ministry of Science and Technological Policy of the Russian Federation).

Credit also should be given to Dr. Maarten van Arkel of the NIOZ and Prof. Dr. D. Y. Puscharovsky (Faculty of Geology, Moscow State University) for their continuous administrative support.

Thanks are due to the administration and staff of the PMGRE (St. Petersburg) for their co-operation and assistance with the cruise organization and execution. Captain V. Pidenko and the skilful crew of the RV Professor Logachev ensured the smooth operations at sea. Staff and students of the UNESCO-MSU Marine Geosciences Centre provided valuable support in processing the acoustic data and in the preparation of illustrations.

INTRODUCTION

The TTR-14 cruise was carried out in the North Atlantic and Western Mediterranean with the RV Professor Logachev, owned and operated by the Polar Marine Geosurvey Expedition (PMGE, St. Petersburg, Russia), from 15 July to 18 September 2004. The cruise started in St. Petersburg (Russia), while embarkation of non-Russian participants took place in Porto (Portugal) on 24 July. The expedition terminated in Naples (Italy) on 17 September. Intermediate port calls were to Cadiz (Spain) on 10 - 11 August, Alicante (Spain) on 19 - 20 August and Barcelona (Spain) on 1 - 2 September. The cruise programme was divided into 4 Legs with a total of 8 study areas.

An international team of fifty three scientists, postgraduate and undergraduate students from the following fourteen countries participated: Argentina, Belgium, France, Georgia, Germany, Italy, Malta, Morocco, Norway, Portugal, Saudi Arabia, Spain, Switzerland and the UK. The participating students were involved in all stages of acquisition and preliminary processing of a multi-disciplinary set of geophysical and geological data. Daily seminars, lectures and discussions of the results facilitated high-level on-the-job training of the students and young scientists.

The objectives of the cruise were twofold: to conduct detailed investigations of geological and biological processes on the deep continental margins of Europe and to

train students in how to conduct research in marine geoscience. The following areas were visited during the cruise:

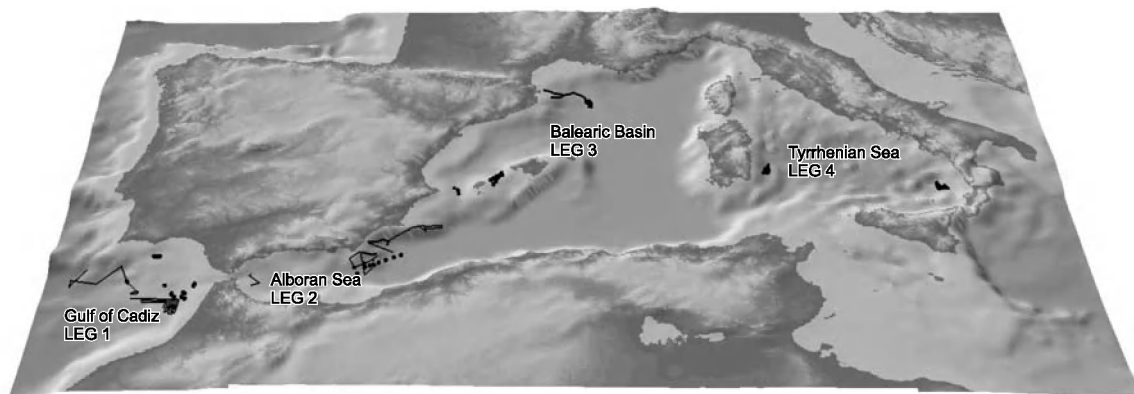
Leg 1: Gulf of Cadiz

The area of the Gulf of Cadiz has been intensively studied during several recent TTR expeditions, focussed mainly on mud volcanism, fluid venting and related phenomena. About 20 mud volcanoes have been discovered and confirmed by sampling. Gas hydrates, carbonate crust and nodules, as well as benthic chemosynthetic communities were sampled from some of these structures. Large carbonate chimneys, related to fluid escape were sampled and recorded by a deep-towed video system. Within the TTR-14 Cruise, further detailed geological and geophysical investigations of known mud volcanoes, fluid escape features, gas hydrate accumulations and other related phenomena were conducted, together with searching for yet unknown structures of similar origin.

Leg 2: Alboran Basin

West Alboran Basin

The mud-diapir province in the West Alboran Basin is formed of over-pressured shales that are early Miocene (Burdigalian) in age. The mud diapirism continued into the Holocene and reaches the sea floor. TTR-14 continued the previous studies of mud vol-



TTR-14 cruise location map

canoes in the Alboran Mud Diapiric Province (Northern and Southern Sectors). The aims were: to enlarge and complete former surveys conducted by TTR-9 (1999) and TTR-12 (2002) on the mud volcano fields on the Spanish and Moroccan margins; to image new mud volcanoes with high-resolution MAK sidescan sonar and to sample mud volcano material and related rocks. The tectonic framework of the area and the volcanic basement were also to be investigated.

Almeria-Palomares Margin and core transect from the East Alboran to the South Balearic Basins

Investigation of the SE Iberian continental margin and its extensive deep-sea depositional systems were conducted with the use of single-channel seismics, long-range and deep-towed sidescan sonars, and bottom sampling.

Studies of Holocene pelagic sedimentation in the area with the view to develop paleoclimate reconstruction in the Western Mediterranean during the last 20,000 years were continued with a gravity core transect.

Leg 3: Balearic basin

Balearic Islands

Four slides in the Balearic Margin of the Eivissa Channel, in water depths ranging from 600 to 900 m, were imaged during the survey. Pre-existing data consists of swath bathymetry and high resolution seismic profiles. There are pockmarks within the slide scars and fluid escape features are also present further upslope.

Acoustic imagery and 5 kHz profiles were also collected on the NW Mallorca margin in order to study sediment dynamics.

Catalan margin and Gulf of Lions

Several tasks were addressed on the Catalan margin and in the Gulf of Lions. An acoustic survey was conducted in the zone between the Cap de Creus and La Fonera canyons in order to gain a better understanding of the sedimentary processes and canyon development.

Another study area was located within

the Rhone neofan, the youngest depocentre on the Rhone fan, with the aim of obtaining a high resolution acoustic map of the scoured area, in order to better visualize the interplay of scouring processes and sand supply from both the Rhône sedimentary systems and the Pyreneo-Languedocian canyons.

Leg 4: Tyrrhenian Sea

Sardinia margin

Investigations on the eastern Sardinian margin were conducted along the Sarrabus Canyon system with the focus on the study of the different segments of the transport pathways in order to determine how sedimentary processes vary in response to the slope sectors traversed. The survey was conducted with deep-towed sidescan sonar and sampling.

Stromboli / Marsili basin

Stromboli Island has been affected by repeated flank collapse events on the Sciara del Fuoco and the structure of its submarine flanks is the result of a complex of sedimentary dynamic processes and volcanic processes.

The recent, December 2002, collapse event on the Sciara del Fuoco and the consequent catastrophic tsunami, rendered the flanks and deeper portions of the Stromboli/Marsili depositional system an important target for understanding the frequency of such events and the fate of the material and the processes involved. Deep-tow sidescan sonar surveys and sampling were conducted in the area.

LIST OF PARTICIPANTS

TTR-14 Cruise
15 July - 18 September 2004
RV Professor Logachev

ARGENTINE

Oscar Romero

BELGIUMEva de Boever
Heleen Vanneste**FRANCE**Bernard Dennielou
Marianne Nuzzo
Laurence Droz
Pierre Ferrer**GEORGIA**

Giuli Kharkheli

GERMANYAlexandra Beckstein
Warner Bruckmann**ITALY**Michael Marani
Fabiano Gamberi
Alessia Del Principe
Alessio Di Roberto
Marco Firetto
Salvatore Distefano**MALTA**

Aaron Micallef

MOROCCOBouchta El Mounni
Ilham Boumatran
Nadia Mhammdi**NORWAY**

Jan Sverre Laberg

PORTUGALLuis Pinheiro
Marina Cunha
Vitor Magalhaes
Ana de Carvalho
Carla Goncalves
Carolina Vieira de Sa
Clara Rodrigues
Joao Duarte
Patrick Reis Santos**RUSSIA**Michael Ivanov
Elena Kozlova
Valentina Blinova
Eugenia BilevaElizaveta Londvina
Eugene Sarantsev
Andrey Ovsiannikov
Dmitry Korost
Igor Kuvaev
Igor Uvarov
Anton Sungurov
Piotr Golinchik
Igor Gur'ev
Andrey Shuvalov
Dmitry Daudin
Daria Titkova
Anna Zotova
Vasilii Kiseliov
Kristina Chumakova
Alexandra Shoronova**SAUDI ARABIA**Najeeb Rasul
Fares Zaki Bahareth
Omar Al-hazmi**SPAIN**Menchu Comas
Miquel Canals
Francisca Martinez-Ruiz
David Amblas
David Gallego Torres
Fermin Fernandez-Ibanez
Francisco Jimenez-Espejo
Galderic Lastras
Guillermo Marro
Manuel Roman Alpiste
Mario Gomez
Marga Garcia
Oskar Vidal
Sergi Costa
Susana Costas**SWITZERLAND**Benoit Hamard
Cornelia Broennimann**UK**Andrey Akhmetzhanov
Neil Kenyon
Victoria Catteral

METHODS

The RV Professor Logachev is a Russian marine geology research and survey vessel equipped with geophysical survey and seabed sampling equipment. She is operated by the State Enterprise "Polar Marine Geosurvey Expedition" St. Petersburg. The vessel has: a draught of 6.66 m, length of 104.5 m, width of 16 m, net tonnage of 1351 ton, displacement of 5700 ton and is powered by two 3500 hp diesel engines.

Navigation

Positioning during the TTR-14 cruise was acquired using an Ashtech GG24 GPS + GLONASS receiver. The use of both GPS and GLONASS satellite configurations allows for greater accuracy than is available from conventional GPS alone, with up to 60% greater satellite availability. Positions are calculated in real-time code differential mode with 5 measurements per second and an accuracy of +/- 35 cm (75 cm at 95% confidence limits)

with optimal satellite configuration. Realistic positioning accuracy under normal satellite configuration for European waters is assumed as ca. 5 m. Positioning when the vessel is moving also utilizes Doppler velocity determinations from the differential code signal to generate a vessel speed accuracy of 0.04 knots (0.1 at 95% confidence limits) with optimum satellite configuration.

The GPS+GLONASS receiver is located centrally with accurate levelling to sampling and equipment deployment positions on the vessel allowing precise back navigation. Seabed sampling positions with the gravity corer are normally 5% of the accuracy of the vessel position due to their rapid deployment. MAK1-M sidescan sonar and deep-towed video system are all fitted with a pinger allowing precise navigation between the vessel and sub-sea surface position. This is necessary as deep-towed equipment is subject to greater spatial differences with respect to the vessel. This underwater navi-



RV Professor Logachev during port call in Barcelona

gation is based on the Sigma-1001 hydroacoustic system. Four stationary aerals, spaced 14 m apart, are hull mounted and receive acoustic signals from pingers attached to deployed equipment in short-base mode operating between 7-15 kHz. The signal emitted by the sub-surface pinger is tracked on board and accurate x,y positioning of the device relative to the vessel is computed taking into account roll, trim and ship's speed. Error positioning of this method usually does not exceed 1-2% of water depth.

The navigation system is linked with the ship's main and additional thrusters enabling highly accurate dynamic positioning, which is routinely used during deep-towed acoustic and video surveys and sampling operations.

Seismic profiling

The seismic source usually consisted of one 3 litre airgun, at a pressure of 120 bar (12 MPa). The airgun was towed at a depth of approximately 2-2.5 m and was fired every 10 seconds (i.e. approximately every 30 m). The streamer consisted of one active section, 30 m long, with 50 hydrophones, towed at a depth of approximately 2.5-3 m. The offset between the seismic source and the centre of the live hydrophone array was 135 m.

The data was acquired digitally using MSU developed software and preliminarily processed with RadExPro software, which was provided to the UNESCO MSU Centre for Marine Geosciences by GSD Productions, Moscow. The signals were low-pass filtered analogically to 250 Hz in the acquisition stage. The sample interval was 1 ms and the record length 3 seconds.

The basic processing sequence consisted of definition of the acquisition geometry, static shift correction, spiking deconvolution, amplitude recovery by spherical divergence correction and Butterworth bandpass filtering (20-60-180-240 Hz).

Hull-mounted acoustic profiler

A hull-mounted 5.1 kHz profiler was routinely used during most of the operations, with a continuous paper output and a selective recording of the digital data.

Sidescan sonar systems

OKEAN

The OKEAN is a long-range sidescan sonar operating at a frequency of 9.5 kHz, which, with its up to 15 km swath range and 6 knots towing speed, is well suited for reconnaissance surveying of large deep-sea areas. The OKEAN vehicle is towed behind the ship at about 40-80 m below the sea surface. Depending on the waterdepth and resolution required the swath could be set to 7 or 15 km.

MAK-1M

The MAK-1M deep-towed hydroacoustic system contains a high-resolution sidescan sonar operated at frequencies of 30 and 100 kHz, with a swath range of up to 2 km (1 km per side) and a subbottom profiler, operated at a frequency of 5 kHz. The sonar has a variable resolution of about 7 to 1 m across track (maximum range to centre) and along track (center to maximum range). During TTR-14, the fish was towed at a nearly constant altitude of about 100-150 m above the seafloor at a speed of 1.5-2 knots for 30 kHz surveys and about 50 m above seafloor for 100 kHz. The positioning of the tow-fish was archived with a short-based underwater navigation system.

The data from the tow-fish was transmitted on board through a cable, recorded digitally, and stored in Seg-Y format, with a trace length of 4096 2-byte integer samples per side. Time-variant gain was applied to the data while recording, to compensate the recorded amplitudes for the irregularity of the directional pattern of the transducers as well as for the spherical divergence of the sonic pulse.

Onboard processing of the collected data

included slant-range-to-ground-range (SLT) correction of the sonographs, geometrical correction of the profiles for recovery of the real seafloor topography, and smoothing average filtering of both types of records. Individual lines were geometrically corrected for the towing speed of the fish, converted into a standard bitmap image format. Some image processing routines, such as histogram equalization and curve adjustment, which are aimed at improving the dynamic range of the imagery, were also applied before printing out. Geographic registration of the acquired images was also done onboard.

Underwater photo and television system

The television system operating onboard cruise TTR-14 is a deep towed system designed for underwater video surveys of the seabed at depths of up to 6000 m. It consists of onboard and underwater units. The onboard part comprises the control units with video amplifier and VCR. The power for the underwater system is supplied through a conductive cable. The underwater equipment comprises the support frame with light unit, the high-pressure housing containing a "Canon M1" digital camera and the power supply unit.

The TV system is controlled from onboard by the winch operator, who visually controls the distance from the camera to the seafloor. This is assisted by a 1.5 m long rope with a weight at the end attached to the frame. It is usually towed along the seafloor enabling the operator to estimate the altitude of the instrument above the seafloor. Lights and video camera are switched on/off by the operator from onboard. The non-stop underwater record on the digital camera lasts for 2 hours in the "LP" mode. Onboard VCR keeps a continuous record during the whole survey, which can be up to 6 hours.

Sampling Tools

Gravity corer

Coring was performed using a 6 m long c. 1500 kg gravity corer with an internal diameter of 14.7 cm.

One half of the opened core was described on deck, paying particular attention to changes in lithology, colour and sedimentary structures. All colours relate to Munsell Colour Charts. The other half was measured for changes in magnetic susceptibility using a Bartington Instruments Magnetic Susceptibility meter with a MS2E1 probe. Magnetic susceptibility reflects the ease with which a material can be magnetised. This property is most strongly influenced by grain-size, heavy mineral content and diagenetic ferric mineral reduction.

Samples were also taken for coccolith and micropalaeontological assays from smear slides. This was done to generate a preliminary chronostratigraphy for the cores.

Box Corer

Box cores were taken using a Reineck box-corer with a 50 x 50 x 50 cm box capable of retrieving 185 kg of undisturbed seabed surface sample. Lowering and retrieving operations are conducted using a hydraulic A-shaped frame with a lifting capacity of 2 ton.

Kasten-corer

The corer is square in cross-section with a weight of about 600 kg and dimensions of 0.4x0.4x1.8 m. The recovery volume is up to 0.3 m³. The closure of the instrument is performed by two sliding plates and triggered during pull-up. The instrument is particularly useful for obtaining large samples of loosely packed coarse-grained sediment.

Dredge

The dredge comprises a 1 m², rectangular steel gate with chain mesh bag trailing behind and a 0.5 ton weight attached to the

wire 3 m in front of the gate. The mesh bag also has a rope bag inside and the mesh size is ~5 cm. The dredge was deployed ~250 m in front of the identified target site and the ship moved at 0.5 kts between 500 and 1500 m ensuring the dredge was pulled up-slope. On some sites, the bottom was monitored with a 3.5 kHz hull-mounted single-beam echosounder. At all times, the ship's velocity and position were monitored using GPS. Tension on the trawl-wire was monitored in the winch cab by both ink-line paper roll and by a tension meter. "Bites" of up to 10 tons on the trawl wire were recorded in this way.

TV-guided grab

SGS-4/1 hydraulically operated grab system was used during the cruise. The 3100 kg system is able to sample dense clayey and sandy sediments as well as deep water basalts and sulphide ores. SGS-4/1 can be used at depths up to 4000 m. The maximum sample volume for soft sediment is 1 m³. The grab is controlled by an operator from onboard and can be opened and closed again at any given time. The grab is positioned with the short base SIGMA 1000 underwater navigation system. The grab is equipped with a built-in digital camcorder with the video signal being both stored locally and transmitted back onboard to enable control for the grab operation as well as back-up recording. The lights are powered by a rechargeable battery, enabling up to 1 hour of continuous operation. A second battery kept on board was used to perform consecutive dives.

I. GULF OF CADIZ (LEG 1)

I.1. Introduction and objectives of TTR-14 Leg 1

During the TTR-9 cruise (1999) a large mud volcano field was discovered in the Spanish and Moroccan sectors of the Gulf of Cadiz (Gardner, 1999; Kenyon et al., 2000; Gardner, 2001), based on the interpretation of a sidescan mosaic collected in the area in 1992 (courtesy of Joan Gardner, Naval Research Laboratory (NRL), Washington D.C.). Five mud volcanoes were then identified: TTR, Kidd and Adamastor, in the Eastern Moroccan Field, and Yuma and Ginsburg, in the Middle Moroccan Field. Gas hydrates were recovered from the Ginsburg mud volcano. The next year, a deep mud volcano field was discovered in the South

Portuguese Margin (Pinheiro et al., 2003). In the subsequent years the Gulf of Cadiz has been extensively investigated during 8 research cruises: TTR-10, Anastasya (Somoza et al., 2001), TTR-11, TTR-11A, Tasyo, Cadipor, TTR-12, GAP and TTR-14. 29 new mud volcanoes have been confirmed by coring, as well as several mud diapirs (e.g. Ibérico) and elongated diapiric ridges (e.g. Guadalquivir, Cadiz, Formosa, Vernadsky and Renard). Extensive areas of carbonate crusts and chimneys were found in the northern part of the Gulf of Cadiz, near the main channel of the Mediterranean Outflow Water (MOW), on several diapiric ridges characterized by a strong-backscatter signature on sidescan sonar images. Up to this cruise, gas hydrates had been recovered from three mud volcanoes in this area: Bonjardim, Captain Arutyunov and Ginsburg. There are

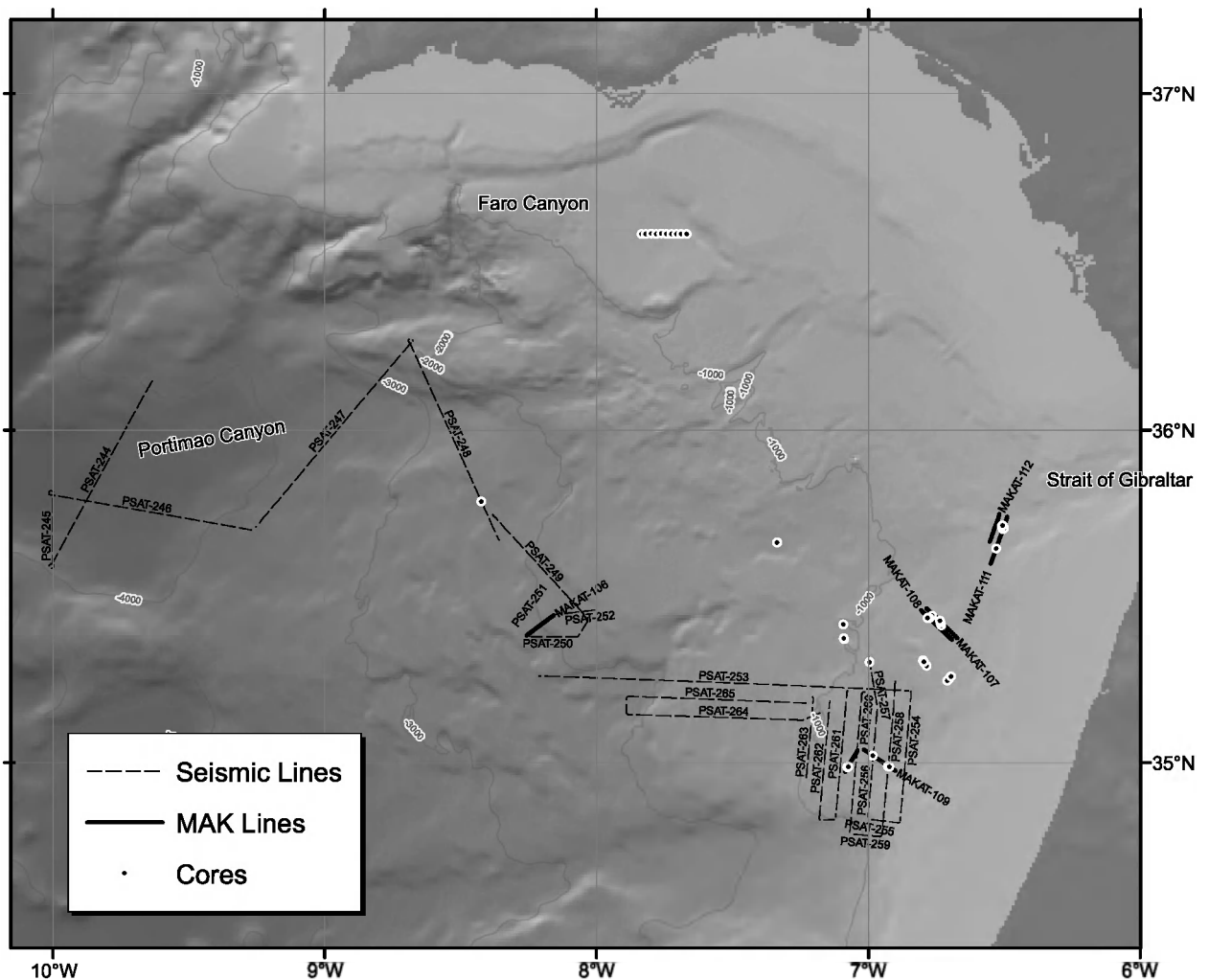


Figure 1. Summary of the research carried out during TTR-14 Leg 1 in the Gulf of Cadiz.

indications that gas hydrates may also occur in the Carlos Ribeiro mud volcano.

The main objectives of TTR-14 Leg 1 were:

To collect a set of gravity cores east of the Faro Canyon for geomicrobiological studies.

To investigate a series of landslides located in the distal part of the Portimão Canyon, as well as several WNW-ESE major tectonic lineaments (strike-slip transfer zones) probably linked to the Africa-Eurasia Plate Boundary. These features had been identified on a high resolution multibeam bathymetric map acquired just prior to this cruise (MATESPRO project).

To investigate several strong backscatter features observed on the NRL Seemap mosaic that may be related to fluid escape.

To investigate the possible continuation to the south of the southernmost known mud volcano field in the NW Moroccan margin.

To collect gas and gas hydrates from active mud volcanoes to complement studies already underway.

To investigate the existence of new areas of carbonate crusts and chimneys near the main channel of the MOW.

To investigate the fauna associated with fluid seepage in new areas of the Gulf of Cadiz, to revisit several known structures for more detailed work and to obtain quantitative samples in one active structure.

To collect specimens for genetic, stable isotope and ultramicroscopy analyses.

To record seismic data within the water section in order to try to image patterns within the water column related to ocean current circulation.

Fig. 1 shows a summary of the work done during the TTR-14 Leg 1.

I.2. Geological setting

The Gulf of Cadiz is located at the front of the Betic-Rifian Arc. It has had a very complex geological history and undergone several episodes of rifting, compression and strike-slip motion, since the Triassic (Wilson et al., 1989; Dewey et al., 1989; Maldonado et

al., 1999). The westward migration of the Gibraltar arc during the Late Tortonian caused the Gulf of Cadiz to form as a forearc basin (Bonnin et al., 1975, Auzende et al., 1981; Maldonado and Comas, 1992; Maldonado et al., 1999). The emplacement of the thrusting units, gravitational sliding of the mobile shale and salt stocks formed a giant mass-wasting deposit, the Gibraltar Olistostrome, that migrated west towards the Horseshoe and Seine abyssal plains. This olistostrome body consists of a chaotic mixture of Triassic, Cretaceous, Paleogene and Neogene sedimentary units, overlying a Palaeozoic basement. On seismic reflection profiles it is characterized by a chaotic pattern, highly diffractive with high-amplitude reflections (Riaza and Martínez del Olmo, 1996). These chaotic units involve a huge volume of mud and salt diapirism of Triassic salt units and undercompacted Early-Middle Miocene plastic marls (Maldonado et al. 1999).

Throughout this area, pockmarks, extensive mud volcanism, carbonate mounds and chimney structures related to hydrocarbon rich fluid venting and mud diapirism are observed (Baraza and Ercilla, 1996; Kenyon et al., 2000; Ivanov et al., 2000; Somoza et al., 2003; Pinheiro et al., 2003). In the northeastern sector of the Gulf of Cadiz, authigenic carbonate chimneys and crusts have been collected from the Iberico mud diapir, discovered in 2000 (Diaz del Rio et al., 2001). To the east of this structure a large NE-SW diapiric ridge, the Guadalquivir Diapiric Ridge (GDR), runs from the shelf break to 1200 m. This ridge controls the orientation of the main channel of the MOW undercurrent and it is composed of a series of wide sub-circular conical mounds surrounded by ring-shaped seafloor depressions. Most of these depressions are filled by contourite deposits of the MOW undercurrent. Some of them, mainly on the right side of the main MOW channel, are developed into sediment "shadows", formed on the down-current side of the mounds and with asymmetrical moats.

I.3. Studied areas

During this cruise, three main areas were investigated. The first area is located east of the Faro Canyon, at a water depth of about 800 m. Ten gravity cores were collected at regular intervals along an E-W profile from 36°34.99N / 7°49.99W to 36°35.00N / 7°40.00W. All cores were sampled at 3 depth intervals (10/50/100 cm); in addition the lowermost part of the recovered material was secured. These samples will be examined in a microbiological study to determine the microbial inventory, especially the distribution of methane-oxidizing and other hydrocarbon-oxidizing bacteria and the variation in their abundance along the cored profile.

The second area to be investigated is located in the distal part of the Portimão Canyon and it covers an area of about 160 nm x 200 nm. In this area, several long seismic lines were acquired to investigate several landslides as well as three main tectonic lineaments that probably represent transfer zones associated with the Africa-Eurasia Plate Boundary. In general, the penetration of the seismic energy is limited (less than 700 ms TWT), because of the significant water depth (over 4200 m, in places).

The third area includes a zone characterized by many semi-circular high-backscatter features that are thought to be related to fluid seepage, as well as the known mud volcano field in the Moroccan sector to the southwest. Apart from revisiting several known mud volcanoes (Kidd, Fiuza, Captain Arutyunov, Ginsburg and Gemini) several new structures were investigated with seismic profiling, OKEAN sidescan sonar and high-resolution deep-towed MAK. Most of these structures were sampled by gravity coring and TV-controlled grab. Box cores were taken on the Kidd mud volcano for biological studies and dredges were performed in a new area near the main MOW channel to recover carbonate chimneys from an area with a very strong backscatter signature. Several structures were investigated with underwater digital TV profiles.

I.4. Seismic and acoustic data

I.4.1. Seismic data acquisition and processing

Single channel seismic reflection profiles were acquired during TTR-14 Leg 1. The seismic source consisted of two 3.5 litre airguns, at a pressure of 150 atm. The airguns were towed at a depth of approximately 3.5 m shooting every 10 seconds (approximately every 30 m). Throughout the seismic acquisition, the average ship's speed was about 6.5 knots.

The data was acquired digitally using MSU developed software and preliminarily processed with the RadExPro software, which was provided to the UNESCO MSU Centre for Marine Geosciences by GDS Productions, Moscow. The trace length is 8s and the sampling rate is 1 ms. The analogue signals were filtered between 30-250 Hz during acquisition.

The preliminary on board processing was carried out using the RadExPro software and also the SPW (Seismic Processing Workshop) processing system. The basic processing sequence consisted of static shift correction, amplitude recovery by spherical divergence correction and simple bandpass filtering (5-20-250-300 Hz). Signature deconvolution and phase-shift deconvolution were also applied to some of the seismic lines to attenuate the bubble pulse and to better image the near-surface geological structure.

I.4.2. Seismic data interpretation

L. PINHEIRO, J. DUARTE AND A. CARVALHO

During the first part of Leg 1, five long seismic lines (PSAT-244, PSAT-245, PSAT-246 and PSAT-247) were acquired in the westernmost sector of the Gulf of Cadiz, to study several WNW-ENE tectonic lineaments and a few possible collapse structures and landslides discovered during the MATE-SPRO multibeam survey (L. Mendes-Victor, Pers. Comm.). This survey was conducted on board the ship N.R.P. D. Carlos 1 from the Portuguese Hydrographic Office (IH) in

June/July 2004, just prior to the TTR-14 cruise.

Distal part of the Portimão Canyon

This is an area of complex geology where several major WNW-ESE tectonic lineaments related to the Africa-Eurasia Plate Boundary affect a sedimentary system related to the deposition and gravitational sliding of sediments originating from the north, south and the east. The combination of major dextral strike-slip movement along these faults and northwest-directed convergence along the Africa-Eurasia Boundary, inferred from the focal mechanism solutions of the major seismic events recorded in this area, has caused asymmetric folding, reverse faulting and many small submarine landslides at various scales, clearly visible on the new seismic data acquired during this cruise as well as on the MATESPRO multibeam survey.

Line PSAT-244 (Fig. 2)

This is a NNE-SSW seismic line, 63 km long, located in the distal part of the Portimão Canyon, in the southward continuation of the VOLTAIRE-14 multichannel seismic line.

The objective of this seismic profile was twofold: (1) to investigate two main WNW-ESE fault zones with superficial rupture, located in the deep S. Portuguese margin. These structures have been interpreted as major transfer zones related to the Africa-

Eurasia Plate Boundary; (2) to investigate several localized features (“Pegadas do Lobo”) observed in the multibeam bathymetry, which could represent collapse structures associated with submarine landslides.

Structure T1, in the south, is a large fault scarp, with a local vertical displacement of at least 150 m; it probably corresponds to a major dextral strike-slip transfer zone. The upper part of the fault wall shows a much smaller dip, indicating collapse of the southern elevated block and the consequent formation of semi-chaotic sediment deposition observed just north of the fault zone (Fig. 2). The sedimentary structures in the southern elevated block are folded, possibly in a transpressional regime. North of the fault zone (SP: 1220-1530), the upper sedimentary units show a gentle apparent dip towards the north, affected by only minor extensional faulting. These units overlie a far more deformed sedimentary section. The interpretation of line VOLTAIRE-14 suggests that this could correspond to the topmost part of the olistostrome body.

Between shotpoints 1100 and 1250 this line crosses a well defined collapse structure with a NNE-SSW headwall scarp with a height of about 100 m, also visible on line PSAT-246. The lateral walls of this collapse structure have heights of ca. 40-60 m and the infill material is fairly irregular, probably related to slumping from the east. This feature is interpreted as a local secondary collapse of a larger pre-existing landslide that

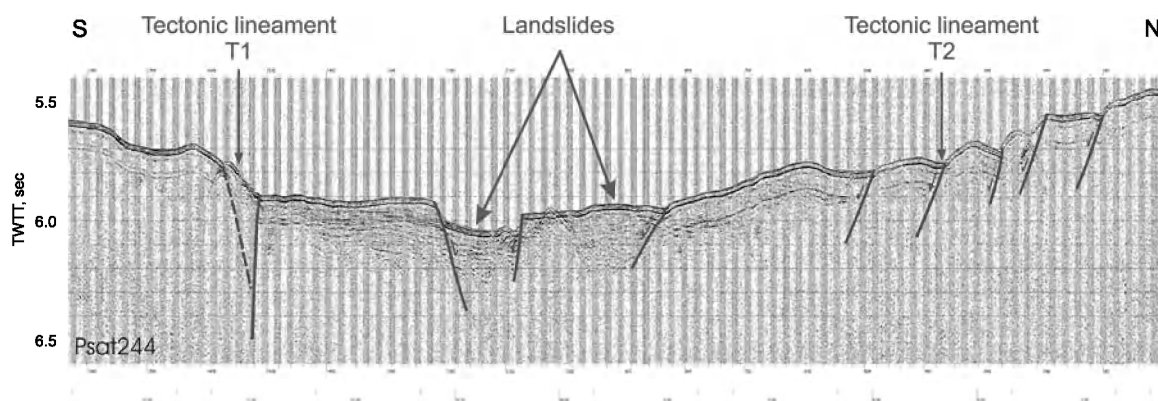


Figure 2. Seismic profile PSAT-244. line is located on Fig. 1.

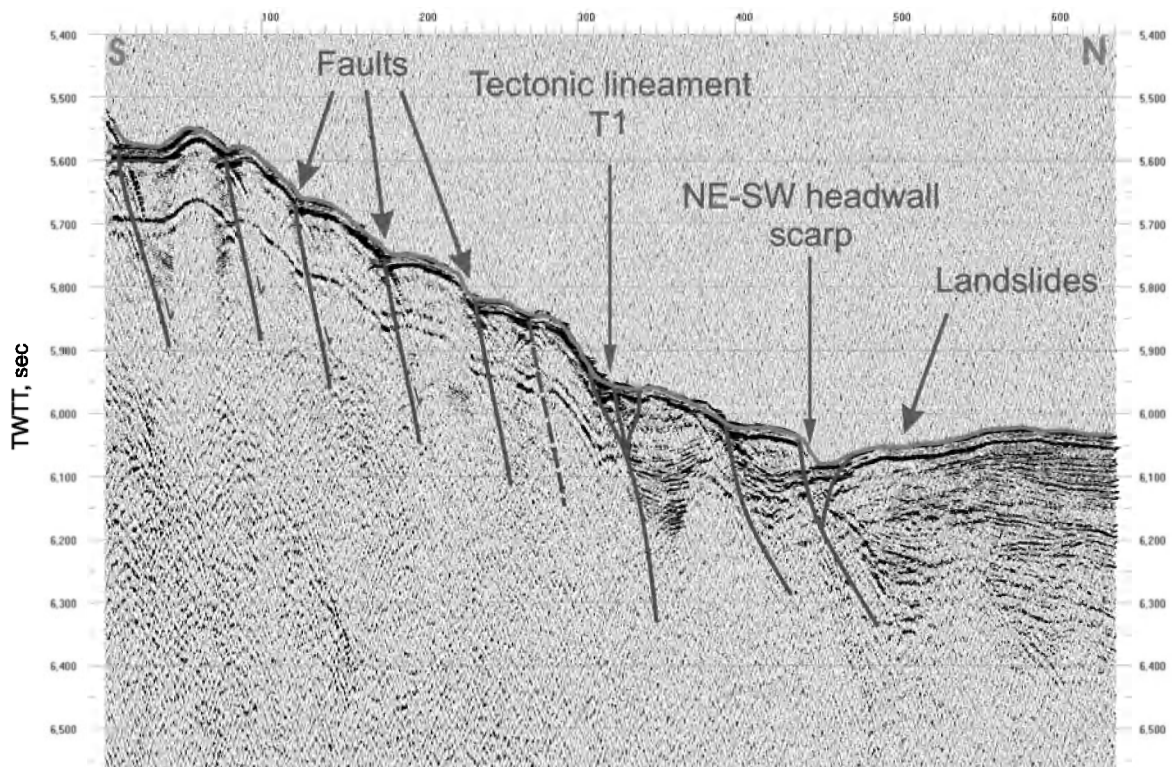


Figure 3. Seismic profile PSAT-245. line is located on Fig. 1.

extends from approximately shotpoints 850 to 1220. Just north of this secondary collapse a positive feature is observed outside the plane of the section, from which a side-reflection can be seen on the seismic profile. This is probably a small compressional ridge similar to many larger features observed on the bathymetry map.

The northern half of the line crosses an area of active NW-SE extensional faulting and slumping that affects the large depositional lobes formed by the sediments transported along the Portimão Canyon. These structures are probably related to strike-slip movement along another major tectonic lineament, more than 175 km long, observed in the MATESPRO multibeam bathymetry (T2 on Fig. 2).

Line PSAT-245 (Fig. 3)

This N-S seismic line, 19 km long, is located just west of Line PSAT-244 (Fig. 1). The objective of this seismic profile was to complement profile PSAT-244 by crossing again the southernmost WNW-ESE linea-

ment T1 as well as another collapse structure located just west of the one referred to in the description of line PSAT-244. On this line, structure T1 appears almost vertical, with a total throw of almost 300 m, accommodated along several normal(?) faults with variable throws of 30-40 m.

Between shotpoints 440 and 470 the seismic line crosses a collapse structure with a NE-SW trending headwall scarp. This structure produces a small landslide out of the plane of the section to the WNW (Fig. 3). North of this structure a complex sedimentary system is observed, with lense-like sedimentary units related to deposition and gravitational sliding of sediments originating from the north, south and east (Fig. 3).

Line PSAT-246 (Fig. 4)

This WNW-ESE seismic line, 60 km long, is also located in the distal part of the Portimão Canyon. The objectives of this line were: (1) to cross 4 landslides observed in the multibeam bathymetry (the easternmost of which was described on lines 244 and 245);

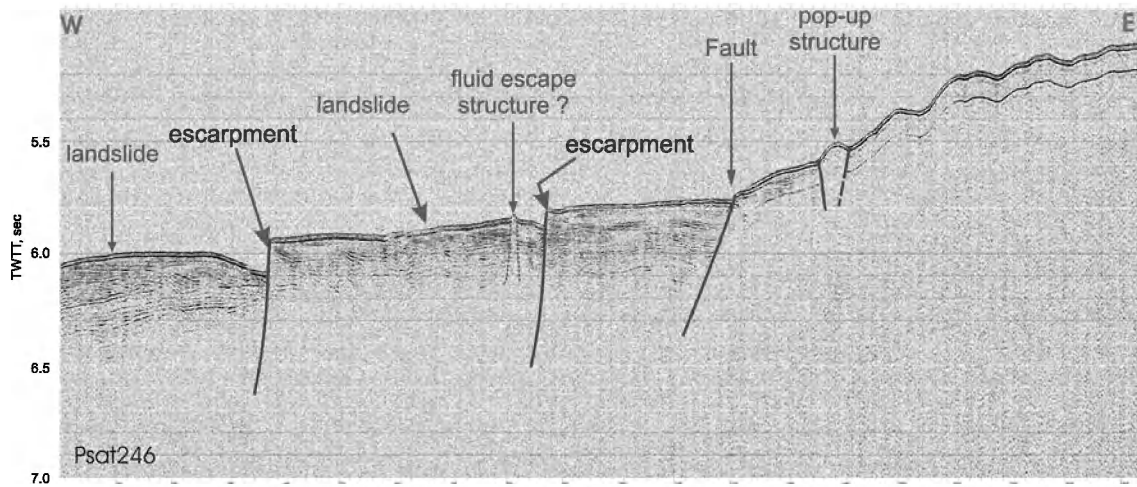


Figure 4. Seismic profile PSAT-246, line is located on Fig. 1.

(2) to study the transition between two very distinct morphological domains: a fairly smooth seafloor west of 9° 30' W (on this line) and an area with much rougher morphology to the east.

As described for Line 244, the westernmost landslide shows a slide scar with a headwall height just over 100 m. Line PSAT-246 is almost perpendicular to the landslide and shows its internal structure. The upper part of the sequence has been affected by

faulting and gravitational sliding to the west. (Editors comment: An alternative explanation is that these are deep scour holes due to turbulence downflow from resistant outcrops. They compare with the Judd Deep in the Faeroe-Shetland channel, although the latter are in an area of oceanic bottom currents rather than turbidity currents (e.g. Fig. 17 in Kenyon et al., 2000)). They overlie a sedimentary half-graben basin that thickens to the east where it is bounded by a former

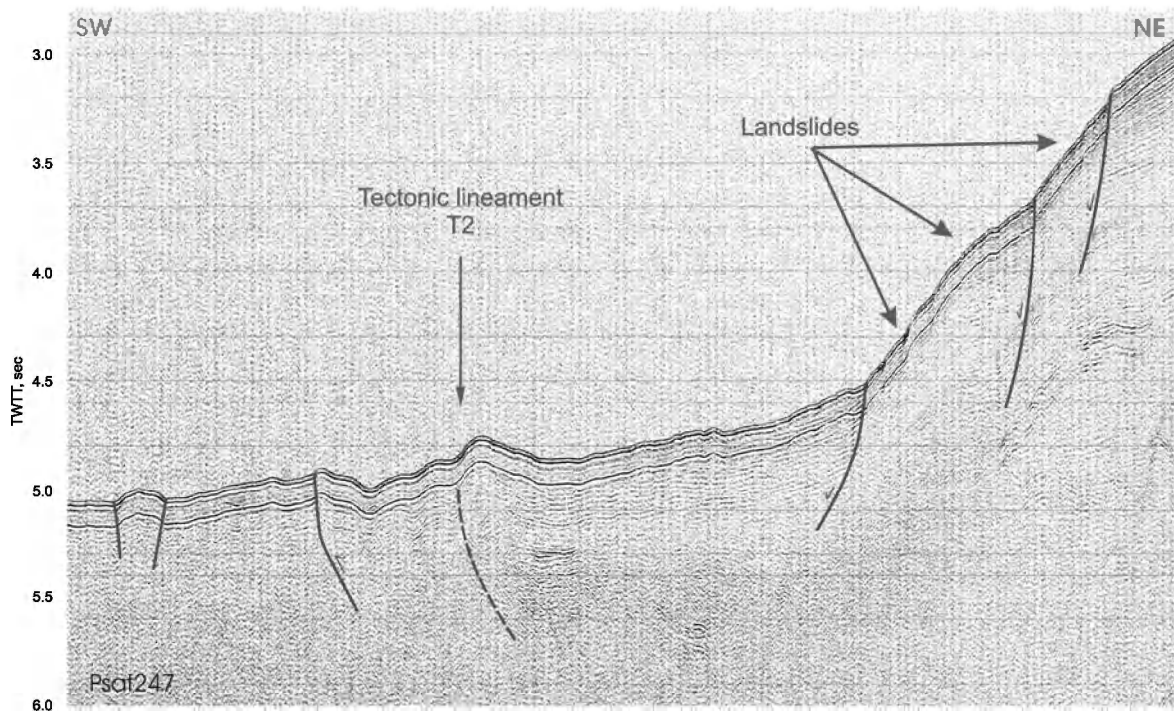


Figure 5. Seismic profile PSAT-247, line is located on Fig. 1.

normal fault, that appears to have been later reactivated as a wrench fault. To the east of this structure the seafloor morphology becomes highly irregular, the topography much steeper and the acoustic impedance contrast at the seabottom much higher, indicating a much stiffer seafloor. These units coincide with the westernmost tip of the deformation front related to the formation of the Gibraltar Arc and correspond to the western tip of the olistostrome/accretionary complex interpreted by Maldonado et al. (1999) and Somoza et al. (1999). These units are strongly deformed and faulted. A small pop-up structure is observed near SP-1360.

Near shotpoint 800 there is a small acoustically transparent structure that may be related to gas seepage (Fig. 4).

Line PSAT-247 (Fig. 5)

This is a SW-NE seismic line, 80 km long. The objectives of this line were: (1) to cross the boundary between the two morphological domains referred to above, which are separated by a major tectonic lineament (T2) that appears to mark the northern limit of the possible olistostrome body; (2) to investigate a major landslide complex locat-

ed in the northeastern part of the MATE-SPRO multibeam survey, just west and south of a large structure of possibly diapiric nature visible on line PSAT-248.

On this line, the boundary between the two distinct morphological domains is marked by a localized asymmetric ridge, similar to that observed on the N-S line PSAT-146, acquired during the TTR-10 cruise. To the south, a NE-dipping thrust is observed near SP-500, as well as a small pop-up structure near the southern end of the line.

In the northern part of this line, a steep slope marks the area where large, multiple landslides controlled by a set of SW-dipping normal faults affect a thick (900 m) sedimentary section (Fig. 5).

Line PSAT-248 (Fig. 6)

This is a NW-SE seismic line, 70 km long. The objectives of this line were: (1) to investigate a large diapiric structure in the NE sector of the multibeam survey; (2) to cross once more the large landslides just south of this structure; (3) to investigate the possible tectonic control of the Carlos Ribeiro mud volcano, which appears to be associated

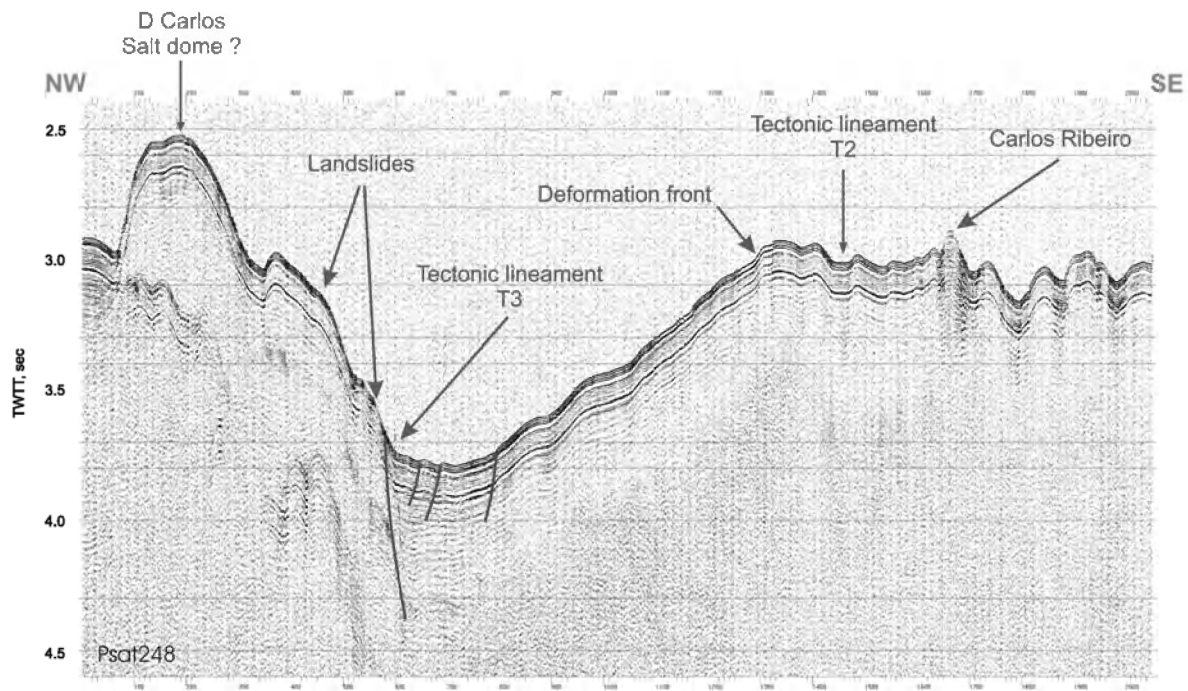


Figure 6. Seismic profile PSAT-248. line is located on Fig. 1.

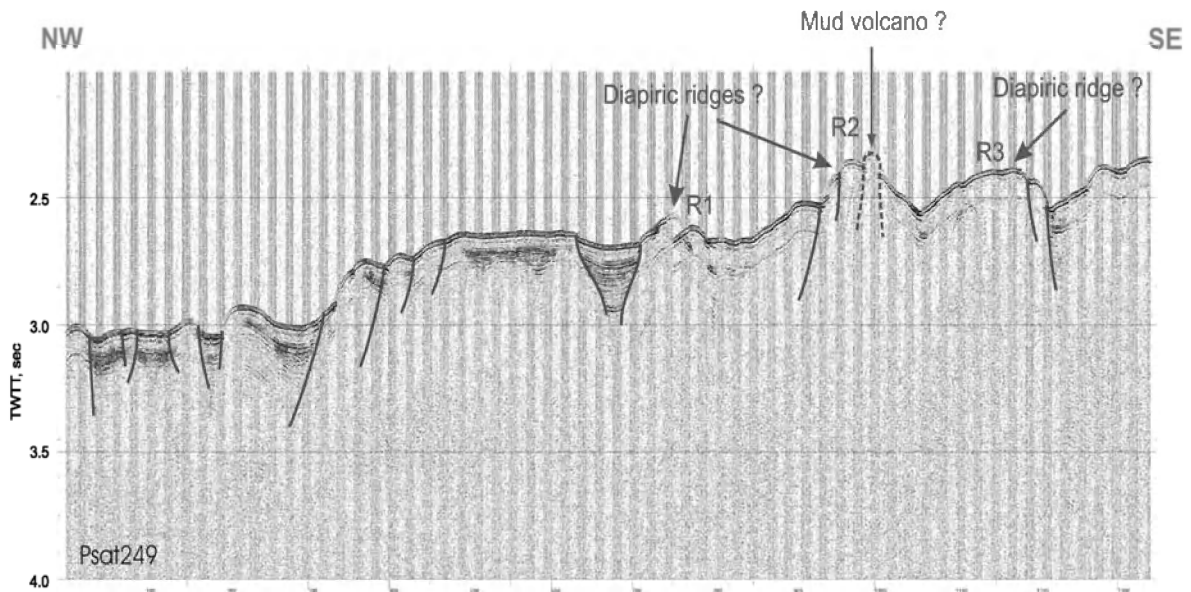


Figure 7. Seismic profile PSAT-249. line is located on Fig. 1.

with the major strike-slip zone T2.

The large diapiric structure (salt dome?) has a diameter of ca. 4.6 km and a height of over 350 m. It has a surrounding moat and is located at the edge of a small sedimentary basin to the north. To the south of this structure this seismic line crosses obliquely two landslides that run in a SW direction. The base of the southernmost landslide coincides with a large ENE tectonic lineament observed on the multibeam bathymetry (T3 in Fig. 6).

The southern part of this line crosses the eastern prolongation of the T2 tectonic lineament which bounds the olistostrome body in the north. In this area, this tectonic lineament seems to split into two main divergent seg-

ments, delimiting a narrow deformation zone where the Carlos Ribeiro mud volcano is situated, near SP-1680. One core (AT-520G) was taken on the top of this mud volcano.

Line PSAT-249 (Fig. 7)

This is a NW-SE seismic line, 40 km long. The objective of this line was to image the geological structure in this area and to investigate a small feature located near shot-point 1000 (35° 40.5' N, 08° 18.3' W), which could be associated with gas seepage.

The geological structure consists of several small basins (with a sedimentary infill that can reach over 200 m), interrupted by NW-SE, possibly diapiric, ridges. This area is

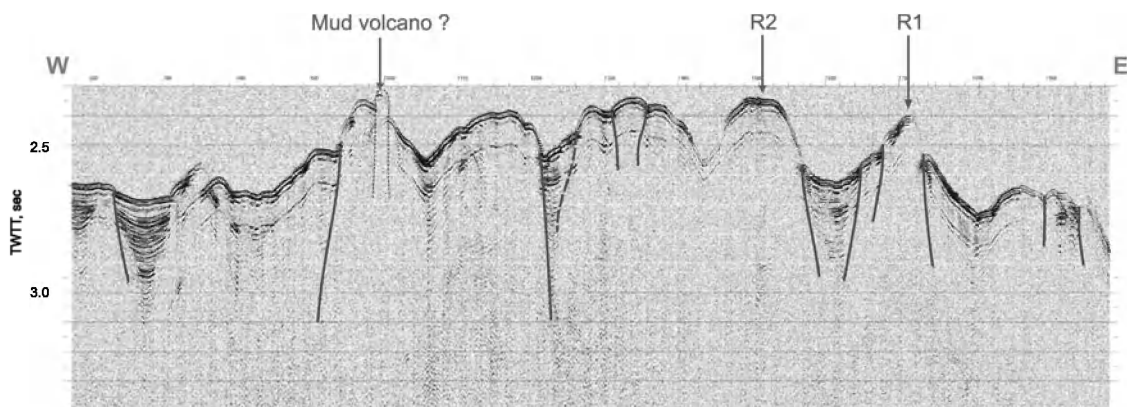


Figure 8. Seismic profile PSAT 250. line is located on Fig. 1.

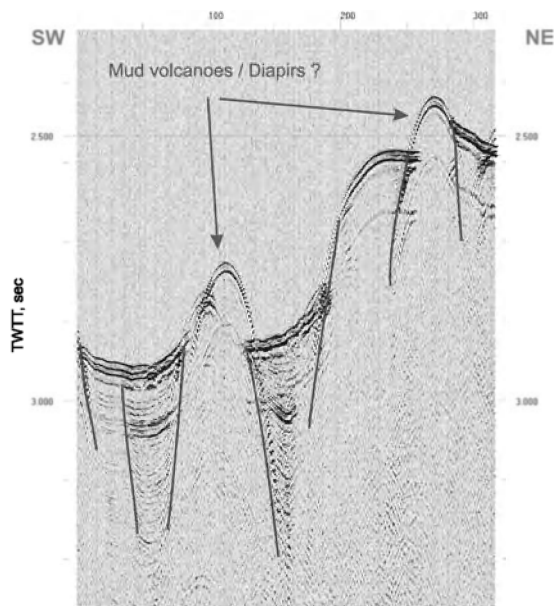


Figure 9. Seismic profile PSAT 251. line is located on Fig. 1.

strongly affected by extensional or, more likely, strike-slip faults; some of which could be important structures, particularly those located near shotpoints 300, 930 and 1220 (Fig. 7). There is no strong evidence of significant compressional features in this area. Between shotpoints 930 and 1210, there are two structural highs with a small basin in between. The consideration of this line, together lines PSAT 250-252, shows that the highs correspond to NW-SE ridges (R1, R2 and R3?; Fig. 7). The small structure near SP-1000 is probably a small mud volcano or mud diapir.

Lines PSAT-250, PSAT-251 and PSAT-252

These three lines form a small loop to the south of line 249 (Fig. 1). They are located in an area of many small semi-circular features that may correspond to fluid escape structures.

Consideration of the three lines shows that the structural highs R1 and R2 observed on line 249 are NW-SE ridges, whose nature is not yet known. The north face of ridge R1 is a steeply-dipping normal fault. In between the two highs there is a deep basin (over 200 m deep), on the top of which small landslides are observed (Fig. 8).

The 9 km long, NE-SW seismic line PSAT-251 shows two features which could be small mud volcanoes or mud diapirs (Fig. 9). The northernmost structure appears to be associated with a normal fault with an apparent dip to the south.

Moroccan Mud Volcano Field

Line PSAT-253 (Fig. 10)

This long E-W seismic line (ca. 95 km) starts in the area of extensive small scale fluid seepage referred to above and it continues east to $6^{\circ} 50' W$. It shows two very distinct areas east and west of approximately $7^{\circ} 45' W$. The western portion has an average depth of about 2000 m whereas the eastern area is 700 m shallower. The transition between these two areas is marked by a very steep slope and a highly diffractive zone approximately 9 km wide. The nature of this structure is still unknown. It could be related to salt diapirism. It has an arcuate shape clearly visible on the NRL sidescan sonar mosaic (Gardner, 1999; 2001). It delimits a small, slightly deformed sedimentary basin, over 200 m deep, to the east. Beyond this transition zone, to the east, several small extensional basins, bounded by east-dipping former normal faults, are observed; some of these basins have been strongly deformed under a compressional regime. At the eastern part of the line there are fairly large half-graben basins, overlying rotated fault blocks. These show only minor compressional deformation and they are bounded by a major normal fault at the easternmost end of this line. Between this area and the arcuate structure in the west, the sedimentary basins are fairly symmetrical and show signs of being affected by probable wrench movement. Two structures, possibly associated with fluid escape, are observed in this area: one collapse structure near SP-2000 and a possible mud volcano or mud diapir near SP-1600.

Lines PSAT-254 to PSAT-263

These are a set of N-S seismic lines, 5 km apart, obtained in order to investigate

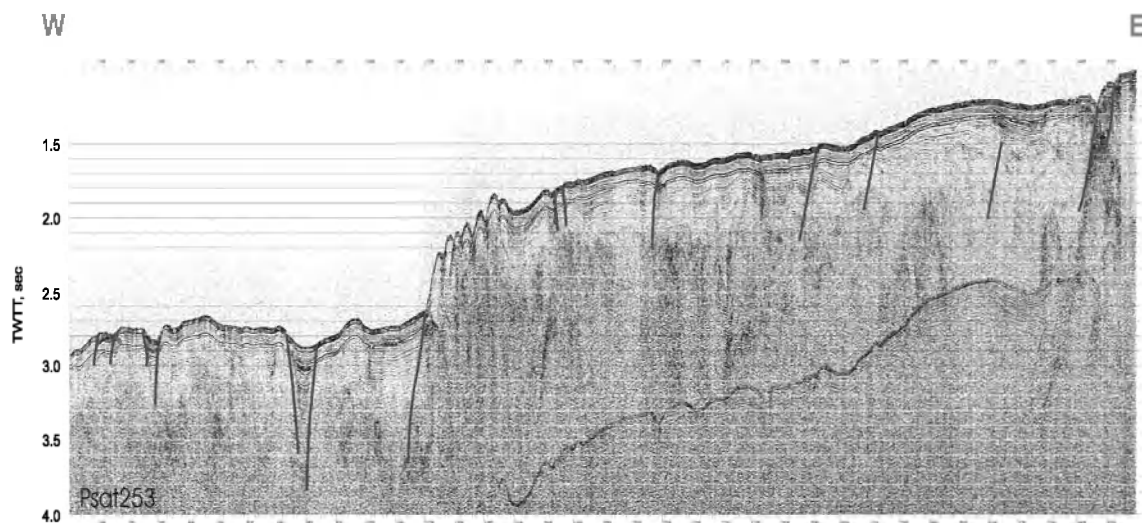


Figure 10. Seismic profile PSAT 253. line is located on Fig. 1.

whether the southernmost known mud volcano fields continue further south. They are perpendicular to and located just south of Line PSAT-253. Their analysis allows lateral correlation of several significant sedimentary and tectonic features.

There is a clear distinction between the northern and the southern segments of these lines. The southern part is more elevated than the northern one by over 100 m in places, and it forms an asymmetric large fold with evidence of intense internal deformation. This fold consists of a deep asymmetric basin (over 350 m in places) that deepens to the south, where it is sharply delimited by a vertical fault that probably corresponds to a strike-slip zone. This is particularly evident on lines PSAT-254, 256, 258, 260 and 261. The boundary between the southern and the northern portions of this line is marked by a WNW-ESE fault zone, most likely strike-slip, along which several diapiric structures (salt domes or mud volcanoes) are observed (lines PSAT-256, 258, 262 and 263). On lines PSAT-254, 260 and 261, instead of intrusions, several collapse structures and small grabens are observed.

The northern part of these lines, in contrast, shows shallower symmetrical sedimentary basins affected by intense strike slip faulting. This interpretation is corroborated by the short E-W trending profiles.

I.4.3. MAK sidescan sonar interpretation

W. BRÜCKMANN, A. AKHMETZHANOV, S. COSTAS
AND A. BECKSTEIN

During the TTR-14 cruise a total of 76 km of MAK deep-towed sidescan sonar data were collected. Table 1 summarizes the work carried out.

MAKAT-106

MAKAT-106 was designed for a closer inspection of two high reflectivity features discovered in the Seamap data (Gardner et al., 1999) in order to check their possible diapiric origin. The MAK data reveals no obvious mud volcanoes but does show areas of contrasting high backscatter on the top and flanks of the diapiric structure. These could be due to outcropping or near surface diapir core material. A depression between the two structural highs accommodates deposits of several debris flows which are covered by a thin hemipelagic veneer. The flows are probably sourced from the slopes of the diapirs as indicated by slide scars observed on the subbottom profiler records (Fig. 11).

MAKAT-107

MAKAT-107 runs NW-SE for 8.5 km,

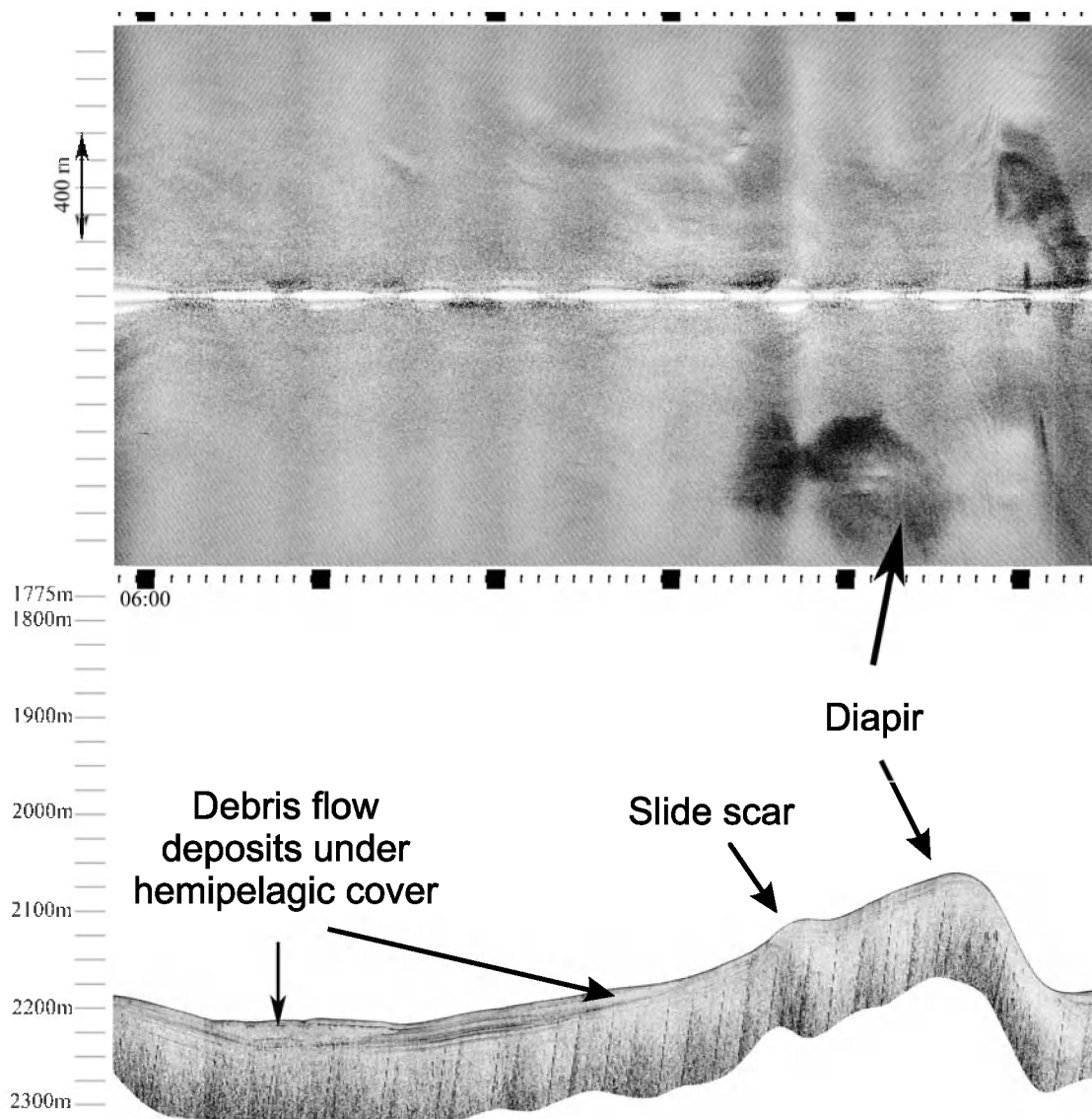


Figure 11. Fragment of MAK sonograph and profile along line MAKAT-106. Line is located on Fig. 1

along the extension of the Vernadsky ridge. The central crater of the Kidd mud volcano was surveyed in order to select possible sampling sites. The mud volcano is clearly imaged with several concentric rings defining its central part. The central crater has an approximate diameter of 350 m. The 5 kHz profile shows an asymmetrically shaped volcanic edifice, with a steep SE slope and a gently sloping NW flank, the base of the volcano is at a depth of 500 m and its top is at 420 m. A circular moat is also clearly imaged (Fig. 12).

Two other areas of high reflectivity were identified. In the SE part of the profile there

is an elevated area with variable to high reflectivity and a rugged surface, spanning a distance of 1.7 km along the crest of Vernadsky ridge, and approximately 0.9 km wide. In the NW a depression of 60 m also exhibits very high reflectivity which could be due to the presence of carbonate crusts or erosive surfaces. This area is also characterised by a bumpy topography.

MAKAT-108

This MAK and 5 kHz profile was run to the southwest of MAKAT-107 along a parallel course. It length is about 10.5 km and it

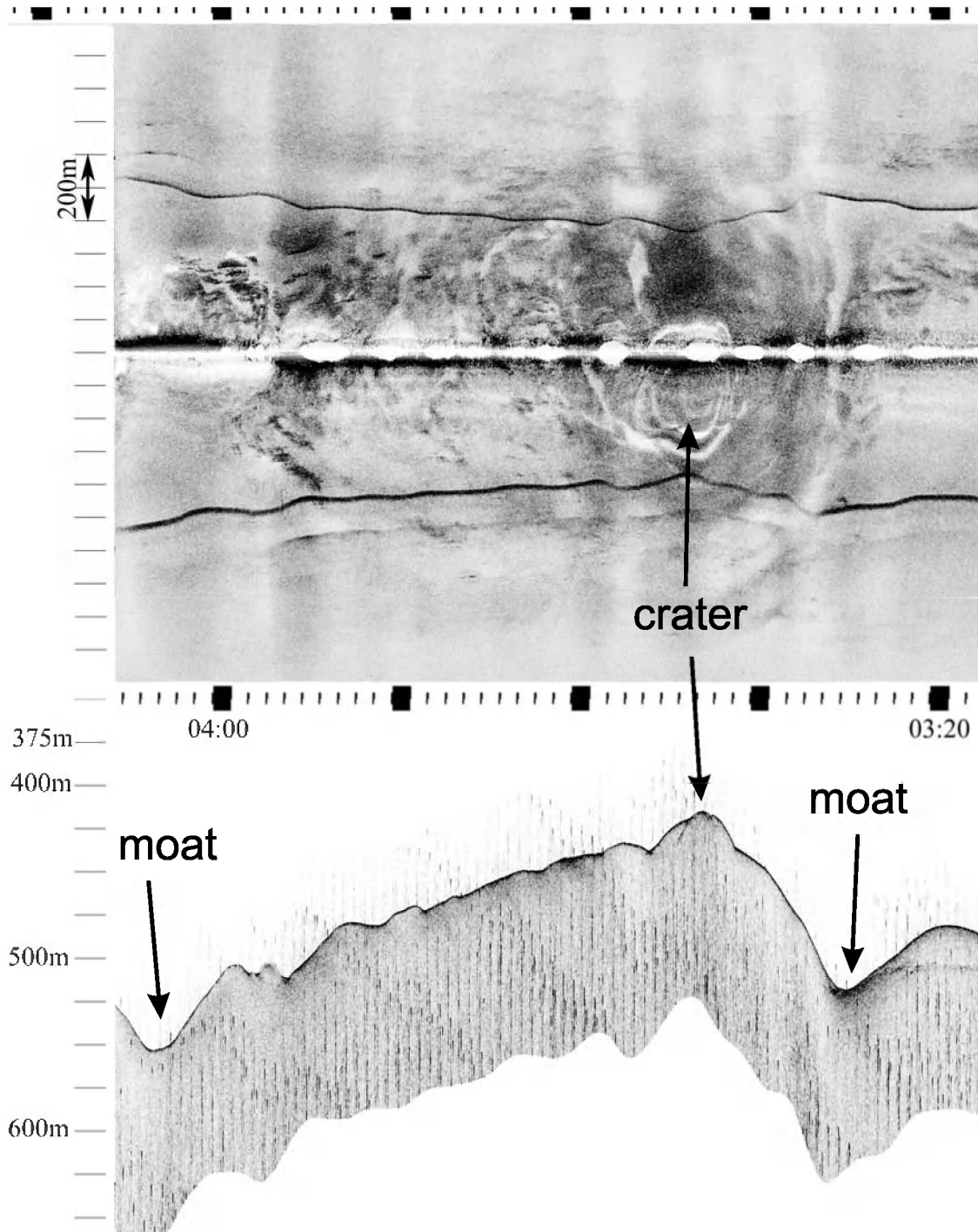


Figure 12. Fragment of MAK line MAKAT-10 over Kidd mud volcano. Line is located on Fig. 1.

duplicates the line MAKAT-64 collected during the TTR-12 cruise.

The line covers the crest of the Vernadsky Ridge and crosses two highs, which possibly are the exposed tops of mud diapirs. The southeasternmost one is a distinct morphological feature rising 60 m above the surrounding sea floor. Its base has a width of 2.4 km, bounded to the NW by a

reflective moat with a depth of 50 m. The top is nearly flat and shows only moderate to low reflectivity. The northwesternmost feature is a highly reflective area made up of linear to lobate ridges up to 20 m high. An area of rough topography is sharply limited by a NW-SE trending slope with an irregular, "bumpy" surface that drops from 480 m to 635 m water depth.

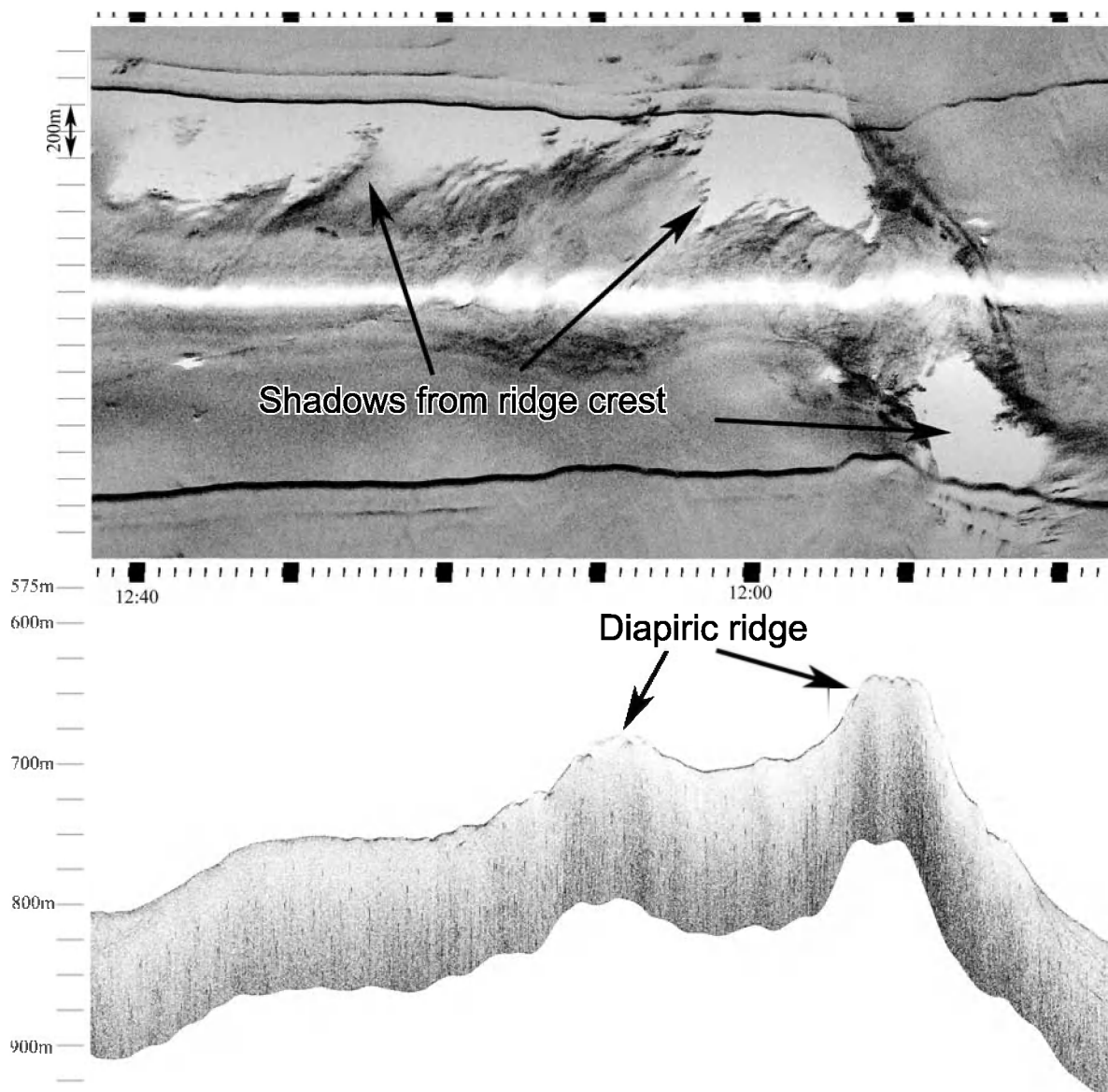


Figure 13. Fragment of MAK line MAKAT-109. Line is located on Fig. 1.

MAKAT-109

Line MAKAT-109 was collected with the aim of inspecting two newly discovered structures, suspected to be of diapiric origin. The length of the E-W trending line is approximately 10 km. Both structures are clearly seen on the sonograph and profile to be distinct seabed highs. They bound a small basin whose infill has the characteristic acoustic signature of a sedimentary drift with convex upper surface and rapid thinning out of the reflectors towards the basin's margins. One of the hills in the eastern part of the line has a 2 km wide base and rises

from a depth of about 700 m to 620 m. It has highly reflective semi-circular ridges crowning its top.

Another hill, in the western part of the profile, has an elongate top with reflective ridges and two separate pinnacles in the W and E, rising to 630 m and 680 m respectively, which cast prominent shadows (Fig. 13).

MAKAT-110

Line MAKAT-110 aimed to look at a newly discovered structural high crossed by seismic line PSAT-256. In the western part of the MAK line there is a newly discovered

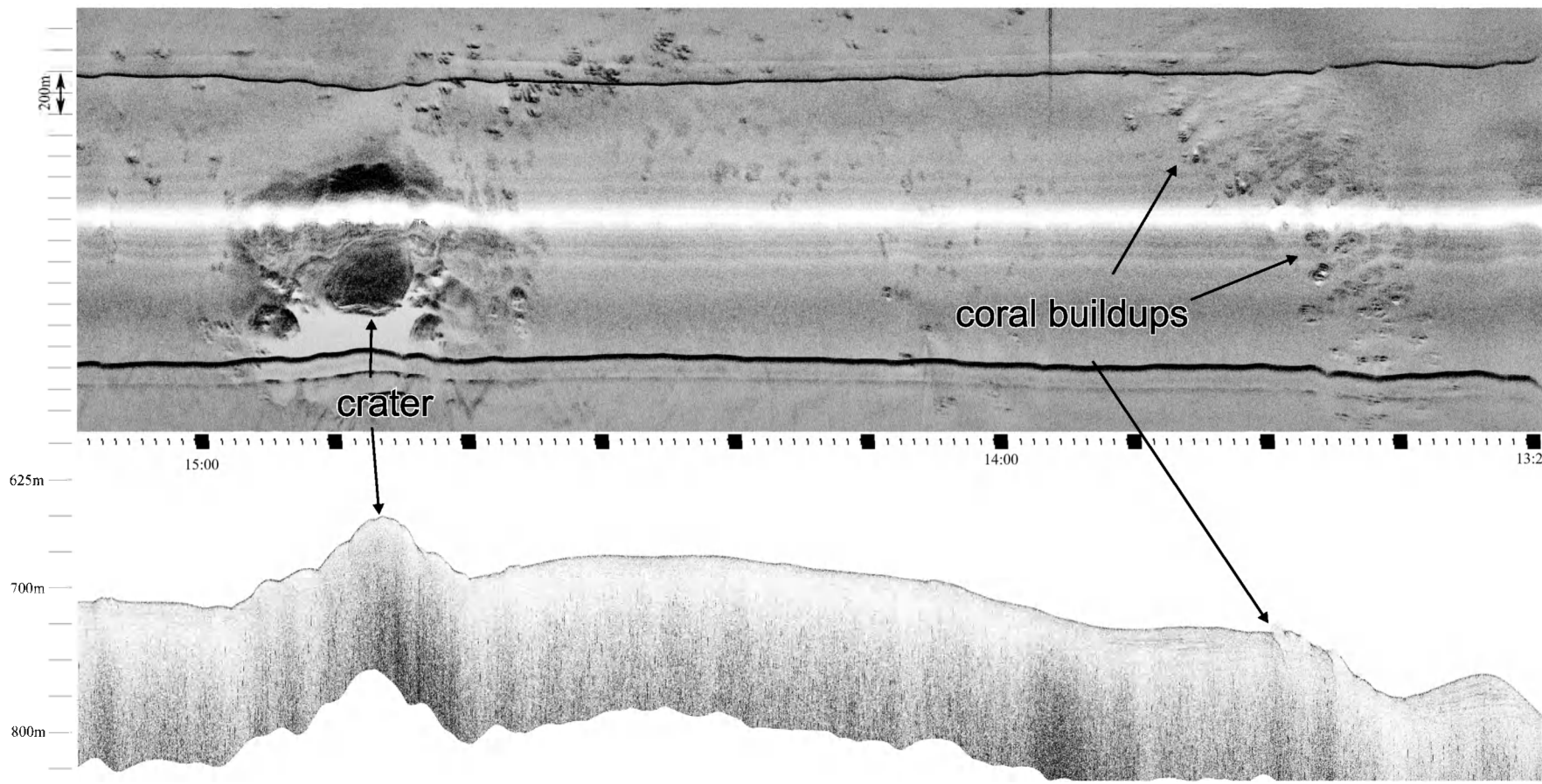


Figure 14. Fragment of MAK line MAKAT-110 near Meknes mud volcano. Line is located on Fig. 1.

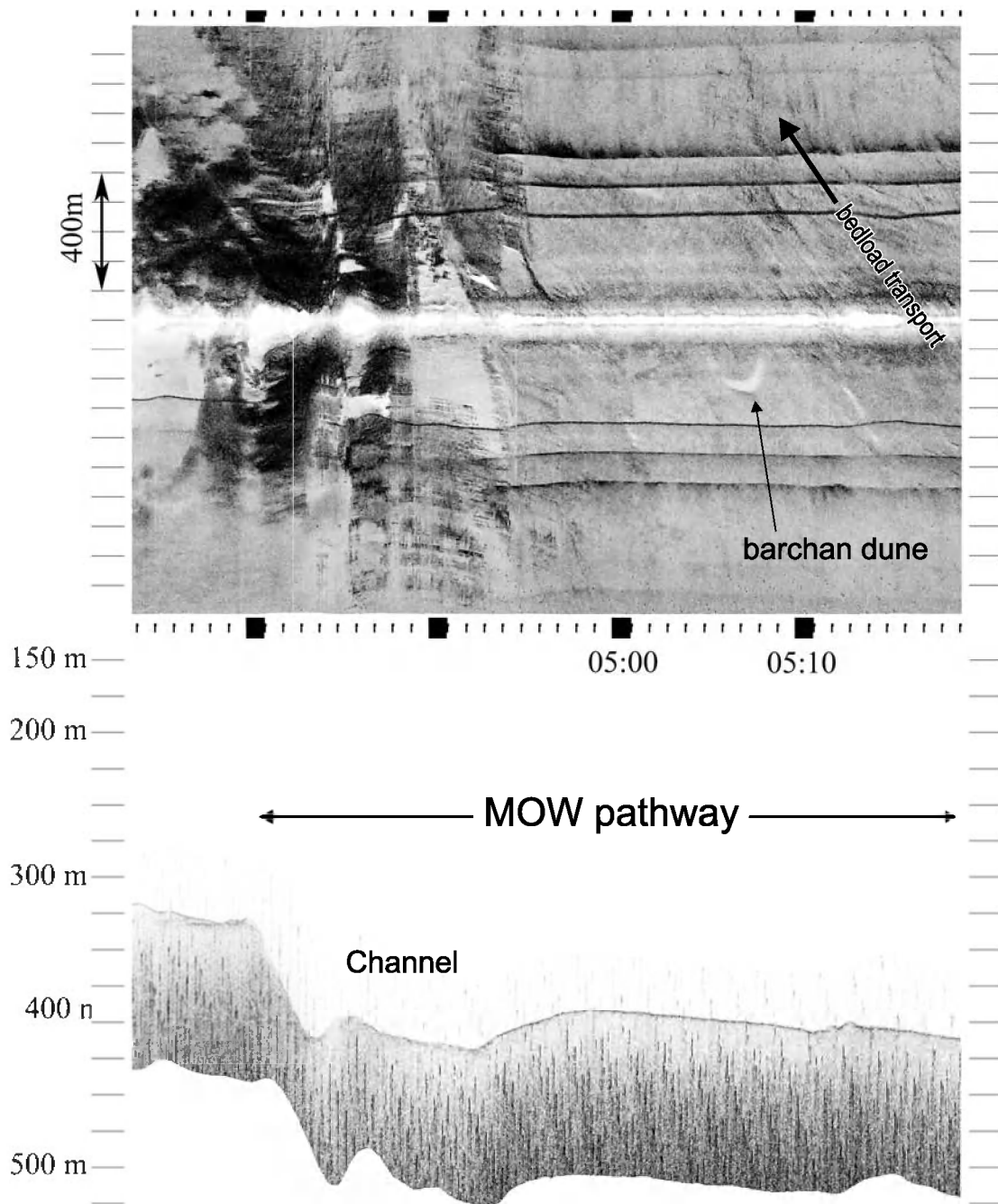


Figure 15. Fragment of MAK line MAKAT-111 over southern rim of the MOW pathway. Line is located on Fig. 1.

mud volcano, named Meknes, with a circular, centrally located crater of high backscatter. The crater is at a depth of approximately 650 m and the base is at 710 m. The width of the mud volcano is about 1 km. The slope dips gently towards the east showing horizontal bedding in the subsurface. The sonograph also shows a large number of small build-ups on the northern slope of the mud volcano as well as on top of an escarpment

located about 5 km to the northeast. The build-ups have high reflectivity and an average diameter of 50 m (Fig. 14). They are thought to be small carbonate mud mounds produced by cold water corals.

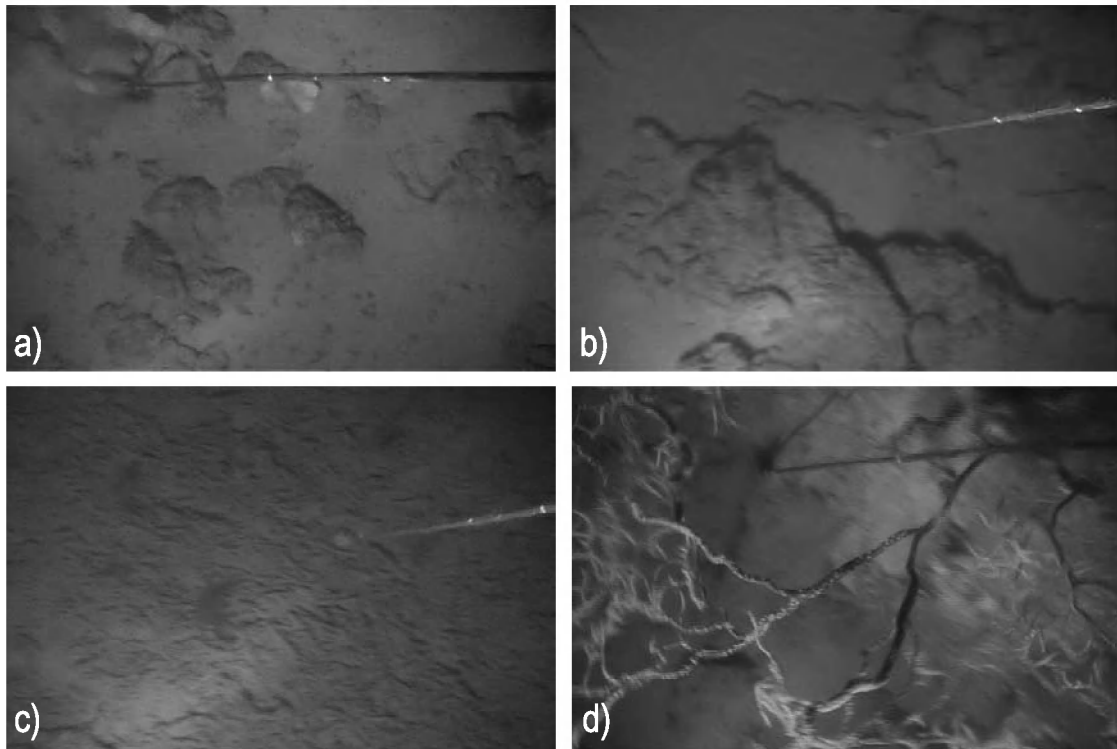
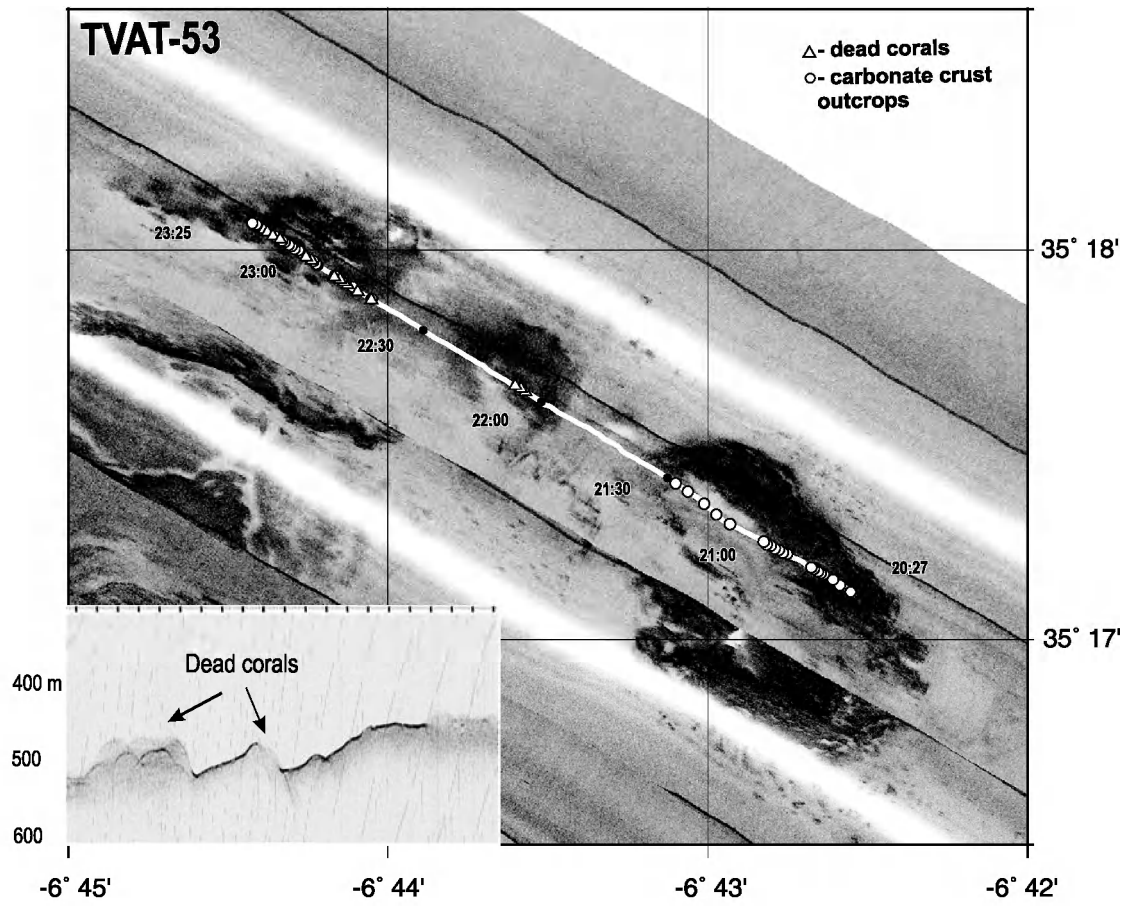


Figure 16. Location and stills from TVAT-53 line in the El Araiche mud volcano field. See text for description.

MAKAT-111

Line MAKAT-111 runs roughly SSW to NNE and is designed for a closer inspection of several high reflectivity areas identified on Seamap imagery (Gardner et al., 1999). The line crosses a circular structural high of about 1 km diameter which is elevated approx. 150 m above the surrounding sea floor. It is bound by a steep 50 m high, south facing slope that may be related to recent slope failure/instability. Two distinct lobate high-reflectivity patches located 500-1000 m SE of the high are thought to be small scale slides. Between this structural high and two high reflectivity areas to the NE the sea-floor is gently rising and shows no distinct reflectivity variations.

The northernmost part of the line covers the southern rim of the MOW channel where there are sedimentary bedforms such as small and large sand waves and longitudinal bedforms characteristic of sand transport by fast flowing currents. The base of the channel is roughly 100 m below the rim of the highly reflective area to the south. At its southern

edge, the MOW pathway is bound by a steep cliff that appears to have been undercut by the current (Fig. 15).

MAKAT-112

This line, parallel to line AT-111, also covers a part of the MOW pathway which has large and small sand waves and erosion-al furrows.

Although this profile is only 3 km to the west of line AT-111 the southern rim of the MOW channel is not as clearly defined. Instead of a steep cliff there are several ridges that form a stepped transition to the high reflectivity area to the south. A field of sand waves, seen as low backscattering features, indicate strong currents and active sand transport along the MOW pathway.

I.5. Underwater video observations

V. BLINOVA, M. IVANOV AND L. PINHEIRO

Seven TV-lines were obtained during TTR14-Leg 1 in the Gulf of Cadiz.

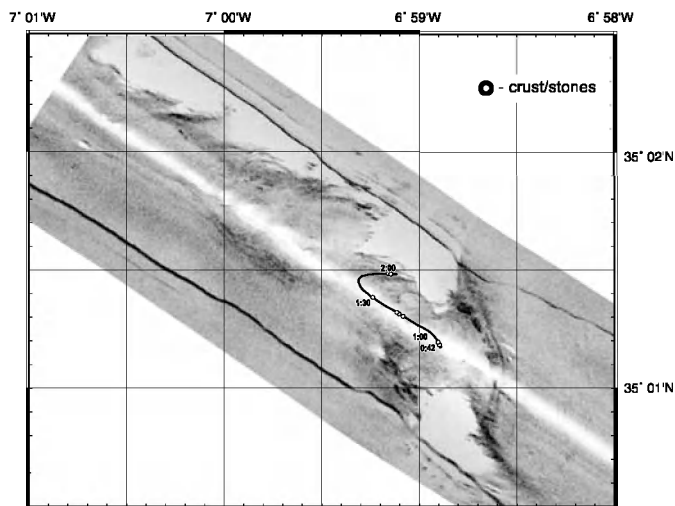


Figure 17. Location of line TVAT-54 on line MAKAT-109 (Fig. 13). Stills show sponges (a) and individual coral thickets (b).

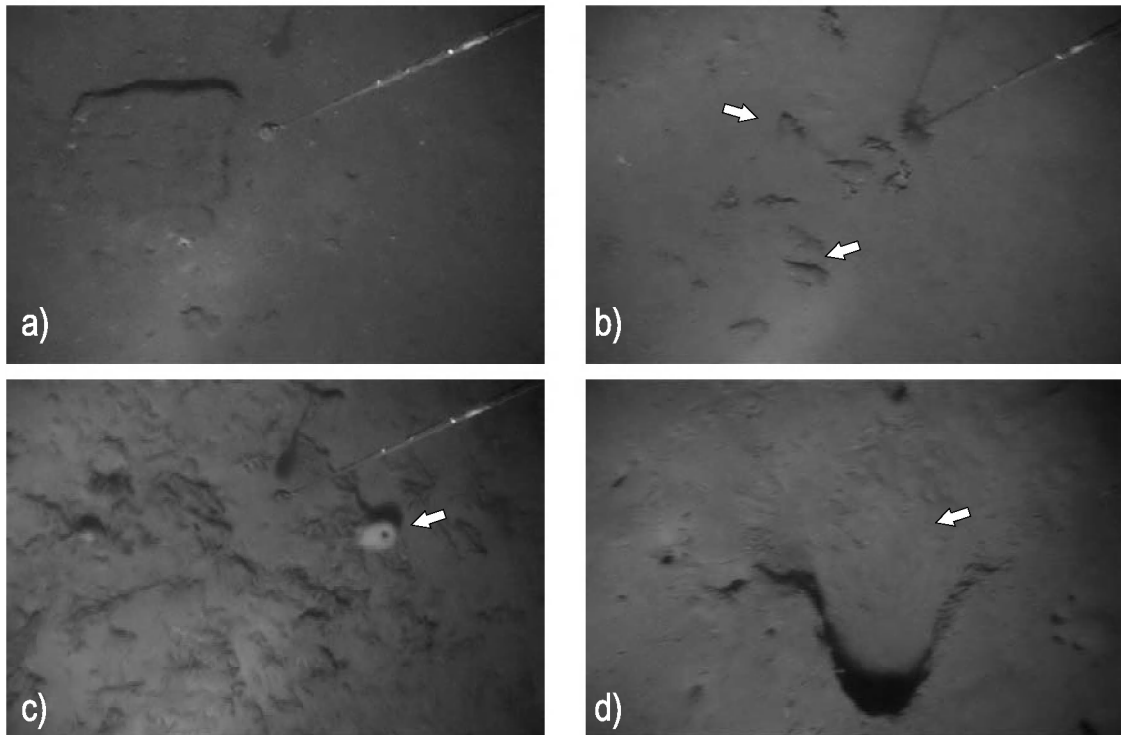
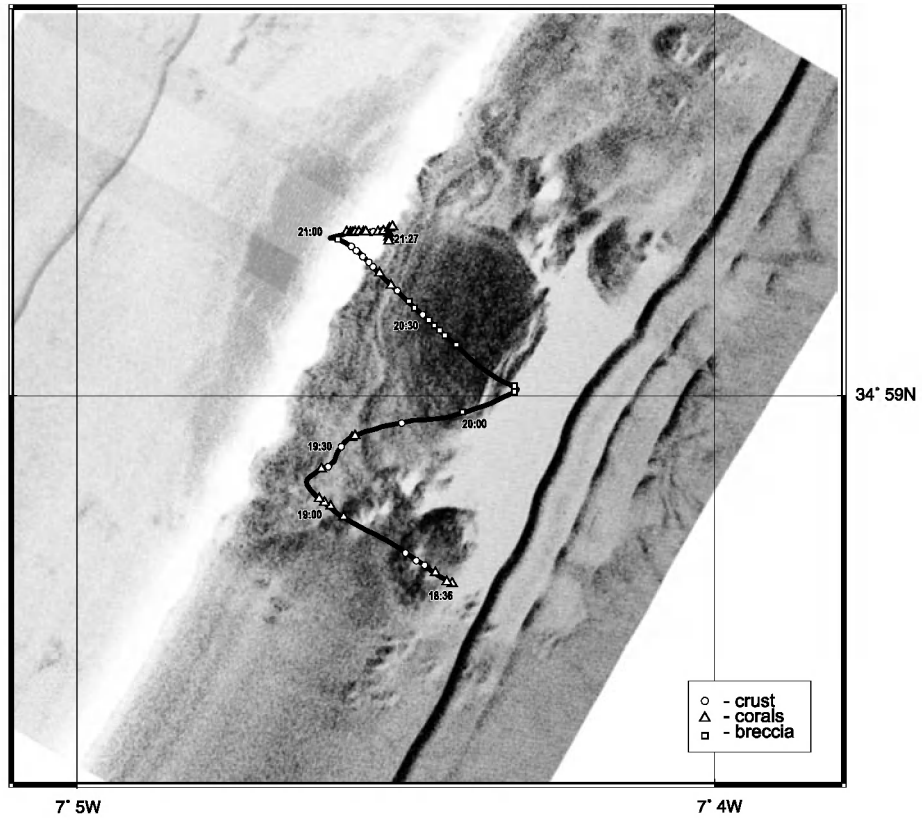


Figure 18. Location and stills from TVAT-55 line across Meknes mud volcano.

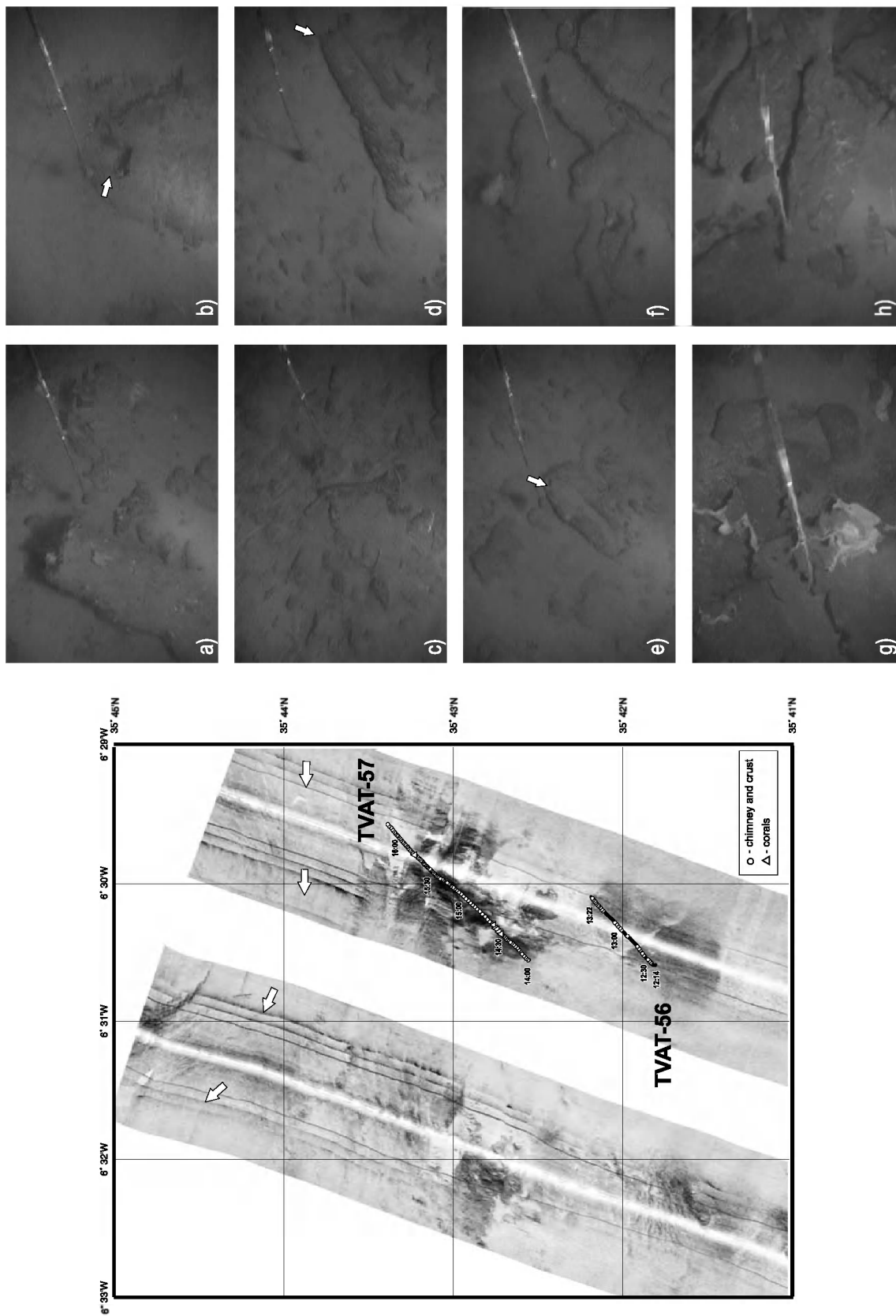


Figure 19. Location and stills from lines TVAT-56 and TVAT-57, located on line MAKAT-III (Fig. 1).

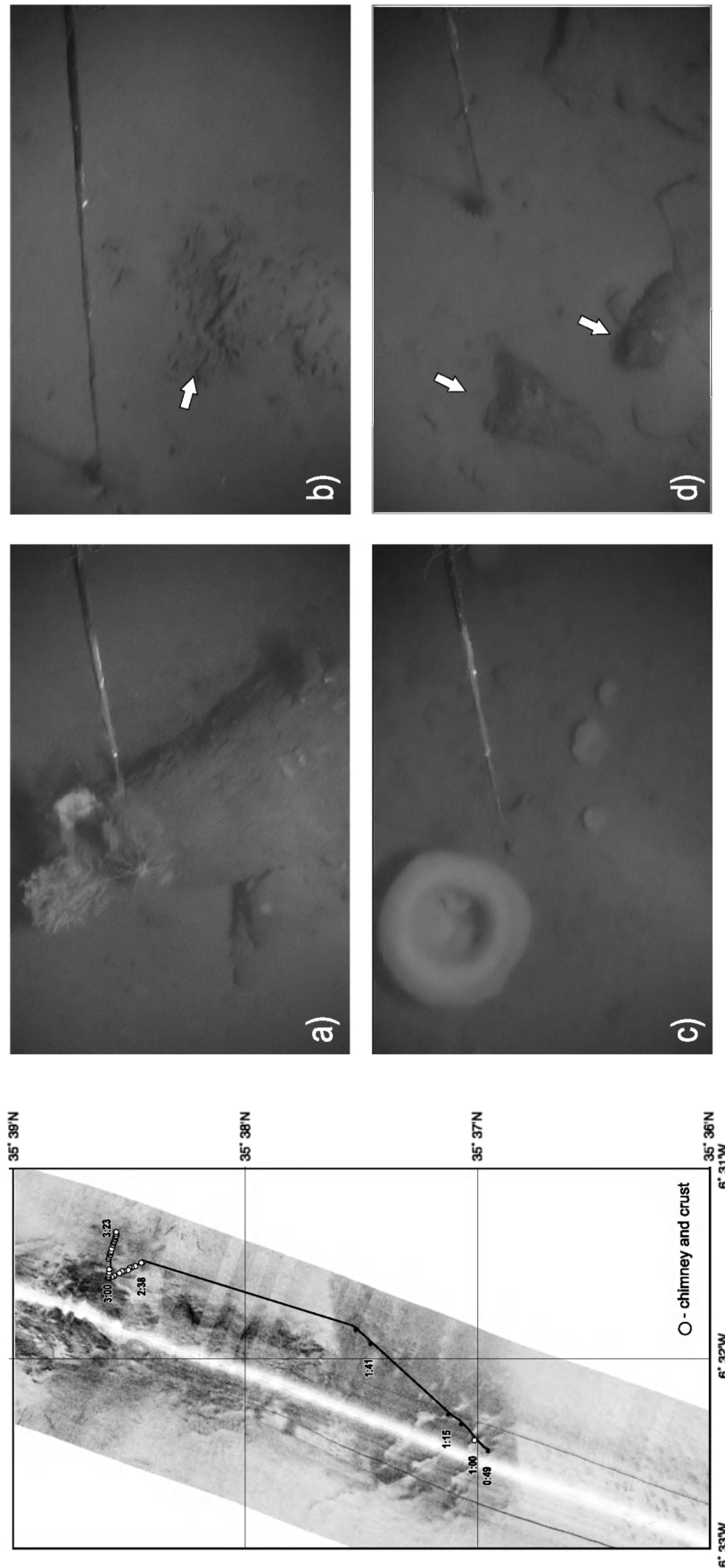


Figure 20. Location and stills from TVAT-58 line showing carbonate chimneys, corals (a, b) and sponges (c), located on line MAKAT-111 (Fig. 1).

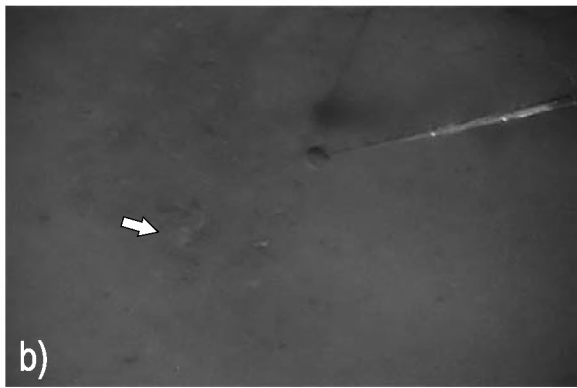
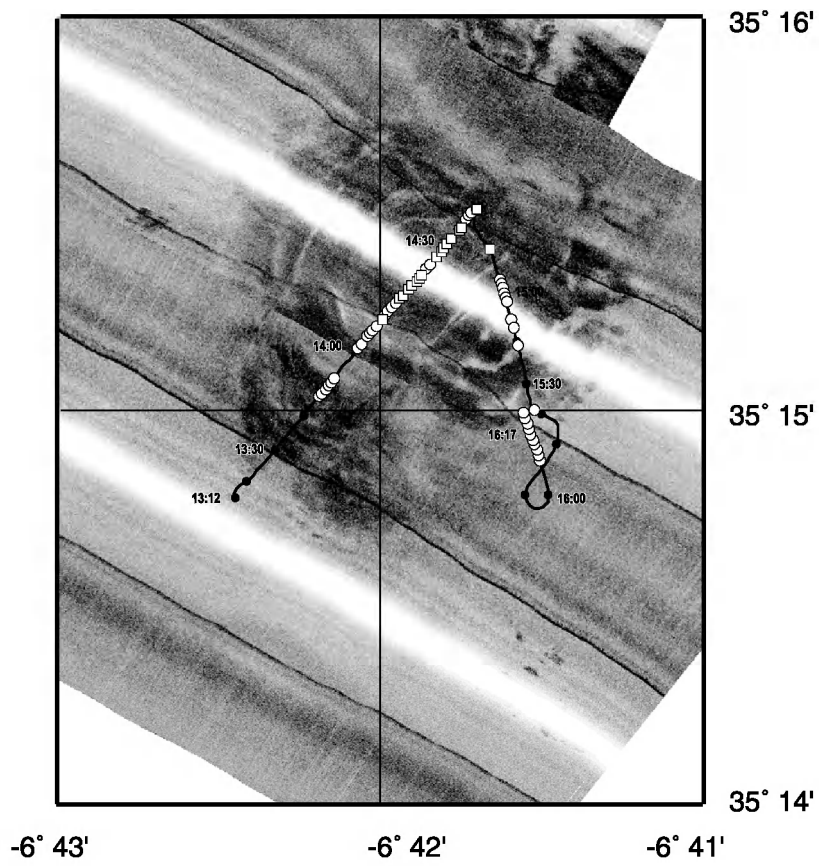


Figure 21. Location and stills from TVAT-59 line across Fuiza mud volcano.

TVAT-53

Line TVAT-53 was selected on the basis of a sidescan sonar mosaic (mainly the line MAKAT-73) made on the TTR-12 cruise in the El Araiche mud volcano field (Kenyon et al., 2003). Three hills, characterized by a strong backscatter, were investigated (Fig. 16).

The video record showed abundant carbonates crusts, concretions (Fig. 16a) and possible outcrops or extensive carbonate slabs (Fig. 16b). On the tops of two hills dense fields of dead corals were observed (Fig. 16c). Sponges and branches of Hydrozoa are also seen along the line (Fig. 16a,d). Between the hills a uniform seafloor is mainly covered by soft bioturbated sediment.

TVAT-54

Line TVAT-54 was selected on the basis of sidescan sonar line MAKAT-109. It runs from the top to the bottom of the seamount (Fig. 17). The seafloor is mainly uniform and covered by soft bioturbated sediment. Several sponges and corals were also seen.

TVAT-55

TVAT-55 was run across the newly discovered Meknes mud volcano (Fig. 18). Carbonate crusts, sandstone blocks, dead corals and fields of mud breccia were observed (Fig. 18). Corals occur mostly on the crusts or blocks of rock present on the slope of the mud volcano (Fig. 18c). The densest field was observed on the north-west slope (water depth about 720 m). Carbonate crusts corresponded to high backscatter on the sonograph. Patches of mud breccia and grey sediments expelled from burrows indicate that the mud breccia is just beneath the surface and mainly in the crater (Fig. 18a,d). On the top of the mud volcano extensive fields of dead *Liptunia contraria* were found (Fig. 18b).

TVAT-56 and TVAT-57

TVAT-56 and TVAT-57 are in the eastern

part of the Gulf of Cadiz, close to the Gibraltar Strait. TV lines were selected to run across seabed hills characterized by high (TVAT-57) and medium (TVAT-56) backscatter on sonographs (Fig. 19). On both lines dense fields of carbonate chimneys, slabs and crusts were observed (Fig. 19). Some chimneys are broken and an internal conduit is seen (Fig. 19e). Outcrops are found on the northern hill characterised by very high backscatter level on the sonograph. There are dead corals on TVAT-57 (Fig. 19a), usually on the southern slopes of hills where more corals must have lived in the past. Large sponges are seen along these two lines and at the end of the TVAT-57 there is evidence of very strong current (MOW). Thus the MOW becomes stronger to the north, forming a variety of bedforms such as sand ripples. Fast moving particles and debris are seen in the water column, indicating the high speed of the bottom current.

TVAT-58

TVAT-58 was run across the southern hill in order to check distribution of carbonate chimneys in this region close to Gibraltar Strait (Fig. 20). The seabed is mainly covered by hemipelagic sediments on the southern part of the line and some chimneys (less than on previous TV-lines) on the northern part. Large outcrops are found to the north in the area characterized by high backscatter on the sonograph. Several sponges and corals are also seen (Fig. 20).

TVAT-59

TVAT-59 runs across Fiuza mud volcano based on the sidescan image obtained during TTR-12 (Kenyon et al., 2003) (Fig. 21). Several carbonate crusts and blocks are seen (Fig. 21c,d). In the crater of the mud volcano mud breccia is found (Fig. 21a,b). It differs from surrounding sediments (yellowish-brown) by its grey colour with some small rock clasts and shell debris.

Table 1. Details of the sites sampled during Leg1 in the Gulf of Cadiz.

Station number	Date	Time (GMT)	Latitude	Longitude	Depth (m)	Recovery (cm)
TTR14-AT-510G	29.07	5:18	36°34.995	7°49.995	768	235
TTR14-AT-511G	29.07	7:16	36°35.004	7°49.003	770	216
TTR14-AT-512G	29.07	8:22	36°35.029	7°47.810	770	175
TTR14-AT-513G	29.07	9:29	36°35.010	7°46.690	760	209
TTR14-AT-514G	29.07	10:30	36°35.022	7°45.595	750	150
TTR14-AT-515G	29.07	11:33	36°35.001	7°44.495	737	166
TTR14-AT-516G	29.07	12:19	36°35.001	7°43.383	715	224
TTR14-AT-517G	29.07	13:00	36°35.002	7°42.280	745	95
TTR14-AT-518G	29.07	13:42	36°34.998	7°41.186	696	139
TTR14-AT-519G	29.07	14:23	36°35.000	7°40.007	710	177
TTR14-AT-520G	31.07	11:57	35°47.127	8°25.335	2215	233
TTR14-AT-521G	02.08	08:29	35°22.284	7°05.276	919	216
TTR14-AT-522G	02.08	09:24	35°22.417	7°05.299	912	202
TTR14-AT-523G	02.08	10:58	35°24.960	7°05.475	962	51
TTR14-AT-524Gr	02.08	12:40	35°24.943	7°05.558	975	1,5 t
		13:20	35°24.973	7°05.461	960	
TTR14-AT-525G	02.08	16:40	35°18.228	6°59.692	881	339
TTR14-AT-526G	02.08	17:32	35°18.135	6°59.693	862	343
TTR14-AT-527G	03.08	11:29	35°25.281	6°43.970	482	28
TTR14-AT-528Gr	03.08	12:09	35°25.281	6°43.969	483	1,5 t
		12:15	35°25.304	6°43.972	489	
TTR14-AT-529G	03.08	13:00	35°25.282	6°43.970	482	77
TTR14-AT-530G	03.08	14:07	35°26.480	6°45.825	580	36
TTR14-AT-531G	03.08	14:46	35°26.078	6°46.485	518	80
TTR14-AT-532G	03.08	15:35	35°26.130	6°46.832	518	107
TTR14-AT-533G	03.08	17:32	35°18.081	6°47.672	573	401
TTR14-AT-534G	03.08	18:20	35°18.410	6°47.812	550	395
TTR14-AT-535G	04.08	17:41	34°59.034	7°04.552	718	281
TTR14-AT-536G	04.08	18:27	34°59.176	7°04.558	735	227
TTR14-AT-537G	04.08	20:15	34°59.248	6°55.621	717	42
TTR14-AT-538G	04.08	22:32	34°59.191	6°55.320	695	279
TTR14-AT-539G	04.08	00:00	35°01.180	6°58.888	742	38
TTR14-AT-540G	05.08	22:22	34°59.070	7°04.413	701	139
TTR14-AT-541Gr	05.08	23:10	34°59.070	7°04.416	706	0,1 t
		23:20	34°59.103	7°04.435	703	
TTR14-AT-542G	06.08	00:16	34°59.175	7°04.364	703	107
TTR14-AT-543G	06.08	07:02	35°39.688	7°19.981	1345	184
TTR14-AT-544G	06.08	09:11	35°39.707	7°20.012	1330	334
TTR14-AT-545G	06.08	10:13	35°39.689	7°20.056	1337	214
TTR14-AT-546Gr	06.08	11:25	35°39.690	7°20.060	1346	1 t
		11:34	35°39.692	7°20.046	1345	
TTR14-AT-547Gr	06.08	14:48	35°39.702	7°20.036	1345	1,5 t
		14:49	35°39.701	7°20.037	1344	
TTR14-AT-548K	06.08	17:41	35°39.708	7°20.034	1345	150
TTR14-AT-549K	07.08	10:27	35°38.612	6°31.657	302	2
TTR14-AT-550D	07.08	17:26	35°42.105	6°30.196	368	0,5 t
		18:12	35°42.257	6°30.000	392	
TTR14-AT-551D	07.08	19:18	35°42.597	6°30.505	445	0,5 t
		20:05	35°42.769	6°30.305	393	
TTR14-AT-552Gr	07.08	21:09	35°42.737	6°30.333	404	0,5 t
		22:45	35°42.816	6°30.234	428	
TTR14-AT-553G	08.08	10:04	35°15.354	6°41.898	398	packed
TTR14-AT-554G	08.08	10:27	35°15.357	6°41.888	398	packed
TTR14-AT-555G	08.08	11:01	35°15.065	6°42.196	457	packed
TTR14-AT-556G	08.08	11:32	35°15.062	6°42.196	457	packed
TTR14-AT-557G	08.08	12:08	35°14.785	6°42.480	542	packed
TTR14-AT-558G	08.08	12:37	35°14.785	6°42.475	541	packed
TTR14-AT-559B	08.08	18:34	35°24.777	6°43.782	552	30
TTR14-AT-560B	08.08	19:30	35°25.306	6°43.976	498	40
TTR14-AT-561B	08.08	20:35	35°25.602	6°44.099	526	90
TTR14-AT-562G	08.08	21:30	35°25.601	6°44.095	526	packed
TTR14-AT-563G	08.08	21:52	35°25.602	6°44.094	526	packed
TTR14-AT-564G	09.08	01:03	35°17.453	6°47.006	538	219
TTR14-AT-565Gr	09.08	02:41	35°18.100	6°47.515	558	1,5 t
		03:29	35°18.180	6°47.656	544	
TTR14-AT-566Gr	09.08	05:53	35°15.494	6°41.657	413	1,5 t
		06:11	35°15.510	6°41.702	414	

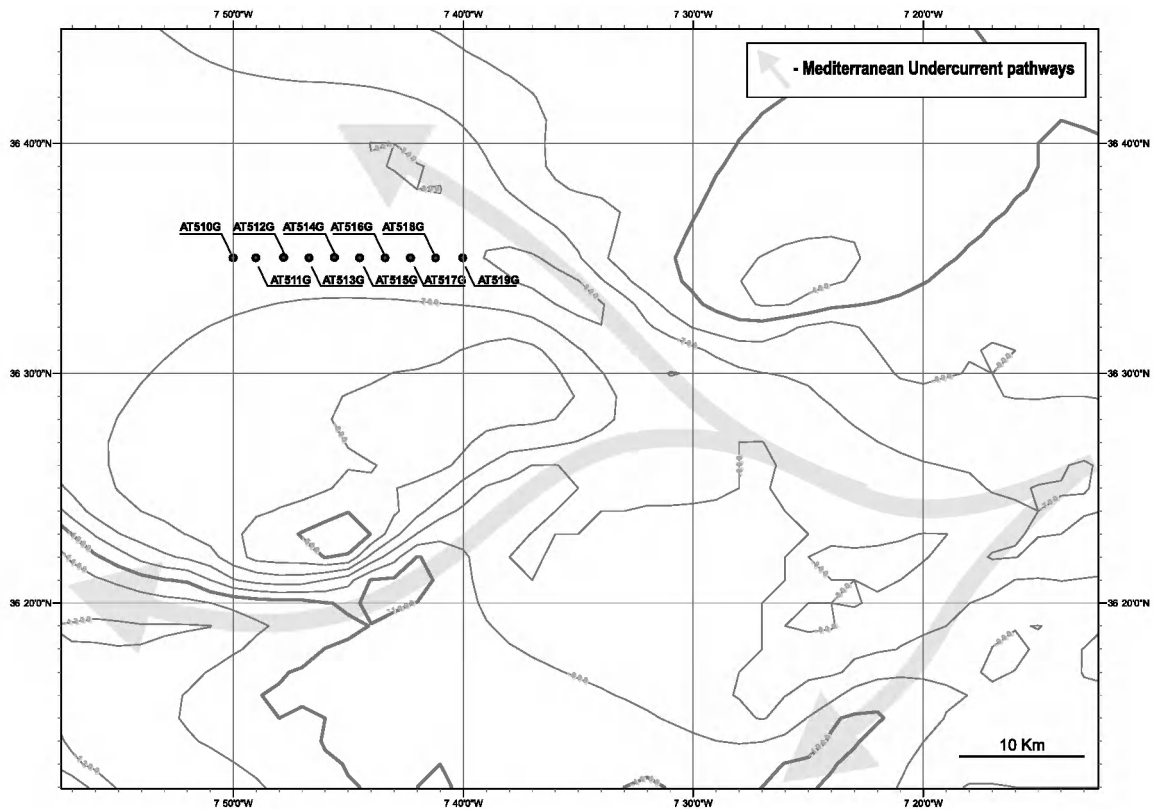


Figure 22. Location of sampling sites AT-510G-519G, east of Faro Canyon.

I.6. Bottom sampling results

E. KOZLOVA, E. SARANTSEV, E. BILEVA, V. BLINOVA,
D. KOROST, A. OVSYANNIKOV, E. LOGVINA,
A. SHUVALOV, I. GURJEV, P. GOLINCHIK,
A. BECKSTEIN, E. DE BOEVER, S. COSTAS, M. CUNHA,
V. MAGALHAES, M. NUZZO, A. CARVALHO,
C. RODRIGUES, C. SA, P. SANTOS, C. GONÇALVES,
J. DUARTE AND B. EL MOUMNI.

Table 1 summarises technical details of the sampling sites and core logs can be found in the Annexe I.

Area 1

The area is located east of the Faro Canyon, at a depth of about 800 m. Ten gravity cores (AT-510 to AT-519) were collected at regular intervals along an E-W profile (Fig. 22). All cores were sampled at 3 depth intervals (10/50/100 cm), in addition the lowermost part of the recovered material was kept. These samples will be examined in a microbiological study to determine the microbial inventory, especially the distribution of

methane-oxidizing and other hydrocarbon-oxidizing bacteria and the variation in their abundance along the cored profile.

Cores AT-510G to AT-516G

Recovery length at these six sites varied from 166 to 236 cm and showed a hemipelagic sequence, usually with two units distinguished. The uppermost unit is about 5 to 15 cm thick and is a light brownish grey clay, rich in foraminifera. The lower unit is a light grey clay with silty admixture.

Cores AT-517G to AT-519G

These cores have a hemipelagic sequence similar to the previous sites but with higher sand content which resulted in reduced recovery (95 to 177 cm). Sand intervals are 5 to 20 cm thick and have either sharp or transitional contacts. The presence of these sand intervals is explained by the proximity of the sampling sites to a pathway of the MOW (Fig. 22) and indicates its recent activity.

*Carlos Ribeiro mud volcano*Core AT-520G

The sampling station was located in the centre of Carlos Ribeiro mud volcano. About 233 cm of sediments were recovered. The upper part of sediments (0-13 cm) is a light brown water-saturated marl with foraminifera. The unit below (13-72 cm) consists of brownish stiff clay with a small amount of sandy admixture in the upper 18 cm and with oxidized patches in the lower part. Dark spots, thin stripes (organic matter?) and a small amount of foraminifera are also seen. At 46-59 cm patches of grey clay with silty admixture are found. The lower unit (72-217 cm) is grey clay with some silty admixture. The lowermost unit (217-233 cm) is a greyish matrix-supported mud breccia with clasts up to 0.5 mm in diameter. The upper boundary is irregular.

Ginsburg mud volcano

Two stations aimed to retrieve gas hydrates from the crater of Ginsburg mud volcano.

Cores AT-521G and AT-522G

Both cores recovered sequences of mud breccia 216 and 202 cm long, respectively, covered by a thin (6 to 8 cm) veneer of hemipelagic sediments. The mud breccia is grey with clasts of different lithology (from 2 mm up to 3 cm in size) in the clayey matrix and a strong smell of H₂S. These sediments indicate that the mud volcano is active at the present time. No gas hydrates were seen.

*Yuma mud volcano*Core AT-523G

The 51 cm long core was collected from the small crater of Yuma mud volcano. It consists of an upper (0-17 cm) brown marl with many small rock fragments and a soupy top and a lower grey mud breccia, with a large amount of small (up to 3 mm) clasts of

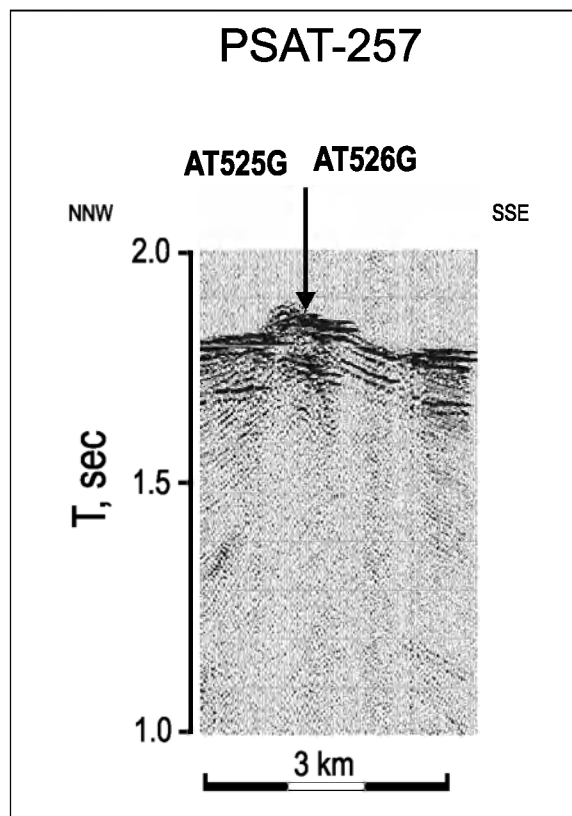


Figure 23. Location of sampling sites AT-525G and AT-526G, on line PSAT-257 (see Fig. 1 for location).

different lithology in the clayey matrix. No H₂S smell was detected.

Grab AT-524Gr

This large volume sample was also collected from the small crater of Yuma mud volcano. The upper part of the sequence (about 5 cm) is brownish marl with foraminifera and shell debris. The lower part is matrix-supported mud breccia. Biological samples include Pogonophora (Fam Sisoglinidae), Bivalves (Fam Sozemyidae) and others. No gas hydrates were recovered.

Dome-like structure

Two cores were collected from a dome-like feature, recognised on the seismic line PSAT-257 which was suspected to be a mud volcano (Fig. 23).

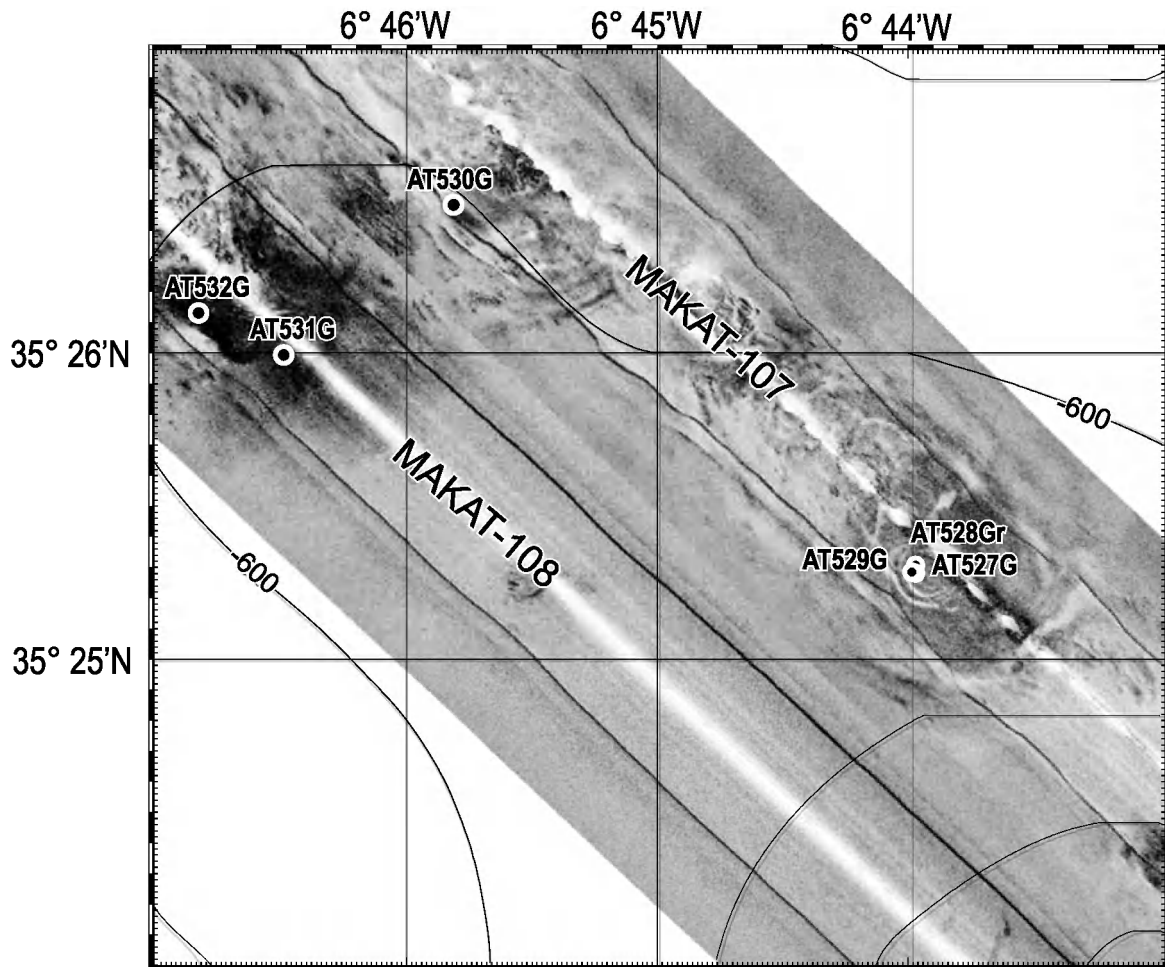


Figure 24. Location of sampling sites AT-527-532G along lines MAKAT 107 and 108 (see Fig. 1 for location).

Core AT-525G and AT-526G

The corer retrieved 339 and 343 cm long sequences of hemipelagic sediments, represented by brownish and grey marls and clays.

Kidd mud volcano (Fig. 24)

Three stations were based on the MAK-1M acoustic imagery obtained during this cruise. The aim of the sampling was to retrieve gas hydrates from the crater of the mud volcano, however no gas hydrates were recovered at these stations.

Core AT-527G

The 28 cm long core consisted of brownish grey coral and shell debris in a clayey matrix with clasts up to 0.5 cm in diameter in

the upper 6 cm. Below (6-28 cm) is an interval of grey matrix-supported mud breccia with shell fragments. A smell of H₂S was detected.

Grab AT-528Gr

The grab retrieved a large volume of grey mud breccia with sandy admixture, and with a smell of H₂S. Large clasts (up to 10-15 cm in diameter) were recovered. Clasts include porous carbonate crusts and bedded sandstones.

Core AT-529G

The core is similar to the core AT-527G. Most of it (14-77 cm) is grey mud breccia overlain by a 14 cm thick hemipelagic clay veneer mixed with clasts from the lower unit.

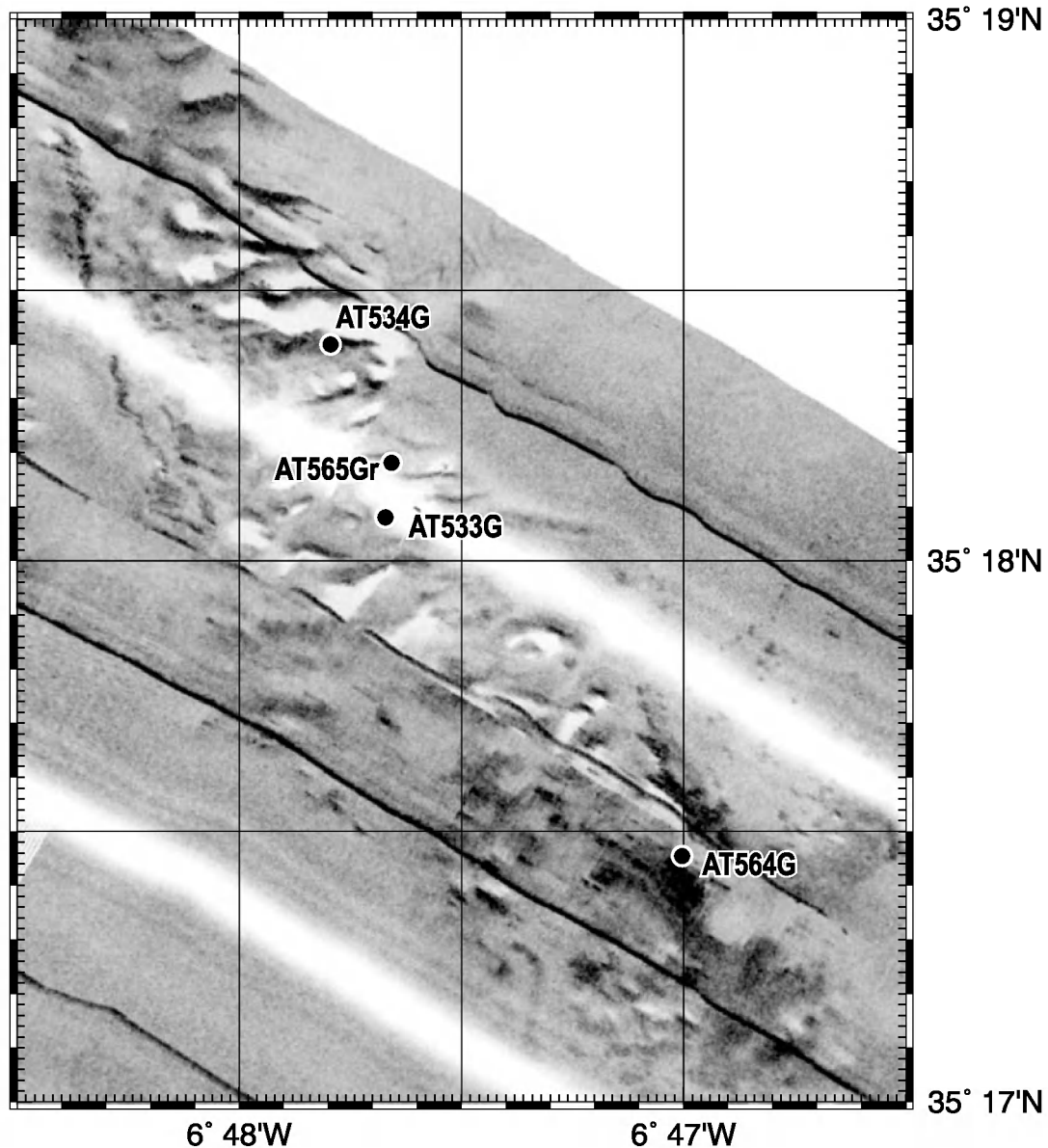


Figure 25. Location of sampling sites AT-533G, AT-534G, AT-564G, and AT-565Gr on the Pen Duick escarpment.

Circular structure and ridge

Core AT-530G

A ridge near the Kidd mud volcano was sampled at this station. The core was 36 cm long. The upper unit is brown sand with silty admixture and coral and shell debris. The lower unit consists of light grey, very stiff bioturbated clay with foraminifera.

Core AT-531G and 532G

A high backscatter area on the top of the ridge was sampled at these stations. The recovery was 80 and 107 cm, respectively and is similar to the previous station. The uppermost unit is 8 to 18 cm of brown sand with silty admixture and coral and shell debris. The lower unit is light grey very stiff clay. The stiff clay is thought to be the cause of the high backscatter and represents older strata cropping out at the top of the diapiric ridge.

Pen Duick escarpment area (Fig. 25)

Core AT-533G

The core was from one of the build-ups growing along the edge of the Pen Duick escarpment. The sequence consists of an upper interval of clayey sand (0-21 cm) overlying an interval of light grey clay (21-56 cm) and below which is a thick interval of coral rubble (56-401 cm).

Core AT-534G

Another build-up was sampled and the recovered sequence is similar to that from the previous station. A coral rubble interval is

found below 37 cm. It is overlain by a hemipelagic veneer topped by a sand interval. Coral fragment distribution within the coral rubble interval is not uniform and there are intervals with almost no debris.

Core AT-564G

The core was from a patch of high backscatter on the MAK image. The recovery is a 219 cm long sequence of mostly coral rubble overlain by a 10 cm thick hemipelagic clay veneer. The coral rubble interval varies in colour from brownish in the top to greenish grey in the bottom. Density of sediment also increases towards the bottom. The sediments smell of H₂S.

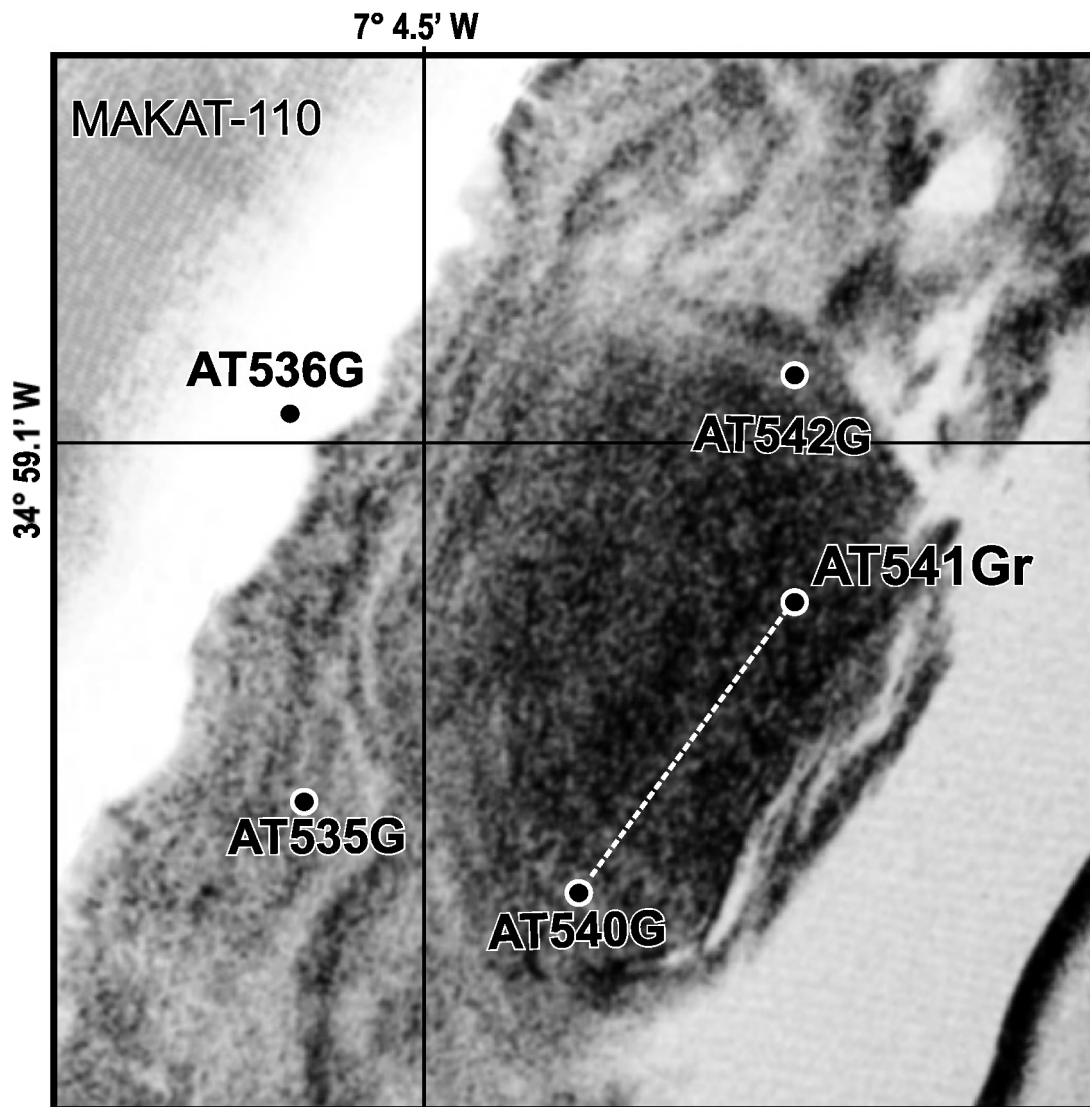


Figure 26. Location of sampling sites AT-535G, AT-536G, and AT-540-542G on Meknes mud volcano.

Grab AT-565Gr

This large volume sample was also collected from a build-up and consists mainly of coral rubble with a high proportion of coral.

Meknes mud volcano (Fig. 26)

Core AT-535G

The 281 cm long core is from the slope of the volcano and is a hemipelagic sequence with several intervals of coral rubble up to 94 cm thick.

Core AT-536G

The core is from the northwestern slope of the volcano. It is a 227 cm long sequence consisting of hemipelagic sediments with noticeable admixture of coral debris. The sequence contains two intervals of mud breccia between 159 and 167 cm and between 201 and 227 cm. The breccia is grey, with clasts up to 1 cm in diameter and coral fragments in the clayey matrix and smells of H₂S.

Core AT-540G

The core is from the crater of the mud volcano and is a 139 cm long section of mud breccia with intervals of different water saturation, density and colour. The sequence is thought to be formed by multiple amalgamated flows. The whole core smells of H₂S.

Grab AT-541Gr

The grab retrieved a large amount of greenish grey mud breccia with clasts of different lithology and size (from 2 mm up to 5 cm in diameter). A representative collection of bottom fauna was preserved from the sample.

Core AT-542G

The station is also within the crater of the mud volcano, close to its northern edge. The core is 107 cm of dark greenish grey mud breccia with clasts of different lithology

mixed in the clayey matrix. A strong smell of H₂S was detected.

Conical structure

Cores AT-537G and AT-538G

The corer recovered 42 and 279 cm long sections of hemipelagic marls and clays.

Clay diapir

Core AT-539G

This short core is 38 cm of hemipelagic sediments topped by a 6 cm thick sandy layer. The lower 22 cm are grey, very stiff clay which is thought to be from old sediments cropping out at the top of the diapir. The short recovery is due to the density of the clay.

Captain Arutyunov mud volcano

Several samples were collected from the crater of the mud volcano.

Cores AT-543G, AT-544G, AT-545G, and AT-548K

The cores contain a sequence of grey mud breccia, up to 214 cm long, with abundant clasts (1 to 2.5 cm in diameter) and a sandy admixture in the clayey matrix. In the upper 5-10 cm of the sequences Pogonophora is very common. A strong smell of H₂S was detected in all cores and all but AT-543G contained gas hydrates.

Grabs AT-546GR and AT-547GR

The aim of these samples was to collect a large volume of gas hydrates. Both attempts were unsuccessful due to slow recovery speed. Otherwise large volumes of grey mud breccia with clasts from 3 mm and up to 5 cm in diameter were recovered.

Sampling data suggest that Arutyunov mud volcano is an active gas seepage site.

Ridge close to Gibraltar Strait

Core AT-549K

A seabed ridge, located close to Gibraltar Strait and characterized by very high backscattering on the MAKAT-111 line, was sampled at this station. The corer retrieved a small amount of sediment represented by greyish brown shell debris with sand and random pebbles (up to 2-3 cm in diameter) and grey soupy carbonate clay.

Dredge AT-550D

The dredge contained only rocky fragments about 90% of which are represented by carbonate crusts and chimneys. Several examples of sandstone fragments were also found. All rocks are covered by attached fauna.

Dredge AT-551D

The dredge contained 12% of sediments and 88% of rock fragments. The rocks are carbonate slabs and chimneys densely covered by attached fauna such as Polychaeta, Decapoda, Hydrozoa, Porifera, Bryozoa and others. All rock fragments were smeared with stiff grey clay with a small amount of silty admixture.

Grab AT-552Gr

The recovery was similar to the previous station, consisting mainly of carbonate crusts from 5 to 60 cm in diameter covered by a diverse attached fauna.

Fiuza mud volcano

AT-566Gr

The grab sample consists of 65% sediments and 35% clasts. The sediments are a greenish-grey mud breccia with sandy admixture and the clasts have different lithologies and are up to 150 cm in size. The larger blocks are predominately sandstones.

Miscellaneous

Cores AT553G-563G

Several stations were repeated on Fiuza and Kidd mud volcanoes for subsequent onshore analyses and were not described onboard.

I.7. Biology

M. CUNHA, C. RODRIGUES, C. SÁ AND
P. REIS SANTOS

I.7.1. Introduction

The geological samples collected during Leg 1 contained a number of organisms that were preserved for further study. Moreover, deep-towed TV runs also provided information on faunal zonation. Their analysis will contribute to knowledge of the faunal assemblages associated with the different bathyal environments and complements the material collected during previous TTR cruises. The specimens will be deposited in the Marine Invertebrate Collection (Department of Biology, University of Aveiro) and will be used for ecologic, taxonomic, morphologic and genetic studies.

I.7.2. Methods

Bottom sampling

Grab samples: Conspicuous animals were picked from the surface of the sediments and rocks. When chimneys and crusts were present, specimens were also recovered from their washings. A variable volume of surficial sediments was also collected when available

Dredge samples: The fauna was picked from the surface of the rocks and/or recovered from rock washings and sieved sediments (the finest sieve used was 0.5 mm).

Core samples: Conspicuous animals were picked from the sediment. Whenever possible at least one quarter of the 25-30 cm of the uppermost part each core was subsampled.

Box-core samples: Three samples for meiofauna were collected in each core from the surficial sediments. The top layer (30-40 cm) was washed and preserved for further analysis.

Except for the box cores, the samples obtained could only be treated in a qualitative way. The specimens picked from sediments and rocks were preserved in 85% ethanol (or deep-frozen) to enable future genetic analysis. Some specimens of selected species were prepared for stable isotope analysis and electronic microscopy observation.

The sediments were washed through a sieve column (2, 1 and 0.5 mm). The fauna in the two coarser fractions was sorted and kept in 85% ethanol. The finer fraction (0.5 to 1 mm) of the sieved sediments was preserved in 10% neutralised formaline stained with Rose Bengal for later sorting under a stereoscopic microscope.

Deep towed TV

Preliminary lists of the fauna, multivariate analysis and mapping were made from data obtained during real time observations of video footage.

1.7.3. Results

Biological results consist of lists of macrofaunal organisms obtained from bottom sampling and observations of megafauna and life traces during TV-lines. These are compiled in Tables 2 and 3, respectively. A preliminary description of the samples is given below based on the material partially processed on board.

A) Bottom sampling

South Portuguese margin (east of Faro Canyon): The sampling in this area included ten gravity cores (AT-510G to AT-519G), only a few Polychaetes, empty tubes and one bivalve were retrieved from the samples.

Carlos Ribeiro mud volcano: The only gravity core sample (AT-520G) collected in this area showed some biological debris but no conspicuous living organisms.

Ginsburg mud volcano: Some

pogonophoran worms (*Siboglinum* sp.) were recovered from the samples (AT-521G to AT-522G).

Yuma mud volcano: Pogonophoran worms (*Siboglinum* sp.) were abundant in the two samples taken at this location (AT-523G and AT-524Gr). Solemyidae bivalves (*Acharax* sp.), polychaete worms and sessile fauna were also retrieved from the grab sample (AT-524Gr).

New structure (1): Some pogonophoran worms (*Siboglinum* sp.) were recovered from the two samples (AT 525-526G)

Kidd mud volcano: Pogonophoran worms (*Siboglinum* sp.) were abundant in the samples taken at this location. (AT-527G, AT-528Gr, AT-529G). The grab sample further yielded numerous specimens of Solemyidae bivalves (*Acharax* sp.) and a diversity of other mobile organisms (several species of Crustacea and Polychaeta) and sessile organisms (Porifera, Cnidaria and Bryozoa). Some of the specimens were fixed for stable isotope analysis. Three box cores (AT-559B to AT-561B) were also collected in different areas of hemipelagic sediments on the outskirts of the mud volcano, crater and mud flow. These samples were washed and fixed on board but were not sorted.

A coral ridge and a dome structure near Kidd mud volcano were also sampled. The gravity core samples (AT-530G and AT-531G to AT 532G, respectively) showed some biological debris but no conspicuous living organisms.

Pen Duick Escarpment: The samples recovered (AT-533G-AT-534G, AT-564G, AT-565Gr) included abundant biological debris, mainly dead corals, but no conspicuous living organisms.

Meknes mud volcano: Cores AT 535G-536G, AT-540G, AT-542G) recovered abundant biological debris, mainly dead coral fragments. The grab sample (AT-541Gr) further yielded numerous specimens of pogonophoran worms (*Siboglinum* sp.) a few Solemyidae bivalves (*Acharax* sp.) and a diversity of other mobile organisms (several species of Crustacea and Polychaeta) and sessile organisms (Porifera, Cnidaria and Cirripedia).

New structure (3): The two core samples

Table 2. Macrofauna and biological debris from the bottom samples.

A) Listing of the macrofauna collected from bottom samples
Stations that were not used for biology subsampling are marked with *.

Class	IPOR	Cnidaria	SIP	MOLLUSCA	NEM	ANN	ARTHROPODA	ECHINODERMATA	BRY									
Order	Hyd	Scy	Ant	Polp	Gas	Biv	Pog	Cir	Melacostraca	Dec	Amp	Iso	Tan	Ast	Cir	Oph	Echl	
AT 510 G																		
AT 511 G						+												
AT 512 G						+												
AT 513 G*																		
AT 514 G						+												
AT 515 G																		
AT 516 G						+												
AT 517 G																		
AT 518 G*																		
AT 519 G																		
AT 520 G*																		
AT 521 G*																		
AT 522 G																		
AT 523 G																		
AT 524 Gr																		
AT 525 G																		
AT 526 G																		
AT 527 G																		
AT 528 Gr																		
AT 529 G*																		
AT 530 G																		
AT 531 G																		
AT 532 G																		
AT 533 G																		
AT 534 G																		
AT 535 G																		
AT 536 G																		
AT 537 G																		
AT 538 G																		
AT 539 G*																		
AT 540 G																		
AT 541 Gr																		
AT 542 G*																		
AT 543 G																		
AT 544 G																		
AT 545 G*																		
AT 546 Gr																		
AT 547 Gr																		
AT 548 K																		
AT 549 K*																		
AT 550 D																		
AT 551 D																		
AT 552 Gr																		
AT 559 B**																		
AT 560 B**																		
AT 561 B**																		
AT 564 G*																		
AT 565 Gr																		
AT 566 Gr																		

B) Biological debris observed in bottom samples

Biological debris	IFor	Cor	Ple	Gas	Biv	Bra	Ech
AT 510 G							
AT 511 G	+						
AT 512 G							
AT 513 G							
AT 514 G							
AT 515 G							
AT 516 G							
AT 517 G							
AT 518 G							
AT 519 G							
AT 520 G	+						
AT 521 G							
AT 522 G							
AT 523 G							
AT 524 Gr							
AT 525 G	+						
AT 526 G							
AT 527 G							
AT 528 Gr							
AT 529 G							
AT 530 G							
AT 531 G							
AT 532 G							
AT 533 G							
AT 534 G							
AT 535 G							
AT 536 G							
AT 537 G							
AT 538 G							
AT 539 G							
AT 540 G							
AT 541 Gr							
AT 542 G							
AT 543 G							
AT 544 G							
AT 545 G							
AT 546 Gr							
AT 547 Gr							
AT 548 K							
AT 549 K							
AT 550 D							
AT 551 D							
AT 552 Gr							
AT 559 B							
AT 560 B							
AT 561 B							
AT 564 G*							
AT 566 Gr							

For: Foraminifera; Cor: Coral fragments; Ple: Pteropod shells;
Gas: other gastropod shells; Biv: Bivalve shells; Bra: Brachiopod shell;
Ech: Echinoderm spicules and plates

POR: Porifera; SIP: Sipuncula; NEM: Nemeritea; ANN: Annelida; BRY: Bryozoa; Hyd: Hydrozoa; Scy: Scyphozoa; Ant: Anthozoa;
Polyp: Polychaeta; Biv: Bivalvia; Poly: Polychaeta; Pog: Pogonophora; Cir: Cirripedia; Ast: Asteroidea;
Cir: Cirripedia; Oph: Ophiuroidea; Ech: Echinoidae; Dec: Decapoda; Amp: Amphipoda; Iso: Isopoda; Tan: Tanaidacea

Table 3. Listing of the megafauna during real time observation of video footage.

Cnidaria	Hydrozoa		+		+	+	+		
	Anthozoa		+	+	+	+	+	+	+
Mollusca	Gastropoda		+	+	+	+	+		+
	Cephalopoda					+	+		+
Arthropoda	Malacostraca	Decapoda	+		+	+	+	+	+
Echinodermata	Crinoidea		+						
	Asteroidea		+			+	+	+	
	Ophiuroidea		+		+	+	+		
	Echinoidea		+		+	+	+	+	+
	Holothuroidea								+
Chordata	Chondrichthyes					+			+
	Osteichthyes		+	+	+	+	+	+	+

(AT-537 and AT-538G) yielded only biological debris.

Captain Arutyunov mud volcano: Pogonophoran worms (*Siboglinum* sp.) were very abundant in all samples (AT-543G, AT-545G, AT-546GAT, AT-547Gr, AT-548K). The grab samples further retrieved several species of Crustacea, Polychaeta and a few bivalves

Ridge close to Gibraltar Strait - Chimney area: The chimneys retrieved in dredge samples (AT-550-551-D), had abundant sessile fauna. Several colonies of different cnidarian species, and small encrusting sponges (Porifera) and bivalves were removed from the surface of the chimneys. Serpulidae (Polychaeta) tubes and Bryozoan colonies were very abundant but difficult to remove. Motile animals like decapods, other small crustaceans, polychaetes and echinoderms were mainly collected in the grab sample (AT-552Gr).

Fiuzza mud volcano: Grab sample AT-566GR collected in this mud volcano contained several different sessile organisms (Porifera, Cnidaria) and motile organisms (Crustacea, Polychaeta) including pogonophoran worms (*Siboglinum* sp.) and solemyid bivalves (*Acharax* sp.).

B) Video observations

A brief description of the video observations follows. It was not possible to process all the lines onboard but all observations are summarized in Table 2.

TVAT-53

This TV-line crossed a coral ridge near Kidd mud volcano. Cnidarian colonies of

several different species were the dominant fauna (70-90% of the observations) but it was possible to identify different megafaunal assemblages associated with areas of high and low backscattering in line MAKAT-107. In the high backscattering areas, covered by coral and coral debris, the assemblage was dominated by one cnidarian species, black coral occurred occasionally and most of the build-ups were covered by unidentifiable epifauna. The low backscattering areas covered by soft sediments were characterized by the presence of pedunculated hexactinellids among other species of sponges that accounted for up to 20% of the observations. Fish, crustaceans and echinoderms were more frequent in these latter areas.

TVAT-55 (Meknes mud volcano)

The observations allowed discrimination of three different sections where changes in the geological setting were clearly accompanied by changes in the benthic assemblage. The first section was characterized by numerous patches of coral build-ups and coral rubble covered by abundant sessile fauna including large sponges and soft corals. Different species of mobile fauna (crustaceans, echinoderms and fish) were recorded and the sediment was highly bioturbated by different kinds of burrows and tracks. The second section, spanning the crater, showed a heavily disturbed greenish mud breccia with scattered clasts as well as a strikingly large number of empty shells of the gastropod *Neptunea contraria* and a very low density of living megafauna (mostly fish swimming or standing near the bottom). Finally in the third section, the benthic

assemblage showed an intermediate abundance mostly of sessile fauna covering the patches of coral rubble, carbonate crusts and clasts.

TVAT-56, 57, 58

These TV lines covered three areas of a ridge close to Gibraltar Strait showing high backscattering on line MAKAT-111. The seafloor was almost continuously covered by carbonate chimneys of different sizes and shapes. In some segments of the video it was possible to observe strong bottom currents. The chimneys were colonized by many different kinds of sponges and other epifaunal organisms that showed a higher abundance in areas with moderate bottom currents. Mobile fauna such as fish, octopuses, crustaceans and echinoderms were also very abundant. TVAT-56 was especially characterized by the frequent observations of galatheids hiding among the chimneys.

1.8. Gas biogeochemistry

Past geochemical analyses of gas from Gulf of Cadiz mud volcanoes have revealed significantly high concentrations of C₂+ hydrocarbons, and shown that differences exist between individual mud volcanoes, some of them exhibiting a much higher proportion of methane (Mazurenko et al., 2002; Blinova and Bileva, 2003). Methane stable isotope measurements might improve understanding of the origin of the gas-bearing fluids. Methane stable carbon and hydrogen isotopes have been used for the purpose of constraining the proportion of gas derived from deep-sourced hydrocarbon reservoirs versus that due to shallower bacterial activity (e.g. Whiticar et al., 1986). Stable isotope interpretation is, however, not straightforward and a comparison with a maximum number of biogeochemical parameters is thus necessary. It has been shown that the gases escaping from the Gulf of Cadiz mud volcanoes originate from deep-seated fluids (Blinova and Stadnitskaya, 2001). On the other hand, microbial processes affecting these fluids as they rise through the sedimentary column are being investigated but remain largely unknown.

In this context, this work aims to study the impact of microbial activity on the molecular and isotopic composition of the escaping gases. The approach is a combined analysis of pore water and gas composition. Pore water composition may yield information on the origin of the fluids (e.g. geothermometers) and diagenetic processes occurring in the sediment, related to the microbial activity. Pore water organic acids may be interpreted by reference to hydrocarbon/organic matter degradation pathways. Also, the characterization of the acetate and CO₂ pore water pool is interesting for the study of methane isotopic biogeochemistry, particularly in some of the mud volcano sediments containing gas hydrates, as it has been suggested that acetate fermentation to methane might predominate in these environments (Cragg et al., 1995), with hypothetical consequences on the methane isotopic signature.

The comparison of results from mud volcanoes distributed in different sectors of the Gulf of Cadiz, and an attempt to understand how they might relate to each other structurally, will be used for the investigation of the biogeochemical processes that affect the fluids in the region.

The specific objectives for the methane biogeochemistry study are:

- To measure the stable carbon and/or hydrogen isotope compositions of methane, light hydrocarbon gases and CO₂;
- To measure the pore water composition and abundance of volatile fatty acids as possible indicators of the microbial degradation of substrate (e.g. hydrocarbons);
- To estimate pore water composition for anions and cations, as well as some metal species.

1.8.1. Gas composition

1.8.1.1. Concentration in methane and higher hydrocarbons (ethane, propane, butane, pentane, hexane)

Stripping of the pore water gas

Sediment pore water methane stripping is realized according to the method of McAullife (1971). A sediment plug is collected with a tip-sliced syringe and injected in a 30 ml glass vial filled with 10 ml of 10 % potassium chloride solution. It is shaken in order to dissociate the sediment plug and stop all bacterial activity. The sample is stored upside down to avoid exchanges with room air, and allowed to equilibrate with the vial headspace for 48 hours. The gas is then extracted in a syringe by injecting an equivalent amount of 10% KCl solution. A blank sample (air equilibrated with 10% KCl solution) is also taken for background corrections. Three replicates are taken from each sampled horizon.

Sample preservation

The gas is immediately injected in a serum vial filled (bubble-free) with a pH1 10% KCl solution by displacement of an equivalent amount of solution. The vials are stored upside down in order to avoid exchanges with air through the septum.

Sample analysis

The gas is extracted in a gas-tight syringe by displacement. Its composition is analyzed in the laboratory (University of Aveiro, Portugal) by flame ionization gas chromatography on a Varian 3400 equipped with a capillary Plot Q column. Laboratory standards for calibration consist of a range of BOC alpha-gravimetric mixtures (multi-point calibration).

1.8.1.2. Methane stable carbon ($d^{13}C$) and stable hydrogen (dD) isotopic composition

The sampling and sample preservation for methane stable isotope composition is as described above. Three replicates are sampled at each depth. The gas samples are then

analyzed in the University of Bristol by continuous flow gas chromatography combustion isotope ratio mass spectrometry (GC-IRMS) on a Thermofinnigan Delta XP mass spectrometer. Micro-litre quantities of gas samples are injected onto a Plot Q column for separation of CH_4 and CO_2 .

$d^{13}C$: Methane is combusted to CO_2 at $1050^\circ C$ in a reactor containing copper and platinum-platinum wires. The carrier gas is helium (2 ml/min) into which a trickle flow of 1% oxygen in helium (0.1 ml/min) is added just before the combustion reactor. The stable carbon-isotope values are reported relative to VPDB.

dD : Stable hydrogen isotope measurements on methane will be conducted on the same instrument for high concentration samples. Separation of gaseous components is achieved using the same PLOT Q column. However, the $1050^\circ C$ combustion reactor is replaced by an empty reactor in which H_2 is formed by pyrolysis of CH_4 at $1400^\circ C$ (Tobias and Brenna, 1997). For low concentration samples, gases are processed in an off-line vacuum extraction line (Hornibrook et al., 1997). Water and CO_2 are separated from samples by freezing in liquid nitrogen. Methane is combusted to CO_2 and H_2O at $900^\circ C$ in a quartz furnace packed with CuO wire and Pt foil. CO_2 is separated from H_2O by cryogenic distillation using an ethanol/LN slush at $-110^\circ C$. The quantity of CO_2 from CH_4 combustion is measured manometrically to determine combustion yield, after which it is transferred to a break-seal for analysis by dual inlet mass spectrometry. The H_2O formed from methane combustion is trapped on zinc shavings ('Indiana Zn') and sealed in a glass break-seal. It is then reacted for 25 minutes at $450^\circ C$ to form H_2 which is then analyzed by dual inlet mass spectrometry.

Standards: Stable hydrogen-isotope data are reported relative to VSMOW. An in-house laboratory CH_4 standard with known $d^{13}C$ and dD values is analyzed along with samples for both online (GC-C-IRMS) and offline methods. Using the same extraction line, microlitre quantities of the IAEA water

standards VSMOW and SLAP are injected and frozen into breakseals containing Indiana Zn. The standards are also reacted at 450°C to form H₂ gas which is used to normalise the D/H ratio data measured for the CH₄-derived water analyses.

1.8.1.3. Carbon dioxide concentration and stable carbon (d13C) isotopic composition

Sampling

A sediment plug is sampled from the core and placed in a 40 ml glass vial. Samples are taken every 20 cm. The plug is sealed and frozen for preservation. Dissolved inorganic carbon will be analysed by an offline procedure because sediment samples cannot be acidified as this might produce CO₂ from carbonate minerals. CO₂ is extracted by vacuum from the sealed samples, and collected by freezing at liquid nitrogen temperatures. Water is removed by cryogenic distillation. The amount of CO₂ collected is measured manometrically before it is stored in a glass break-seal for subsequent analysis by conventional dual inlet mass spectrometry.

1.8.2. Pore water volatile fatty acids (VFA), anions and cations

Sampling and preservation

A sediment plug is collected with syringe and injected in a sterile centrifuge vial. The sample is frozen for preservation until analysis in the laboratory (University of Bristol).

Analysis:

The sample is thawed and centrifuged at 4°C (4500 rotations/min) for pore water extraction. The VFA's (acetate, propionate and butyrate), anions (Cl, SO₄) and cations (Na, Ca, K) are analyzed by High Performance Liquid Chromatography (HPLC, Dionex, USA).

Sediment samples for metal analysis will be thawed and centrifuged for pore water collection under an N₂-atmosphere, and analyzed at the Analytical Chemistry Department of the University of Aveiro (Portugal).

Table 4. Sampling sites for sediment biogeochemical study (University of Bristol and University of Aveiro).

Site	Core ID	Depth (cmbsf)	CH ₄ Conc. & isotopes	CO ₂ conc. & isotope	Pore water (VFA)	(metals, anions, cations)
Coast of Algarve	AT513G	10-180	X	X	X	X
Coast of Algarve	AT518G	10-140	X	X	X	X
Carlos Ribeiro MV	AT520G	10-200	X	X	X	X
Ginsburg MV	AT521G	10-200	X	X	X	X
Ginsburg MV	AT522G	10-200	X	X	X	X
Yuma MV	AT523G	10-60	X	X	X	X
New Structure	AT525G	10-300	X	X	X	X
New Structure	AT526G	10-320	X	X	X	X
Kidd MV	AT529G	10-70				X
New Structure	AT532G	10-100				X
New Structure	AT536G	10-200	X		X	X
New Structure	AT540G	10-130	X		X	X
New Structure	AT542G	10-110	X			X
Captain Arutyunov	AT543G	10-150	X		X	X
Captain Arutyunov	AT545G	10-300	X		X	X

(1) Pore water (anions, cations) & methane sampling interval: 10 cm;

(2) VFA, CO₂ sampling interval: 20 cm.

1.8.3. Sampling sites

All samples were collected from gravity cores (max. 6 m) every 10 cm along the core. Samples have generally been collected from cores recovered in known mud volcanoes and in structures discovered during this cruise (Table 4), with the exception of two cores that have been sampled out of a set of eight in a W-E transect, off the coast of Algarve. These cores were collected for the purpose of microbiology studies. Hydrocarbon oxidation is likely to be an important process in this area, located to the north of the carbonate chimney field. The results might be used as a reference for oxidation isotopic effect on sedimentary hydrocarbons (methane, ethane) in the region.

Cores have been recovered from known active or fairly active mud volcanoes all across the Gulf. They include Carlos Ribeiro (AT520G), Ginsburg (AT521G and AT522G), Yuma (AT 523G) and Captain Arutyunov (AT543G and AT545G) mud volcanoes.

Cores have been sampled from the less active Kidd mud volcano (AT529G) and the new structures (AT532G, AT536G and AT540G) as indicated by the presence of coral fragments throughout the cores and the light brown colour.

Two cores (AT525G and AT526G) have been sampled from a new structure, which seems to be fairly active (degassing dark grey sediments).

II. SOUTHEASTERN IBERIAN MARGINS: THE ALBORAN BASIN AND THE PALOMARES AND CARTAGENA MARGINS (LEG 2)

II.1. The mud diapiric province of the West Alboran Basin

II.1.1. Introduction

M. COMAS AND M. IVANOV

Previous surveys during TTR-9 and TTR-12 in the West Alboran Basin (WAB)

demonstrate the occurrence of mud volcanoes on the Iberian and Moroccan margins behind the Gibraltar Arc (Comas et al., 2000; Talukder et al., 2000, Sautkin et al., 2003). Mud volcanoes build up in the Diapiric Province of the WAB, and are always connected to underlying mud diapir structures. The Diapiric Province is formed of over pressured shale and olistostromes from the lowermost marine sedimentary sequences (early to middle Miocene in age) laid down in the basin. The Diapiric Province built up in a sedimentary depocentre that is up to 8 km thick, and overlies the metamorphic basement (Comas et al., 1999, and references therein). Regional tectonism was the main triggering mechanism for mud diapirs and volcanoes, and distinct stages of active diapirism and volcanism are punctuated by events of mud-flux activity and over pressured material rising, stepping forward from the middle Miocene to Present. Older mud diapirs match to processes of widespread crustal extension during middle and late Miocene (between 18 and 9 Ma), being linked to extensional faults and concurrent tectonic subsidence in the basin. Major diapiric structures are consistent with the W to SW-directed extension disturbing the basin during those times. The younger stages of diapirism (Pliocene to Holocene) proceed with pierced diapirs and mud volcanoes. Actual or sub-actual mud volcanoes result from the latest episode of diapirism, mainly along faults, leading to the extrusion of olistrotrome material, mud-breccias and fluids from the older and deeper sediments. Pliocene to Recent mud diapirs and related mud volcanoes build up while the WAB is undergoing submeridional contraction and roughly E-W transtension. Mud-volcano features in the Alboran Sea back-arc basin are comparable to mud-volcanoes from the Gulf of Cadiz accretionary prism (Pinheiro et al., this volume) and the Mediterranean Ridge, but occur in quite different tectonic settings.

In order to improve on TTR-9 and TTR-12 investigations on mud diapir structures and mud volcanoes, two areas for survey were selected on the basis of previous data (Fig. 27). Single channel seismic and concur-

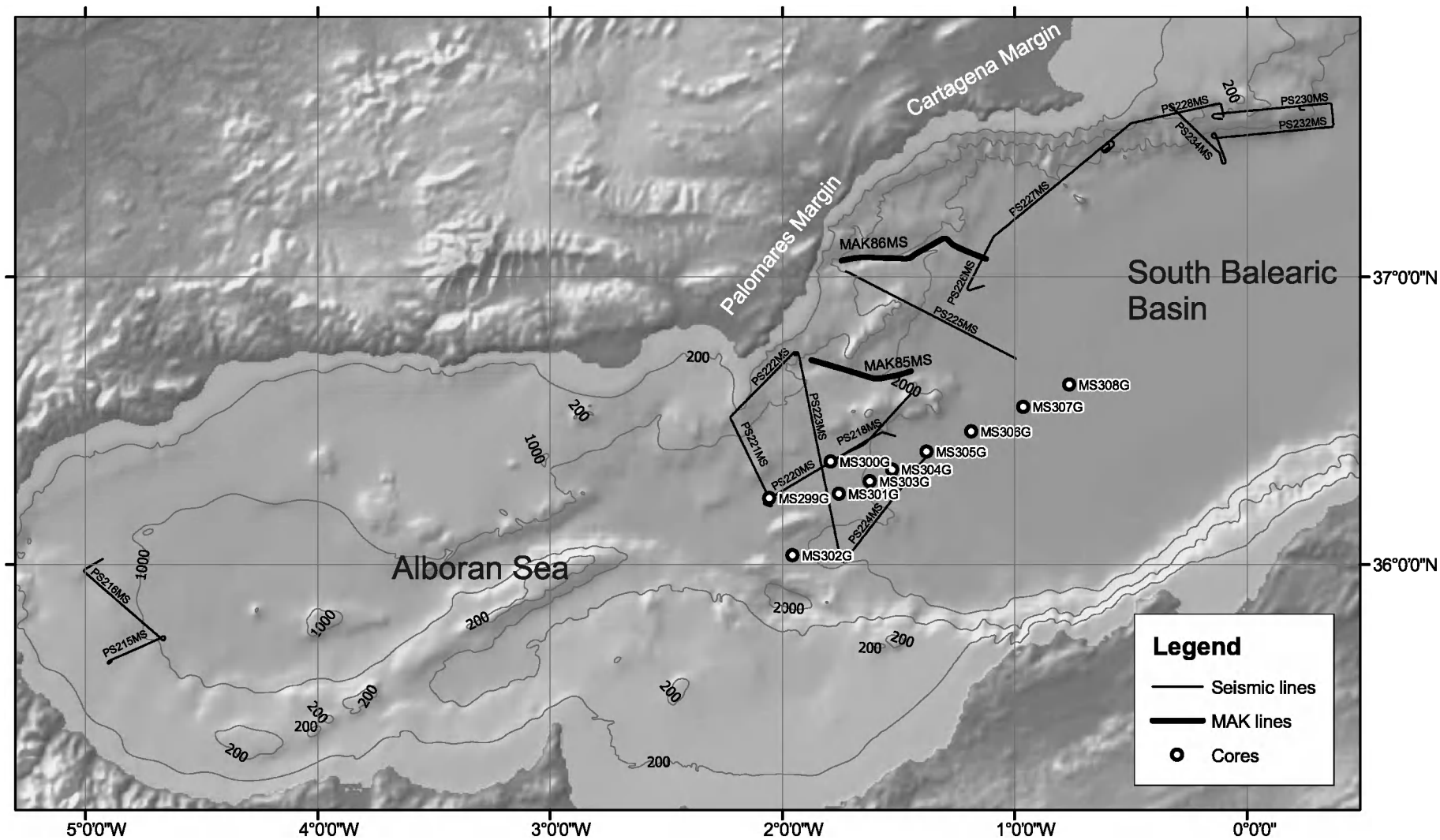


Figure 27. Location map of TTR-14 Leg 2 surveys in the Alboran Sea.

rent OKEAN profiles were obtained across previously known seafloor structures suspected to be mud volcanoes. The survey carried out in the WAB has revealed the presence of one new mud volcano which was named Carmen, which is located between the Northern and Southern Mud Volcano Provinces, and the occurrence of a giant pockmark SW of the Kalinin mud volcano. The two seismic lines will also be useful for seismic stratigraphy correlation between the northern and central WAB.

II.1.2. Seismic interpretation and sidescan sonographs from the West Alboran Basin

F. FERNÁNDEZ-IBÁÑEZ, G. MARRO, M. SÁNCHEZ-GÓMEZ, M. ROMAN-ALPISTE, M. GARCÍA, N. MHAMMDI, H. VANNESTE AND M. COMAS

The four seismic units recognized in the Plio-Quaternary sequence of the Alboran Basin have been differentiated in the seismic profiles:

a) Seismic Unit Q1 is limited by the seafloor reflector and its base is the the erosional q1 horizon that dips gently southwards. The unit can be divided into two subunits: Q1a and Q1b. The Q1a subunit is the most recent one, and presents a bedded seismic facies, with medium to high acoustic amplitudes and low lateral continuity. Thickness varies between 115 and 200 ms TWTT. Locally, below the Q1a subunit, the Q1b subunit can be differentiated. This subunit has a transparent seismic facies and is wedge-shaped. The maximum thickness of the subunit is 110 ms TWTT.

b) The base of Seismic Unit Q2 is the q2 horizon, which is seen as a very strong acoustic amplitude reflector. The Q2 unit has a bedded seismic facies with high acoustic amplitude and high lateral continuity. The thickness of the unit varies between 150 and 280 ms TWTT.

c) The base of Seismic Unit P1 is the p1 horizon, marked by an important change in the acoustic amplitude. The unit has a bedded seismic facies, with high acoustic amplitude and lateral continuity. The unit thickness varies laterally in relation to the growth

of diapirs, from a maximum value of 180 ms TWTT, to almost disappearing at some diapiric highs.

d) The base of Seismic Unit P2 is the M reflector. This seismic unit is a transparent seismic facies. The observed thickness of this unit is over 510 ms TWTT.

One line (PS-215MS) was run using the OKEAN deep towed sidescan sonar. The images are of poor quality, but a new mud volcano in the region can be distinguished. The mud volcano has been named "Carmen".

Seismic Line: PS-215MS

This is a 5.30 nm long line that runs ENE-WSW across the centre of Carmen mud volcano (Fig. 28). This mud volcano is located in the distal part of the Ceuta contourite

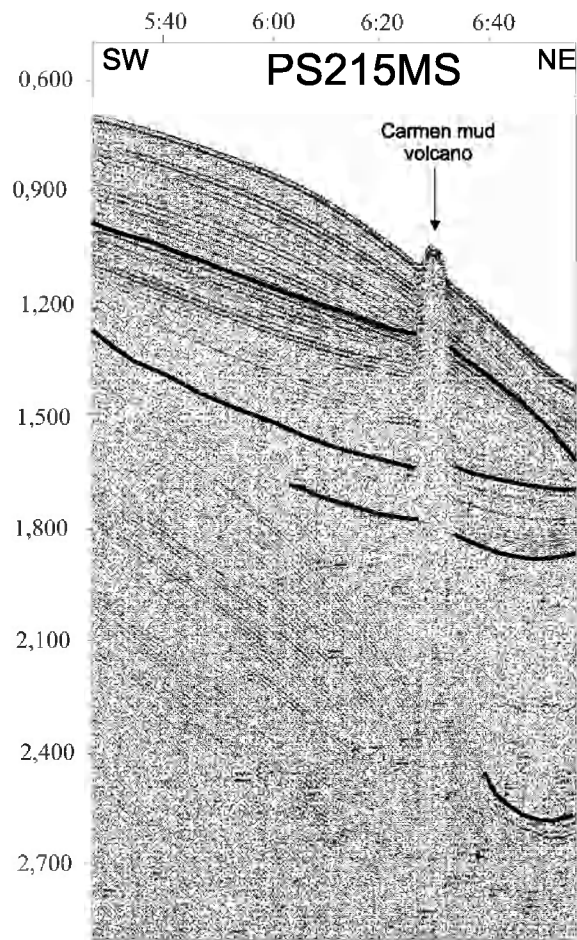


Figure 28. Seismic line PS-215MS across the Carmen Mud Volcano. Line located on Fig. 27.

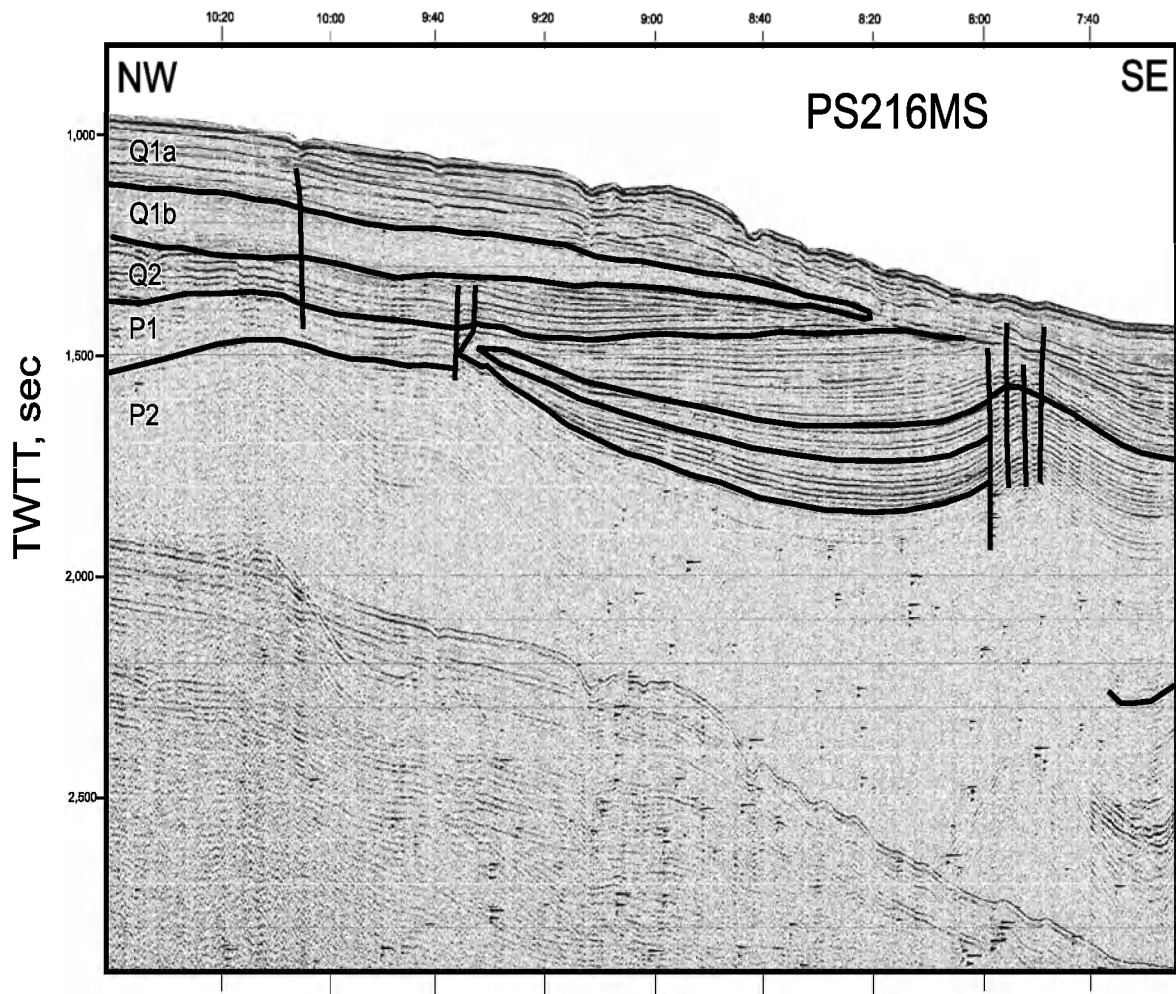


Figure 29. Seismic line PS-216MS showing the main seismic units distinguished in the west Alboran basin. The Ceuta drift sediments and diapiric structures are seen. Line located on Fig. 27.

drift and outcrops as a positive structure of 800 m diameter and about 40 m height. The mud volcano cuts through the whole sedimentary thickness shown in the seismic profile i.e. 2 s TWTT.

The units with bedded facies, above the p1 horizon, are deformed towards the walls of the surrounding moat, while the deepest units, with a semi-transparent seismic facies, seem to remain undeformed.

All the units have parallel bedded seismic facies with medium to high acoustic amplitude and lateral continuity.

Note that towards the ENE of the mud volcano there is a steep downwards crosscutting reflector that may be a BSR, but further research is needed to confirm this assessment.

Seismic Line: PS-216MS (Fig. 29)

The PS-216MS profile is a 21.18 nm long line oriented SE-NW showing the top of mud diapirs and concurrent folds. The line is located in the distal Ceuta drift.

The main features observed in this profile are diapirs that deform most of the sedimentary sequence. In the SE sector two diapirs cross-cut the M reflector and deform the P2, P1 and Q2 seismic units. Towards the NW, two diapirs gently deform the p1 reflector, and the overlying sediments remain undeformed. There is a local depocenter in the central area, related to the progressive growth of the two sets of diapirs which bound it, as inferred from the onlapping of reflectors in the northwestern diapirs. Sub-vertical faults appear at the top of the diapirs,

grouped in penetrative sets. They reach the lower Quaternary (Q2) unit in the NW sector and the Upper Quaternary unit and even the seafloor in the SE sector.

The Q1 seismic unit can be divided into two subunits: the uppermost Q1a subunit has a bedded seismic facies, with medium to high acoustic amplitudes and low lateral continuity. The lower, wedge-shaped Q1b subunit has transparent seismic facies.

The Q1a and Q2 units have channel incisions with lateral migration. A wave field can be identified in the Q1a seismic subunit.

Seismic Line: PS-217MS

This 1 nm long seismic line is the continuation, with a NNE-SSW trend, of the PS-216MS line. Seismic unit subdivisions are similar to those previously described.

Bottom reflector and Quaternary units are affected by a huge pockmark that results in a negative relief. From the start of the seismic line to the border of the pockmark there is a sediment wave field. The striking characteristic of the subunit Q1b is the presence of an approximately 0.130 ms fracturation due to gas. The subunit Q1a decreases in thickness in comparison with the same unit described in PS-216MS.

II.2. Eastern Alboran margin: the transition between the Alboran and the Balearic-Algerian Basins

II.2.1. Introduction

M. COMAS AND M. IVANOV

The transition between the East Alboran Basin and the Balearic-Algerian Basin is gradual. The surface morphology shows a gradual deepening and significant basin widening towards the 1600 m deep basin plain in the east.

The nature and ages of the Pliocene to Pleistocene sedimentary record in the transition zone is well constrained by results from ODP Sites 977 and 978 (Leg 161 drill-sites, Comas, Zhan, Klaus et al., 1996). The "M reflector", that marks the basal limit of the

Plio-Quaternary sequence, is ubiquitous in the Mediterranean and corresponds to a strong erosional and locally angular unconformity overlying diverse older sedimentary sequences.

At a crustal level this transition corresponds to a very thin continental crust (less than 13 km) and concurrent lithosphere thinning (Torné et al., 2000), giving way eastwards to the oceanic crust of the Balearic-Algerian basin. The oceanic crust is thought to develop beneath the Messinian salt diapirs, which are well developed in the basin. Furthermore, the region has been the site of high magma production (during the late Miocene), which results in numerous volcanic residual highs that accommodate the Plio-Quaternary sequence. Deep structural features of this transition are imaged in the ESCI-Alb deep multichannel seismic sections. Nevertheless, few high-resolution data were available until now to understand the basin architecture at shallower levels in this transition.

TTR-14 Leg 2 objectives aimed to investigate the shallow structure and the sedimentary architecture of this peculiar region (Fig. 27) using high resolution seismic reflection profiles

Seismostratigraphy of the Plio-Quaternary depositional sequences in the Alboran-Balearic transition is based on correlations with ODP Leg 161 drilling results (Comas, Zhan, Klaus et al, 1996). ODP Site 977 was crossed by two seismic profiles, and the seismic grid also allowed for correlations with Site 978.

Four seismic units are recognised within the Plio-Quaternary sediments bounded by discontinuities:

The Quaternary sequence is subdivided into two seismostratigraphic units:

Unit Q 1: a late Quaternary unit, bounded at its base by the q1 discontinuity.

Unit Q 2: an early Quaternary unit. The lower limit of Unit Q 2 (top of Pliocene unit/s or lower limit of the Quaternary unit/s) correspond to the q2 discontinuity

Both units are included in the general Quaternary Unit 1a distinguished in the Alboran Basin at ODP leg 161 Sites

The Pliocene sequence is subdivided into two regional seismic units, bounded by an angular unconformity. The boundary between these two units is usually marked by the occurrence of the significant hiatus in the middle Pliocene (i.e. at ODP Site 976, and 977, Comas et al., 1999). These two units have been called from bottom to top:

Units P1: Roughly late Pliocene in age, that corresponds to Unit Ib in ODP Sites. The lower limit of Unit P1 is the p1 discontinuity (intra Pliocene boundary)

Unit P2: Roughly early Pliocene in age, that corresponds to Unit Ic in ODP Sites.

The regional M unconformity, usually at the base of Unit P2, and well known around the whole Mediterranean, corresponds to the lower boundary of the Plio-Quaternary sequence, associated with a strong and prominent high-amplitude reflector. The M discontinuity is usually an erosional truncation of the underlying sequences (Miocene in age), or marks the top of the acoustic (even volcanic) basement in the basin margins.

Seismic interpretation indicates a region dominated by post-Messinian contraction and recent or active strike-slip tectonics, which strongly conditioned the sea floor morphology.

Mapping the seismic units and performing subsidence analysis (1D and 2D, through correlation between single channel profiles, offshore commercial wells and ODP sites 877 and 978 logging data) will be carried out over the Plio-Quaternary sedimentary sequence found in the TTR-14 profiles in order to determine tectonic versus thermal subsidence, and subsidence/elevation rates through time.

II.2.2. The transition between the Alboran and the Balearic-Algerian Basins: seismic interpretation

M.SÁNCHEZ-GÓMEZ, F. FERNÁNDEZ-IBÁÑEZ,
G. MARRO, M. GARCÍA, M. ROMAN-ALPISTE,
H. MHAMMDI, H. VANNESTE AND M. COMAS

The transition between the Alboran and South Balearic-Algerian Basins (Fig. 27) is marked by several volcanic highs (from

north to south: Maimonides, Al-Mansour and Yusuf) that individualize the isolated basins. The basin enclosing the Al-Mansour Seamount was drilled by the ODP Sites 977 and 978, that enable correlation of seismic and stratigraphic units. The deep Balearic-Algerian basin and the Al-Mansour Basin are bounded by steep strike-slip faults with local extensional and compressive slip components that can be seen in the seismic profiles. The Al-Mansour Basin, at the western rise of the Balearic-Algerian Basin, shows a thick sedimentary sequence with little disturbance. The deeper basin has Messinian salt diapirs that fold the lower sedimentary units. These diapirs may indicate the presence of underlying oceanic crust.

Seismic Line: PS-219MS

Line PS-219MS is about 11 nm long and trends SW-NE. It cuts across the Maimonides volcanic high which is limited to the southwest by a high angle normal fault.

Plio-Quaternary sediments are about 0.2 ms in thickness and run from the Maimonides high to the end of the line.

Seismic Line: PS-220MS

Line PS-220MS runs for 26 nm in an ENE-WSW direction, from the south slope of the Maimonides high to ODP Site 978. Seismic units Q1, Q2, and P1 are differentiated, overlying the M reflector. The M reflector appears as a high-reflectivity limit between 2.9 and 3.3 s TWTT. The reflectors are nearly horizontal and locally they are affected by faults that reach the Q1 limit. Most of the faults appear as subvertical structures. Small channel-like features are found towards the NE end of the line, and the Quaternary units fill the erosional structures.

Seismic Line: PS-221MS

Line PS-221MS is a 20 nm long seismic profile running SSE-NNW, from the 978 ODP Site to the Cabo de Gata apron. Two major domains are differentiated, separated by a major fault. The southern domain has a

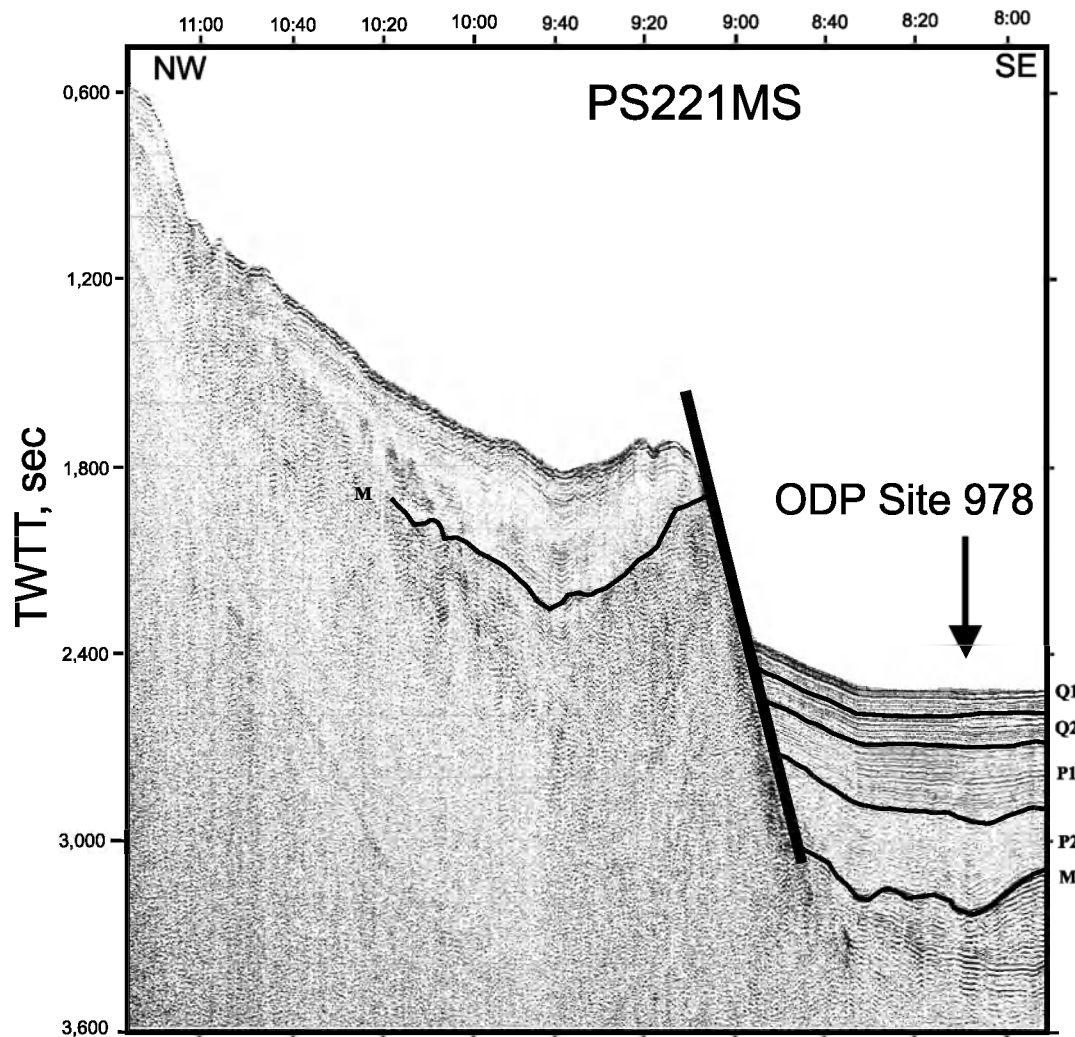


Figure 30. Seismic line PS-221MS showing position of ODP Site 978. Located on Fig. 27.

thick sedimentary sequence and the northern domain has a shallow acoustic basement covered by gently folded sediment. The southern domain shows bedded seismic units that are disturbed near the main fault and progressively folded at depth. The northern domain is affected by a few sets of high angle faults, with apparent normal and reverse throw (Fig. 30) and result in a wide fault zone. Faults penetrate down through the acoustic basement. Within the fault zone the pre-q1 seismic units are chaotic, with some vestiges of bedding.

Seismic Line: PS-222MS

This line runs for 17 nm in a SW-NE direction, crossing the Cabo de Gata apron and the head of the Gata Canyon. Only the

Q1 seismic unit can be differentiated. It overlies layers with disturbed bedding. The profile crosses the wide Carboneras Fault Zone, which bounds the NE end of the Cabo de Gata apron and affects the seafloor. At depth, this fault zone appears as a penetrative set of vertical faults with normal and reverse movement. Gently folded layers develop in the fault zone and to the east. The outstanding morphological feature is the 2 km wide Gata Canyon with more than 450 ms TWTT depth (Fig. 31). Slumps are seen on both the fault scarps and the canyon walls.

Seismic Line: PS-223MS

Line PS-223MS begins at the Gata Canyon and ends 45 nm to the SSE. The line crosses ODP single channel seismic line S3

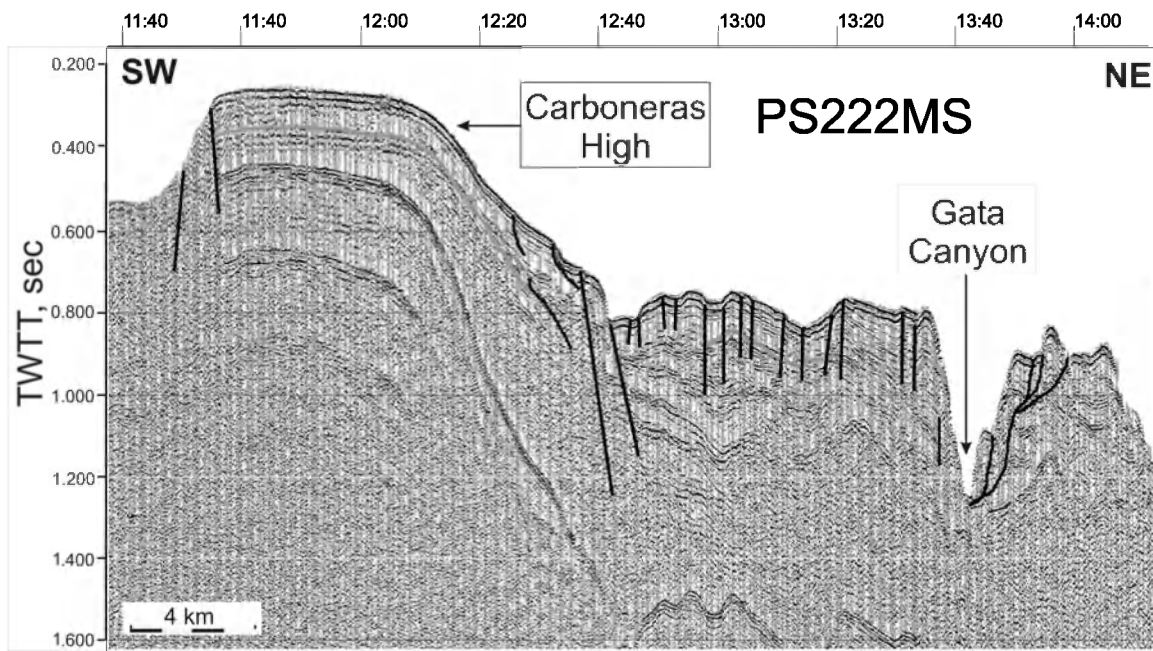


Figure 31. Seismic line PS-222MS. Located on Fig. 27.

where Site 977 is located. The line crosses a thick sedimentary pile within which the Q1 unit is well-differentiated, lying over a bedded and a transparent seismic facies. The entire section is a wide deformed zone where compressive and extensional structures coexist. The Gata Canyon is developed over a

high angle fault set that merges at depth (Fig. 32). The northern wall of the canyon shows numerous slumps, while the southern wall is steeper and terraced, presenting a more erosive character. Normal and reverse faults, and related folds, characterize the general pattern. Most of these faults affect the

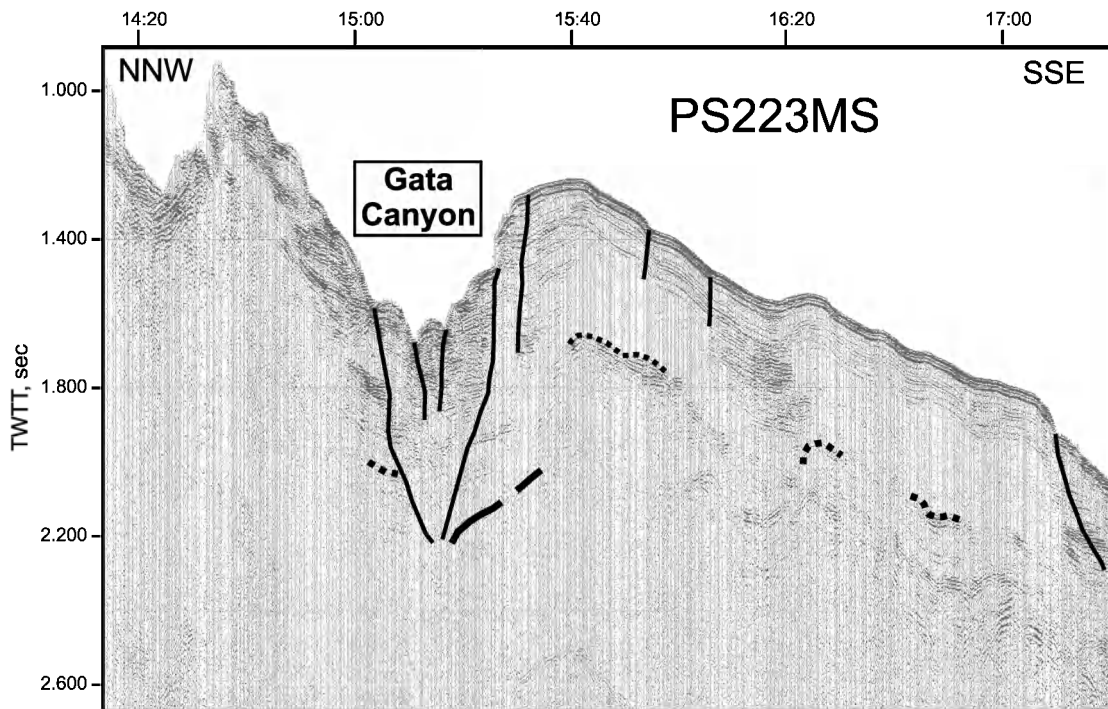


Figure 32. Seismic line PS-223MS showing the head of the Gata Canyon. Located on Fig. 27.

Quaternary sediments, causing steep slopes where several slumps and slump scars are seen. The slope dips gently to the south and a few sets of subvertical faults affect the entire sedimentary sequence and are marked by sudden lateral seismic facies changes that may be related to a strike slip component. Graben-like structures are developed in the lower seismic units.

Seismic Line: PS-224MS

Line PS-224 MS is 25.5 nm long and trends from SW to NE. The line has a 400 ms to 800 ms thick continuous sedimentary sequence, that drapes a basement horst in its central part. Above this basement high and towards the SW, bedded sediments are almost horizontal, disturbed by a few normal faults. Northeast of the horst there are high angle faults affecting the youngest sediments and occasionally reaching down to the acoustic basement. Messinian salt diapirs deform reflectors in the deep basin sediment, causing open folds below the q1 discontinuity limit.

II.3 Bottom sampling

F. MARTINEZ-RUIZ, E. KOZLOVA, E. SARANTSEV, A. OVSYANNIKOV, F. J. JIMENEZ-ESPEJO, E. BILEVA, D. KOROST, V. BLINOVA, O. ROMERO, D. GALLEGO-TORRES, E. LOGVINA, A. SHUVALOV, I. GURJEV AND P. GOLINCHIK.

A paleoceanographic core transect from the East Alboran Sea to the South Balearic basin (Fig. 33) was designed to obtain gravity cores for the reconstruction of climate variability and paleoceanographic conditions in the western Mediterranean since the Last Glacial Maximum (LGM).

The Alboran Sea basin, the westernmost in the Mediterranean, has a complex sea floor morphology with different sub-basins, ridges and seamounts (Comas et al., 1999). This narrow basin is positioned between two large converging plates and has a very high sedimentation regime. Such high sedimentary input generated one of the best archives in the Mediterranean, in which high resolution

regional and global climate changes are recorded. Other than its exceptional geological setting, its oceanographic setting is also a key to understanding water mass exchange with the Atlantic Ocean and for determining Mediterranean-wide circulation patterns. Additionally, the semi-enclosed character of the Mediterranean has provided a very sensitive record of climate variability.

Paleoclimate evolution since the Last Glacial Maximum

Classical climate periods since the LGM include the last Heinrich event (H1), the Older Dryas, the Bølling-Allerød transition, the Younger Dryas and the Holocene. The deposition of the last sapropel (S1) in the Mediterranean (~ 9000-6000 yr BP) was also climate controlled and derived from enhanced humidity and increased precipitation. The different Mediterranean basins exhibit distinct responses to climate change through time. Thus, while the last deglaciation warming recorded after the the H1 occurred as an extremely rapid pulse in the Gulf of Cadiz and the Tyrrhenian, in the Alboran Sea it followed a stepwise pattern (Cacho et al., 2001). In general the whole Bølling-Allerød pattern varies from place to place which suggests a significant heterogeneity in the climate response. Export production rates also varied regionally in response to basin-wide climate changes (Martinez-Ruiz et al., 2003).

Studied areas and site locations

TTR-9 and 12 cruises in the Alboran Sea and the South Balearic basins provided a paleoceanographic transit from the West Alboran basin (WAB) to the East Alboran basin (EAB), and some records of the South Balearic basin (Kenyon et al., 2000; Kenyon et al., 2003). Studies of these cores and ODP cores from Leg 161 have shown significant differences in the climate response of both basins to forcing mechanisms of climate change (Martinez-Ruiz et al., 2003). Furthermore, the comparison of records of the S1 time interval shows important differ-

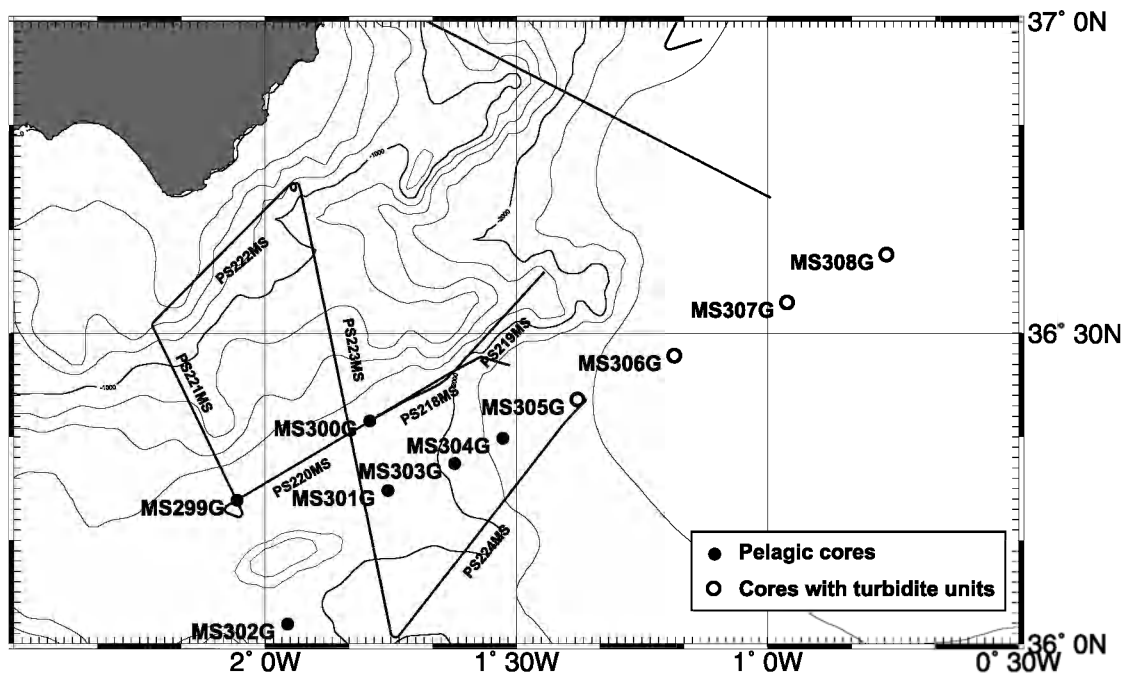


Figure 33. A paleoceanographic core transect from the East Alboran Sea to the South Balearic basin.

ences from East to West through the whole Mediterranean. The transition from the Alboran Sea to the South Balearic basin is a key location to identify regional factors vs. global influence, the causes for different climate responses and to understand the highly sensitive Mediterranean climate record. TTR-14 sites (Fig. 33) were designed to obtain a sedimentary record along a transect in the easternmost Alboran-South Balearic basin in order to understand the East-West evolution of the climate responses in the Mediterranean. Sites were selected to ensure records with high sedimentation rates and without sedimentary discontinuities. Gravity cores recovered a sediment interval spanning approximately the last 16 to 18 Kyr providing a high-resolution record of the main climate events since the LGM at a centennial to decadal scale. In the South Balearic basin turbidite sedimentation interrupted the pelagic record, but the uppermost sediment also provides evidence of paleoceanographic conditions. The most recent pelagic sediments deposited in the Alboran Sea (gravity cores 4 to 5 m long) correspond to calcareous rich clays with greenish grey colours. The main mineral components of the sediments are

clays, calcite and quartz, with traces of feldspar (also pyrite in the Alboran sea basin) and accessory minerals such as zircon, apatite, biotite, etc. Clay and quartz percentages are high for the Alboran Sea basin as expected from the high terrigenous input.

High resolution analyses of the sediment cores aim to reconstruct paleoproductivity, sea surface temperatures (SSTs), salinity and evolution of seasonality, paleocirculation and oxygen conditions, eolian input and atmospheric response, and to study biogeochemical cycles (carbon and nutrients cycles), ocean-continent interactions, the impact of climate change on human and cultural evolution in the Iberian Peninsula, rapid climate changes and the influence of Messinian salt on sediment diagenesis and preservation of paleoproxies.

Core transect

A total of 10 cores (Table 5, Annexe I) were recovered in the transect, which together with previous TTR sites within the Alboran Sea basin completed a whole transect from the WAB to the South Balearic basin.

Table 5. Details of the sites sampled during Leg 2 in the Alboran Basin.

Station	Date	Time (GMT)	Latitude	Longitude	Depth (m)	Recovery (cm)
TTR14-MS-299G	13.08	00:15	36°13.897'N	2°03.350'W	1938	469
TTR14-MS-300G	13.08	04:12	36°21.532'N	1°47.501'W	1860	458
TTR14-MS-301G	13.08	06:58	36°14.813'N	1°45.342'W	1965	487
TTR14-MS-302G	13.08	10:44	36°01.906'N	1°57.317'W	1989	420
TTR14-MS-303G	13.08	17:06	36°17.429'N	1°37.380'W	2094	461
TTR14-MS-304G	13.08	19:19	36°19.873'N	1°31.631'W	2382	454
TTR14-MS-305G	16.08	03:14	36°23.603'N	1°22.710'W	2512	564
TTR14-MS-306G	16.08	06:15	36°27.846'N	1°11.166'W	2574	489
TTR14-MS-307G	16.08	09:24	36°32.977'N	0°57.692'W	2676	169
TTR14-MS-308G	16.08	12:30	36°37.586'N	0°45.835'W	2675	96

Core MS-299G

This station is at the same location as ODP Leg 161 978A (where the upper sediments were washed out and the most recent pelagic sediments were not recovered, although site information was already available). It is located in the EAB to the south of Cabo de Gata in a small east-west trending basin north of the Al-Mansour Seamount. The corer retrieved about 469 cm of sediments, predominantly brownish grey clay, with greenish grey clay in the lower 259 cm, and a small amount of silty admixture and foraminifera. Throughout the succession some patches filled with rich water clay are observed. Between 210-469 cm dark spots and stripes (organic matter?) were found. The upper 13 cm is brown structureless water-saturated marl with a small amount of silty admixture and foraminifera.

Core MS-300G

A 458 cm long core of hemipelagic sediments was recovered to the north-east of Core MS-299G, at a slightly shallower site. The lowermost unit is brown water-saturated structureless marl with a small amount of silty admixture and foraminifera. Most of the core consists of grey clay, brownish in the upper 7 cm, with foraminifera and a small amount of silty admixture. Sediments become more greenish towards the bottom.

Core MS-301G

The core was 487 cm long. The upper

part is brown water-saturated marl with foraminifera and small amount of silty admixture. The lower boundary is irregular. The unit between 3 and 487 cm is grey clay, brownish in the upper 60 cm, with foraminifera, a small amount of silty admixture and dark (organic?) spots and stripes throughout the succession.

Core MS-302G

420 cm of hemipelagic mud was collected at the same site as 977A of ODP Leg 161. This site is located south of the Al-Mansour Seamount in a 36 km wide graben that is limited by the Yusuf Ridge to the south and the Maimonides Ridge to the north. There is brownish marl with foraminifera in the upper 14 cm, grey clay between 14 and 164 and greenish grey clay with small amount of silty admixture, foraminifera, dark (organic?) spots and rare shell fragments in the lower part of the core.

Core MS-303G

Core 303 is located east of Core 301 at a deeper site. The 461 cm long core is similar to the previous cores: upper brown marl (0-6 cm), medium grey clay (6-292 cm) and lower dark grey clay (292-461 cm).

Core MS-304G

454 cm of hemipelagic sediment consisted of greyish clay, brownish in the upper part, with some silty admixture, and a number of foraminifera, dark (organic?) spots and

stripes throughout the succession. Oxidized layers are recognized between 30 and 40 cm. The lower part has several greenish, clayey layers. Rare shell fragments occur throughout.

Core MS-305G

564 cm of sediments consist of brownish grey marl and clay in the upper 48 cm and grey clay below. Below 68 cm the grey clay contains a number of silty and sandy beds up to 6 cm thick. In most cases they have sharp upper and lower contacts and some of them are clearly graded while others appear to be more uniform. These beds are interpreted as turbidites.

Core MS-306G

489 cm of sediments consist of a light greyish brown water-saturated marl unit overlying a grey clay interval. As in the previous core the grey clay contained a number of silty and sandy turbidites, but they are usually much thinner, being mostly under 2 cm. Some of them are topped by a dark grey silty clay representing the mud cap of a turbidite.

Core MS-307G

This shorter core (169 cm) contained four turbidite units up to 30 cm thick separated by hemipelagic marl and clay. Sands are graded and in some places there is evidence of planar or even cross lamination. The turbidites have distinct mud caps represented by dark grey silty clay.

Core MS-308G

This is similar to the previous core but shorter, being only 96 cm long. Three turbidite units are recognised and they correlate well with those found in the Core MS-307G. The turbidites also have sandy bases and distinct mud caps but the thickness of sandy beds increases, which possibly explains the short recovery.

II.4. The Palomares and Cartagena margins

Introduction

M. COMAS AND M. IVANOV

The Palomares and Cartagena margins in the northeast Alboran Basin, were studied during TTR-9 Leg 3 using OKEAN sidescan sonar records together with high resolution seismic reflection profiles (Comas et al., 1999). These margins have so far not been discussed in detail, and investigations during TTR-14 Leg 2 (Fig. 27) aims to better understand the interaction of surface processes and tectonic behavior, as well as the cause of the marked morphologic contrast between them.

The NNE-SSW trending Palomares margin has an extremely narrow fault-controlled shelf and a large talus with quite heterogeneous relief. There are two deeply incised, submarine-canyons (the Aguas-Almanzora Canyon and Gata Canyon) that presently connect to onshore seasonal flood channels. Canyon pathways give way downslope to meandering channels. Both canyons and downslope channels are thought to be controlled mainly by a wrench-fault zone (related to the Palomares Fault Zone) and the topography of residual highs made up of volcanic or metamorphic basement rocks (either outcropping or sub-outcropping). Down slope the two canyons give way to turbidite systems that extend to the basin plain. Sedimentary processes, including significant mass wasting processes, slumps and slides, shape the morphology of the lower talus in the Palomares margin.

The Cartagena Margin has a wider shelf that connects eastwards with the Balearic Promontory platform, and the talus corresponds to a steep linear escarpment associated with high angle faulting from the EW trending Cartagena Fault System. The steep talus slope is mainly a zone of sediment bypassing and shows erosion features interpreted as sub-aerial paleo-relief, probably from the Messinian, when the Mediterranean dried up. It was submerged during the

Pliocene-Pleistocene flooding. Furthermore, an area of sediment removal has been identified on the Cartagena continental slope. The slide deposits, Cartagena Slide, can be followed down slope from the lower talus to about 2200 m water depth and covers an area of several km². Detached sediment ridges and sediment streams have been identified within the Cartagena Slide. Sediments affected by the slide are Pleistocene and probably late Pliocene in age.

The Palomares and Cartagena Margins, encompassing sites of active tectonics related to recent episodes of strike-slip and transpressive faulting (locally transtensive), have been in existence from the lower Pliocene until the Holocene. These faults deform the sea floor, control the morphodynamic systems (channeling, slump and slide structures) and some of them may be located above shallow earthquake epicenters. An old lineament (the Cartagena Fault System) controlled the active tectonics in the Cartagena margin from the Pliocene to the Pleistocene. Large earthquakes related to this fault system, which produced uplift of the continental shelf, probably triggered submarine slumps and large slides.

Integrated studies of high-resolution seismic reflection data and sidescan sonar images, will be used to determine the tectonic and/or sedimentary control on seafloor morphology as well as sediment instability processes.

Interpreting high-resolution seismic profiles acquired during this cruise plus available commercial and academic multi-channel seismic profiling data in the region, will provide fault geometries, as well as the Plio-Quaternary stratigraphic response to margin evolution. The aim is to map the geometry and offset of structures, to determine the tectonic control on seafloor morphology and study "source to sink" sedimentary processes controlling the morphostructure of these margins. Structural analysis on major tectonic lineaments and associated active faults will illustrate the along-strike margin segmentation, the tectonic inheritance from Miocene rifting processes, and the kinematics of the actual con-

vergent plates. Maps of the surface expression of deformation and of isopachs of the sedimentary basin infill will be produced. We also plan for further studies to integrate onshore and offshore data through structural sections crossing the coast line.

Main objectives on the Palomares and Cartagena margins focus on:

Morphodynamics: Identification of morphodynamic domains and their tectonic and/or sedimentary control.

The main morphodynamic formations such as turbidite systems, slope provinces, basin realm, etc.

Area and character of induced catastrophic phenomena (slides, slumped mass, sedimentary instability). Mass-transfer estimates.

Margin architecture: Stratigraphic and tectonic shallow organization: Seismic unit identification within Plio-Quaternary sediments,

The limit of the Messinian salt diapirs.

Active tectonics: Identification of the main fault zones, with emphasis on active faults.

Correlation between submarine and continental faults in the region and the distinction of the main and secondary fault directions

Estimation of slip rate and relevant vertical throw along recently active faults.

The main result of the TTR-14 survey points to a highly deformed margin of very recent or even active, wrench tectonics which conditioned sediment dispersal and mass wasting. Morphodynamic provinces are shown to encompass impressive turbidite systems, from incised canyons to deep sea fan lobes, developed at the Palomares margin, and ubiquitous slide deposits and mass wasting structures at the Cartagena margin.

II.4.1. Palomares margin: seismic interpretation

G. MARRO, M. SÁNCHEZ-GÓMEZ, F. FERNÁNDEZ-IBÁÑEZ, M. GARCÍA, M. ROMAN-ALPISTE, N. MHAMMDI, H. VANNESTE AND M. COMAS

The Palomares margin is described in the introduction.

Seismic Line: PS-225MS

Line PS-225MS is 50 nm long and runs SE-NW from the deep basin, across the Abu-Bacer volcanic high and to the Carboneras margin (Fig. 27). The most conspicuous feature of the deep basin is the gentle folding that affects the bedded seismic facies sequence. The folds are tighter at depth and towards the SE, and they barely affect the upper Quaternary unit. The deep basin area is separated from the slope by a vertical fault that causes relief of about 1400 ms TWTT. Northwest of the fault (Fig. 34) the sedimentary sequence is thinner and pinches out

towards the acoustic basement, presenting a more transparent seismic facies that could be due to contourite sedimentation. Slumps and slump scars are found on the steepest part of the slope. At the NW end of the profile the sedimentary cover is thinner (up to 700 ms TWTT) and the acoustic basement nearly outcrops in the Abu-Bacer volcanic high. The sedimentary sequence has a bedded seismic facies with low acoustic amplitude and low lateral continuity. Near-vertical faults cross-cut the sedimentary sequence up to the sea-floor reflector and the acoustic basement.

II.4.2. Palomares margin: sidescan sonar interpretation

M. GARCÍA, N. MHAMMDI AND M. COMAS

Line MAK-85MS: Gata Canyon

The line follows the axis of the Gata Canyon, east of Cabo de Gata (Fig. 35). The line has a length of 21 nm, with a direction that changes from ESE to ENE, and a lateral

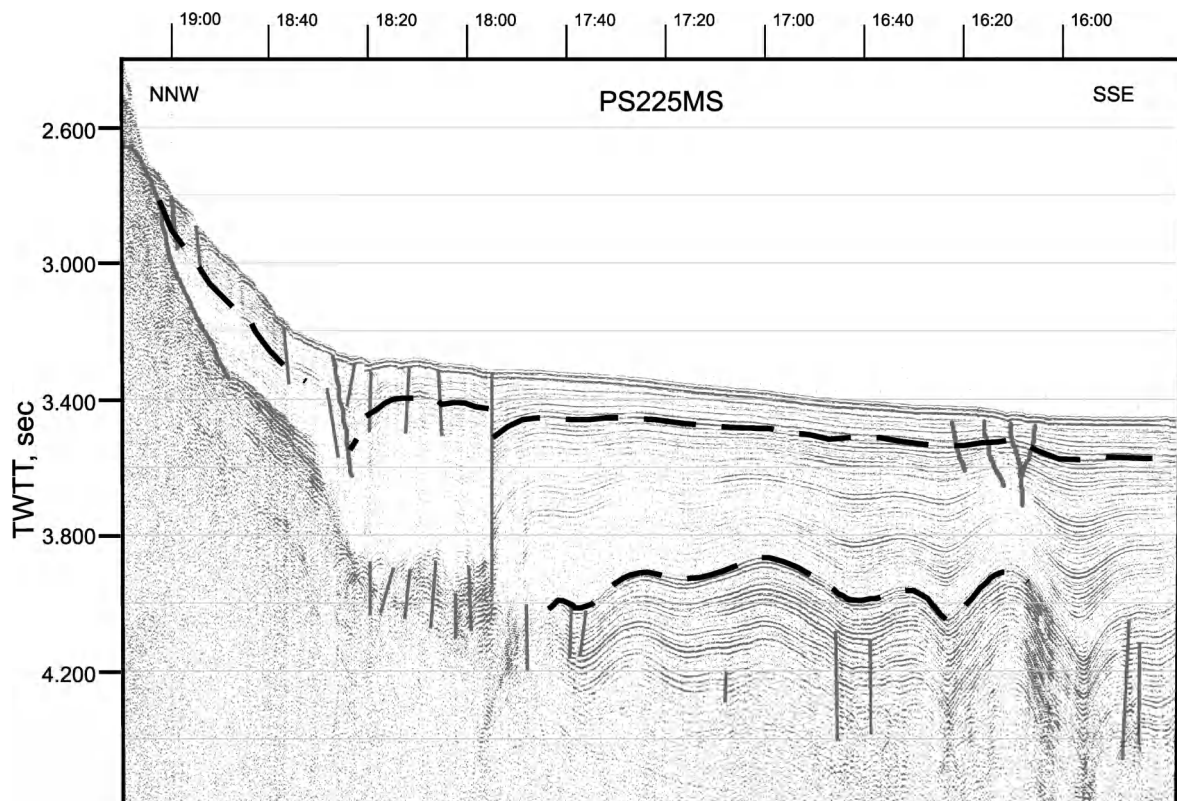


Figure 34. Southern part of seismic line PS225MS, located on Fig. 27. Diapirs affecting deep basin sediments and a narrow fault zone towards the margin slope are seen.

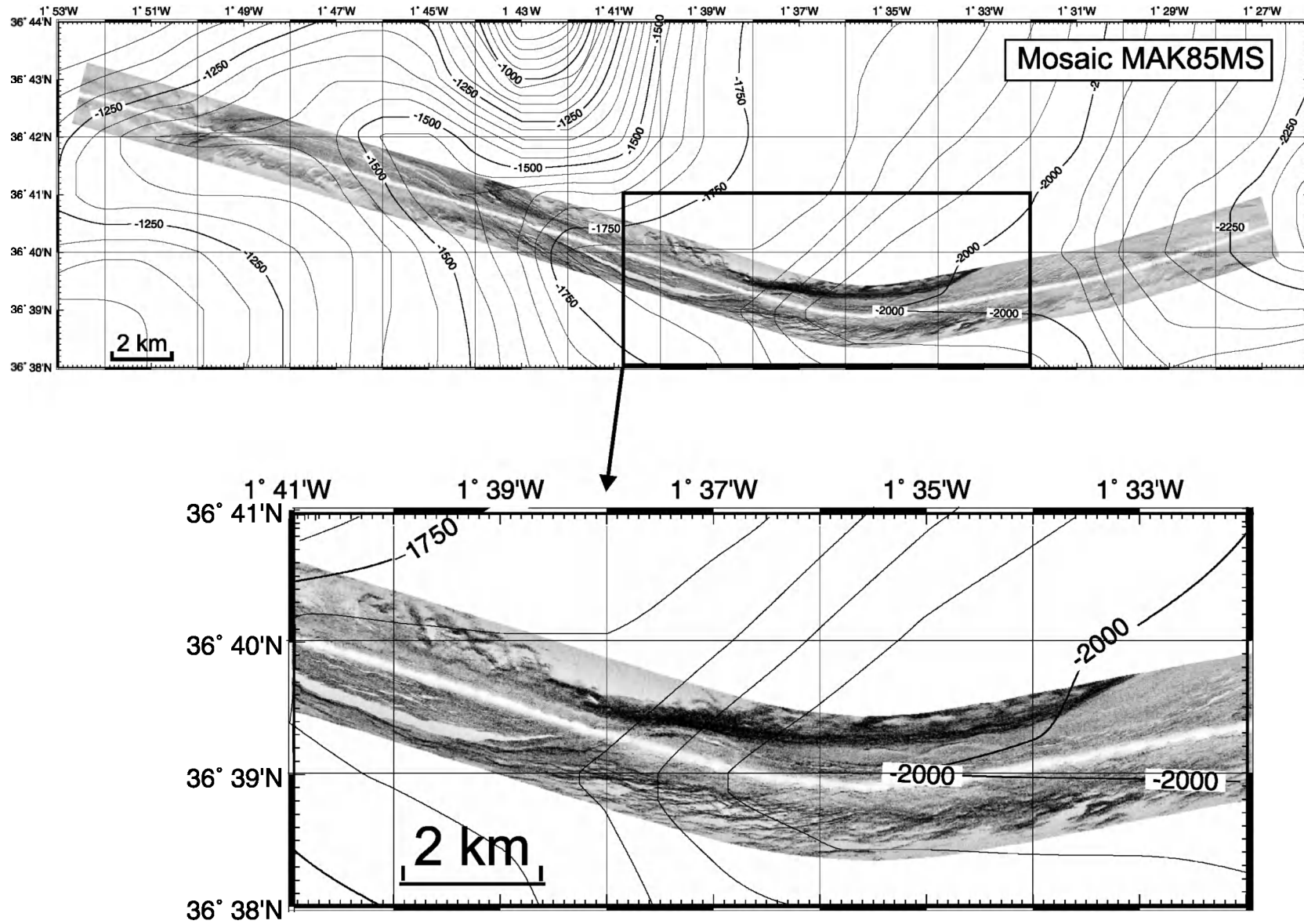


Figure 35. Details of MAK-85MS line along the Gata Canyon, located on Fig. 27.

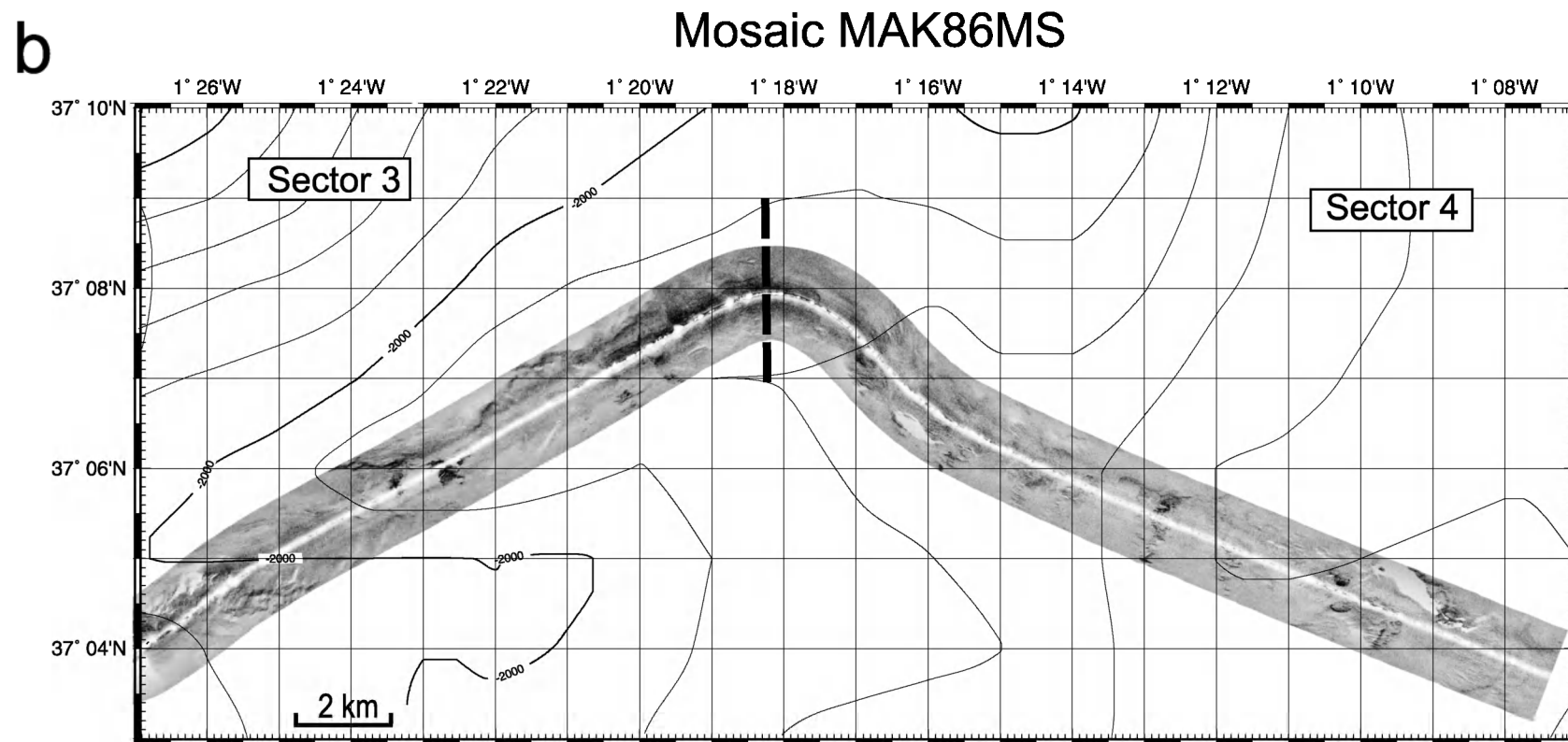
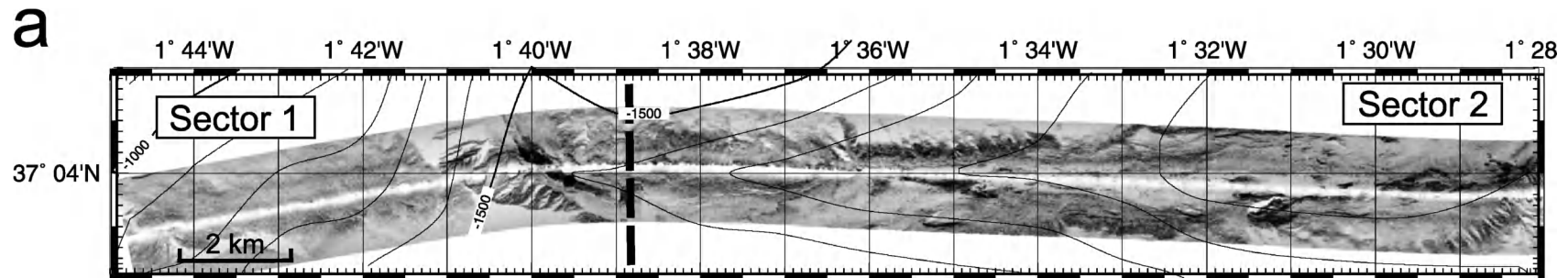


Figure 36. MAK86MS line along the Aguas-Almanzora Canyon. a - northeast part, b - southeast part. Located on Fig. 27.

coverage of about 1 nm. The depth increases from 1080 m to 2400 m. The sonograph shows a sinuous canyon with a steeper northern wall, corresponding to the southern side of the Abu Bacer volcanic high, and a more gentle southern wall, limited by the Maimonides volcanic high.

The sonograph is divided into three sectors. The proximal sector is 7 nm long and has wide semi-circular scarps that mark the rim of the canyon. The 90 m wide thalweg is flat in this area, where the profiler shows sedimentary channel infilling. A fringe with low reflectivity is seen on the southern side of the thalweg. The 9 nm long middle sector is constrained by the volcanic highs, especially by the Abu Bacer high in the north (Fig. 35). The canyon walls have high-reflectivity lineations that probably correspond to rock outcrops. The thalweg is wide and has low reflectivity in the beginning of the sector and it narrows progressively showing higher reflectivity and a braided pattern related to the flow direction. In the distal sector the canyon widens as the physiographic control of the volcanic highs is reduced and the thalweg is up to 100 m wide. The reflectivity is more homogeneous in this sector, nevertheless the thalweg is easily differentiated as a

relatively low reflectivity channel limited by higher reflectivity narrow walls. Some flow-related lineations are also observed in this sector.

Line MAK-86MS: The Aguas-Almanzora Canyon

The line runs for about 30 nm following the axis of the Aguas-Almanzora Canyon, starting at a depth of 1780 m and ending in 2450 m. The canyon has been divided into four sectors (Fig. 36).

The first sector (Fig. 36a) is 5 nm long and shows the confluence of the two branches of the canyon. The northern branch trends NW-SE and has a deeply incised asymmetric relief, with a steep northern wall up to 400 m high and a very irregular profile deeply incised by erosive gullies. The southern wall has gentler relief and is up to 70 m high. The southern branch has low relief and has a low reflectivity sinuous patch. In the confluence area the width of the canyon is about 1 nm. In the second sector (Fig. 36b) the canyon runs eastwards and is also asymmetrical, with a steeper northern wall covered in gullies and slide scars. The southern wall is gentler and is limited locally by some WSW-ESE

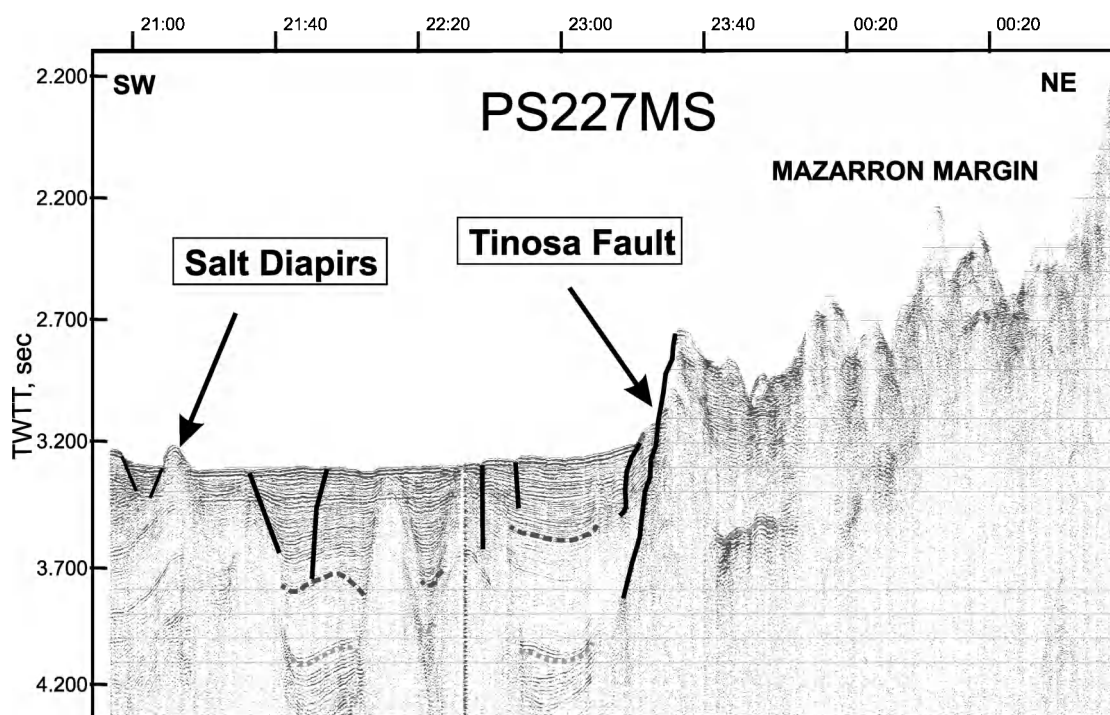


Figure 37. Seismic line PS-227MS crossing the Tinosa fault. Located on Fig. 27.

lineations. The canyon has a flat floor, with some high-reflectivity patches marking the presence of boulders and flow lineations. In the third sector (Fig. 36b), the canyon changes direction to the NE and it widens progressively towards the east. The more proximal area has deeply incised gullies on both walls and outcropping hard rock layers. The fourth sector (Fig. 36b) runs in an ESE direction. The relief of the canyon is reduced, and is limited by a morphological high in the northern wall. Some SW-NE orientated lineations create steps along the canyon axis.

II.4.3 The Cartagena margin: seismic interpretation

G. MARRO, M. SÁNCHEZ-GÓMEZ, F. FERNÁNDEZ-IBÁÑEZ, M. GARCÍA, M.J. ROMAN-ALPISTE, H. VANNESTE AND M. COMAS

The Cartagena Margin is summarised in the introduction.

Seismic Line: PS-226MS

The line runs NE for 12.5 nm. The main feature of the line is a channel with well developed asymmetric levees corresponding to the distal part of the Aguas-Almanzora turbidite system. The width of the channel is about 750 m, with an infill of 40 ms. As the orientation of the seismic line is parallel to the margin and therefore to the main structures, most of the reflectors show a chaotic aspect. The positive relief is due to sedimentary processes related to the neighboring turbidite system.

Seismic Line: PS-227MS

The line runs to the NE for 33 nm from the deep basin towards the Mazarrón margin, crossing the Tiñosa fault at shot point 900. The Tiñosa fault is a major tectonic feature that bounds the deep basin in this area (Fig. 37). Active salt diapirism affects the entire sedimentary fill, locally outcropping at the sea floor and giving positive relief. Diapirs perforate the sequence and deform the reflectors near the diapir walls. The

Tiñosa fault has a large exposed scarp marking the beginning of the Mazarrón margin. The Tiñosa fault appears to have a normal displacement. The Mazarrón margin consists mainly of basement outcrops with abrupt relief. Locally sediments have accumulated between basement highs. The steep slopes cause diffractions, that obscure the deeper reflectors.

Seismic Line: PS-228MS

The line is 18.6 nm long and runs WSW-ENE across the Palos Canyon on the Cartagena Margin. The sedimentary cover is thinner, with well-bedded facies draping the acoustic basement. In the westernmost part of the line the Palos Canyon has a well-developed incision with steep flanks and a few slides. Sets of penetrative high angle faults affect the sedimentary sequence, reaching down to the acoustic basement and also constraining the canyon location. Eastwards some negative relief features can be observed mostly in relation to faults affecting the youngest sediments.

Seismic Line: PS-229MS

The line is 2 nm long and trends N-S across the Cartagena Margin. This line shows a steep southwards facing basement outcrop, bounded by a few faults and partially covered by a thin sedimentary layer.

III. BALEARIC BASIN (LEG 3)

Several locations on the Balearic Basin margin were surveyed (Fig. 38). Most of the study was with the MAK deep towed system and focused on slope processes and sediment transport in the deep sea.

III.1. The Eivissa Channel area

III.1.1. Introduction

G. LASTRAS AND M. CANALS

The Eivissa Channel is located between La Nao Cape north of the coastal city of

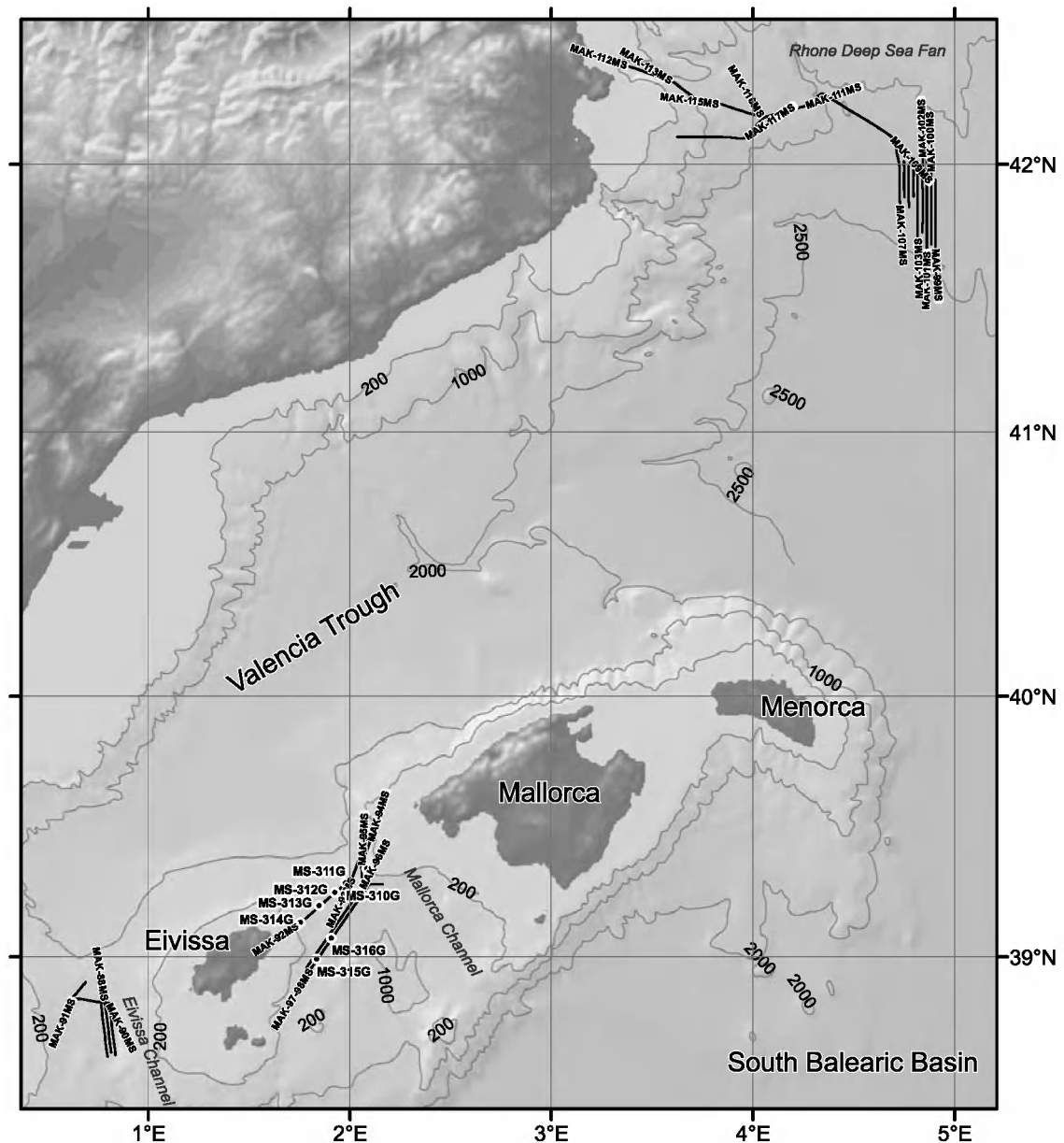


Figure 38. Location map of the TTR-14 Leg 3 in the Balearic Basin.

Alacant (Alicante), on the Iberian Peninsula, and the islands of Eivissa (Ibiza) and Formentera. It lies at the western end of the 350 km long and 120 km wide Balearic Promontory, which includes the Menorca, Mallorca and Eivissa structural blocks, the depressions between them, and the Eivissa Channel. The Promontory is the northeastward prolongation of the external zone of the Betic Ranges. The maximum height of the Balearic Promontory is ca. 3.000 m above the surrounding seafloor. Neogene volcanic centres are quite common in the area (e.g. Acosta et al., 2001a).

Three physiographic elements can be distinguished in the Eivissa Channel (Lastras et al., 2004): the 100 to 130 m deep continental shelves off Alacant and SW Eivissa – Formentera, the continental slopes down to 800 m deep, and a generally smooth median depression that only locally exceeds 900 m water depth. Overall, the saddle morphology of the north-south trending Eivissa Channel is slightly asymmetric, with the Iberian Margin to the west steeper than the Balearic Margin to the east. The smoothness of the median depression is interrupted by the prominent ca. 200 m high east-west trending

Xàbia Seamount, which divides the deep Eivissa Channel into two latitudinal sectors. The northern Eivissa Channel opens to the north to the València Trough, while the southern sector is connected to the South Balearic Basin. The rough northern sector, with a seafloor texture often disrupted by fluid escape features that give it an orange peel texture, contrasts markedly with the essentially smooth floored southern sector (Acosta et al., 2001b). Maximum water depths in the Eivissa Channel reach 826 m and 925 m in the northern and southern sectors respectively (Lastras et al., 2004).

Most of the sediment reaching the Eivissa Channel is thought to come from the Iberian Peninsula, from rivers to the north such as the Ebre, Túria and Xúquer. Despite this riverine influence, patches of benthic carbonate-dominated sedimentation exist on the Balearic continental shelf west of the channel axis (Canals and Ballesteros, 1996). No permanent rivers exist on the Balearic Islands, favouring the development of carbonate-pro-

ducing benthic communities.

The Eivissa Channel plays a major role in the exchange of water masses between the South Balearic Basin and the València Trough. Surface waters with Atlantic influence enter the València Trough through the Eivissa Channel. Northward-directed bottom currents are dominant during summer. When they weaken during winter, deep waters originating in the Ligurian Sea and the Gulf of Lions exit the València Trough through the Eivissa Channel (López Jurado and Díaz del Río, 1994). The interaction between near-bottom currents and the Xàbia Seamount produces a typical contouritic ridge and associated base-of-slope depression (moat) south of the seamount (Lastras et al., 2004).

Four slides, the Ana, Joan, Nuna and Jersi slides, have been described on the seafloor along the Balearic margin of the Eivissa Channel (Lastras et al., 2004). They have areas of up to 16 km² and occur in water depths ranging between 600 and 900 m.

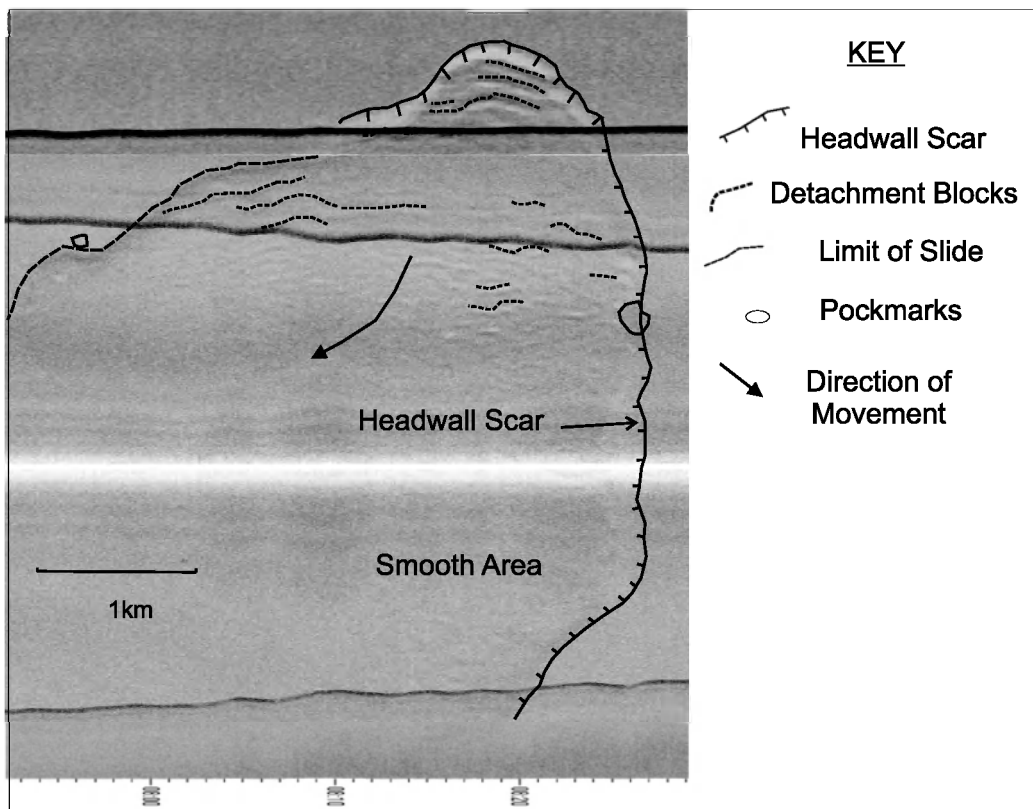


Figure 39. Mosaic of lines MAK87MS to MAK89MS west of Eivissa showing the limit of the Jersi slide and its detached blocks. There are pockmarks near the headwall and to the south of the slide. Located on Fig. 38.

Volumes range from 0.14 to 0.4 km³. In general, they show horseshoe-shaped headwall scarps and distinct depositional lobes with positive relief. Internally, the slide bodies consist mostly of transparent seismic facies. Chaotic facies are observed at the toe of some of the slides, and blocks of coherent stratified facies embedded in the slide deposit have also been identified. Very-high resolution seismic reflection profiles demonstrate that the four slides share the same slip horizon that corresponds to a distinctive continuous, high amplitude reflector (Lastras et al., 2004). Furthermore, the geometry of some of the headwall scars reveal evidence of pockmarks, and fluid escape features are also present further upslope. This indicates a possible link between fluid escape features and destabilisation of the upper sediment layers. Both the slides and the pockmarks were the target of the first part of Leg 2.

III.1.2. MAK-1M sidescan sonar data

G. LASTRAS AND C. BROENNIMANN

Five lines were acquired in the study area. Lines MAK-87-89MS formed a complete acoustic coverage of the Ana, Joan, Nuna and Jersi slides (Lastras et al., 2004) on the Eivissa margin. Line MAK-90MS runs across Xabia Seamount and Line MAK-91MS was intended to study an underwater promontory to the north of the seamount, where a field of pockmarks was reported from the multibeam data.

MAK-87 to 89MS sonographs

The lines run N-S covering an area of approximately 260 km² through the southern and northern Eivissa Channel. They terminate at the contourite ridge south of the

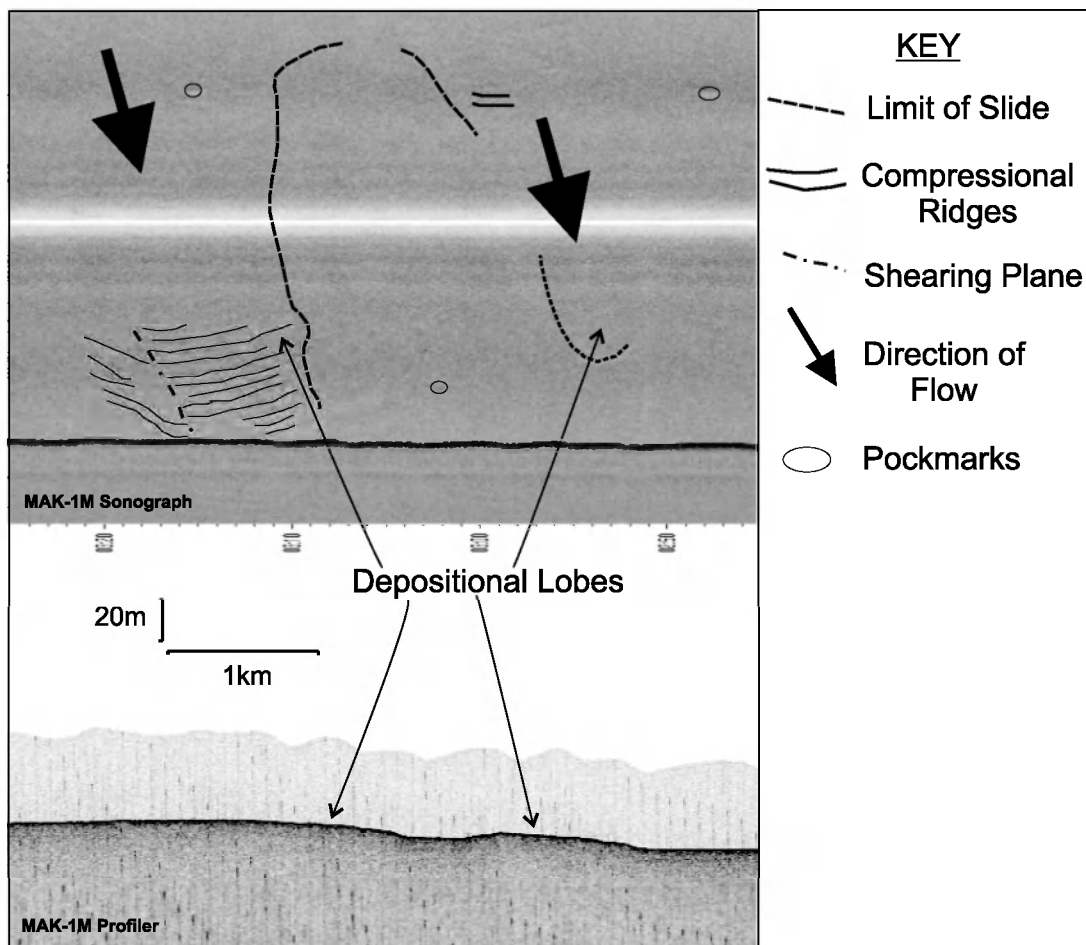


Figure 40. Sonograph of line MAK-87MS showing compressional ridges and the two depositional lobes associated with the Nuna slide. West of Eivissa (Fig. 38).

Xabia Seamount. The following description of the sonograph mosaic provides a general overview of the four types of acoustic features found in the area.

An area of shadow or high backscatter which is noticeably wider than any other feature indicates an escarpment-type of seabed morphology. This feature is often semi-circular or horseshoe-shaped and is interpreted to be the headwall scar of a slide.

High-low backscatter couplets which are linear and trend north-south and which are located within the headwall scars, indicate a stepped-type morphology. This morphology is interpreted to have formed by blocks of deposit which have been detached and rotated/glided downslope.

Very subtle changes of backscatter can be seen as linear features and are located in an area close to the headwall scar but not within it. These features are interpreted to be the limits of the slide and are confirmed by previously collected swath bathymetry data (Lastras et al., 2004).

Multiple, parallel and linear changes of backscatter (dark-light) but this time located up to 8 km away from the headwall scar (Nuna slide) are related to the Ana, Joan and Nuna slides. These features are interpreted to be compressional ridges created by sediment disruption at the toe of the slide.

Ana Slide

The narrowest part of the Ana slide headwall scar is horseshoe-shaped and is approximately 1 km wide. This headwall scar widens to form a semi-circular embayment which at its greatest visible extent is approximately 3 km wide. The Ana slide shows evidence for detached blocks and compressional ridges which are located approximately 5.6 km away from the headwall scar and indicate that the slide has travelled to the northeast.

Jersi Slide

The north-east trending headwall scar of the Jersi slide is recognisable from its morphology (Fig. 39). The subtle east-west trending lineation which marks the continuation of the headwall scar is confirmed by the break of slope seen on the profile. The slope of the seafloor has caused the slide to travel in a northerly direction with compressional ridges forming at its toe. In an area west of the detachment blocks there is uniform backscatter. This may be either due to blanketing of slide morphology by sediment, or because the slide surface is smooth. It corresponds to an area with a chaotic seismic facies (Lastras et al., 2004).

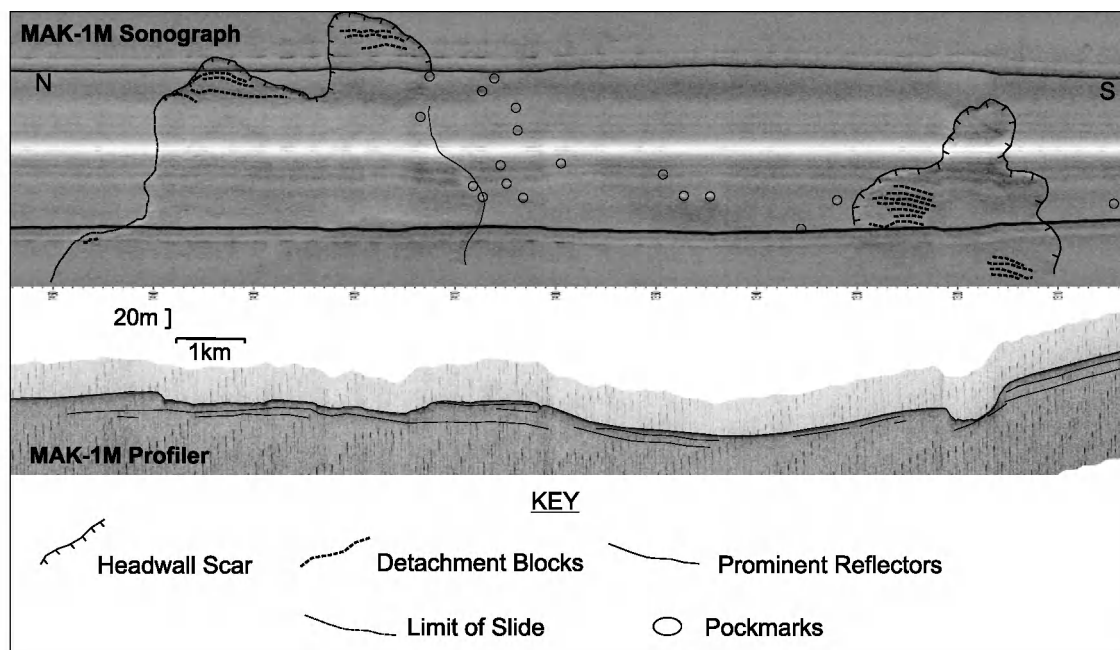


Figure 41. Sonograph and profile from line MAK-89MS, west of Eivissa (Fig. 38) showing the Joan slide.

Nuna Slide

Evidence for detached blocks is seen within the headwall scar of the Nuna slide and also within the depositional lobe. The largest cluster of compressional ridges is associated with this slide and indicate that the slide has travelled in a southeast direction (Fig. 40).

Joan Slide

The Joan slide appears to have two complex arcuate headwall scars that are between 1.6 km to 3.1 km wide at their greatest visible extent (Fig. 41). There is evidence for detachment blocks in the northern headwall scar and compressional ridges approximately 7 km away from the headwall scar which indicate that the slide has travelled southeastward. There appear to be two families of compressional ridges, one of which truncates the other. Comparisons with the accompanying profiles indicate that there are two depositional lobes. These are confirmed by swath bathymetry data (Lastras et al., 2004).

MAK-87 to 89MS subbottom profiles

Line MAK-87MS

The maximum penetration on the profile is about 40 m. The seafloor slopes gently to the north and deepens from 660 m to 840 m. Two seismic facies are identified: (1) a stratified facies with strong and continuous reflectors, and (2) a transparent facies. The first is found all along the profile while the second is related to some irregularities in the seafloor caused by sliding (Lastras et al. 2004).

The southern end of the profile crosses the distal deposit of the Ana slide and the northern end crosses the southern sidewall of Joan slide.

The seismic reflectors in the northern part of the profile have the typical internal geometry of a contouritic sequence. The contourite sequence is north of the Xabia seamount, which has an opaque seismic character.

Line MAK-88MS

The southernmost Ana slide has a 3.5 m high headwall at the seabed. The depositional part of the slide is 850 m wide and appears as a chaotic, lens-shaped package. The presence of a scar bounding deposits of the Ana slide in the south may indicate that the slide has a complex pattern of movement with a major westward component and a minor northward component.

Further to the north the Joan slide scar is a 2.5 km wide depression with an 8.5 m high stepped southern headwall. The transparent seismic facies is about 5 m thick. The northern headwall is 6 m high and has a simple concave profile. The complex topography observed within the slide scar suggests that there were at least two episodes of sliding. The earlier episode was in the south and the later failure, responsible for the second headwall, was in the north, partially affecting the first scar.

To the north of the Joan slide is a similar sized depression (800 m wide). A 20 m high peak with hard acoustic return is located within the depression. The peak is associated with several high amplitude wave reflectors at a depth of about 10 m below the seafloor. North of the peak is a 10 m deep depression whereas sediments are piled up against its southern slope. Such a distribution of erosion and deposition is common for obstacles on the seafloor affected by bottom current. The peak belongs to a cluster of highly backscattering features, which may represent irregularities of the volcanic basement outcropping on the seafloor. This conclusion is supported by multibeam data, which show that the outcrops could be the continuation of a large volcanic ridge located to the east of the study area.

The Nuna slide is immediately north of the peak. The scar width is about 1000 m. The headwall is about 7-9 m high and has a simple concave profile at the both crossings. It extends down to the prominent reflector indicated by Lastras et al. (2004) as a slip surface. Within the southern sector of the scar the seabed is smooth for approximately 200 m and the slip surface is exposed onto the

seafloor. The remaining surface of the scar is hummocky due to the presence of the displaced material.

The Jersi slide is crossed by the line further to the north. The width of the slide is about 3 km. The headwall is about 10 m high and the slide surface is exposed for about 1.5 km. A 4-5 m thick, acoustically chaotic lens shaped body, representing the slide deposit, occupies part of the slide depression.

Line MAK-89MS

The slides are also seen on line MAK-89MS and are similar to the previous lines. In addition to the slides there are two 30 km wide pockmarks in the area between the Ana slide and the Joan slide. There are 25 pockmarks north of the Nuna slide, with an average of density of 3 pockmarks per km² and a width ranging between 20 m and 40 m.

Line MAK-90MS

Xabia seamount is crossed by the line and the sonograph shows a mostly featureless seafloor. The eastern slope of the seamount appears to be unstable with the upper sedimentary cover being removed by sliding. The high backscatter area corresponds to more competent sediments or rocks exposed by sliding. Upslope from the scar there is a series of small pockmarks, aligned in a SW-NE direction, which probably develop along a fault. There are also small patches and stripes of high backscatter on the western slope of the seamount that appear to be associated with 3 m deep notches in the seafloor. These could be small scale scars or exposed hard grounds at fluid seepage sites. A few more pockmarks, 50-55 m wide, are found at the NW end of the line. Penetration by the profiler is poor.

Line MAK-91MS

The underwater promontory is draped by a hemipelagic cover which is characterised by a low backscatter on the sonograph. The promontory is best seen on the profiler record which shows a flat-topped

rise with moats on either side. The top of the promontory is densely covered by circular pockmarks. They are about 50-70 m in diameter and, according to one crossing, are about 5 m deep. The pockmarks are not found outside of the promontory where the acoustic penetration is better and up to 25 m of stratified sediments are seen.

III.2. The Mallorca Channel

III.2.1. Introduction

G. LASTRAS

The Mallorca channel is located between the Eivissa (Ibiza) and Formentera islands, to the west, and the Mallorca island to the east. It is in the middle of the Balearic Promontory.

Swath bathymetry of Mallorca channel, obtained during the Spanish Exclusive Economic Zone surveys, showed a complex seafloor morphology. The bordering Mallorca and Eivissa continental shelves have shelf breaks at 160 m and 130 m respectively. Extensive carbonate sand fields characterize large areas of the Mallorca shelves, originating from seagrass-derived biogenic sediments (Acosta et al., 2002).

The northern sector of the Mallorca channel is a depression which deepens northwards towards the Valencia Trough, while the southern sector is an almost enclosed basin bounded by the two margins and a northeast-southwest trending high along the top of the Emile-Baudot escarpment (Acosta et al., 2004). Linking these two sectors is a slight high, the Mallorca Collado high, that is cut by a narrow north-trending channel (Acosta et al., 2004) formed by an alignment of pockmarks, reaching a water depth of 740 m. The Mallorca Collado high is linked with the Mallorca continental shelf by a submarine terrace. Maximum water depths over 1500 m are reached in the northern sector, while the southern basin reaches ca. 1050 m water depth. The slope off Mallorca has two distinct morphologies: it is smooth in the vicinity of the Mallorca Collado while the rest is irregular, cut by gullies and disturbed

by several landslides and headwall scars (Acosta et al., 2004).

The present-day seafloor morphology of the Mallorca channel has been shaped by a network of normal faults cut into the Plio-Quaternary sediments and by fluid escape processes. The fault network may have resulted from downslope gliding over a deformable water saturated layer of latest Messinian–early Pliocene age (Acosta et al., 2004). Large pockmarks are one of the most important features on the seafloor of the Mallorca channel, and they are often aligned (Acosta et al., 2001) as in the Eivissa channel (Lastras et al., 2004). They are most likely formed by the expulsion of thermogenic gas somehow associated with the volcanic field

between Mallorca and Eivissa islands and the Valencia Trough.

The study of the sedimentary processes in the Mallorca channel, and specially the Mallorca Collado, and slides on both the northern and southern Mallorca margin, and the aligned pockmarks in the southern Eivissa margin were the main targets of the second part of Leg 3, the results of which are presented below.

III.2.2. MAK-1M sidescan sonar and profiles

G. LASTRAS AND C. BROENNIMANN

Line MAK-93MS

The objective in this area is mainly to investigate the boundary between the shallow Balearic promontory and deep sea area.

Two main units are observed in the seismic profile: the upper one is approximately 10 m thick and the lower one, at depths of 10 to 20 m, is also 10 m thick. The upper unit has low amplitude, high frequency stratified seismic facies, and the lower is a transparent seismic facies with some faint stratified reflectors. The sonograph shows no distinct features apart from four pockmarks and a possible horseshoe shaped slide scar related to another three pockmarks. In places the two units pinch out against a very strong seafloor reflector and gullies and pockmarks are identified.

Slope gradients reach 25° in this part of the margin where there are significant escarpments, the highest of which is up to 70 m. These high escarpments could be due to normal faults within a horst and graben structure. Many faults disrupting the seafloor in the Mallorca channel, often related with pockmarks, have been described by Acosta et al. (2002). Some of the faults seem to be quite recent as they cut the upper sedimentary layers.

Line MAK-95MS

Line MAK-95MS is orientated north-south and is located along the western side of the island of Mallorca.

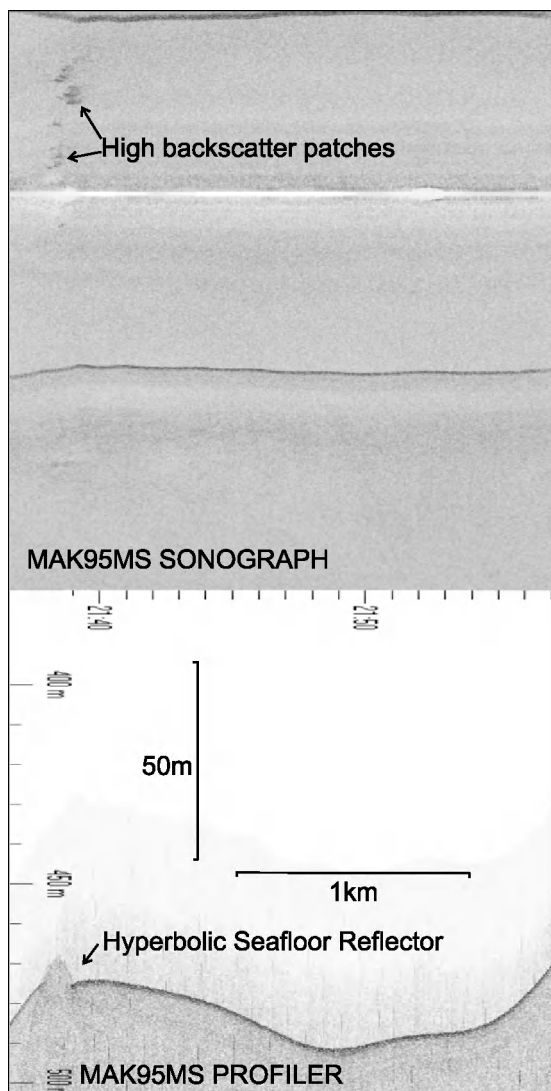


Figure 42. Fragment of line MAK-95MS in Mallorca Channel. Located on Fig. 38.

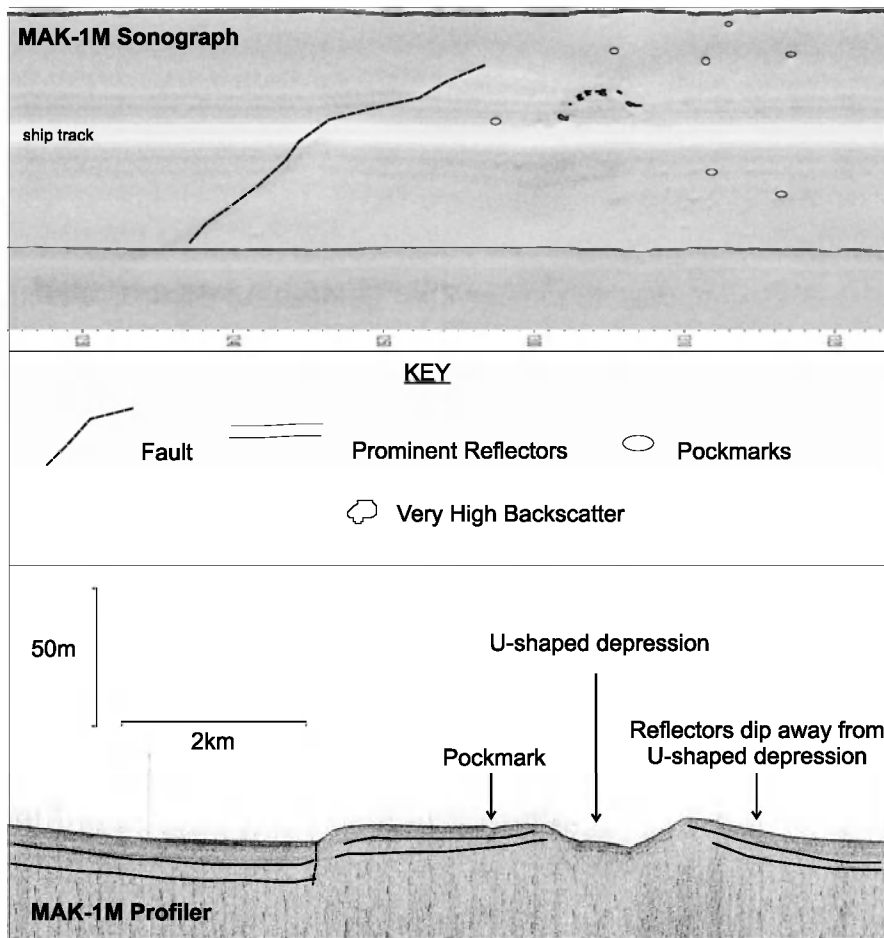


Figure 43. Fragment of line MAK-97MS in the Mallorca channel, showing a possible giant pockmark. Located on Fig. 38.

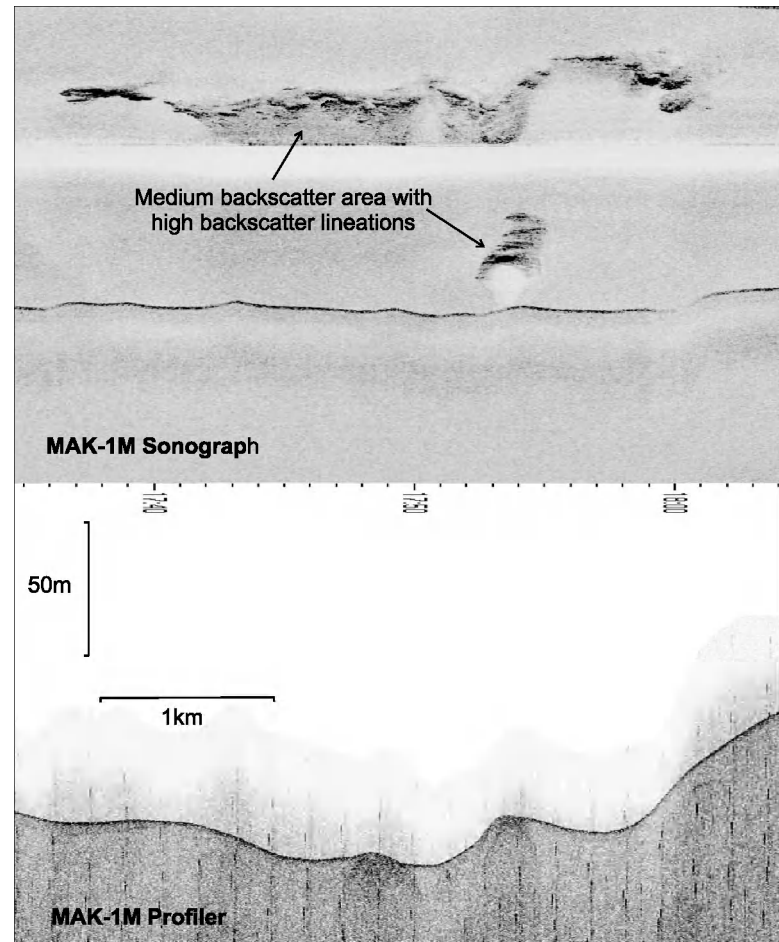


Figure 44. Fragment of line MAK-97MS in the Mallorca channel, showing rocky outcrops. Located on Fig. 38.

Table 6. Details of the sites sampled during Leg 3 in the Mallorca Channel.

Station	Date	Time (GMT)	Latitude	Longitude	Depth (m)	Recovery (cm)
TTR14-MS-309G	23.08	22:23	39°20.302'N	2°05.242'W	333	
TTR14-MS-310G	23.08	23:52	39°16.980'N	1°58.797'W	606	
TTR14-MS-311G	24.08	00:38	39°17.018'N	1°58.824'W	606	333 cm
TTR14-MS-312G	24.08	01:53	39°14.822'N	1°55.610'W	740	
TTR14-MS-313G	24.08	03:22	39°11.697'N	1°50.998'W	610	
TTR14-MS-314G	24.08	04:55	39°07.901'N	1°45.401'W	428	
TTR14-MS-315G	24.08	07:09	38°59.324'N	1°50.305'W	663	
TTR14-MS-316G	24.08	08:48	39°04.212'N	1°54.611'W	714	431 cm

Most of the sonograph has a medium backscatter response, which is possibly due to a cover of hemipelagic sediment. At one place there is an 800 m long line of high backscatter patches, which coincide with a hyperbolic seafloor reflector (Fig. 42). The hyperbola is probably produced by an outcrop at the seafloor. Its location close to the island of Mallorca, linear arrangement and comparison with bathymetry data suggest the outcrop to be a structural feature of the Mallorcan continental slope.

Line MAK-97MS

The line runs between the islands of Eivissa and Mallorca, across the Balearic promontory from SW-NE. It is characterised by low backscatter with the following three exceptions:

The SW end of the line has depressions that are interpreted as pockmarks. The pockmarks are found in clusters or lineations.

Very high backscatter patches are arranged in a semicircle and the individual patches are approximately 100 m wide (Fig. 43). On the profiler record this area is seen as a U-shaped depression approximately 20 m deep and 1.5 km wide with prominent reflectors dipping away from the depression. High backscatter lineations are found within medium backscatter in an area on the Majorcan continental slope that runs approximately parallel to the track. It is interpreted to be outcropping sedimentary layers from the continental slope sequence (Fig. 44).

A narrow area of medium backscatter that trends N-S has a 10 m vertical offset and is interpreted to be the surface expression of a fault.

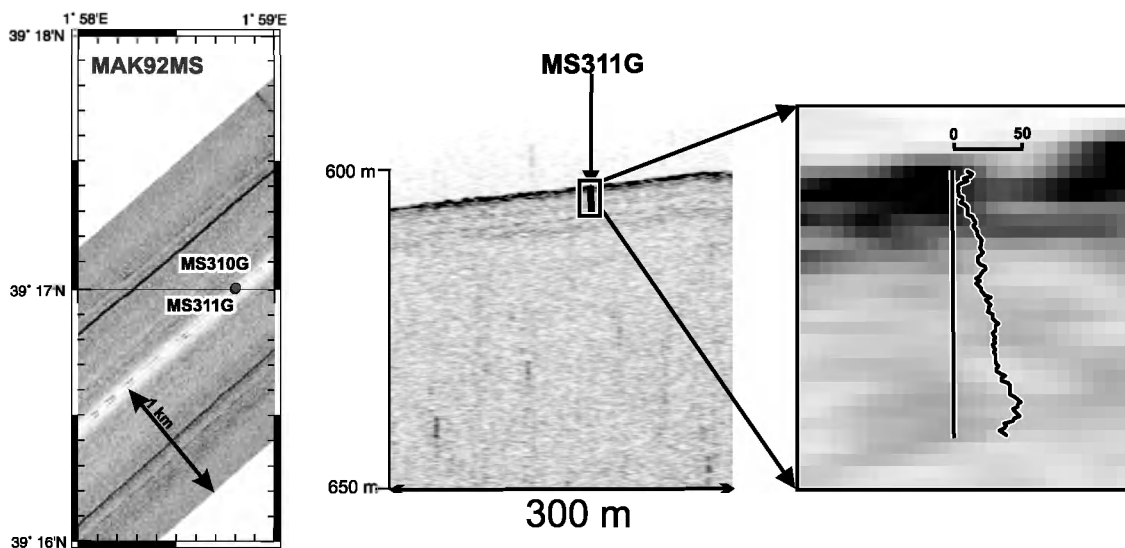


Figure 45. Sampling sites MS-310G and MS-311G in the Mallorca channel. Located on Fig. 38.

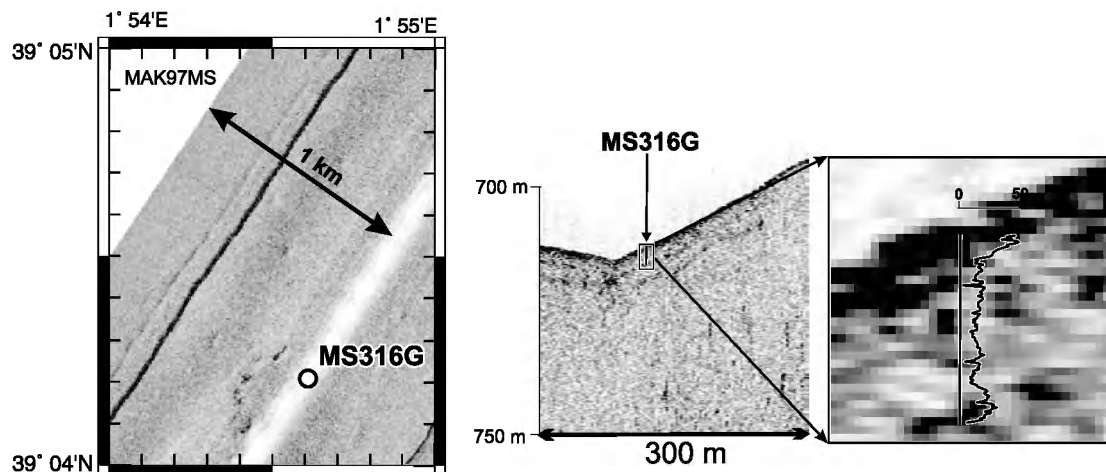


Figure 46. Sampling site MS-316G over possible pockmark in the Mallorca channel. Located on Fig. 38.

A structural control is suggested for the location of pockmarks within the Mallorca channel because of the clustering and linear arrangement of the pockmarks on the sonograph, the presence of a fault on the profiler and comparison with multibeam bathymetry data. The arcuate shape of the very high backscatter patches could be the relict remains of a pockmark. The u-shaped depression may have been created by the failure of the pockmark and the very high backscatter patches may have a biological origin linked to fluids escaping from the pockmark. Alternatively the depression may have been initiated by tectonism. A thick cover of hemipelagic sediment over the Mallorca channel would explain why most of the sonograph shows low backscatter and why landslide material sourced from the Mallorcan continental shelf is not visible.

III.2.3. Bottom sampling data

A. OVSYANNIKOV, D. KOROST, E. KOZLOVA,
A. AKHMETZHANOV, E. SARANTSEV, E. BILEVA,
E. BLINOVA, E. LOGVINA, A. SHUVALOV, I. GURJEV
AND P. GOLINCHIK

8 cores including 5 along a regional profile were collected in the area (Table 6, Annexe I). The purpose of the coring was to test geotechnical properties of sediments of the area. Only two of the cores (MS-311G and MS-316G) were split and described.

Station MS-311G

This station was chosen along line MAK-92 MS (Fig. 45). About 333 cm of uniform bioturbated hemipelagic brownish grey and grey clays were recovered. The magnetic susceptibility pattern indicates an increase of the terrigenous material towards the bottom.

Station MS-316G

This station was at a possible giant pockmark seen on line MAK-98 MS (Fig. 46). 431 cm of hemipelagic brownish grey and grey clays were found but no features related to fluid escape.

III.3. The Rhone Neofan: A high resolution survey of a turbidite channel-lobe transition zone

III.3.1. Geological setting

B. DENNIELOU AND L. DROZ

Rhône Deep-sea fan

The sedimentary systems of the northern margin of the Western Mediterranean have been the object of numerous researches since the beginning of the 1970's. The architecture is well known thanks to an important data base, including EM12 and EM300 swath bathymetry and acoustic backscatter, high resolution deep-towed sidescan sonar data, seismic data from high to very high resolution and coring.

The Petit-Rhone fan, 1.5 km thick and about 300 km long, is the main turbidite system of the Gulf of Lions (Fig. 47). It was fed by alpine inputs brought to the Mediterranean by the Rhone River. The fan began to develop during the Lower Pliocene as a multiple source fan with numerous small channel/levee systems with little organisation (Droz, 1983). During the

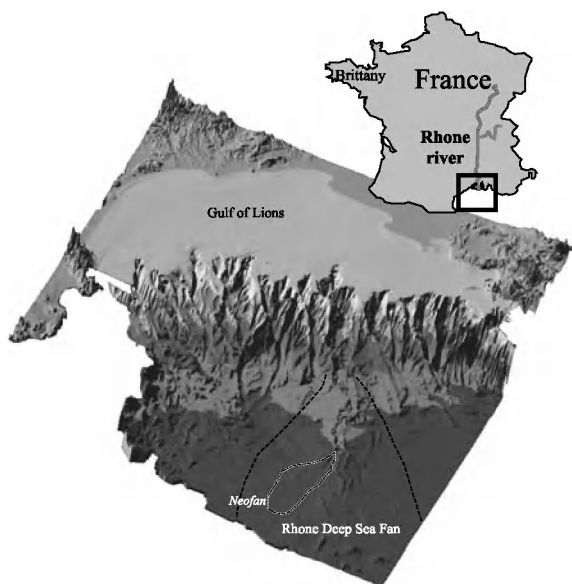


Figure 47. Perspective view of the Gulf of Lions and location of the Rhone deep-sea fan and neofan.

Quaternary, the Petit-Rhone Canyon became the principal feeding canyon of the Rhone Fan, and the fan grew through successive westwards avulsions. In the Late Quaternary, instabilities of the margin, perhaps linked to an increase in underlying Messinian salt layers, resulted in the collapse of sediments of the continental slope and upper fan and the deposition of two transparent bodies, the western and eastern transparent bodies, one on each levee. These transparent bodies rest unconformably through an erosional surface on the fan sediments. Following this period of instability, a last avulsion of the Rhone channel occurred westwards and deposited a small lobate feature, the Neofan, that partially overlaps the western transparent body between the Pyreneo-Languedocian Ridge and the main body of the Rhone fan. The Rhone fan has been inactive since about 11 ka B.P (Torres et al., 1997), in response to the Holocene rise of sea level that cut the fan off from its direct fluvial inputs.

Rhone Neofan

The Rhône neofan is a lobe shaped sedimentary body lying unconformably on the western levee of the Rhone deep-sea fan and on the western mass transport deposit (Droz, 1983). It was deposited after the last bifurcation of the Rhône deep-sea fan submarine channel (Fig. 48). First investigations carried out by Droz (1983), Méar (1984) and Droz and Bellaiche (1985) concluded that there was a rather straight channel, a highly discontinuous layered seismic facies, sandy deposits in the coarsest sediment sampled on the Rhone deep-sea fan, and that some sandy deposits were very recent (130y BP). These authors concluded that the Rhône Neofan was a rare example of a fan still active during a high stand despite the disconnection of the feeder canyon from the river.

More recent investigations (Limonov et al., 1993; Kenyon et al., 1995) outlined the presence of large asymmetrical scour holes that were attributed to the interplay of turbidity currents from the neo-channel with a change in the slope gradients. These authors

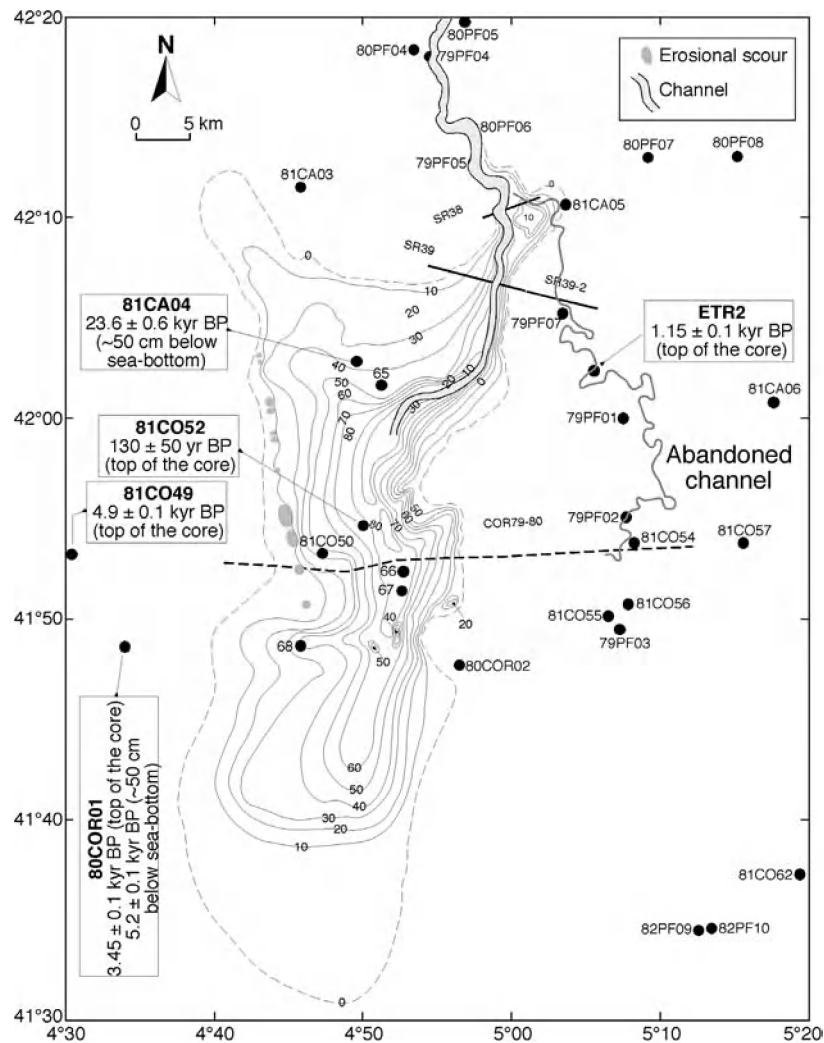


Figure 48. Isopach map of the Rhone neofan, core sites and ages obtained from selected core samples (Torres et al., 1997).

described several sizes of scours, the biggest being close to the neochannel and the smallest being in a more distal position, in relation with the decreasing power of the currents.

Torres et al. (1997) published the first isopach map of the neofan and distinguished a single unit of elongated shape of maximum length of 80 km, maximum width of 36 km and maximum thickness of 80 ms (Fig. 48). The total volume was estimated to be 27 km³. Gaullier et al. (1998) also published an isopach map and distinguished also a single unit estimated to be 60 km long, 20 km wide and 80 ms maximum thickness. The total volume was estimated to be 24 km³.

Recently obtained swath bathymetry, seismic and coring surveys of the area (Marion cruise from IFREMER, MD123-

Geosciences cruise from IFREMER/IFRTP, GMO2-CARNAC cruise from IFREMER, Progres cruise from UBO-IFREMER) provided a better insight of the neofan surface morphology (Fig. 49), internal structure and composition (Bonnell et al., 2005). The surface morphology and backscatter revealed a thicker right levee shaped by sediment waves probably related to sediment spillover from the neochannel. In the southern part of the area several small secondary channels may represent the beginning of the distal lobe of the Rhône neofan (Fig. 49). The scour holes, west of the channel, incise a planar area. They are semi-circular to elongate along a NW-SE direction. The width of scours range between 1 and 2 km while their lengths range from 1 to 5 km. The longest

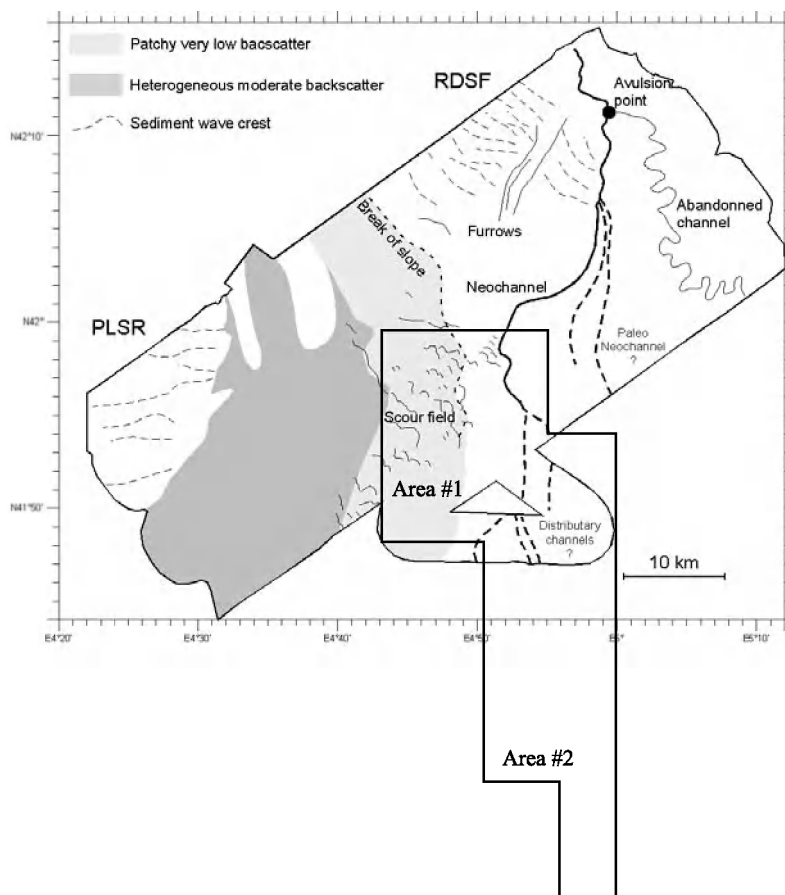


Figure 49. Bathymetric and backscatter features of the Rhone neofan (Bonnell et al., 2005). Location of the areas surveyed by MAK1 sidescan sonar on TTR-14 Leg 3.

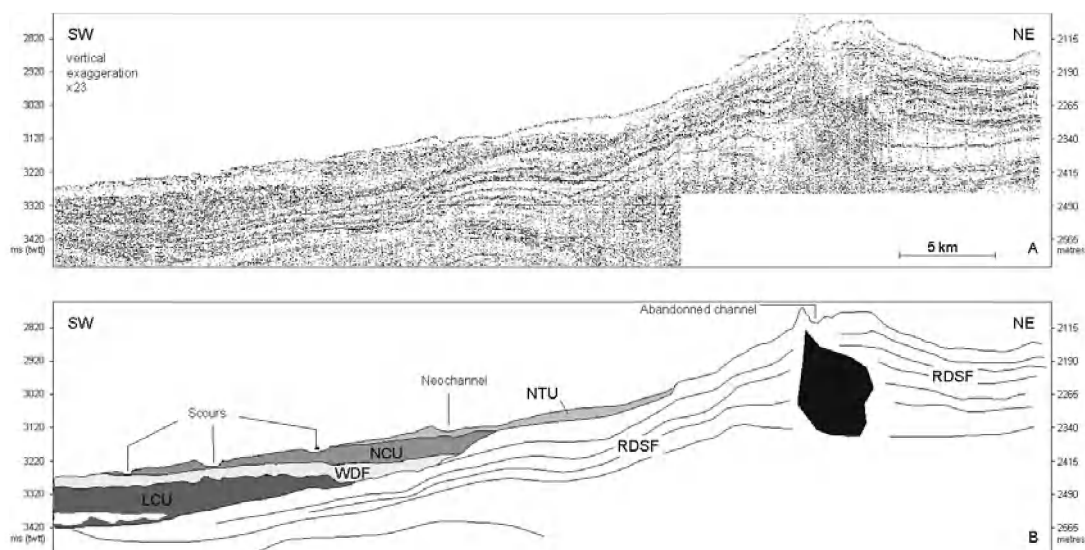


Figure 50. Seismic line across the Rhone neofan and the abandoned channel (Bonnell et al., 2005). See text for explanation.

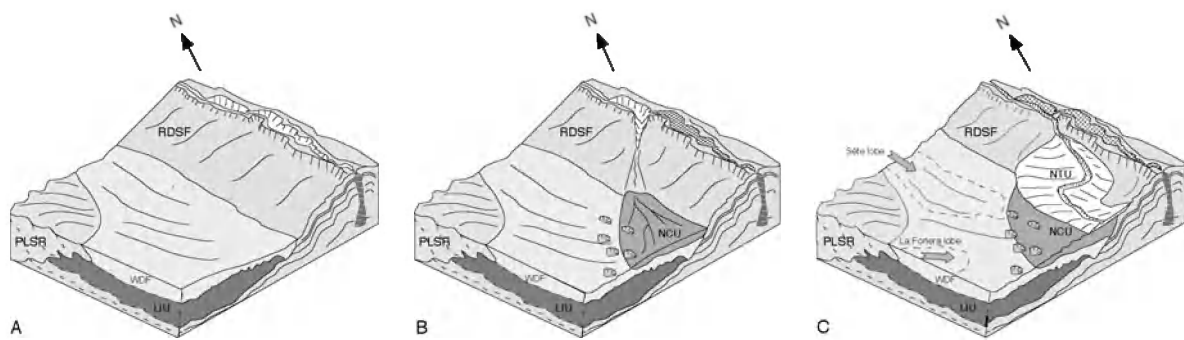


Figure 51. Scheme for the depositional sequence of the Rhone neofan (Bonnell et al., 2005).

scours are coalescent. A characteristic feature is the asymmetry of these scours. Their north-eastern flank is steep and their south-western flank is gentle. The average depth is about 10 m. The overall surface of scours in the mapped area is about 20 km² and the volume of eroded sediment about 0.20 km³. The internal structure revealed that the neofan is actually composed of two subunits (Fig. 50 and Fig. 51). A lower unit, the neofan chaotic unit (NCU), corresponds to the seismic facies described by previous authors, and the upper unit, the neofan transparent unit (NTU), is of channel-levee shape. This two-stage construction fits well with the model admitted for channel avulsions (Flood, 1991). The NCU corresponds to a HARP (High-Amplitude Reflection Packet), interpreted as the product deposited during the retrogressive erosion of the channel upstream of the avulsion point. The NTU corresponds to the aggradational channel-levee stage following the end of erosion in the channel. A sediment core from the right levee of the neofan revealed fine-grained turbidite sequences interpreted as deposits from spillover processes from the neofan channel. The turbidite facies are overlain by hemipelagic sediment, showing that the neofan channel is presently inactive. The base of the hemipelagic drape is dated at 15.1 ky BP (radiocarbon) (Bonnell et al., 2005). Since that date the area received up to ten fine sand layers (Bonnell et al., 2005) that are believed to have transited via the canyon network and whose source may be unstable sand banks at the canyon heads (Berné, 2001). Low backscatter patterns,

observed on 12 kHz swath bathymetry and interpreted as surficial deposits from the Sète canyon network and La Fonera canyon (Droz, 2001) may be the acoustic expression of these sand layers.

III.3.2. Objectives on the Rhone fan

Our study deals with the submarine turbidite channel termination and the sedimentary processes and deposits associated with the transition of turbidity currents from a confined to an unconfined environment. During this transition turbidity currents undergo severe changes of their hydrodynamic characteristics that may produce various depositional and/or erosional processes. These particular areas are named Channel-Lobe Transition Zones (CLTZ) (Wynn et al., 2002) or Channel Mouth Lobe (CML) (Klaucke et al., 2004), mainly because lobe shaped bodies are commonly found at the termination of the turbidite channels.

One objective was to obtain a comprehensive 30 kHz sidescan sonar map of a scoured area (study area #1 on Fig. 49) located southwest and south down the neochannel. These scour holes are already partly documented (Limonov, 1993; Kenyon et al., 1995; Wynn, 2002) and display complex backscatter patterns that will be better understood by a sidescan sonar mosaic. While the scours are a striking feature on the bathymetric map, the product of the erosion remains invisible, even on the acoustic backscatter. The sidescan sonar mosaic should allow identification of these deposits

if they are present. The giant scours surveyed during the TTR-2 cruise do not show any filling (Kenyon et al., 1995), suggesting that these were created at a very late stage of the neofan built up. We wish to know if this is the case for all the scours and if there were several episodes of scouring.

A second objective is to map the termination of the neofan channel (study area #2 on Fig. 49). A lobe shaped pattern on EM300 backscatter suggests that a terminal lobe could lie at the mouth of the neofan channel. A MAK mosaic should constrain the morphology and upper internal structure of this suspected terminal lobe.

III.3.3. MAK-99MS to MAK-107MS sidescan sonar and profiles

V. CATTERAL, A. MICALLEF, P. FERRER, S. COSTA,
D. AMBLAS AND C. BROENNIMANN

The mosaic of nine lines covers an area of approximately 422 km². The lines are orientated north-south and cross the Rhone neofan (Fig. 52). The following four types of feature are present on the mosaic:

Channels

Most of the channel features are on MAK lines 99MS, 100MS and 101MS, although smaller and isolated channels are also located on MAK lines 102MS, 103MS and 104MS. The most discernible element is a number of distributaries flowing south and southeast from the main channel near to 41°58N and 4°54E (Fig. 52). This channel is the main Petit-Rhone neochannel, and has an initial channel width of 1.3 km, which it maintains for a length of 4.6 km. It is sinuous and reaches a depth varying between 10 m and 20 m. The bed of the channel is flat, underlain by up to seven reflectors, indicating a relative transparency of the sediments. The channel banks on the western side of the channel have a gentle but slightly uneven surface that is crossed by a number of smaller sinuous channels. This body of sediment is underlain by up to 20 reflectors, which indicates a more transparent sedimentary body.

It should correspond to the same depositional events that emplaced the sediment in the main channel, as the reflectors of both features are continuous.

At 41°53N and 4°53E the main channel splits into six distributary channels, with a channel width that varies from 77 m to 230 m. Four of these channels merge into one at 41°51N and 4°53E. The channel reaches a maximum width of 770 m and is divided into two by a depositional sediment bar in the middle of the channel. The channel flows southwest and is also asymmetric, with the eastern bank showing evidence of terracing. It separates into two channels at 41°50N and 4°52E. The one to the east flows sinuously southwards. It is asymmetric although the banks are less clearly defined than for the previous channels, with evidence of terracing and mass movement identifiable along most of its length.

On the eastern bank, at 41°48N and 4°53E, the channel moves into an elliptical slide scar some 2 km long and 1.3 km wide. The surface is traversed by a number of parallel and irregular channels that in some areas reach a depth of 15 m. Reflectors underlying this scar are few and only 5 m deep. Another shorter channel flows into the scar area. It is thought that the former channel is younger than this second one because it flows regularly for a longer distance. The slide scar is thought to have occurred between the two channel cutting episodes and may have disrupted the regular flow of the older one. The western channel, on the other hand, is up to 1000 m wide, flows south in a less sinuous fashion, and displays a braided character whereby the channel banks have a very irregular form as does the channel bed.

West of this complex of channels is a very similar network of channels. Here the channels only reach a maximum width of 230 m. The eastern channel flows towards the southwest in an almost straight line for almost 6 km, and has a very smooth channel bed. The western channel is identical, apart from the fact that at 41°51N and 4°50E, another distributary flows southwards through the eastern bank. This channel is 615

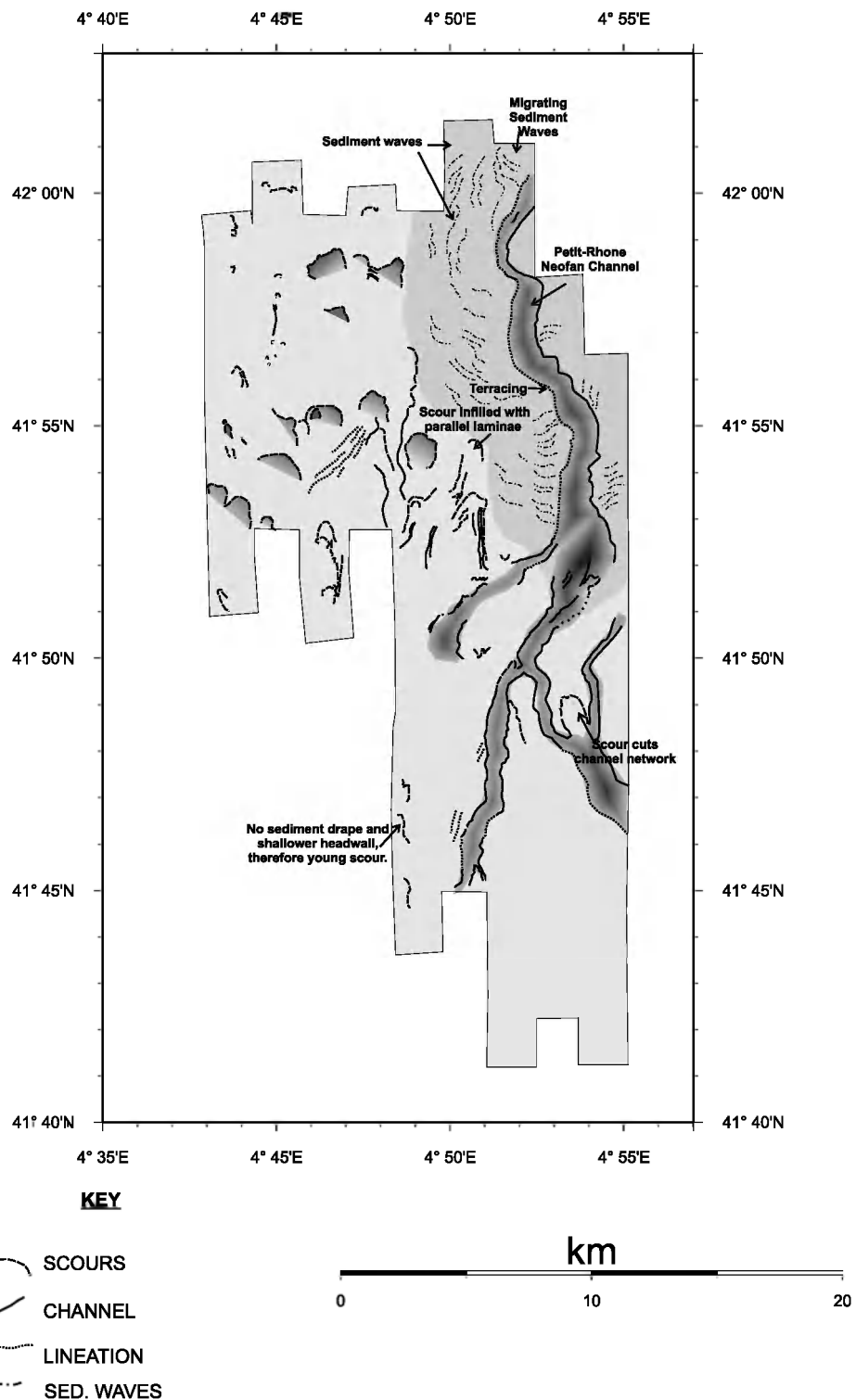


Figure 52. Interpretation of MAK-1M acoustic mosaic.

m wide and distinguished by a rougher channel bed and irregular channel banks, very similar to the braided pattern mentioned earlier.

At 41°50N and 4°54E, to the east of all

the channels that have been described, there is another channel that flows southwards for 4400 m in a slightly sinuous fashion. It is 385 m wide, with a smooth channel bed and banks. The point where this channel starts is

difficult to identify, although it can be seen that it converges with the depositional sediment lobe described earlier at $41^{\circ}48'N$ and $4^{\circ}53'E$.

To the south of this whole complex of channels is an area towards which all the channels seem to flow. It covers up to 88 km^2 of almost flat sea bed, with very few reflectors being located in the upper 5 m.

An unusual feature at $41^{\circ}54'N$ and $4^{\circ}50'E$ is a scar from which a 230 m wide channel flows straight and to the southwest.

At $42^{\circ}0'N$ and $4^{\circ}52'E$ a break in the levee leads to a new network of channels in the north central part of the mosaic. The direction of flow is to the southwest and the width is 230 m. The channels are shallow and there are no levees on the banks. At $41^{\circ}59'N$ and

$4^{\circ}50'50''E$ the channel turns southwards over a complex topography and at $41^{\circ}58'N$ and $4^{\circ}50'50''E$ the channel continues flowing southwest to reach the scour complex.

Sediment waves

The main over-bank area mapped on the sidescan mosaic is covered with sediment waves (Fig. 52). The wave field is bounded by the neofan channel and the scoured area is located between $42^{\circ}01.5'N$ and $41^{\circ}53.0'N$ of latitude, and $4^{\circ}50.0'E$ and $4^{\circ}53.0'E$ of longitude. The northern limit of the over-bank area has not been covered by this survey.

These over-bank deposits are well seen on line MAK-101MS (Fig. 53). The waves have a wavelength of 250 m and a maximum

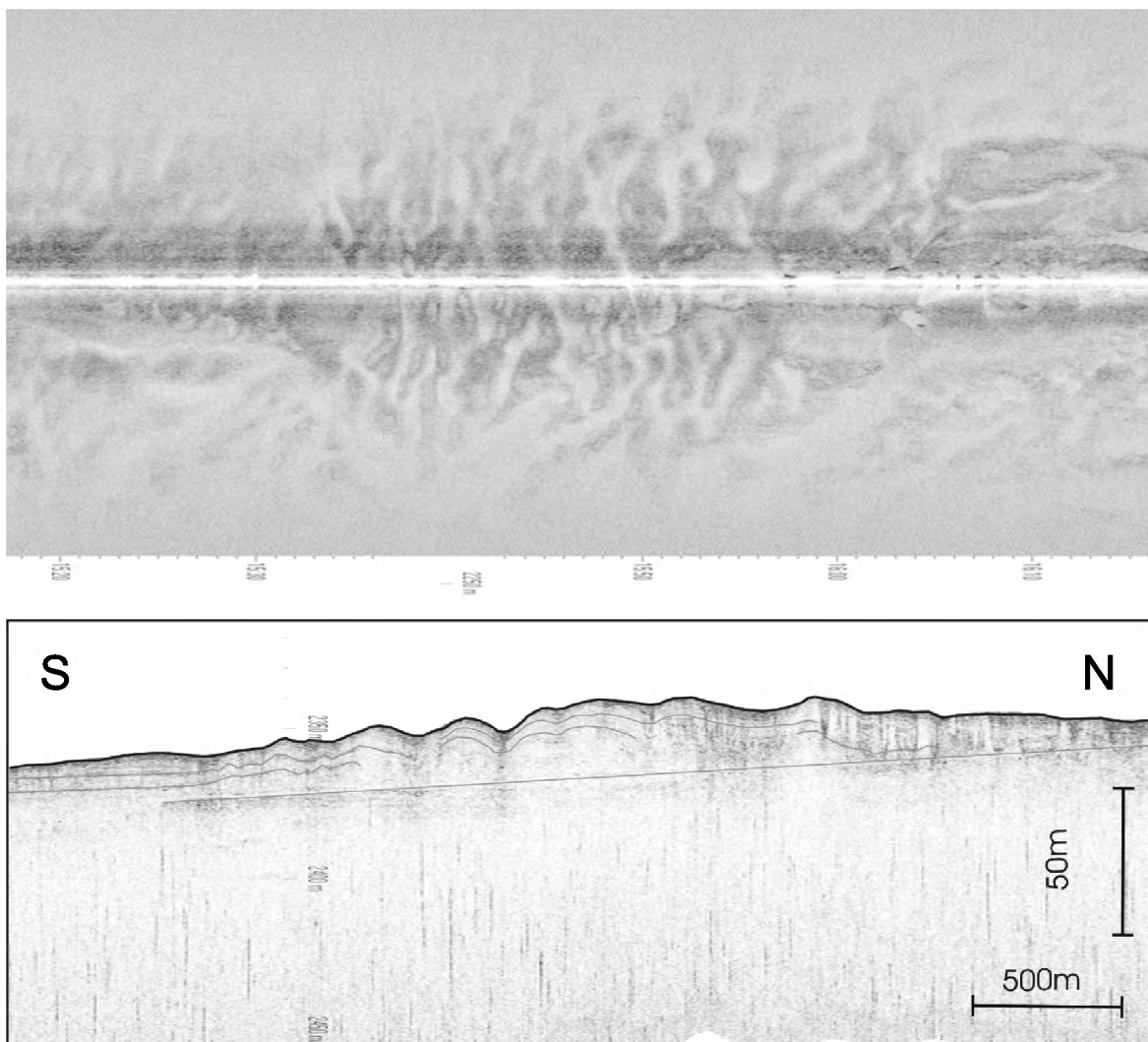


Figure 53. Fragment of line MAK-101MS showing sediment waves developing beyond a channel bend.

amplitude of about 8 m. The wave amplitude decreases down-slope and the waves are roughly asymmetric, with a steeper northern flank.

The seismic facies has high amplitude, continuous and parallel reflectors. The maximum thickness of this deposit is about 30 m, decreasing southwards to 15 m. This seismic facies has a planar high amplitude reflector at its base.

These morphologies are interpreted to result from over-flow processes related to the neofan channel dynamics. The waves are transverse to the main flow direction. The southwards decrease in amplitude is due to the flow losing competence.

Scours

A large number of scours are mapped. Two different types of scours have been differentiated. The area covered by lines 99 to 102 has shallower scours that are followed by a channel. The area of lines 103 to 105 has large scours that are not followed by channels. The 10 m to 20 m of layered deposits beneath the scours are believed to be neofan deposits.

Shallow scours.

These have a regular horseshoe shaped

headwall and are connected to longitudinal low backscatter features, possibly channels, that run downslope out of these erosional scours (Fig. 54). The scour width ranges from a few hundred metres to up to a kilometre. The overall slope in the area of these features is less than 1° (0.3° was measured on line 102). The scours are only a few metres deep.

Deep scours.

The overall gradient of the section shown in Fig. 55 is only 0.1°. The walls of the scours are steep and have an average angle of headwall slope in a range from less than 10° up to 40°. Some scours are symmetrical but most have a headwall steeper than the downflow wall. They are up to 20 m deep and have a length from 100 m up to more than a kilometre. The plan view of the headwalls is irregular but mostly close to crescentic. Some of them have a complex shape and seem to show different generations. In Fig. 55 the scour in the top left corner seems to be created later on top of the “M-shaped” scour. In places the scours reach a density of almost one per square kilometre. The scours seem to have no sediment fill.

The origin of these erosional scours is not well understood. They are thought to be related to recent turbidity currents. Because of a change in slope upstream, on the eastern

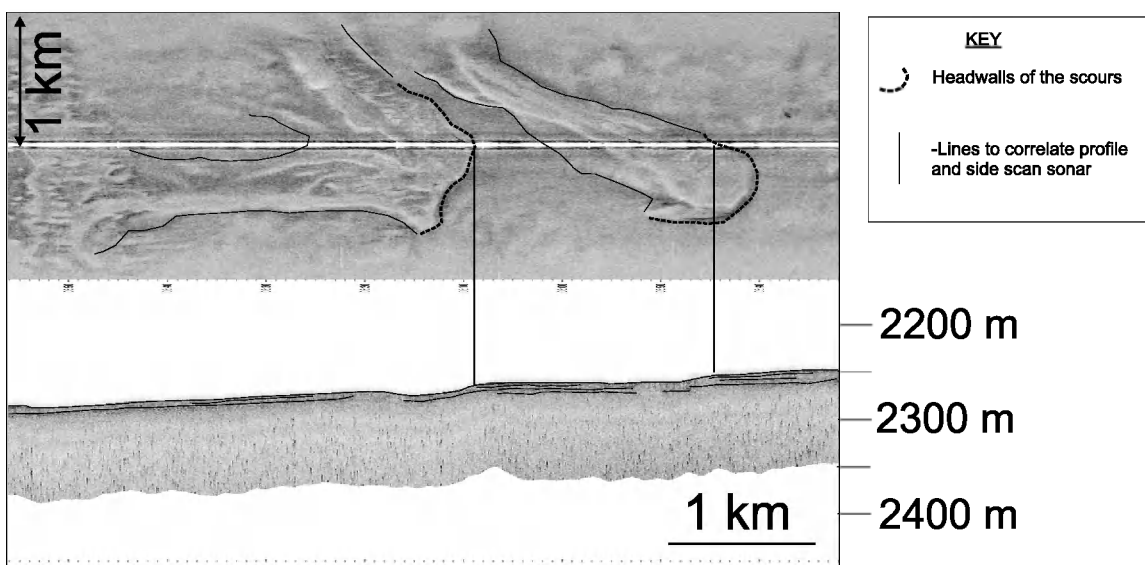


Figure 54. Fragment of MAK-1M line showing an example of the shallow scours.

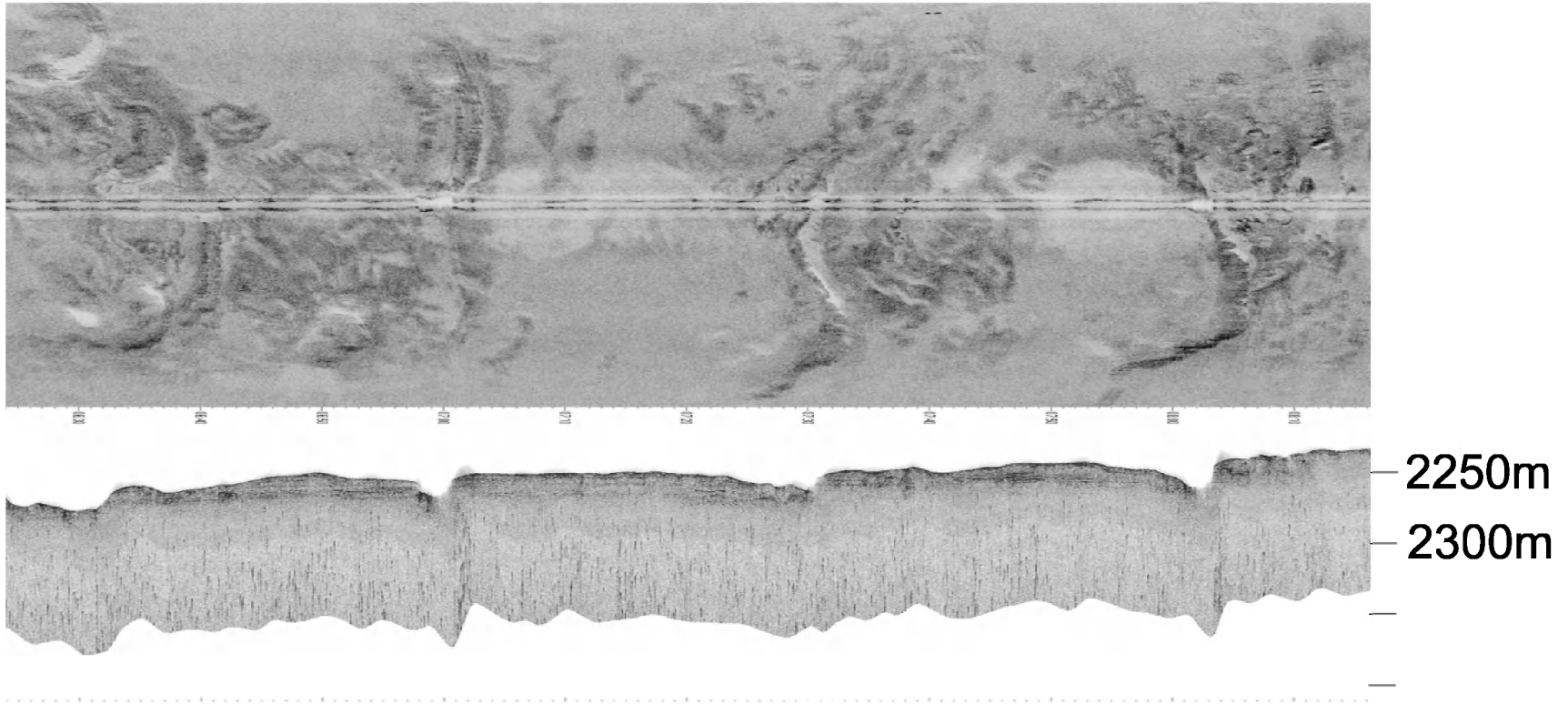


Figure 55. Fragment of MAK-1M line showing examples of the deep scours.

levee of the Rhone neofan, the current may become much more turbulent. This turbulence could explain the deep erosion into the sediments with a low slope. Deep scours were already known from here (Kenyon et al., 1995) and were interpreted as features connected with a high energy flow connected with a break of slope and with the expansion of flow as it leaves the Rhone neofan channel. The shallow scours were not known before.

Alternative scenarios are that: 1. the shallow scours could result from smaller flows with less energy than those which have created the deep ones. 2. the deep scours could be more developed features than the shallow scour type. The shallow scours would form at the initial stage of seafloor scouring by a bypassing turbidity flow.

III.4. The Cap de Creus Canyon system

III.4.1. Introduction

D. AMBLAS

The Cap de Creus Canyon lies offshore of the eastern limit of the Pyrenees and is the westernmost canyon in the Gulf of Lions. It belongs to the Pyrenean canyon system, which from west to east also includes the canyons of Lacaze-Duthiers, Pruvot, Aude, Hérault and Sete.

The 95 km long Cap de Creus Canyon has a WNW-ESE general trend. Its head is located 5 km northeast of Cap de Creus and ends as a hanging valley of the southeastwards oriented Sete Canyon. The Cap de Creus Canyon head and upper course are deeply cut (up to 750 m) into the continental shelf. Upper canyon walls reach slope gradients of up to 23°. Recently conducted swath-bathymetric mapping has revealed a modern narrow inner axial incision or thalweg channel. A prominent slope break at a depth of about 1600 m marks the widening of the canyon, at a place where depositional processes are assumed to become dominant. Large levees are seen in the most distal sector, mainly on the southern flank, which indicates the relevance of this canyon as an active sediment conveyor to the deep basin.

Thus Cap de Creus Canyon is one of the main feeders of the fan-like deposit known as Deep Pyrenean Canyons Sedimentary Body (Canals, 1985), or the Pyreneo-Languedocian Ridge (Berné et al., 1999).

The genesis of the Cap de Creus Canyon is likely related to a NW-SE right-lateral transfer fault system called the Catalan Transfer Zone (Berné et al., 1999; Mauffret et al., 2001). The presence of this tectonic structure led to the development of the canyon system, which was fed by sediments coming from Pyrenean rivers. This canyon pre-existed the Messinian salinity crisis, when it probably was further entrenched by subaerial erosion related to the drying up of the entire Mediterranean Basin. Sediment trapping and downslope transfer efficiency were enhanced during Quaternary sea-level lowstands (Canals, 1985; Berné et al., 1999). Headward and sidewall erosion induced by downslope-eroding sediment flows contributed to enlarge the canyon both along and across strike (Pratson and Coakley, 1996).

The hydrographic setting of the Gulf of Lions enhances the role of the Cap de Creus Canyon as the main sedimentary conduit located at the westernmost end of the system. The Northern Current flows southwestwards along the continental slope following the isobaths. When canyons interfere with the path of the Northern Current, up-canyon/down-canyon circulation cells develop because of the current entry into the canyons. The proximity of the Cap de Creus peninsula to the canyon head creates a promontory effect that helps funnel flow towards the canyon head. Therefore, the modern Cap de Creus Canyon is suspected to be the most active of all Pyrenean canyon system.

The deep-towed sidescan survey of the whole Cap de Creus Canyon system was intended to improve knowledge of both tectonic and sedimentary processes from source to sink.

III.4.2. MAK sidescan sonar data

A. AKHMETZHANOV

A series of MAK-1M profiles were run along the axis of the Cap de Creus Canyon for almost 200 km from an area just below the shelf break down to the basin plain where it connects with the Rhone neofan survey (Fig. 38). Two of the lines were acquired to the south of the canyon axis covering several large features observed on the multi-beam bathymetry in order to evaluate slope instability processes.

Line MAK-112MS is the uppermost one starting about 9 km downslope from the canyon head and running down the slope from 400 m to 900 m waterdepth. The beginning of the line shows a gentle bend of a 1.3 km wide sinuous thalweg. According to the multibeam data this area is the junction of several tributaries forming the head of the canyon. The inner part of the bend has a smooth appearance on the sonograph and almost no penetration on the subbottom profiler record. There are subtle variations of the backscatter, with a repetitive pattern of linear features transverse to the thalweg axis which could represent sediment waves built of coarse grained material. The outer part of the bend seems to be rougher, probably due to scouring. The profile shows that the seabed is eroded and a 500 m wide and 20 m deep channel is seen. Good penetration under the channel's floor suggests that there are no accumulations of coarse material and gravity flows are eroding underlying sedimentary rocks. To the north and south of the channel a spectacular seabed lineation is seen (Fig. 56). The pattern is produced by numerous closely spaced narrow furrows, which are 20-30 m wide and up to 3 km long. From their shadows it is estimated that they are up to 4 m deep. The profile shows an up to 10 m thick sedimentary unit with poor subsurface penetration probably due to scattering of the acoustic energy over the rough seafloor. According to the multibeam data the bedforms develop on the flatter areas along channel banks and are likely to be furrows produced by overbanking turbidity flows. In

places the furrows are parallel to the channel course while in others they converge towards the channel. This usually happens when slopes become steeper and, as a result, overbanking flows are redirected into the channel. Interestingly, downstream from the places where the seabed lineation converges into the channel, the seafloor is scoured, suggesting a sharp increase of flow energy. At the depth of 900 m the channel is about 40 m deep and remains erosional.

Line MAK-113MS is mostly along the channel within depths of 900-1170 m. The channel maintains a width of about 400-500 m. A crosssection at the depth of 1050 m shows that the channel floor becomes aggradational with a possible coarse sediment infill, as penetration on the profiler record is limited and the profile shows a sediment wave field along the northern bank of channel. The waves have a wavelength of about 360 m, height of 10 m and form a well-stratified sequence up to 50 m thick. On the sonograph the waves have uniform low backscatter and their surface is decorated by a very fine lineation, which probably also represent furrows left by overbanking flows. According to the multibeam data the development of the sediment wave field begins once the channel enters the broader portion of the canyon with a gentler northern flank.

Line MAK-114MS also follows the channel axis which now runs in a west-east direction. The channel is about 50 m deep and is poorly expressed on the sonograph as its flanks become less steep and do not produce distinct reflections and shadows. The seabed is scoured and furrows are seen on both flanks, although they are more pronounced on the southern one. The profile shows that furrows are usually associated with outcrops of acoustically transparent units, which are interbedded with high amplitude reflector packages. These acoustically transparent units may represent intervals of soft material with high erodibility, e.g. clays.

At the end of the line the channel depth increases to 70 m. On line MAK-115MS this incision results in the northern flank becoming unstable and sediment failures develop. Several slides are observed as arcuate fea-

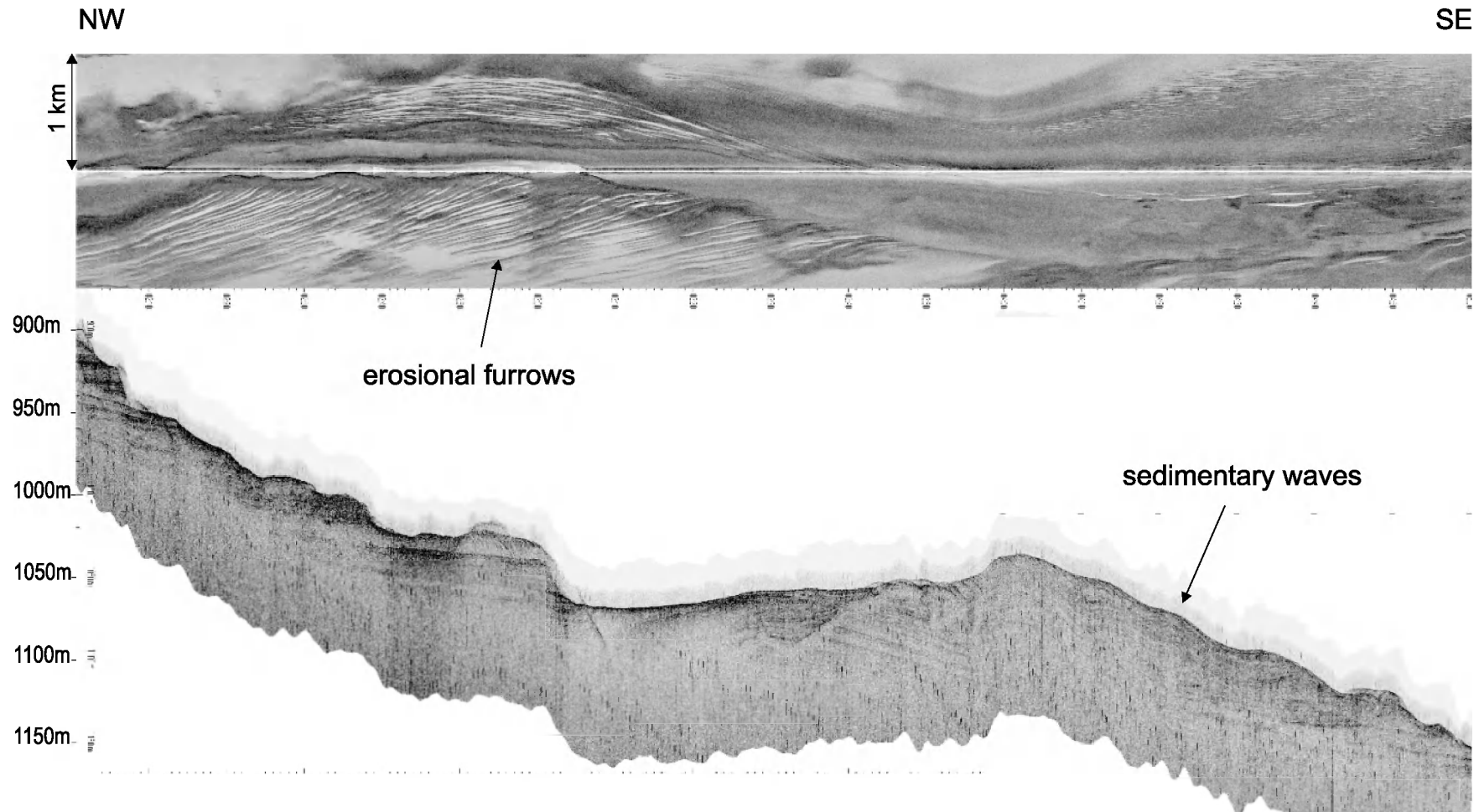


Figure 56. Fragment of the line MAK-113MS. Sinuous channel cutting the Cap de Creus Canyon floor. Fields of erosional furrows have developed on both flanks of the channel. Profile shows sediment waves developing on the channel levee.

tures with highly backscattering headwalls and a wrinkled pattern due to compression ridges. Downslope the channel disappears to the south and the line runs through a field of sediment waves. The waves are up to 30 m high and the profile shows that their slopes are sometimes effected by failures and associated debris flow deposits can be seen as chaotic lens-like bodies incorporated in the acoustically well-stratified sequence. The channel is crossed by the line again at the depth of 1550 m. It broadens up to 1 km and is 50 m deep. Truncated reflectors are seen on both flanks with a southern one being steeper and terraced. The channel floor has a patchy pattern of medium to high backscatter. The profiler shows that both deposition and erosion take place. There is a transparent lens-like body within the channel infill, which is probably a debris flow deposit resulting from a flank collapse. Several faults are seen along the channel flank suggesting that gravity flows are exploiting a weak zone. The channel forms broad levees. The line crossed the southern levee and the profile shows a well-stratified sequence up to 70 m thick. A sharp bend of the channel is

crossed at the end of the line at the depth of about 1670 m. It occurs where the channel negotiates a local basement high seen on the multibeam bathymetry map. The channel is almost 1.5 km wide and several low backscatter patches are seen on the sonograph which are characterised by poor penetration on the profiler record. This may be due to sheets of fine-medium sand covering the seabed.

Line MAK-111MS follows the channel further down the slope along an almost flat portion of the seafloor at the depth of about 1670 m. The channel becomes broader, up to 2.5 km, and is about 15-20 m deep. The profile shows a 20 m thick sequence filling the channel, with the upper 10 m being almost transparent and the lower part well stratified with continuous parallel reflectors. On the sonograph the floor of the channel has low to medium backscatter and at some places is characterised by a pattern of fringes of low and medium backscatter (Fig. 57). They are usually seen at some distance from the fish track and the pattern could be produced by interference within superficial layers of interbedded mud and sand layers, of near

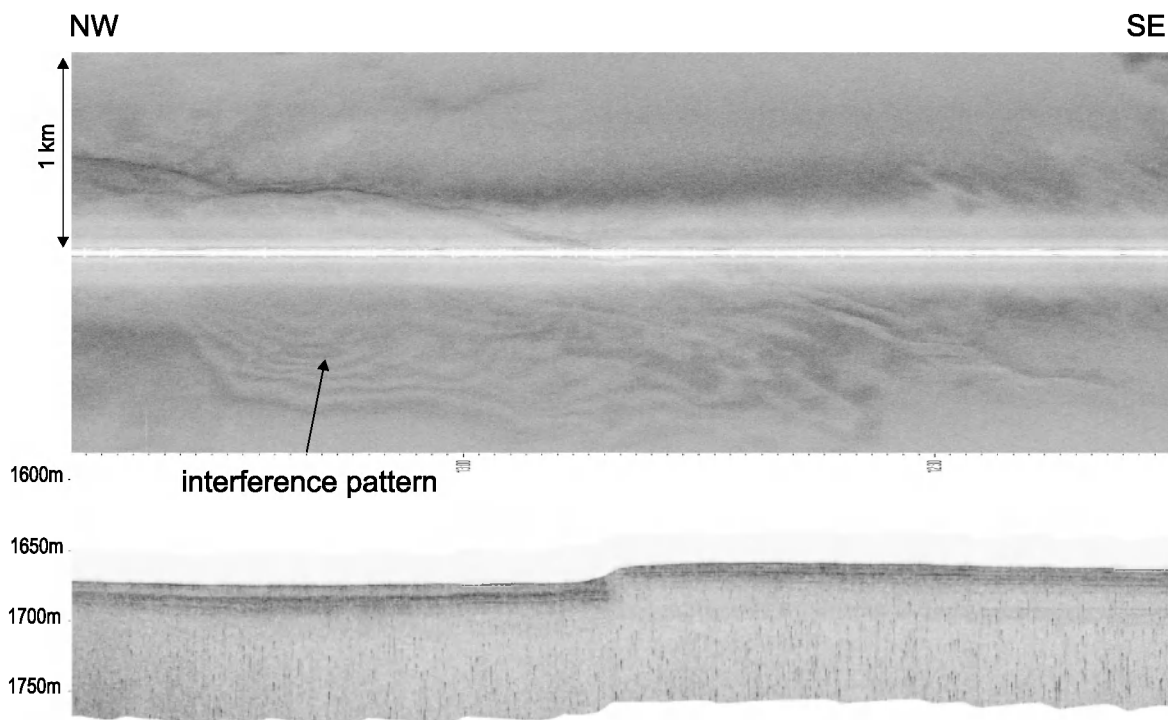


Figure 57. Fragment of line MAK-111MS showing a pattern of interference fringes, an acoustic artefact in thin, parallel layers on the channel floor.

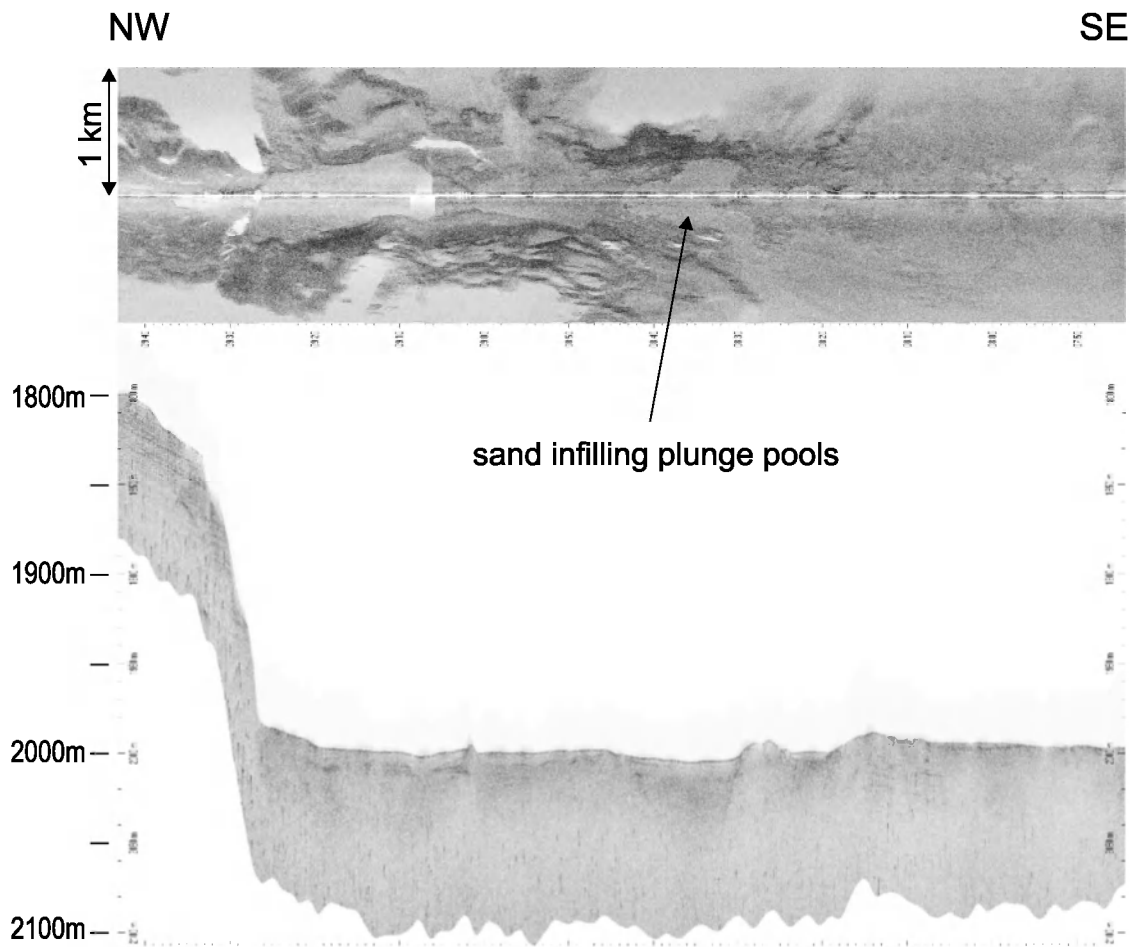


Figure 58. Fragment of line MAK-110MS across the site where the Cap de Creus channel enters the Sete Canyon. The seafloor has rugged topography due to severe erosion of basement outcrops and possible sandy deposits infilling the deeps.

constant thickness, infilling the channel. In places the walls of the channel are steeper as a result of sliding and associated 3-5 m thick debris flow deposits are seen at the foot of the walls.

The end of the line and most of the line MAK-109MS runs across a 180 m high escarpment marking the place where the channel enters the lower reaches of the Sete Canyon. The sonograph shows that the escarpment and the base of the escarpment have a complex pattern of medium to high backscatter areas due to the presence of basement outcrops and rough topography which are observed for almost 4 km further down the slope from the escarpment (Fig. 58). The outcrops are confined within a gentle, 10-15 m deep depression which could be a plunge pool eroded by gravity currents cascading

down the escarpment. The deeps have flat floors characterised by low backscatter, which suggests that they are filled by sandy deposits. The flat seafloor at a depth of almost 2000 m immediately beyond the outcrops is the floor of the Sete Canyon which also is characterised by limited penetration on the profiles.

Line MAK-109MS runs almost along the axis of a broad valley emanating from the Sete Canyon which is a conduit for sediment transport further down to the basin plain. At the start of the line a portion of the levee complex, with at least 50 m of well stratified overbank deposits, is crossed. The top of the levee is severely eroded and giant scour marks up to 1 km across are seen. Partially buried by the overbank deposits is a 30 m thick, chaotic complex. This chaotic interval

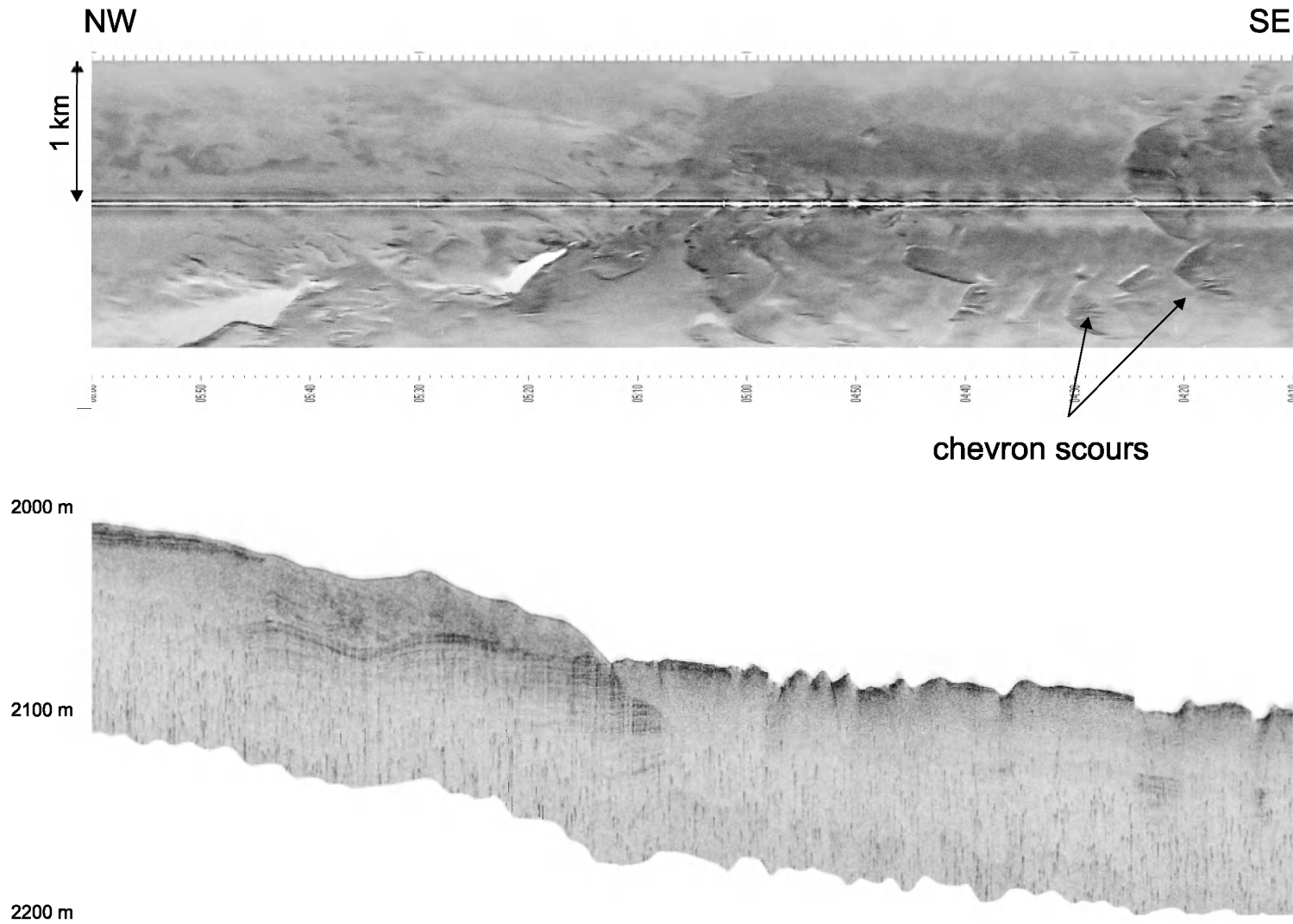


Figure 59. Fragment of line MAK-109MS across the flank of the valley beyond Sete Canyon, showing a partially buried chaotic complex, erosional surface filled with valley deposits and chevron scours on the valley floor.

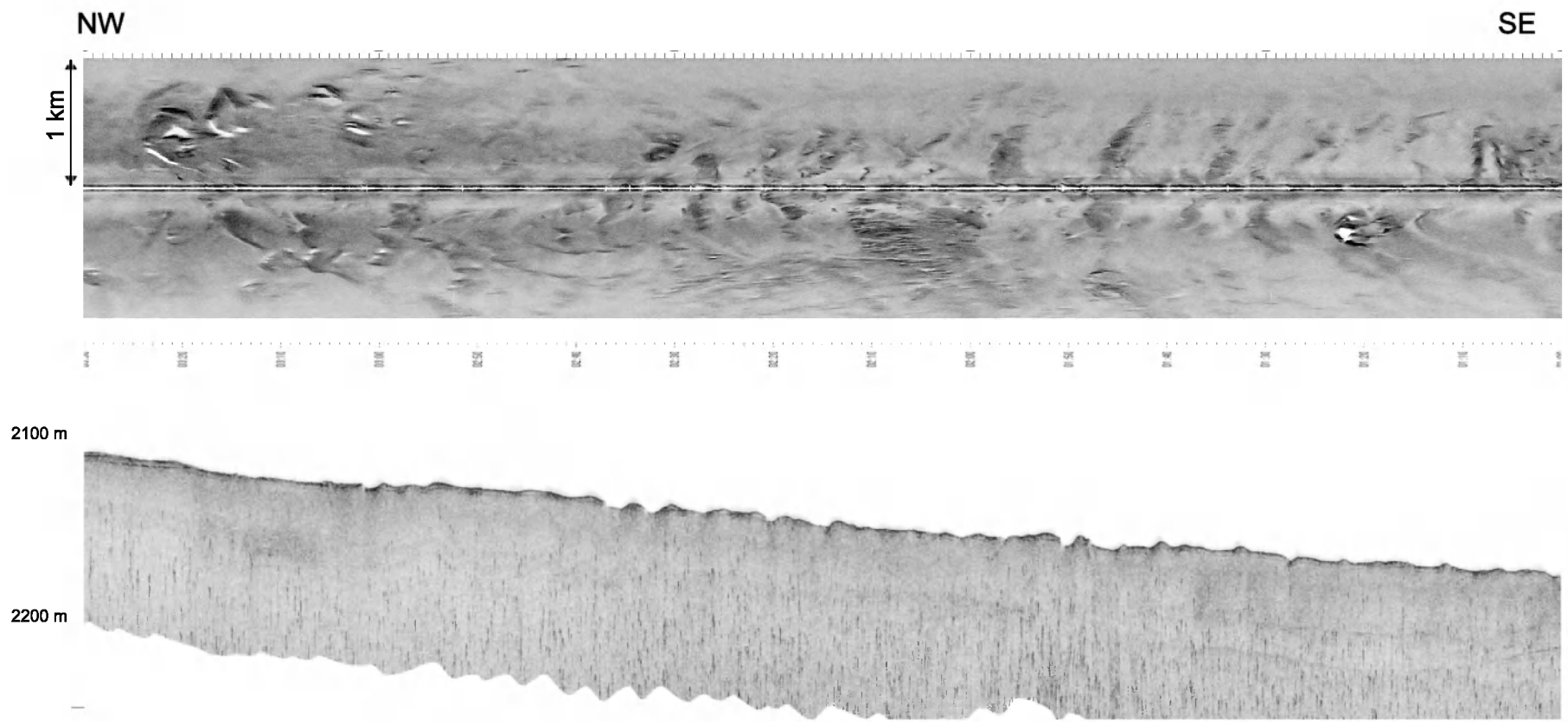


Figure 60. Fragment of line MAK-109MS showing a field of scours, thought to be produced by a single event.

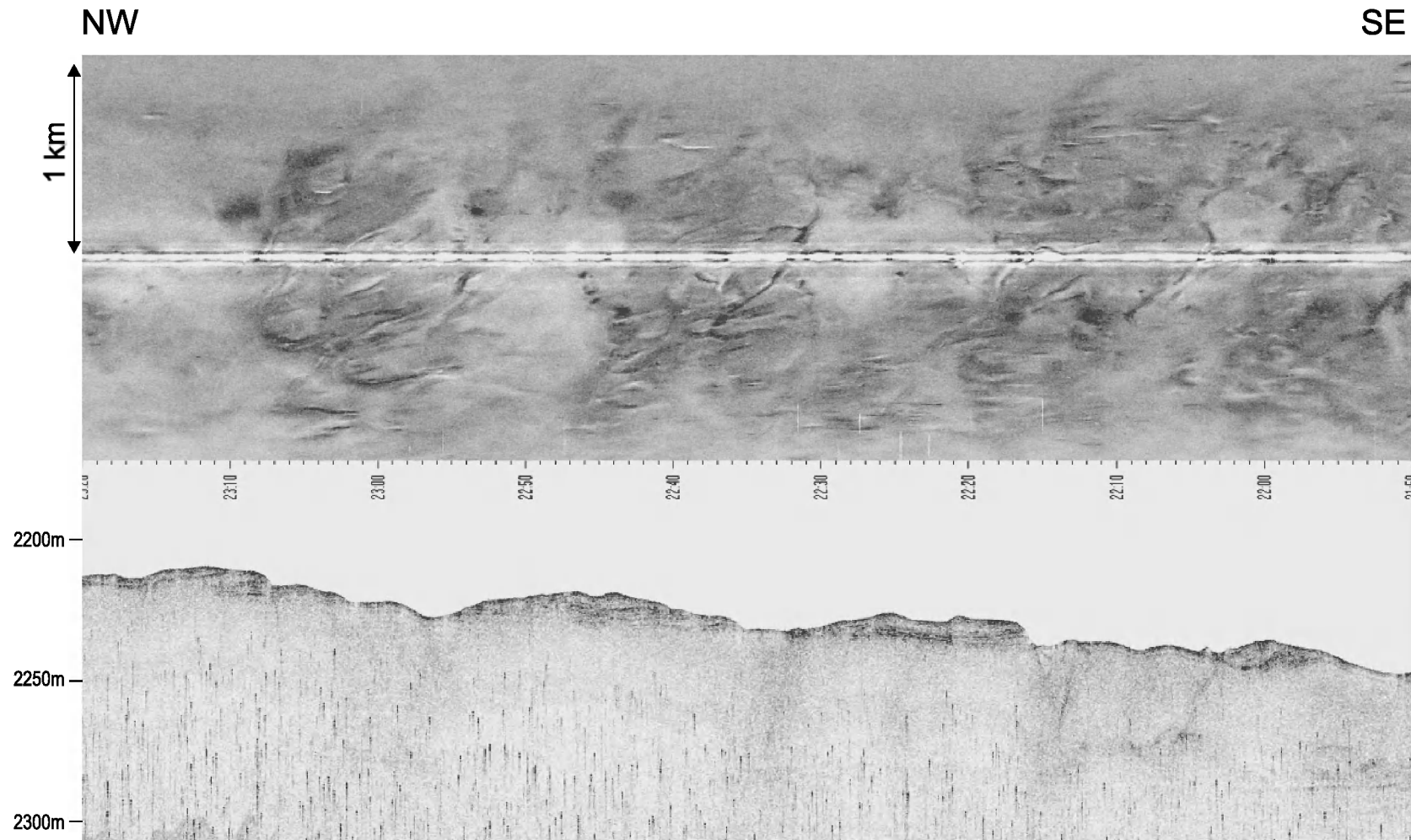


Figure 61. Fragment of line MAK-108MS across three giant isometric scours cut through a 10 m thick sedimentary cover.

is believed to be formed by a slide on the levee and, according to the multibeam data, left a 3-4 km wide arcuate scar situated to the north of the surveyed area. The valley is crossed further down the slope from the slide complex and its depth is about 50 m. The profile across the valley flank shows an erosional surface overlain by an almost 30 m thick valley infill sequence (Fig. 59). The character of the seafloor changes dramatically once the line runs along the valley floor which gently dips to the southeast from 2080 to 2200 m waterdepth. The seafloor has a complex pattern of medium to high backscatter features. They are depressions which come in various shapes and dimensions, from a few tens of metres and up to 1 km wide. One of the commonly observed shapes is chevron-like with a tip pointing upslope. There are also arcuate and elongate features, transverse to the slope direction. They are interpreted as giant, deep-water scours left by vigorous turbidity currents. They are up to 5 m deep and have a symmetrical box-shaped profile. The profile shows that most of the area is covered by a 2-3 m thick layer, beneath which the penetration is poor. However, underneath the scours, where this layer has been removed, penetration increases and the pre-valley well stratified sequence is seen at the depth of about 30 m. From its acoustic signature it is inferred that this layer is a sheet of sand. At one place the sidescan record is particularly interesting as it images scours which may be related to a single event (Fig. 60). The upslope part of the scour field has a large scour, 2 km long and 1.5 km wide, which may be an amalgamation of several small chevron-shaped scours. Downslope from this giant scour are a series of several chevron scours nested into each other. Downslope of the nested chevrons there is a slightly sinuous trail of transverse elongate scours. The width of the elongate scours increases downslope from 300 to 1000 m and the spacing between them increases from 300 m to 1.2 km. The length of the scours is constant at about 200 m.

Another type of scour is found further downslope along line MAK-108MS. They are almost isometric features, being 1-1.2 km

across and up to 10 m deep (Fig. 61). At least four of them are imaged and each is formed by amalgamation of several smaller, 200-300 m wide, scours. As the line runs oblique to the scour axis their along current profile is not clear. However they seem to be asymmetrical in across current direction, being deeper on the right hand side. The profile has a step-like shape and shows that scours develop in the 10 m thick acoustically stratified sequence with parallel to wavy reflectors. From the present data set is not clear whether this sequence represents the redeposited material from the scours or that this type of scour develops in the areas of the well-stratified sequence.

Another two lines were run to the south of those described above. They run upslope from east to west. The depth ranges from 1650 m to 450 m. The main objective of the survey was to identify slope instability features.

Line MAK-116MS runs across two 100-120 m high ridges. There is excellent penetration on the profile, down to over 70 m through a drape of hemipelagic sediment which covers the ridges. The western slope of the eastern ridge seems to be particularly unstable as there are truncated reflectors along a slip plane developing on the ridge flank. Several chaotic intervals at the base of the ridge represent debris flow deposits resulting from the flank failures. Sonographs show a band of medium to high backscatter along the failed flank, which is probably due to outcropping of older strata.

Line MAK-117MS runs across two cascading downslope mini-basins and the resulting profile has a stepped geometry. The steep part of the slope seems to be affected by small scale instability, though no slides were observed. A common feature are irregular patches of medium to high backscatter on the steeper slopes. Profiles show that there is a loss of reflector coherence within the upper 5 m of the sequence. The zone of poor coherence appears to have a basal high amplitude reflector. The formation of such a zone may be related to enhanced shearing within the sediments. Eventually these sediments may be transported through downslope channels.

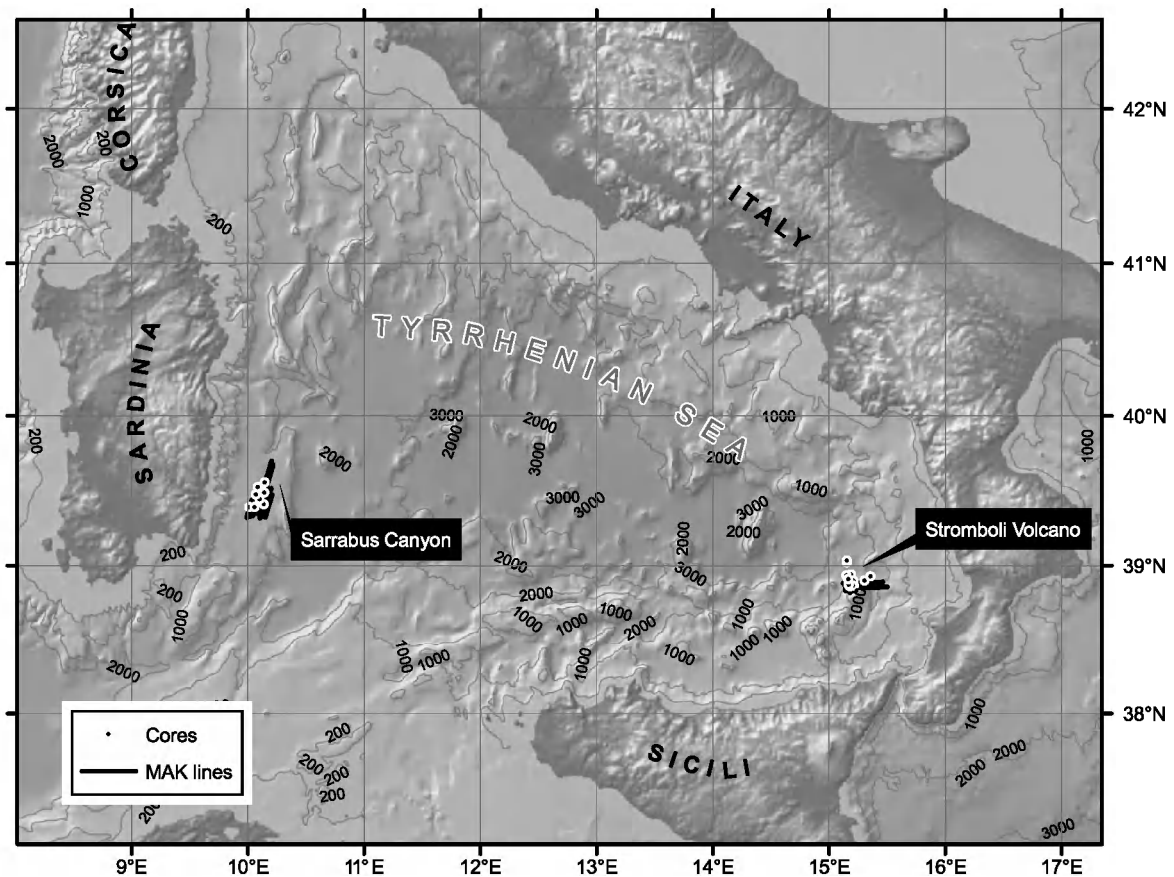


Figure 62. Location map of Leg 4 in the Tyrrhenian Sea.

An example of such a channel is seen within the medium to high backscatter field. It is about 50 m wide and up to 1.8 km long. The flat areas are featureless apart from one, which is a north-south lineation on the seafloor. The profile shows that a 5 m thick and 900 m wide chaotic body forms the upper part of the sedimentary sequence. There also seems to be another chaotic interval at the same place but at a depth of about 20 m. The source for this deposit is seen on the multibeam data as three overlapping arcuate slide headwalls to the north of the line. The most prominent slide, which is believed to be responsible for the most recent event, is located at a distance of 8 km from the track. To the east is another slide which could be the source of the buried chaotic complex. The lineation on the sonograph is interpreted as furrows caused by a turbidity current which was associated with the failure and arrived at the site after the debris flow.

IV. TYRRHENIAN SEA (LEG 4)

Studies during the 4th Leg in the Tyrrhenian Sea were concentrated at two locations (Fig. 62). The first study was of part of the depositional system of Sarrabus Canyon which develops on the southeastern Sardinian margin. The second study was of the large slope failures on the northwestern submarine flank of Stromboli volcano.

IV.1. Sarrabus Canyon

F. GAMBERI, M. MARANI, A. AKHMETZHANOV,
M. CARLINO AND S. DISTEFANO

IV.1.1. Introduction

The Sardinian margin has an upper (around 1700 m deep) intraslope basin, the Sardinian Basin, and a lower (around 2500 m deep) intraslope basin, the Cornaglia Basin (CB). They are separated by the Quirra structural high (QH) (Fig. 63).

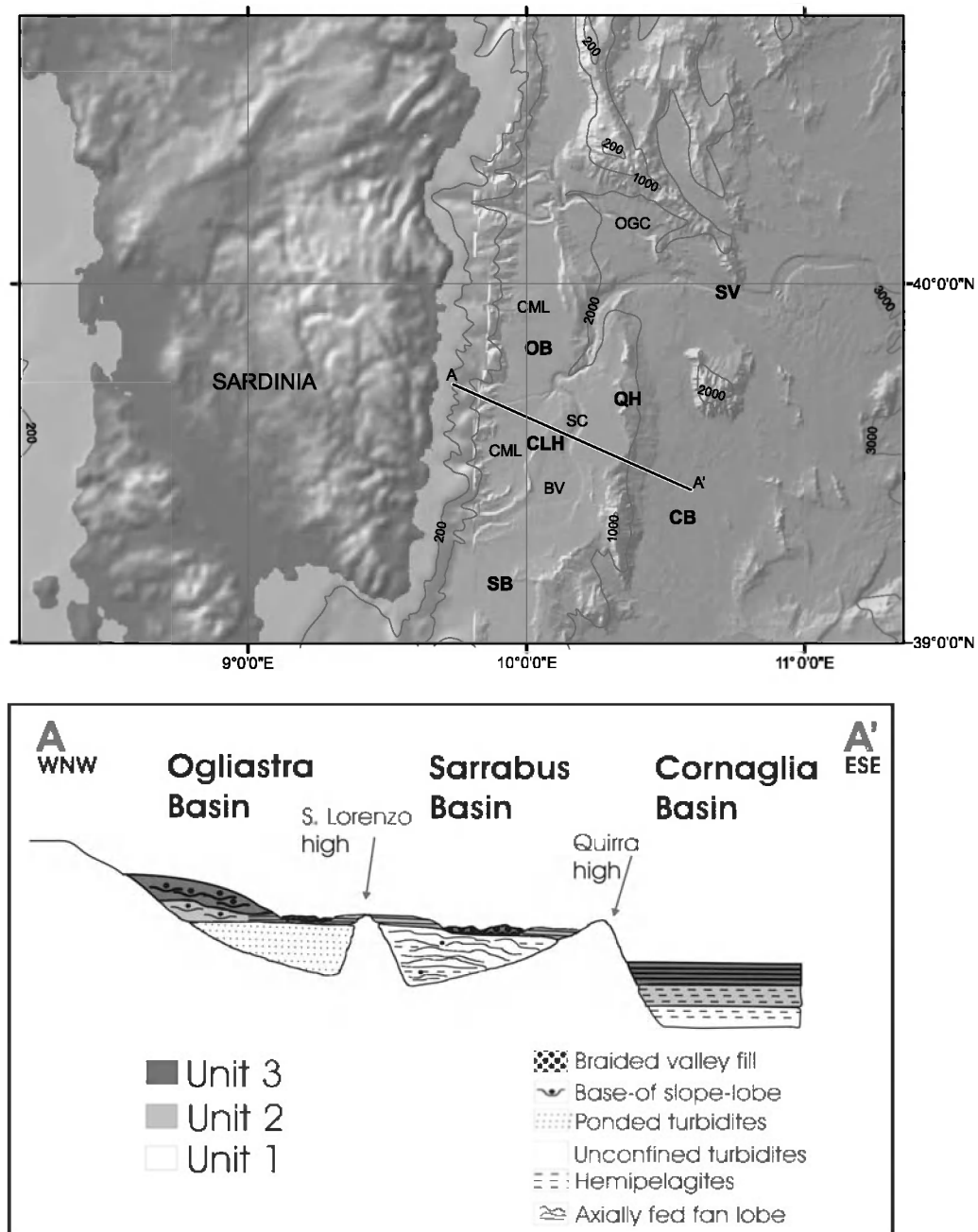


Figure 63. Main morphological features of the Sardinian margin and basin fill history based on a regional seismic line.

An elevated basement block, the Capo S. Lorenzo high (CLH), inherited from the rift stage extensional tectonics, separates the Sardinian Basin into the inner Ogliastro Basin (OB) and the outer Ichnusa-Sarrabus Basin (SB). Many canyons, with highly variable morphology, dissect the Sardinian slope.

The base of slope is mainly characterized by channelized lobes (CML), up to 20 km

wide, that develop at the mouth of the major canyons.

In the centre of the Ogliastro Basin the main bathymetric feature is the Sarrabus Canyon (SC). It originates at a depth of around 1600 m and enlarges downslope to reach a width of 2 km and a relief of 150 m. The Sarrabus channel finally breaches the Sardinian Basin margin, cutting through a relay ramp in the Quirra tectonic lineament.

Upslope of the Sarrabus Canyon the central portion of the Sarrabus Basin is a large erosional belt with features typical of submarine braided valleys (BV). In addition, an axial braided valley develops in the axial sector of the Ogliastra Basin. After crossing the Quirra tectonic lineament, the Sarrabus Canyon joins the Orosei-Gonone canyon system (OGC) in the aggradational Sardinian Valley (SV) that feeds sediments to the lower Cornaglia Basin.

Thus, the present-day setting of the Sardinian Basin is characterized by canyon mouth lobes (CML) and by widespread axial erosion and sediment bypass through the Sarrabus Canyon to the Sardinian Valley and finally to the Cornaglia Basin.

The present-day depositional setting of the Sardinian Margin contrasts with the depositional architecture for older stages. The latter being deduced from interpretation of seismic lines for older infill stages (Fig. 63). The earliest post-Messinian infill stage (Unit 1 in Fig. 63) consists of a package of ponded turbidites in the Ogliastra Basin, an axially fed fan in the Sarrabus Basin and hemipelagites in the Cornaglia Basin. A second depositional phase (unit 2 in Fig. 63) is, on the contrary, characterized by canyon mouth lobes in the Ogliastra Basin, unconfined turbidites in the Sarrabus Basin and hemipelagic deposition in the Cornaglia Basin.

We interpret this evolution as reflecting the progressive infill of the Sardinian intraslope basins, first of the inner Ogliastra Basin, then of the outer Sarrabus Basin. At this stage, with no more space available, a deeper depositional base-level was established, coinciding with the deeper Cornaglia Basin. Sediment bypass to this deeper level was accompanied by widespread erosion in the axial portions of upper basins resulting in the incision of the Sarrabus Canyon and in the formation of the axial braided valley and by the progradation at the base of slope of the canyon mouth lobes. At the same time, a turbidite depositional system fed by the Sardinian Valley was initiated in the Cornaglia Basin.

IV.1.2. Lines MAK-118MS to MAK-127MS

The aim of the 30 kHz MAK survey was to obtain a higher resolution acoustic image of a portion of the Sarrabus Basin where a possible braided pattern had been recognised on EM12 bathymetry and backscatter data.

Braided Valley

The lower resolution backscatter image of the area does not show a distinct braided pattern. Instead the seabed has a patchy backscatter distribution with most of the seafloor characterised by a low backscatter. The new survey shows that the seabed is severely eroded. Three zones with different types of features have been distinguished in the area (Fig. 64). To the southeast the seafloor is dominated by large scours which stand out by their high backscattering headwalls and, in some instances, by their floors. The scours are 1-2 km across and 10 to 30 m deep (Fig. 65). The zone has very low penetration on the subbottom profiles, probably due to very irregular topography and the presence of coarse-grained deposits. The zone merges down slope with the head of the Sarrabus Canyon. The transition is marked by a 40 m high escarpment. To the north the scours are smaller, being 200-400 m wide and 5-10 m deep. High backscatter is less common. The penetration on the profile is greater than in the zone of deep scours. North of the zone of shallow scours the sonographs show that the seafloor has a streaked pattern caused by subtle variations in backscatter (Fig. 65). The penetration on the profile record is up to 30 m and shows a well stratified sedimentary sequence.

These zones are thought to reflect the energy of the gravity flows passing through the area and scouring the seafloor. The main pathway of the flows towards the Sarrabus Canyon is through the zone of deep scours left by the central, most energetic portions of the flows. The zone of the shallow scours is probably formed by the outer portion of the flows or by the flows overbanking from the main pathway and is characteristic of

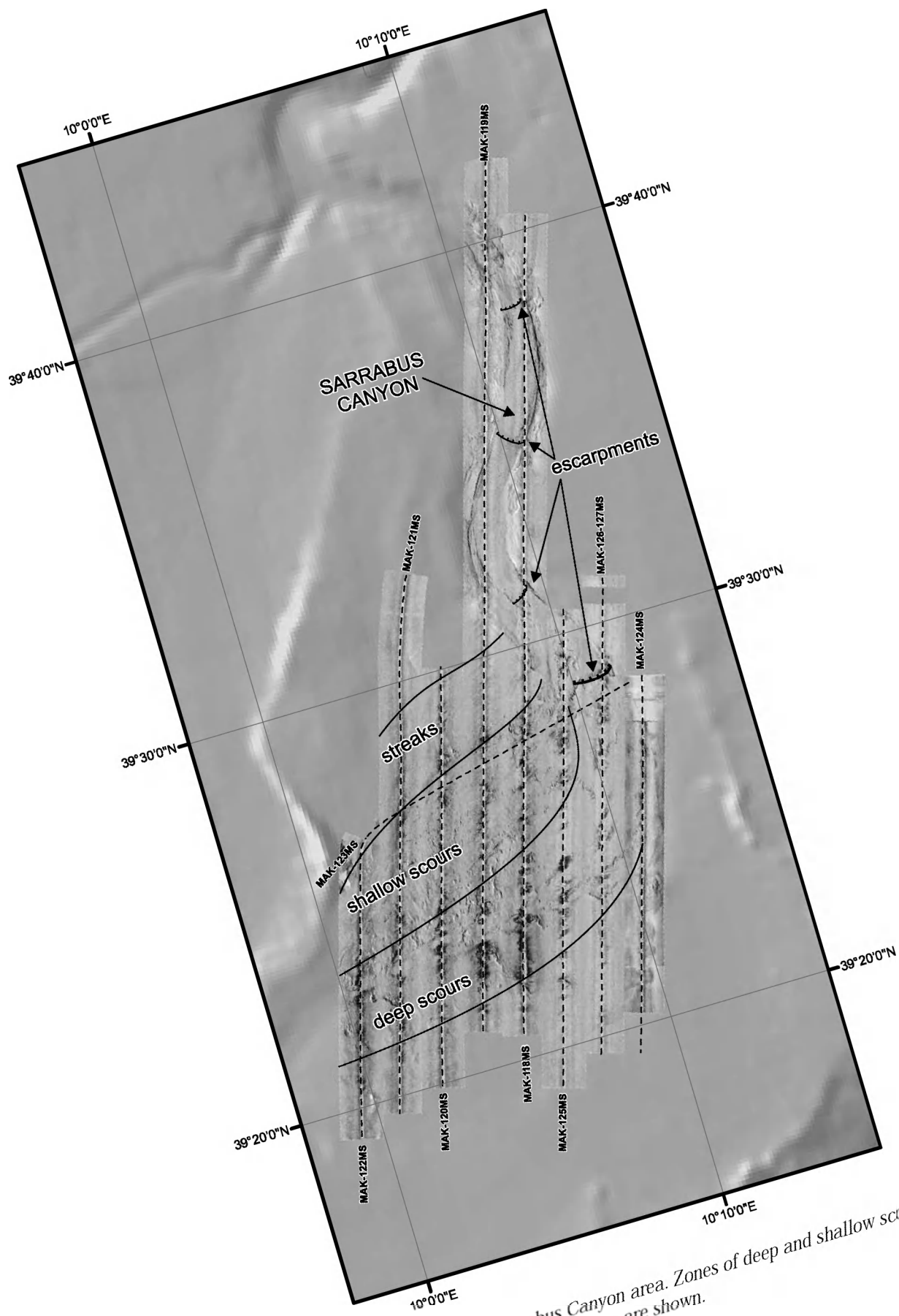


Figure 64. MAK-1M mosaic of the Sarrabus Canyon area. Zones of deep and shallow scours and streaked pattern are shown.

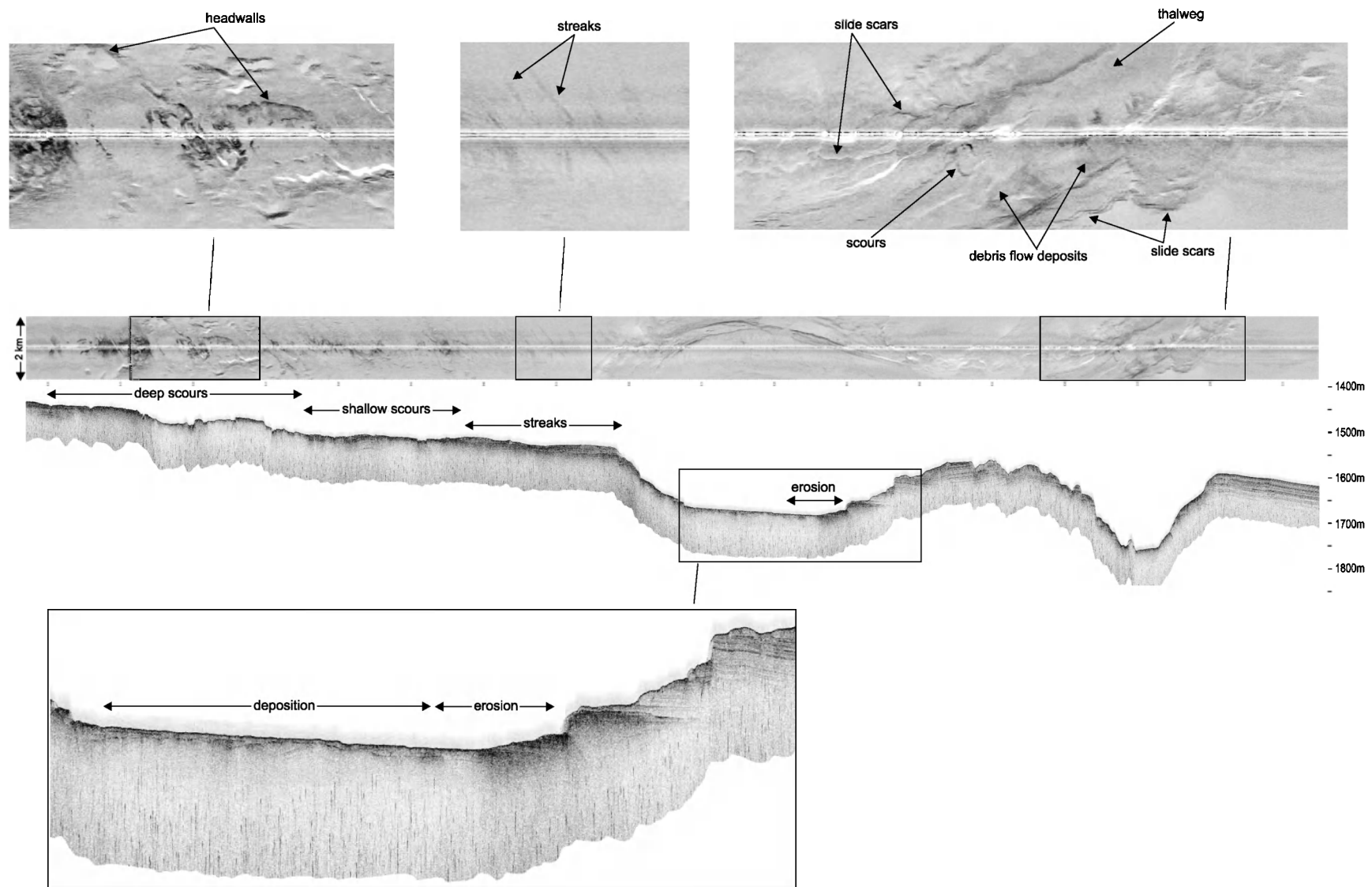


Figure 65. Line MAK-119MS showing some of the details from the Sarrabus Canyon area.

reduced flow energy. The zone of the streaked pattern is produced by peripheral flows with insufficient energy to erode the seafloor.

Sarrabus Canyon

The Sarrabus Canyon follows a NNE direction and is a sinuous feature (sinuosity about 1.2) with steep walls and flattened thalweg.

The more proximal loop is terraced on the western, outer flank (Fig. 65) while the eastern flank has multiple sediment failures producing amphitheatre-shaped scars. The scars cut the bedded sedimentary sequence which is characterised by acoustic penetration of up to 50 m. At the base of the canyon wall there are debris flow deposits resulting from the instability. The canyon depth is about 140 m.

The downslope bend has less terracing on the outer flank and is more strongly affected by instability with numerous scars developing along the wall. Canyon depth increases to 170 m. The width of the canyon is about 2.6 km.

The floor of the canyon is flat and seen as a high amplitude reflector on profiles. The width of the thalweg varies from 0.9 to 1.5 km. Variations of backscatter on the sonographs are interpreted as due to bedforms such as sediment waves with a wavelength of about 100 m. Erosion is evident on the outer part of the thalweg bend. The rest of the thalweg appears to be depositional. There is a series of escarpments crossing the thalweg. They usually have a characteristic zigzag shape and height between 5 and 10 m. The zigzag shape is thought to result from amalgamation of several v-shaped scours. These escarpments are possibly due to retrogressive erosion whereby the canyon works out its equilibrium profile. A large escarpment marks a break in slope of about 1° between the Braided Valley and the Canyon.

IV.1.3. Bottom sampling

A. OVSYANNIKOV, D. KOROST, E. KOZLOVA,
A. AKHMETZHANOV, E. SARANTSEV, E. BILEVA,
E. BLINOVA, E. LOGVINA, A. SHUVALOV, I. GURJEV
AND P. GOLINCHIK

Bottom sampling was done at 8 stations to ground-truth the acoustic image obtained during the MAK survey (Table 7, Annex I).

Station MS-317G (Fig. 66)

The station is within the shallow scour zone in the Braided Valley. The core consists of about 52 cm of brownish grey bioturbated silty clay with foraminifera and shell debris.

Station MS-318G (Fig. 67)

The station was an attempt to sample one of the deep scours of the Braided Valley. About 42 cm of bioturbated brownish grey silty clay, very rich in foraminifera, was obtained.

Station MS-319Gr (Fig. 68)

A high backscatter patch within the deep-scour zone in the Braided Valley was sampled with the TV-guided grab. The upper part of retrieved sediments (0-70 cm) consists of light brownish grey carbonate clay rich in foraminifera. The lower part (about 10 cm thick) is rounded and sub-rounded pebbles to gravels with large shell fragments (Fig. 69).

Station MS-320K (Fig. 70)

The 47 cm long core was collected from the zone of streaks. It consists of brown water-saturated marl with sandy admixture and foraminifera in the upper 3 cm. The unit below (3-47 cm) consists of bioturbated brownish grey silty clay with foraminifera.

Station MS-321K (Fig. 71)

The station was another attempt to sample the shallow scour zone in the Braided

Table 7. Details of the sites sampled during Leg 4 in the Tyrrhenian Sea.

Station	Date	Time (GMT)	Latitude	Longitude	Depth (m)	Recovery (cm)
TTR14-MS-317G	07.09	07:16	39°23.442N	10°00.802E	1606	52
TTR14-MS-318G	07.09	09:30	39°23.318N	10°03.392E	1626	42
TTR14-MS-319GR	07.09	12:57	39°24.519N	10°08.040E	1692	1.5 t
		13:32	39°24.533N	10°08.125E	1693	
TTR14-MS-320K	07.09	16:07	39°29.059N	10°08.500E	1719	47
TTR14-MS-321K	07.09	18:00	39°26.560N	10°06.138E	1685	48
TTR14-MS-322K	07.09	20:01	39°28.458N	10°04.089E	1663	54
TTR14-MS-323G	08.09	10:22	39°31.343N	10°05.194E	1651	478
TTR14-MS-324G	08.09	12:21	39°33.241N	10°08.735E	1842	85
TTR14-MS-325G	10.09	11:17	38°56.219N	15°11.427E	2535	1
TTR14-MS-326B	10.09	13:22	38°56.217N	15°11.428E	2533	15
TTR14-MS-327GR	12.09	12:47	38°53.792N	15°12.702E	2334	1 t
		14:36	38°53.836N	15°12.510E	2324	
TTR14-MS-328B	12.09	18:02	38°55.800N	15°09.018E	2515	21
TTR14-MS-329K	13.09	04:55	38°55.801N	15°09.020E	2520	3
TTR14-MS-330G	13.09	08:06	38°53.915 N	15°18.466E	2340	1
TTR14-MS-331B	13.09	10:14	38°53.915 N	15°18.466E	2340	26
TTR14TVMS20	13.09		38°51.657 N	15°10.749 E	1802	
TTR14-MS-332Gr	13.09	13:21	38°51.660 N	15°10.779 E	1803	
TTR14-MS-333D	13.09	16:18	38°53.765N	15°12.665E	2330	1 t
		17:20	38°53.691N	15°12.394E	2288	
TTR14-MS-334B	14.09	03:25	38°51.658 N	15°11.205E	1812	22
TTR14-MS-335B	14.09	05:19	38°51.699 N	15°12.929E	1754	
TTR14-MS-336B	14.09	07:35	38°53.830N	15°12.445 E	2318	36
TTR14-MS-337GR	14.09	11:24	38°53.796N	15°12.708E	2334	0.3 t
		12:00	38°53.778N	15°12.695E	2332	
TTR14-MS-338B	14.09	15:21	38°51.690 N	15°12.255E	1810	17
TTR14-MS-339B	14.09	17:47	38°52.049N	15°10.280E	1909	25
TTR14-MS-340B	14.09	21:54	38°54.374N	15°10.003E	2358	1
TTR14-MS-341B	15.09	09:07	38°55.581N	15°21.533E	2415	21
TTR14-MS-342B	15.09	12:59	39°01.098N	15°09.297E	2514	28
TTR14-MS-343G	15.09	15:17	39°01.100N	15°09.299E	2512	0.5
TTR14-MS-344G	15.09	17:02	39°01.819N	15°09.300E	2542	0.5

Valley. The recovery was a 48 cm long section of hemipelagic marl and clay similar to previous cores. A few gravel clasts found at the bottom of the core suggest that there is a coarse-grained bed beneath the hemipelagic cover.

Station MS-322K (Fig. 72)

The core was also collected from the streaked pattern zone but upslope from MS-320K. The recovery was about 54 cm and had a similar hemipelagic sequence.

Station MS-323G (Fig. 73)

The station was located outside of Braided Valley and intended to recover a basin hemipelagic sequence. The core is 478 cm long. The sediment on the top (0-54 cm) is

brownish water-saturated marl with foraminifera and shell debris and light brownish clay with foraminifera and shell debris. Below (54-478 cm) is an interval of grey stiff clay with foraminifera and shell fragments. There are subtle colour variations in shades of grey throughout the interval which are thought to reflect paleoclimatic changes.

Station MS-324G (Fig. 74)

The 85 cm long core was taken from the thalweg of the Sarrabus Canyon. Most of the section is bioturbated brownish grey silty clay. Three distinct brownish grey water-saturated layers of fine sand with a small amount of clayey admixture and with sharp upper and lower contacts are found at 33-35 cm, 53-57 cm and at 68-69 cm.

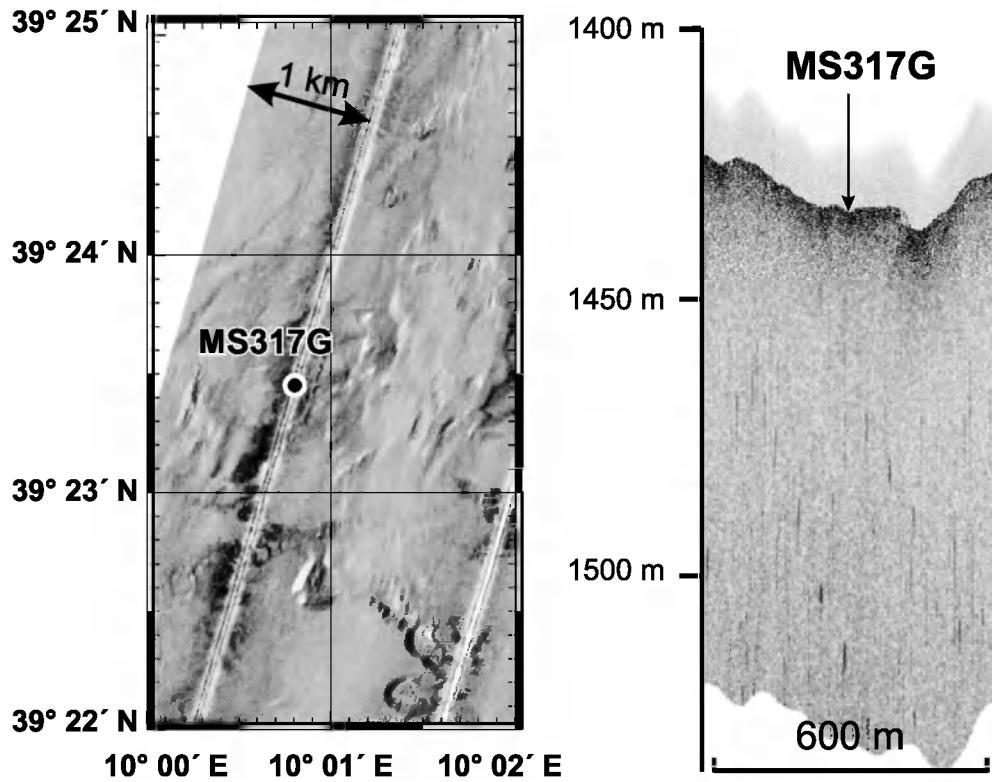


Figure 66. Location of sampling site MS-317G in the zone of shallow scours.

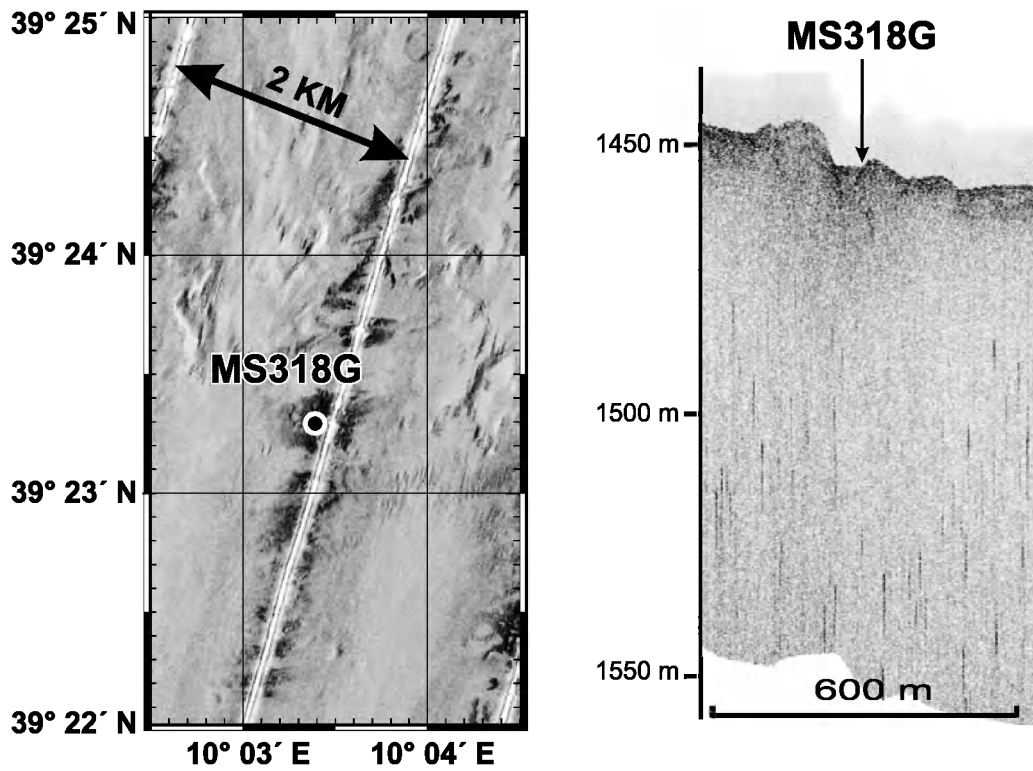


Figure 67. Location of sampling site MS-318G in the zone of deep scours.

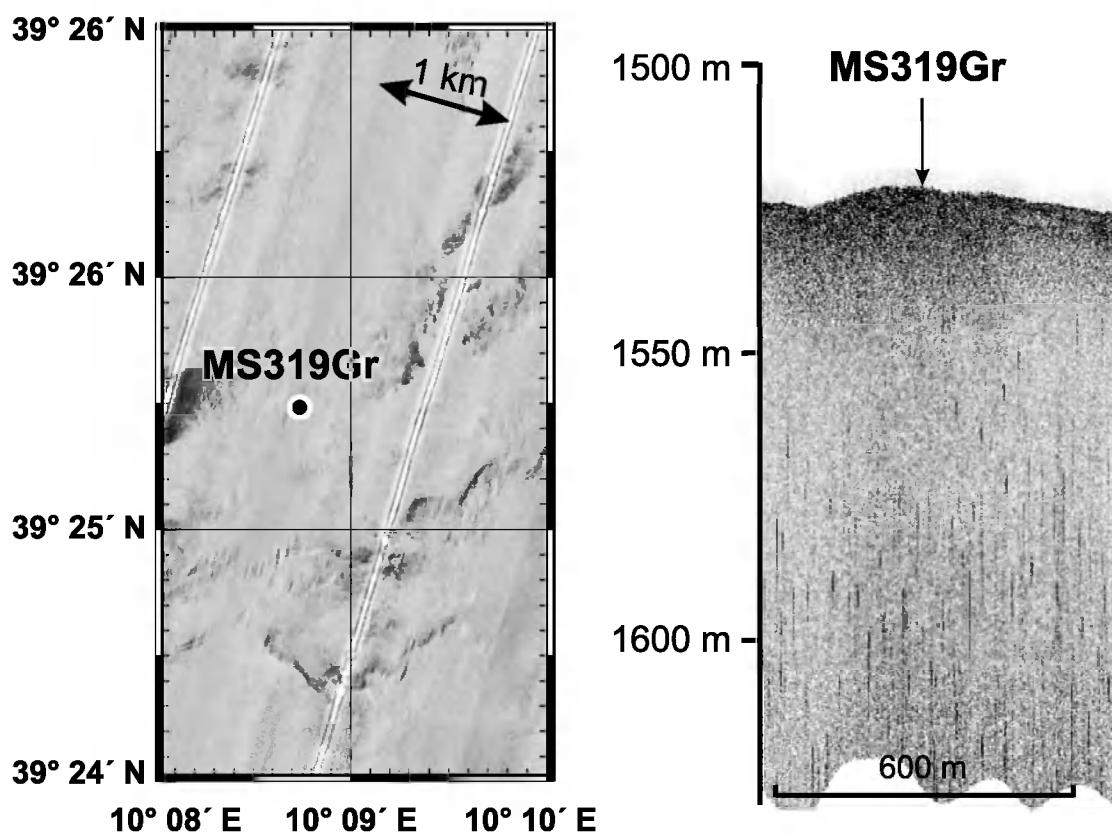


Figure 68. Location of sampling site MS-319Gr in the high backscattering patch.



Figure 69. Gravel and pebbles from the grab sample MS-319 Gr in the high backscattering patch.

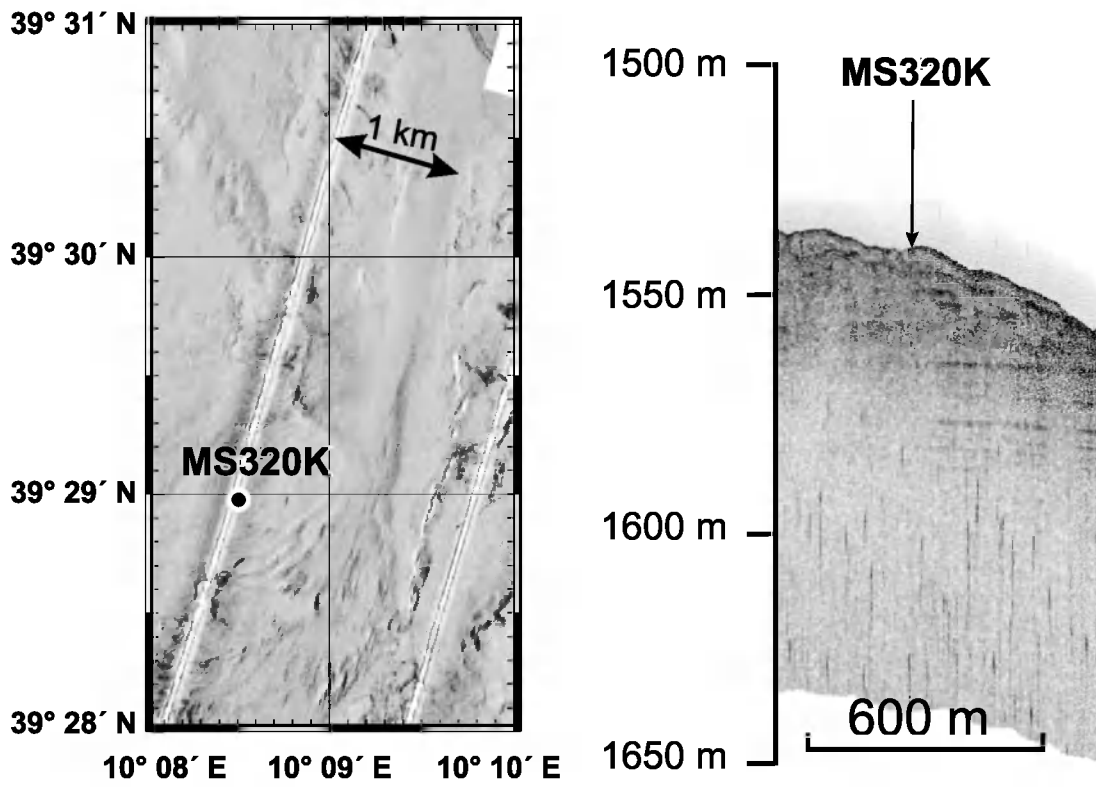


Figure 70. Location of sampling site MS-320G in the zone of streaks.

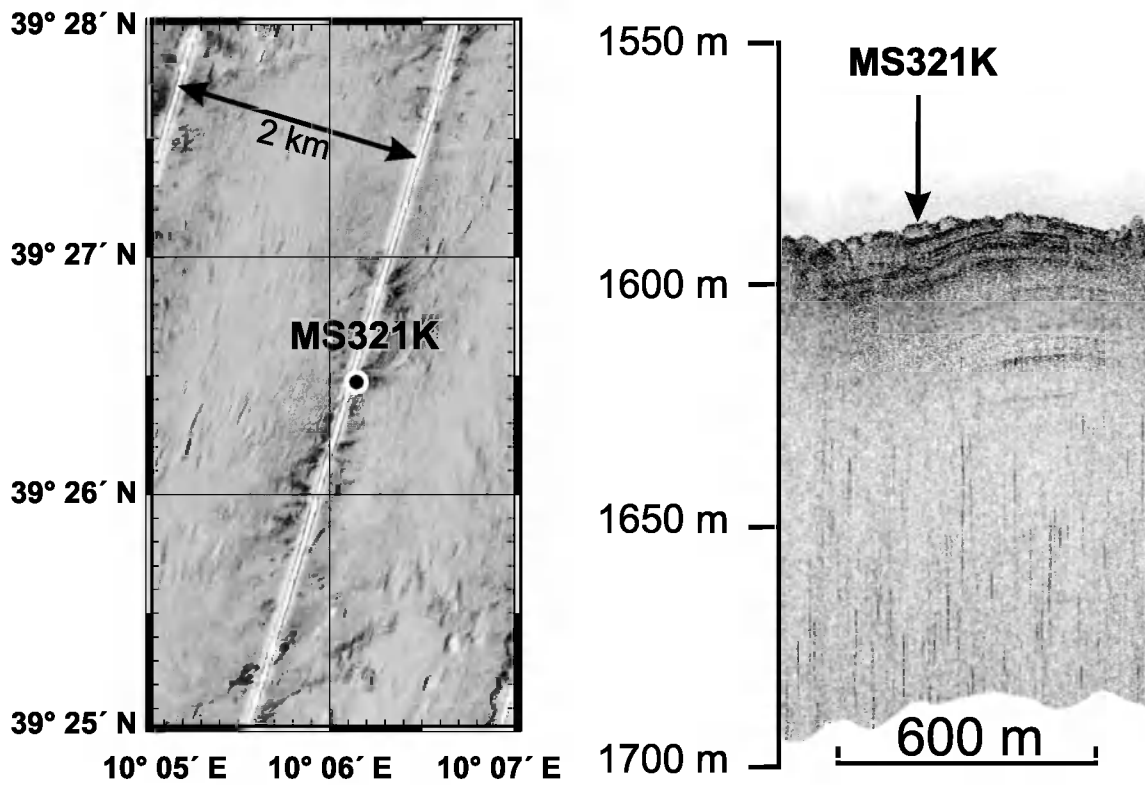


Figure 71. Location of sampling site MS-321G in the zone of shallow scours.

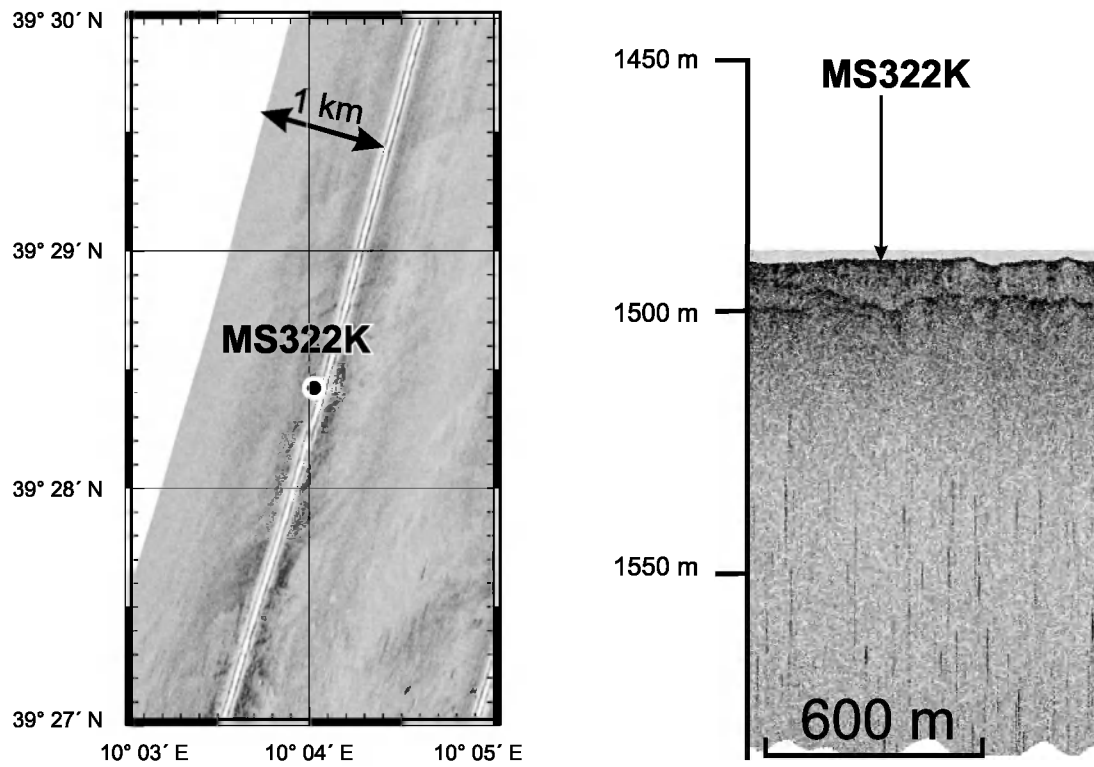


Figure 72. Location of sampling site MS-322G in the zone of streaks.

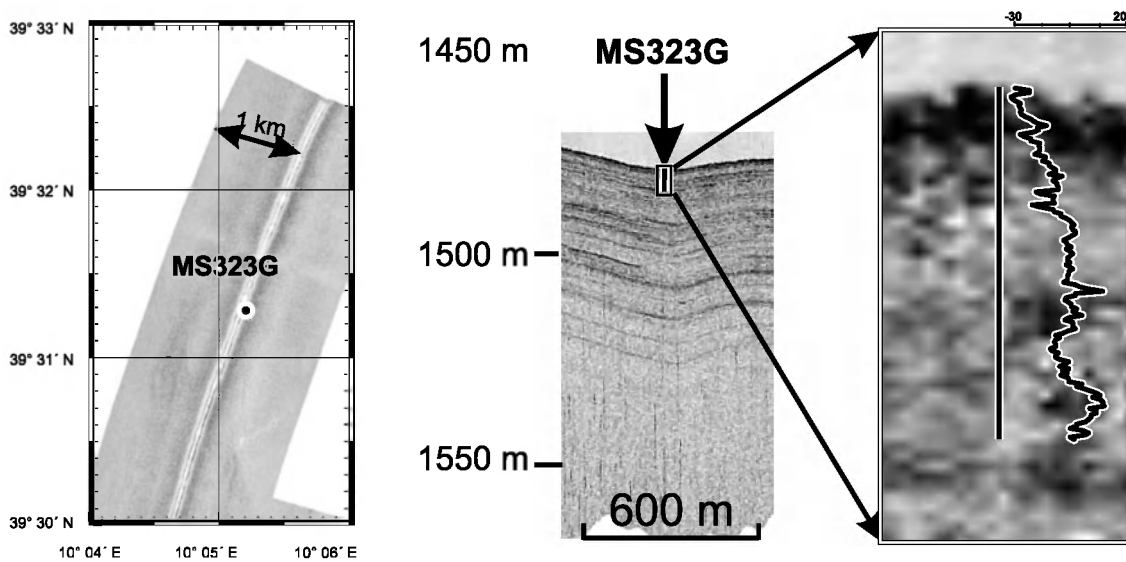


Figure 73. Location of sampling site MS-323G in the basin hemipelagic area.

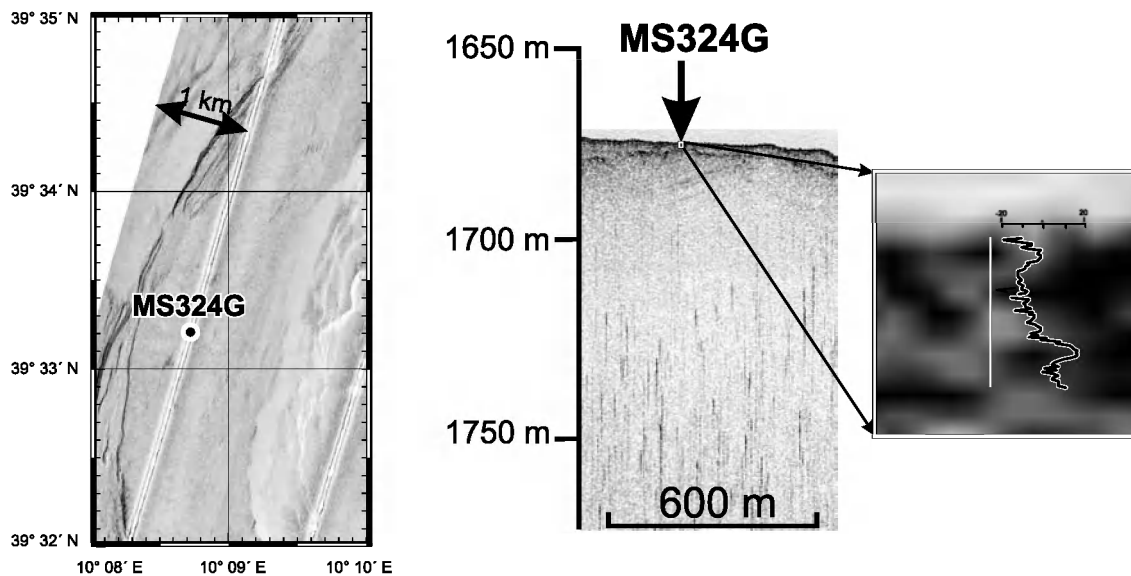


Figure 74. Location of sampling site MS-324G in the Sarrabus Canyon thalweg.

Conclusions

Bottom sampling indicates that the studied area is covered by an approximately 0.5 m thick veneer of hemipelagic sediments. Within the Braided Valley the veneer overlays a coarse-grained bed represented by gravel and pebbles which was successfully sampled at the station MS-319GR. The presence of this bed resulted in short recoveries at most of the other stations in the area. Several sand beds recovered from the thalweg of Sarrabus Canyon are thought to be deposits of turbidity flows passing through the canyon.

IV.2. History of catastrophic slope failures of Stromboli Volcano

M. MARANI, A. DI ROBERTO, N. RASUL,
F. GAMBERI, N. KENYON, M. IVANOV,
A. AKMETZHANOV, E. SOLOVA, J-S. LABERG,
O. HAZMI, A. DEL PRINCIPE, S. DISTEFANO,
M. FIRETTO AND H. BENOIT

IV.2.1. Introduction

The second part of leg 4 was aimed at probing for signatures of recent collapse events on the flanks of the Stromboli Volcano with particular interest in the collapse event

of December 2002. The research is a significant part of the tsunami hazard assessment that is being undertaken by the Italian Civil Protection authority.

Stromboli's summit is 924 m above sea level and rises about 3000 m from the seafloor. Approximately 2000 people inhabit the two villages at the foot of Stromboli Island. Stromboli, known as the "Lighthouse of the Mediterranean", is the northernmost active volcano of the volcanic Aeolian Islands in the Calabrian Arc. The most important feature of Stromboli Volcano is a large horseshoe shaped depression on the NW flank of the island called Sciara del Fuoco. It is the remnant of a series of big flank failures caused by the presence of two parallel (NE-SW) trends of weakness.

Stromboli is the type example of Strombolian Activity characterized by persistent, mid to low energy explosive activity and episodic large explosive and lava flow occurrences. The volcanic activity takes place in the three principal craters on a terrace, approximately 750 m above sea level. It is characterized by the intermittent extrusion of small amounts of volcanic materials composed mostly of incandescent black scoria, lapilli and ash, and lithic blocks of varying size accompanied during severe explosions by crystal-poor golden pumice. Generally,

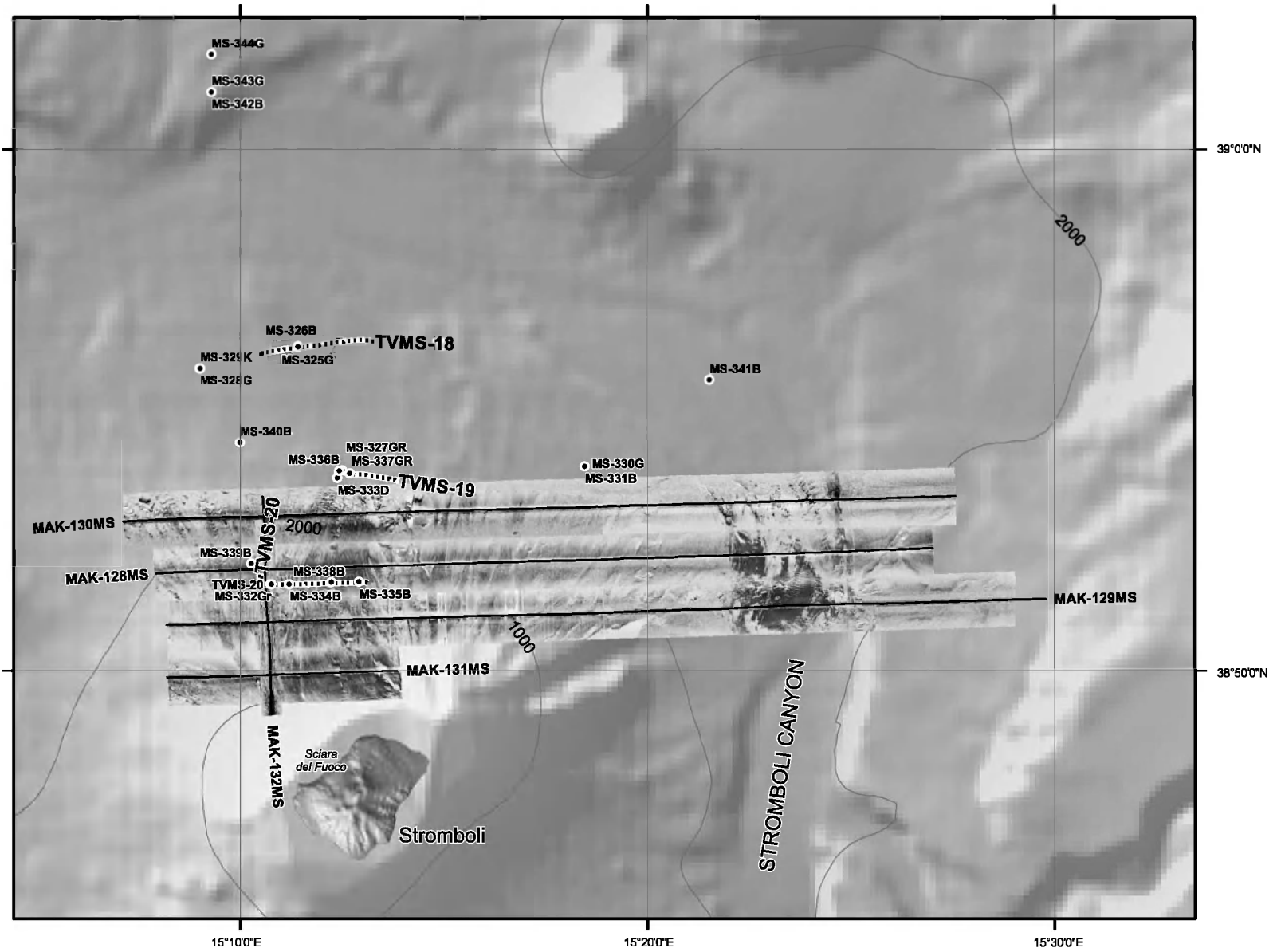


Figure 75. Location map of the Stromboli Volcano study area.

the frequency of mild explosions is 4 times/hour. Periodically, the short-lived normal activity is interrupted by a larger explosion and lava flows. Five major explosions have been reported in the last decade. It is believed that the volcanic activity has been steady for the last 2000 – 2500 years. However, historical sources older than 1000 A.D. are not reliable for conclusions about the frequency and characteristics of the volcanic activity. The last major episode of activity was observed in 1949 followed by a tsunami with wave heights of about 10 m which caused destruction to part of the main village.

Most research has been aimed at understanding the characteristics of the Stromboli Volcano. It is reported that the current activity is associated with the emission of gases in quantities of up to 6000 – 12000 tons/day. The most common are H₂O (3200-6300 tons/day), CO₂ (2900 – 5800 tons/day), SO₂ (400 800 tons/day) and minor amounts of HCl and HF (Allard et.al. 1994).

Stromboli is the sub-aerial part of a much larger volcanic edifice (Fig. 75). On December 30, 2002, a flank collapse of 15-20 million m³ provoked a tsunami causing significant damage to buildings on the eastern coast of the island up to 10 m above sea level. The Sciara del Fuoco and its submarine prolongation acts as a manifold for mild explosive activity and episodic flank collapse events, creating a deep-sea fan covering almost the whole eastern portion of the Marsili basin. The marine environment, being the ultimate depositional site of landslide and related sediment-gravity flows, can be the best repository of information about collapse events. This implies that the deep-sea depositional systems surrounding Stromboli Island could provide a good archive of information about the recent history of the volcano.

IV.2.2. Results

About 200 km² of MAK deep-towed sidescan sonar imagery were acquired in the area in order to investigate the deep canyon axis, the base of the Stromboli edifice and the

median flank characteristics of the volcano (Fig. 75).

The sonographs showed scour marks and sand waves related to the latest sediment pathway (Fig. 76). The subbottom profiler showed distinct areas of erosional and depositional features including small channels, small canyons and slump scars. The debris avalanche deposits derived from the year 2002 collapse event was also imaged. The deposits are positioned between 1550 m and 2000 m on the flank of the Stromboli edifice and about 5 to 7 km from the coastline.

IV.2.2.1. Underwater TV survey

V. BLINOVA, M. IVANOV AND M. MARANI

Three TV camera runs were chosen to groundtruth the acoustic imagery.

TVMS-18 (Fig. 77)

Line TVMS-18 was selected on the basis of a sidescan sonar image made in 1994 during the TTR-4 cruise in the area (Limonov et al., 1995). The TV-line crossed a flat area with uniform low backscatter on the sonograph.

The video record shows a monotonous seafloor covered by a very thin layer of hemipelagic marl (0.5-1 cm) interrupted by fields of black volcanic sand. Various bed-forms are seen, mostly sand ripples (Fig. 78a). Several thin but extensive crusts and slabs are found (Fig. 78b). Large blocks (2-3 m in size) and clasts of volcanic rocks are also seen (Fig. 78c,d). Debris is both rounded and angular in shape.

No seabed fauna was observed.

TVMS-19 (Fig. 79)

This TV line was also selected on the basis of a TTR-4 sidescan sonar image (Limonov et al., 1995). It starts in an area of high backscattering features and rough topography and ends in a flat area.

The video record shows complex topography, abundant volcanic blocks, escarpments and crusts. From 5:45 to 6:30 pillow-lavas are seen. They have a characteristic

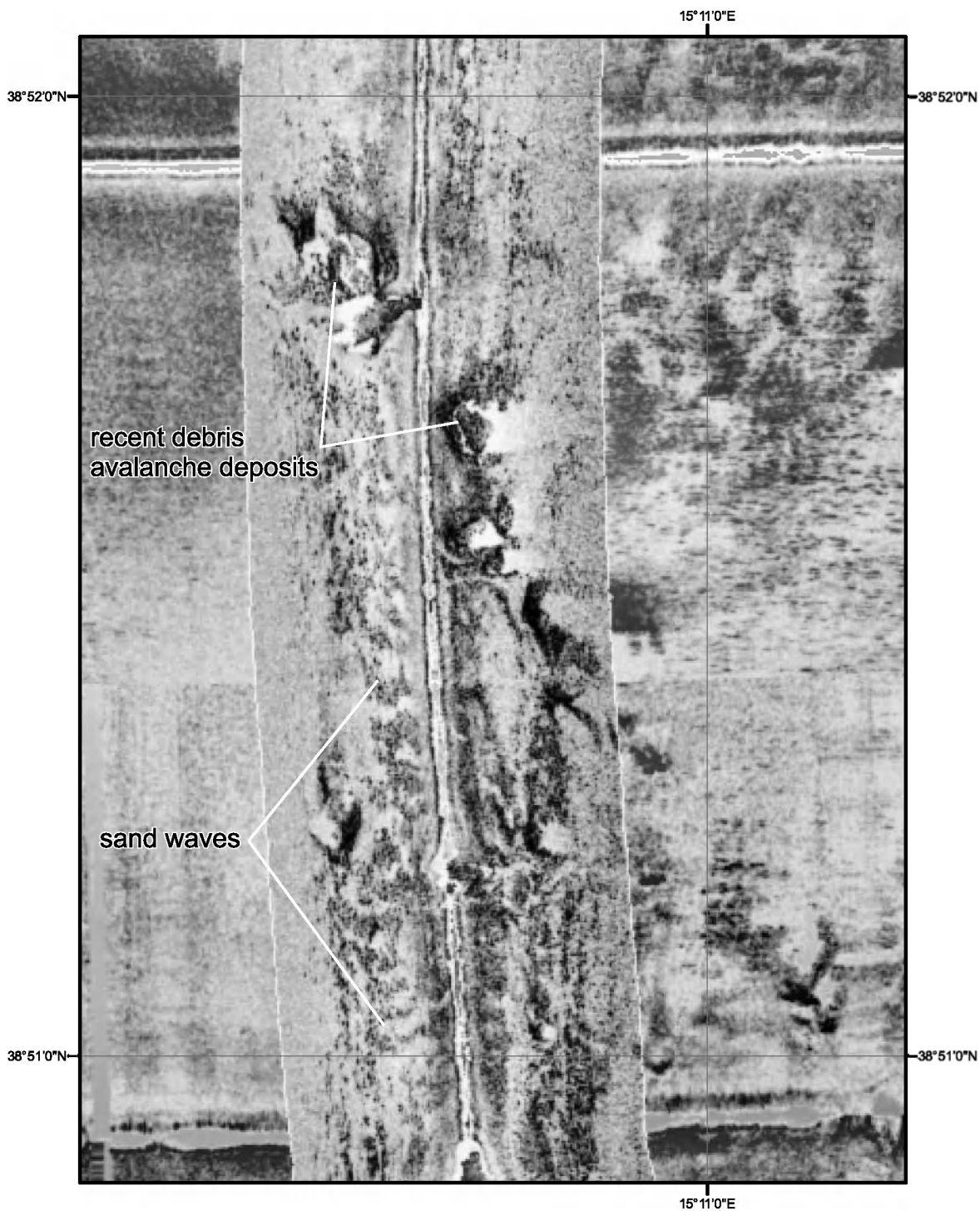


Figure 76. Fragment of MAK-1M mosaic showing details of recent collapse pathway.

round or cylindrical shape (Fig. 80b) and a striated surface texture (Fig. 80c). Some of pillows have collapsed and holes or cracks are formed.

TVMS-20 (Fig. 81)

TVMS-20 was run along line MAK-129MS. The video record shows mainly volcanic rocks and pillow-lavas. At the start of the line volcanic debris scattered over the seafloor is observed (Fig. 82b). Several radial

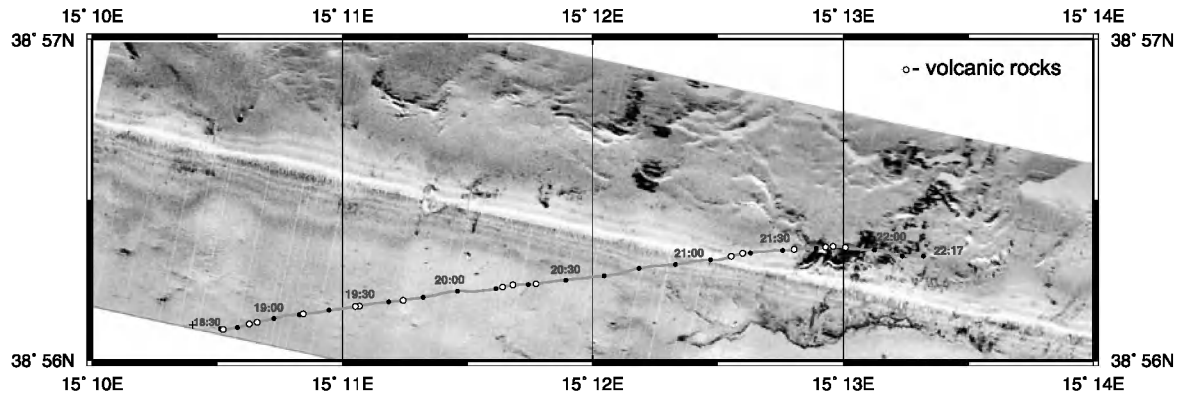


Figure 77. Location of the video run TVMS-18 on the Stromboli avalanche slope.

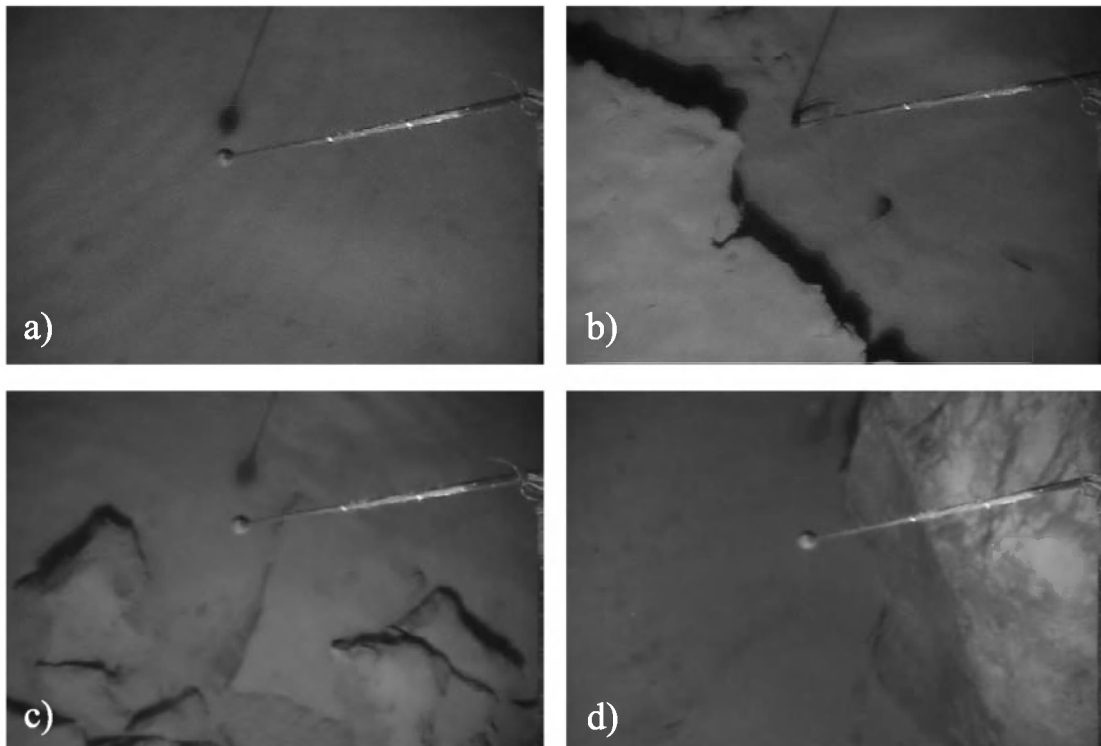


Figure 78. Stills from TVMS-18.

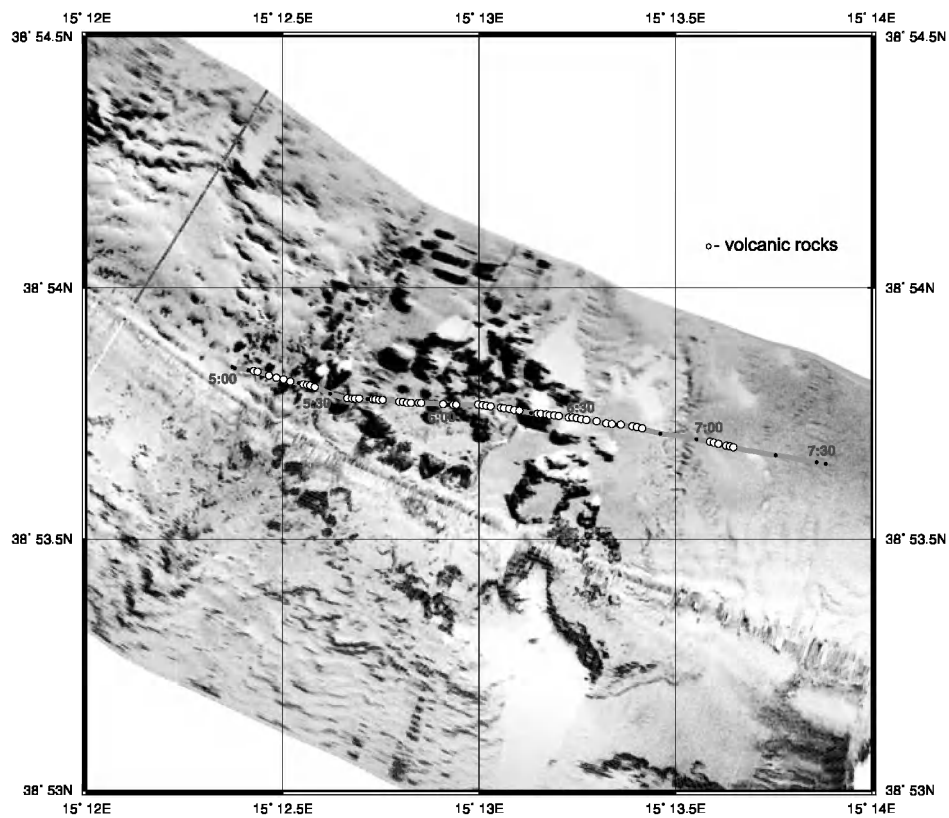


Figure 79. Location of the video run TVMS-19 on the lower slope of Stromboli.

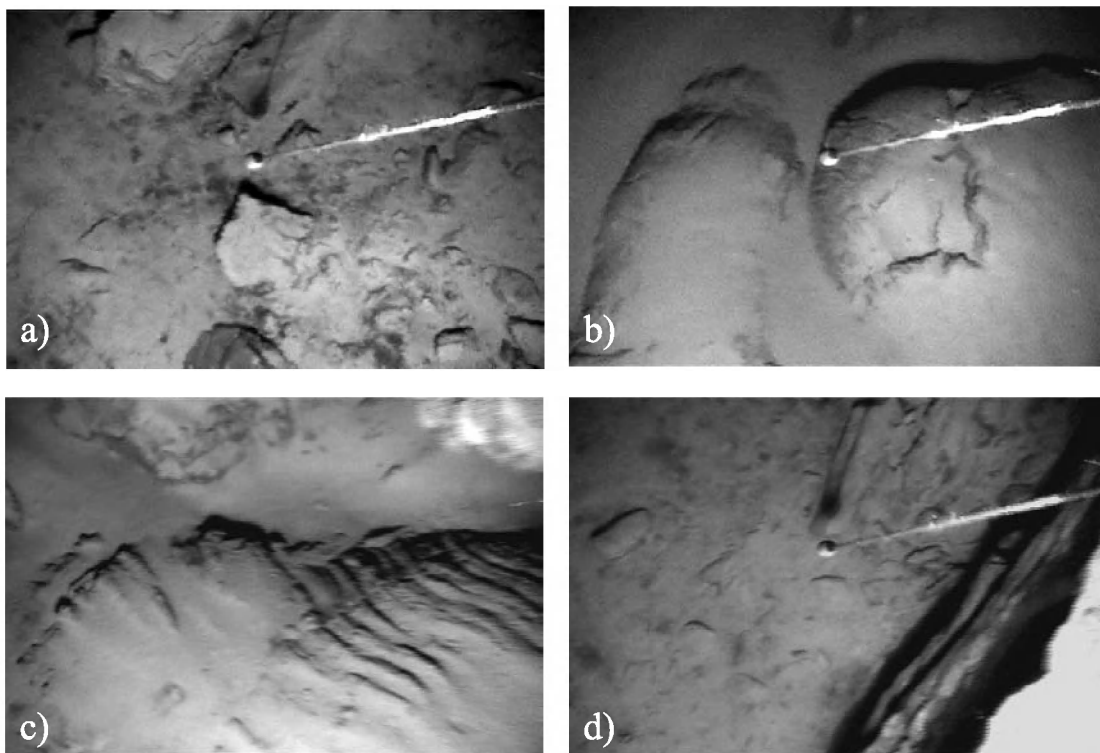


Figure 80. Stills from TVMS-19 showing pillow lava.

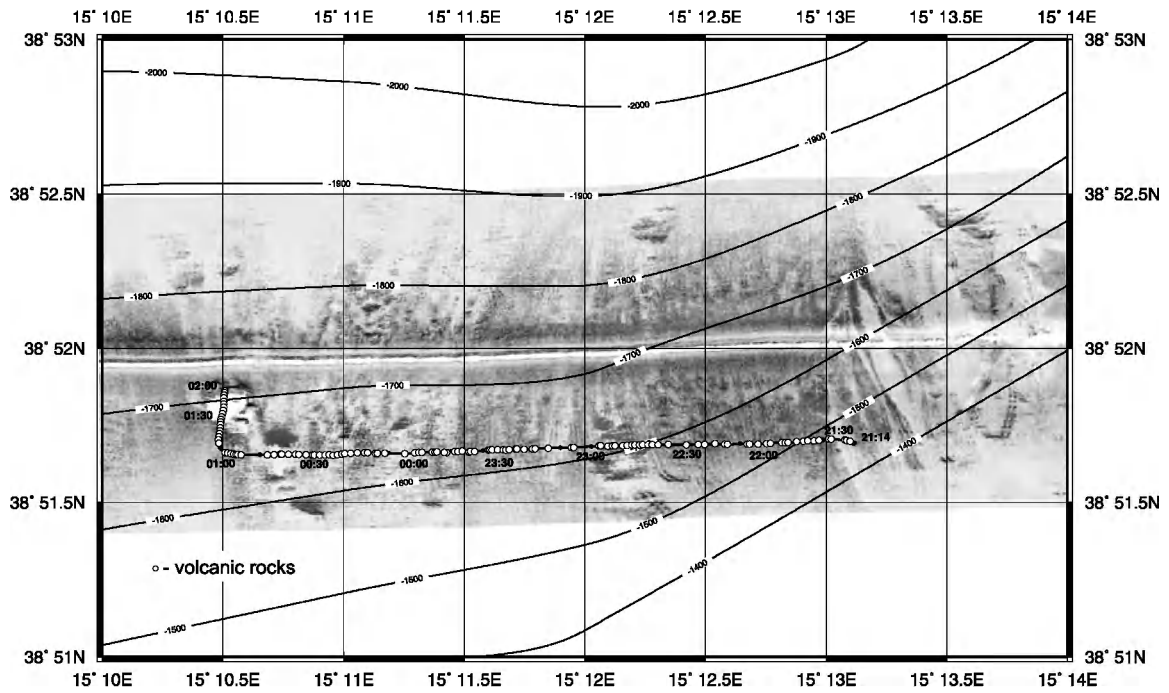


Figure 81. Location of the video run TVMS-20 on the slope of Stromboli.

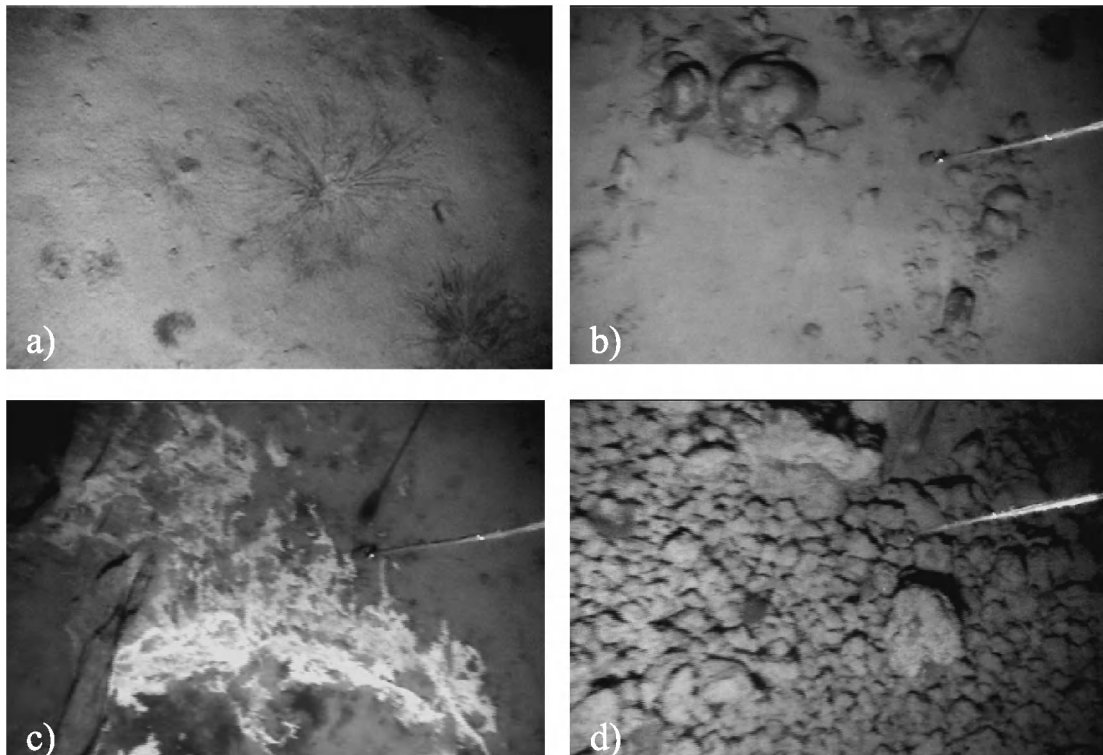


Figure 82. Stills from TVMS-20 showing a) spoke burrows, b) volcanic debris, c) white sediment, d) round volcanic clasts.

circles are found on the flat hemipelagic seabed (probably bottom feeding traces/spoke burrows). From 21:36 till 21:41 white material (probably clay) in the cracks and layers in the escarpments is seen. At one place a boulder covered with white sediment is observed (Fig. 82c)

Two hills are crossed at the end of the line. They have very steep slopes and large blocks are seen. The upper parts of the hills are covered by rounded volcanic clasts (Fig. 82d). Size of clasts becomes smaller towards to the top. The uppermost part has very complicated relief and is difficult to survey with a towed camera. Large escarpments, blocks and precipices are seen here. Based on the MAK image these hills were interpreted as deposits at the edge of a recent debris avalanche.

IV.2.2.2. Bottom sampling

A. OVSYANNIKOV, D. KOROST, E. KOZLOVA,
A. AKHMETZHANOV, E. SARANTSEV, E. BILEVA,
E. BLINOVA, E. LOGVINA, A. SHUVALOV, I. GURJEV
AND P. GOLINCHIK

The aim of bottom sampling in this area was to groundtruth acoustic facies and obtain samples from the sites identified on the TV records. 14 samples were taken (Table 7). The sites were selected on the basis of MAK-1M data obtained during TTR-4 and TTR-14 cruises.

Station MS-325G (Fig. 83)

Only a very small amount of dark volcanoclastic sand was recovered at this station.

Station MS-326B (Fig. 83)

A 17 cm long sedimentary core had brown, very water-saturated marl in the

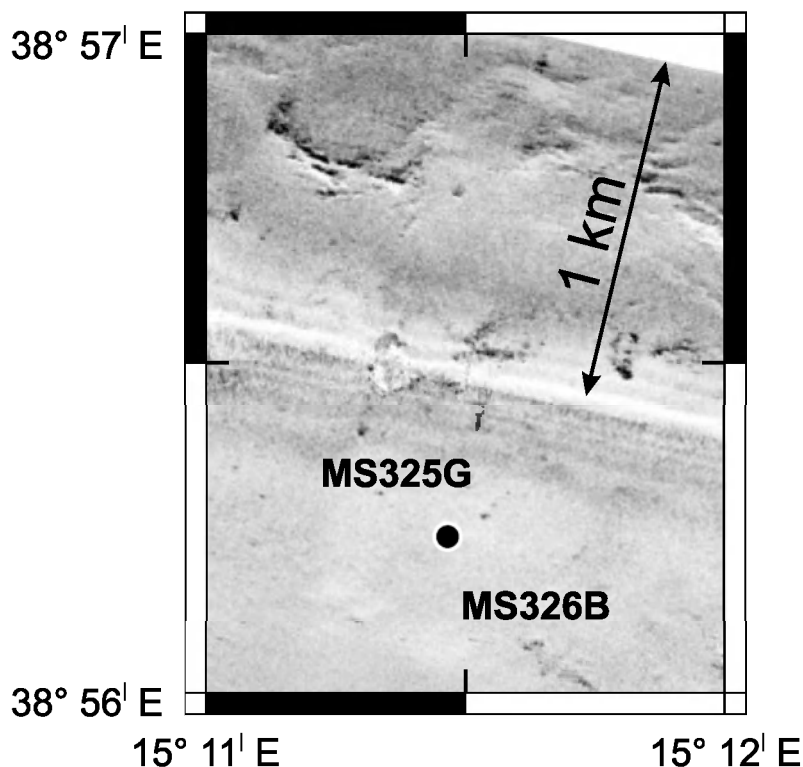


Figure 83. Location of sampling sites MS-325G and 326G on the distal slope of Stromboli.

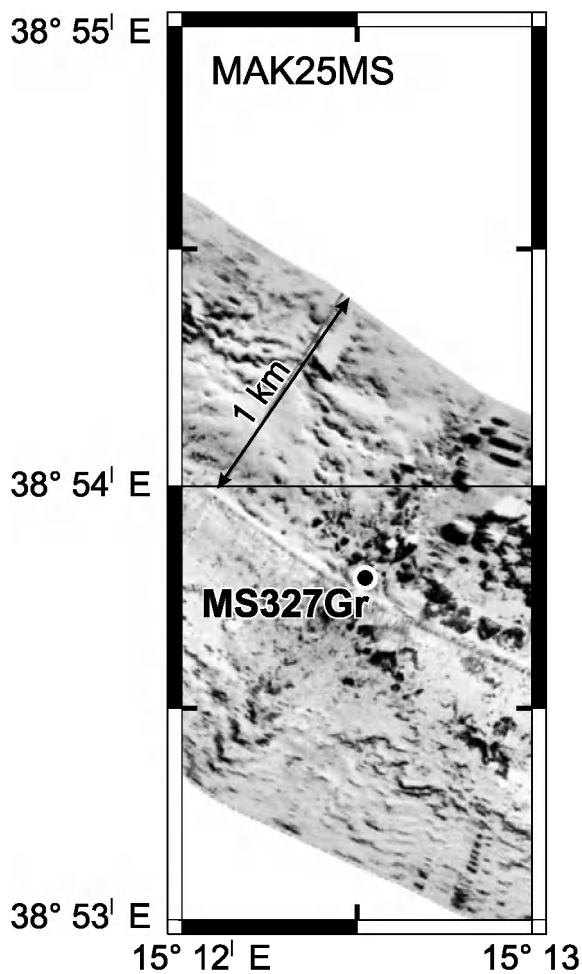


Figure 84. Location of sampling site MS-327Gr.

upper 0.5 cm. The unit below is 16 cm of black, fine to coarse, volcanoclastic sand with lamination and lenses of coarse sand. At 13 cm a layer of very coarse sand is seen.

Station MS-327Gr (Fig. 84)

A large (90x50x60 cm) block of lava, covered by a thin veneer of hemipelagic sediment, was recovered. A small amount of black volcanoclastic sand was also retrieved.

Station MS-328B

A 21 cm long sequence of black, medium to coarse volcanoclastic sand with lamination and lenses of coarse sand was taken at this station.

Station MS-329K

A small amount of black medium to coarse sand was retrieved at this station.

Station MS-330G

A small amount of brownish grey hemipelagic clay with foraminifera and a small amount of silty admixture was recovered.

Station MS-331G

The 26 cm long core consisted of a layer of fine black volcanoclastic sand, overlaid by 16 cm of hemipelagic brownish grey silty clay.

Station MS-332Gr

A large amount of black porous lava fragments were obtained. Fragments vary in shape (angular to rounded) and size (5-50 cm). Some fragments are oxidised on the surface.

Station MS-333D

Numerous blocks of weathered brownish pillow-lava were obtained. The freshly broken surfaces are black in colour. Several black fragments of lava were also recovered.

Station MS-334B

The 23 cm long core consisted of an uppermost 10 cm interval of black medium to fine volcanoclastic sand, with cross lamination in the middle part of the unit. The lowermost interval (10-23 cm) consists of black medium to coarse volcanoclastic sand, with parallel lamination between 10-20 cm and with gravel in the lower part of the unit.

Station MS-335B

A small amount of black volcanoclastic sand was obtained at this station.

Station MS-336B

The upper 7 cm of sedimentary section were washed out during recovery. The sediment below consists of black medium to coarse volcanoclastic sand, with parallel lamination in the upper 3 cm. The lower boundary is irregular. The lowermost interval is 3 cm of black coarse to very coarse volcanoclastic sand with gravel.

Station MS-337Gr

A small amount of black volcanoclastic sand is obtained.

Station MS-338B

A 17 cm long section of black volcanoclastic sand is recovered. The upper 9 cm is fine to medium sand and the interval below is very coarse sand.

Station MS-339B

The core has a 25 cm long section of black volcanoclastic sand. The sand is medium to coarse in the upper 11 cm and becomes coarse below.

Station MS-340B

Only a small amount of fine black volcanoclastic sand was obtained. The sedimentary section is topped by a thin cover of brownish clay.

Station MS-341B

The 21 cm long sedimentary section is topped by brownish clay. The unit below (1-2 cm) consists of medium black volcanoclastic sand. From 2-8 cm there is black fine volcanoclastic sand. The lowermost interval is 13 cm of black fine to medium sand with parallel lamination. Lamination is due to grain size variations.

Station MS-342B

The core was collected about 31 km to

the north of Stromboli volcano. The site is situated on the right hand flank of the Stromboli Canyon which is elevated above the canyon's floor by about 190 m. The aim of the sampling was to recover deposits of large volume turbidity flows which were expected to originate during flank collapse events and were believed to be capable of crossing the Stromboli Canyon. The recovery is 28 cm long. The upper part of the section contains a 3 cm thick turbidite with coarse sandy base and muddy top. Another turbidite with fine sand base and muddy top is found immediately underneath (3-4 cm). The unit below (7-16 cm) is bioturbated brownish silty clay. The lowermost unit (16-28 cm) is another turbidite with a complex sequence. The upper part (16-22 cm) is essentially muddy but contains 4 distinct thin beds of black sand. The lower part of the turbidite is massive black fine to medium volcanoclastic sand. Turbidites with such a sequence are thought to originate during multi-stage collapse events (Wynn and Masson, 2003).

Station MS-343G and MS-344G

Only a small amount of black fine volcanoclastic sand, mixed with brownish hemipelagic clay is recovered in the core catcher.

IV.2.3. Preliminary conclusions

The investigated areas are the northern submerged flanks of Stromboli volcano, facing the major sector of flank instability, the Sciarra del Fuoco, and the deep-water zones of the Stromboli Canyon, running along the base of the volcano.

The TV images showed that the deposit consists of a disorganised body made up of numerous decimetric blocks amidst larger blocks and with a matrix of black volcanoclastic sand. The volcanoclastics are more abundant over the distal edges of the deposit, where they are organised into ripple sized bedforms. The limits of the debris avalanche are represented by sharp contacts with a hemipelagic sediment covered seafloor characterised by spoke burrows and

sedimented, older blocky deposits. TV-controlled grab samples consist of numerous angular black lava blocks. The blocks display bimodal characteristics, being either massive or scoriaceous. The absence of rounded clasts suggests a deposit generated directly by proximal subaerial flows, without evidence of any residence time in the coastal zone. Macroscopically, the lavas are analogous to the eruptive products emitted by Stromboli shortly before and after the collapse event.

An important and unexpected result was the discovery, and sampling, of an extensive pillow lava field at the base of the volcano. The analyses of these samples offer important information on the petrography of the deeper magmas of Stromboli which are at the base of the largest explosive eruptions of Stromboli due to their high volatile content.

REFERENCES

- Acosta, J., Muñoz, A., Herranz, P., Palomo, C., Ballesteros, M., Vaquero, M. and Uchupi, E., 2001a. Geodynamics of the Emile Baudot Escarpment and the Balearic Promontory, western Mediterranean. *Marine and Petroleum Geology*, 18, 349-369.
- Acosta, J., Muñoz, A., Herranz, P., Palomo, C., Ballesteros, M., Vaquero, M. and Uchupi, E., 2001b. Pockmarks in the Ibiza Channel and western end of the Balearic Promontory (western Mediterranean) revealed by multibeam mapping. *Geo-Mar. Lett.*, 21, 123-130.
- Acosta, J., Canals, M., López-Martínez, J., Muñoz, A., Herranz, P., Urgeles, R., Palomo, C. and Casamor, J.L., 2002. The Balearic Promontory geomorphology (western Mediterranean): morphostructure and sedimentary processes. *Geomorphology*, 49, 177-204.
- Acosta, J., Canals, M., Carbó, A., Muñoz, A., Urgeles, R., Muñoz-Martín, A. and Uchupi, E., 2004. Sea floor morphology and Plio Quaternary cover of the Mallorca Channel, Balearic Islands, western Mediterranean. *Marine Geology*, 206, 165-179.
- Allard, P., Carbonnelle, J., Metric, N., Loyer, H. and Zettwoog, P., 1994. Sulfur output and magma degassing budget of Stromboli volcano. *Nature*, 368, 326-330.
- Auzende, J.M., Olivet, J.L. and Pastouret, L. 1981, Implication structurales et paléogéographiques de la présence de Messinien a l'ouest de Gibraltar. *Marine Geology*, 43, 9-18.
- Baraza, J. and Ercilla, G. 1996: Gas-charged sediments and large pockmark like features on the Gulf of Cadiz slope (SW Spain). *Marine and Petroleum Geology*, 13, 253-261.
- Berné, S., Loubrieu, B. i la tripulació de la campanya CALMAR, 1999. Canyons et Processus Sédimentaires Récents sur la Marge Occidentale du Golfe du Lion. Premiers Résultats de la Campagne Calmar. *C. R. Acad. Sci. Paris*, 328, 471-477.
- Berné, S., Carre, D., Loubrieu, B., Maze, J.-P., Normand, A., 2001. Carte morphobathymétrique du Golfe du Lion. Ifremer-Region Languedoc-Roussillon, Brest.
- Blinova, V. and Bileva, E., 2003. Some geochemical characteristics of relatively active and passive mud volcanoes (Gulf of Cadiz and Alboran Sea), IOC Workshop Report, 187, 17-18.
- Blinova, V. and Stadnitaskaia, A., 2001. Composition and origin of the hydrocarbon gases from the Gulf of Cadiz mud volcanic area. IOC Workshop Report, 175, 45-46.
- Bonnell, C., Dennielou, B., Droz, L., Mulder, T. and Berne, S., 2005. Architecture and depositional pattern of the Rhone Neofan and recent gravity activity in the Gulf of Lions (western Mediterranean). *Marine and Petroleum Geology*, 22, 827-84.
- Bonnin, J., Olivet, J.L., and Auzende, J.M., 1975. Structure en nappe a l'ouest de Gibraltar. *C.R. Acad. Sci. Paris*, 280, 559-562.
- Cacho, I., Grimalt, J.O., Canals, M., Sbaiffi, L., Shackleton, N.J., Schonfeld, J., Zahn, R., 2001. Variability of the western Mediterranean Sea surface temperature during the last 25,000 years and its connection with the Northern Hemisphere climatic changes. *Paleoceanography*, 16, 40-52.
- Canals, M. and Ballesteros, E., 1996. Production of carbonate particles by phyto-benthic communities on the Mallorca-Menorca Shelf, northwestern Mediterranean Sea. *Deep-Sea Research*, 44, 611-629.
- Canals, M., 1985. Estructura Sedimentaria y Evolución Morfológica del Talud y el Glacis Continentales del Golfo de Leon: Fenomenos de Desestabilizacion de la Cobertura Sedimentaria Plio-Cuaternaria. Tesis doctoral de la Universitat de Barcelona, 618 p.
- Comas, M. C., Platt J. P, Soto, J. I. & Watts, A. B., 1999. The origin and tectonic history of the Alboran basin: insights from Leg 161 results. In: Zahn, R., Comas, M. C. and Klaus, A. (Eds) *Proceeding Ocean Drilling Program, Scientific Results*, 161, 555-579.

- Comas, M. C., Soto, J. I. and BASACALB cruise (TTR-9 Leg 3) Scientific Party 2000. A tectonic overview of mud diapirs and related mud volcanoes in the Alboran Basin. In: Comas, M. C. and Akhmanov, G. G. (Eds) Geological Processes on European continental margins, Intergovernmental Oceanographic Commission (UNESCO), Workshop Report, 168, 29-30.
- Comas, M.C., Zahn, R. Klaus, A. et al. 1996. Preliminary results of ODP Leg 161. Proceeding Ocean Drilling Program, Preliminary Results, 161, 1679 pp.
- Cragg, B. A., Parkes, R. J., Fry, J. C., Weightman, A. J., Rochelle, P. A., Maxwell, J. R., Kastner, M., Hovland, M., Whiticar, M. J., and Sample, J. C., 1995. The impact of fluid and gas venting on bacterial populations and processes in sediments from the Cascadia Margin accretionary system (sites 888-892) and the geochemical consequences, Proceedings of the Ocean Drilling Program, Scientific Results, 146, 399-410.
- Dewey, J.F., Helman, M.L., Turco, E., Hutton, D.H.W. and Knott, S.D., 1989. Kinematics of the western Mediterranean. In: Coward, M. (Ed) Alpine Tectonics. Spec Publ. Geol. Soc. London, 45, 265-283.
- Diaz del Rio, V., Somoza L., Martinez-Frias J., Hernandez-Molina, F.J., Lunar, R., Fernandez-Puga, M.C., Maestro, A., Terrinha, P., Llave, E., Garcia A., Garcia, A. C. and Vazquez, J.T., 2001. Carbonate chimneys in the Gulf of Cadiz: Initial report of their petrography and geochemistry. In: Akhmanov, G. and Suzyumov, A. (Eds.), Geological processes on deep-water European margins. IOC-UNESCO Workshop Report 175, 53-54.
- Droz, L., 1983. L'éventail sous-marin profond du Rhone (Golfe du lion): grands traits morphologiques et structure semi-profonde. PhD Thesis, Université Paris VI, Paris, 195 pp.
- Droz, L. and Bellaiche, G., 1985. Rhone deep-sea fan: morphostructure and growth pattern. AAPG Bulletin, 69, 460-479.
- Droz, L., Kergoat, R., Cochonat, P., Berne, S., 2001. Recent sedimentary events in the western Gulf of Lions (western Mediterranean). Marine Geology, 176, 23-37.
- Flood, R.C., Manley, P.L., Kowsmann, K.O., Appi, C.J. and Pirmez, C., 1991. Seismic Facies and late Quaternary Growth of Amazon Submarine Fan. In: Weimer, P., Link, M.H. (Eds), Seismic Facies and Sedimentary Processes of Submarine Fans and Turbidite Systems. Springer, New York, 415-434.
- Gardner, J.M., 1999. Mud volcanoes on the Moroccan Margin. EOS Transactions, 80(46), 483.
- Gardner, J.M., 2001. Mud volcanoes revealed and sampled on the Moroccan continental margin. Geophysical Research Letters, 28, 339-342.
- Hornibrook, E. R. C., Longstaffe, F. J., and Fyfe, W. S., 1997. Spatial distribution of microbial methane production pathways in temperate zone wetland soils: stable carbon and hydrogen isotope evidence, Geochimica et Cosmochimica Acta, 61, 745-753.
- Ivanov, M.K., Kenyon, N.H., Nielsen, T., Wheeler, A., Monteiro, J., Gardner, J., Comas, M., Akhmanov, G., Akhmetzhanov, A., and Scientific Party of the TTR-9 cruise., 2000. Goals and principal results of the TTR-9 cruise. Geological processes on European Continental Margin (TTR-9) Post-Cruise Conference. IOC Workshop Report, 168, 3-4.
- Kenyon, N.H., Millington, J., Droz, L. and Ivanov, M.K., 1995. Scour holes in a channel-lobe transition zone on the Rhone cone. In: Pickering, K.T., Hiscott, R.N., Kenyon, N.H., Lucchi, F.R., Smith, R.D.A. (Eds), Atlas of Deep-water Environments: Architectural Styles in Turbidite Systems. Chapman & Hall, London, 212-215.
- Kenyon, N.H., Ivanov, M. K., Akhmetzhanov, A. and Akhmanov, G. G., 2000. Multidisciplinary Study of Geological Processes on the North East Atlantic and Western Mediterranean Margins. IOC Technical Series, 56, UNESCO, 119 pp.
- Kenyon, N.H., Ivanov, M. K., Akhmetzhanov, A. and Akhmanov, G. G. (Eds.), 2003. Interdisciplinary geoscience research on the North East Atlantic margin, Mediterranean Sea and Mid-Atlantic Ridge. IOC Technical Series, 67, UNESCO, 152 pp.
- Klaucke, I., Masson, D.G., Kenyon, N.H. and Gardner, J.V., 2004. Sedimentary pro-

cesses of the lower Monterey Fan channel and channel-mouth lobe. *Marine Geology*, 206, 181-198.

Lastras, G., Canals, M., Urgeles, R., Hughes-Clarke, J.E. and Acosta, J., 2004. Shallow slides and pockmark swarms in the Eivissa Channel, western Mediterranean Sea. *Sedimentology*, 51, 837-850.

Limonov, A.F., Woodside, J.M. and Ivanov, M.K. (Eds), 1993. Geological and geophysical investigations of Western Mediterranean deep sea fans. UNESCO reports in marine science, 62, 154 pp.

López-Jurado, J.L. and Díaz del Río, G. 1994. Dinámica asociada a las masas de agua en el Canal de Ibiza en noviembre de 1990 y marzo de 1991. *Bol. Inst. Esp. Oceanogr.*, 10, 3-22.

Maldonado, A. and Comas, M. C., 1992. Geology and geophysics of the Alboran Sea: An introduction. *Geo-Marine Letters*, 12, 61-65.

Maldonado, A., Somoza, L. and Pallarés, L., 1999. The Betic orogen and the Iberian-African boundary in the Gulf of Cadiz : geological evolution (Central North Atlantic). *Marine Geology*, 155, 9-43.

Martinez-Ruiz, F., Paytan, A., Kastner, M., Gozalez-Donoso, J.M., Linares, D., Bernasconi, S.M. and Jimenez-Espejo, F.J., 2003. A comparative study of the geochemical and mineralogical characteristics of the S1 sapropel in the western and eastern Mediterranean. *Paleoceanography*, 190, 23-37.

Mauffret, A., Grossouvre, B.D., Dos Reis, A.T., Gorini, C. and Nercessian, A., 2001. Structural geometry in the eastern Pyrenees and western Gulf of Lion (Western Mediterranean). *Journal of Structural Geology*, 23, 1701-1726.

Mazurenko, L. L., Soloviev, V. A., Belenkaya, I., Ivanov, M. K. and Pinheiro, L. M., 2002. Mud volcano gas hydrates in the Gulf of Cadiz. *Terra Nova*, 14, 321-329.

McAullife, C., 1971. GC determination of solutes by multiple phase equilibration. *Chem. Tech.* 1, 46-51.

Mear, Y., 1984. Sequences et unités sédimentaires du glacier rhodanien (Méditerranée occidentale). Thesis Doct. 3ème cycle, University of Perpignan.

Pinheiro, L.M., Ivanov, M.K., Sautkin, A., Akhmanov, G., Magalhaes, V.H., Volkonskaya, A., Monteiro, J.H., Somoza, L., Gardner, J., Hamouni, N. and Cunha, M.R., 2003. Mud volcanism in the Gulf of Cadiz: results from the TTR-10 cruise. *Marine Geology*, 195, 131-151.

Pratson, L.F. and Coakley, B.J., 1996. A model for the headward erosion of submarine canyons induced by downslope-eroding sediment flows. *GSA Bulletin*, 108, 225-234.

Riaz, C. and Martinez del Olmo, W., 1996. Depositional model of the Guadalquivir-Gulf of Cadiz Tertiary basin, In: Friend, P.F. and Dabrio, C.J., (Eds), Tertiary basin of Spain: the stratigraphic record of crustal kinematics: Cambridge University Press, 330-338.

Sautkin, A., Talukder, A. R., Comas, M. C., Soto, J. I. and Alekseev, A., 2003. Mud volcanoes in the Alboran Sea: evidence from micropaleontological and geophysical data. *Marine Geology*, 195, 237-261.

Somoza, L., Maestro, A. and Lowrie, A., 1999. Allochthonous Blocks as Hydrocarbon Traps in the Gulf of Cadiz. Offshore Technology Conference OTC 10889, 571-577.

Somoza, L., Ivanov M.K., Pinheiro, L., Maestro, A., Lowrie, A., Vazquez, J.T., Gardner, J., Medialdea, T. and Fernandez-Puga, M.C., 2001. Structural and tectonic control of fluid seeps and mud volcanoes in the Gulf of Cadiz. In: Akhmanov, G. and Suzyumov, A. (Eds.), Geological processes on deep-water European margins. IOC Workshop Report, 175, UNESCO, 41-42.

Somoza, L., Diaz-del-Rio, V., Leon, R., Ivanov, M., Fernandez-Puga, M.C., Gardner, J.M., Hernandez-Molina, F.J., Pinheiro, L. M., Rodero, J., Lobato, A., Maestro, A., Vazquez, J. T., Medialdea, T. and Fernandez-Salas, L.M., 2003. Seabed morphology and hydrocarbon seepage in the Gulf of Cadiz mud volcano area: Acoustic imagery, multi-beam and ultra-high resolution seismic data. *Marine Geology*, 195, 153-176.

Talukder, A. R., Comas, M. C., Soto, J. I. and BASACALB cruise (TTR-9 Leg 3) Scientific Party, 2000. Diapirs and related structures in the mud volcano area of the West Alboran basin. In: Comas, M. C. and Akhmanov, G. G. (Eds.). Geological

Processes on European continental margins, IOC Workshop Report, 168, UNESCO, 22-23.

Tobias, H. J. and Brenna, J. T., 1997. On-line pyrolysis as a limitless reduction source for high-precision isotopic analysis of organic-derived hydrogen, *Analytical Chemistry*, 69, 3148-3152.

Torne, M., Fernandez, M., Comas, M.C. and Soto, J.I., 2000. Lithospheric structure beneath the Alborán Basin: Results from 3D gravity modelling and tectonic relevance. *J. Geoph. Res.*, 105, 3209-3228.




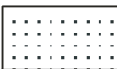
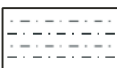







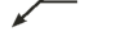
















Torres, J., Droz, L., Savoye, B., Terentieva, E., Cochonat, P., Kenyon, N.H. and Canals, M., 1997, Deep-sea avulsion and morphosedimentary evolution of the Rhone Fan Valley and Neofan during the Late Quaternary (north western Mediterranean). *Sedimentology*, 44, 457-477.

Wilson, R.C.L., Hiscott, R.N., Willis M.G. and Gradstein, F.M., 1989. The Lusitanian Basin of West-Central Portugal: Mesozoic and Tertiary tectonics, stratigraphy, and subsidence history. In: Tankard, A.J., Balkwill, H.R. (Eds), *Extensional tectonics and stratigraphy of the North Atlantic margins*. Am. Assoc. Pet. Geol. and Can. Geol. Found. AAPG Mem., 46, 111-130.

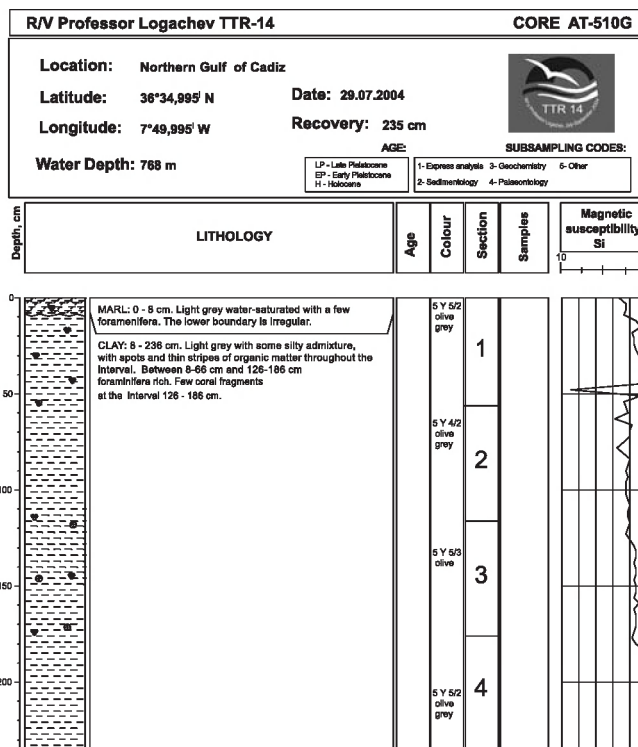
Whiticar, M. J., Faber, E. and Schoell, M., 1986. Biogenic methane formation in marine and freshwater environments: CO₂ reduction vs. acetate formation-Isotope evidence. *Geochim. Cosmochim. Acta*, 50, 693-709.

Wynn, R.B. and Masson, D.G., 2003. Canary Islands landslides and tsunami generation. In: Mienert, J. and Locat, J., (Eds.), *Proc. 1st Int. Symposium on Submarine Mass Movements and their Consequences*, Kluwer, Dordrecht, 325-332.

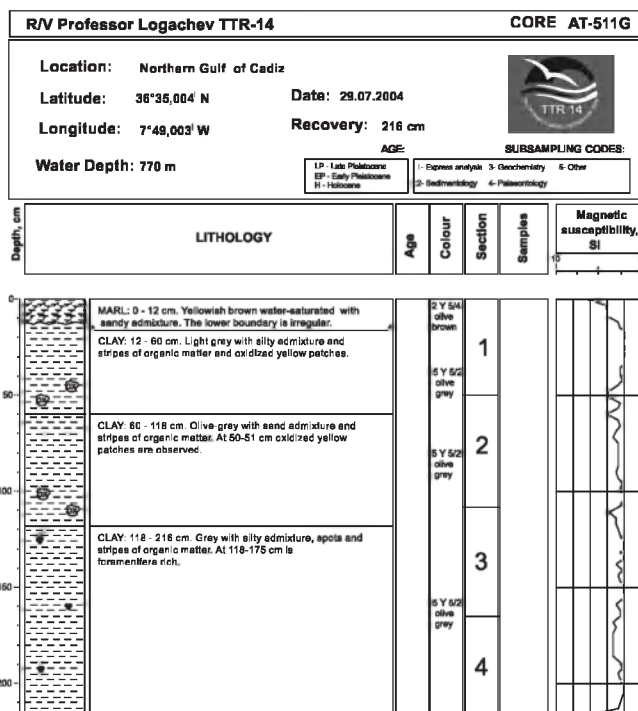
ANNEX I. CORE LOGS

LEGEND	
	Foraminifera rich sediment
	marl
	mud/clay
	sand
	silt
	turbidite
	debris flow
	slump
	planar lamination
	cross lamination
	gradational boundary
	irregular boundary
	fault
	firm ground
	hard ground
	corals
	echinoderms
	gastropods
	plant debris
	shell fragments
	gas hydrate
	drop stones
	others
	lithoclasts
	oxidized layer
	dark layer
	flow in
	bioturbation
	burrows
	soupy sediment

ANNEX I. CORE LOGS (LEG 1, Gulf of Cadiz)

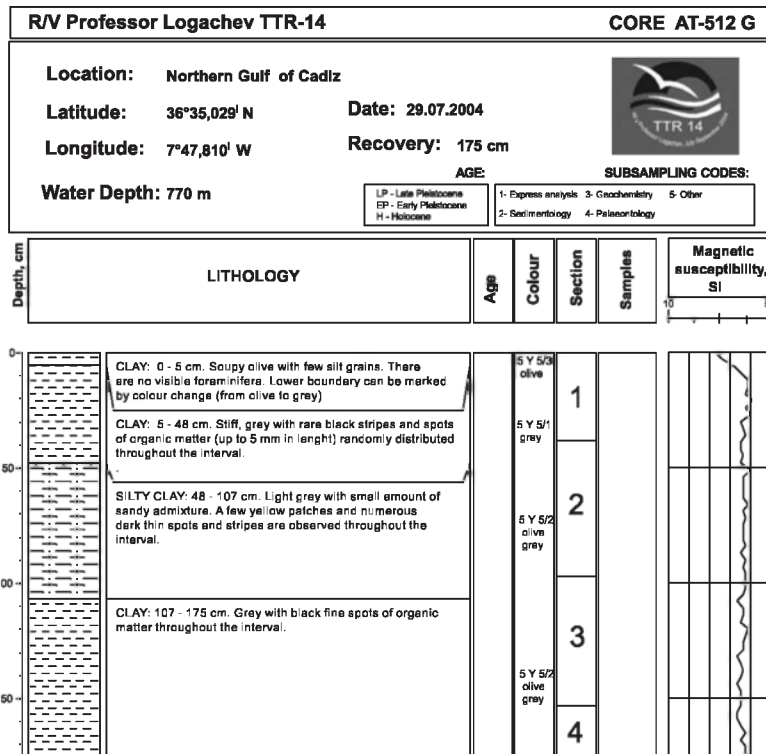


Core log TTR-14-AT-510G

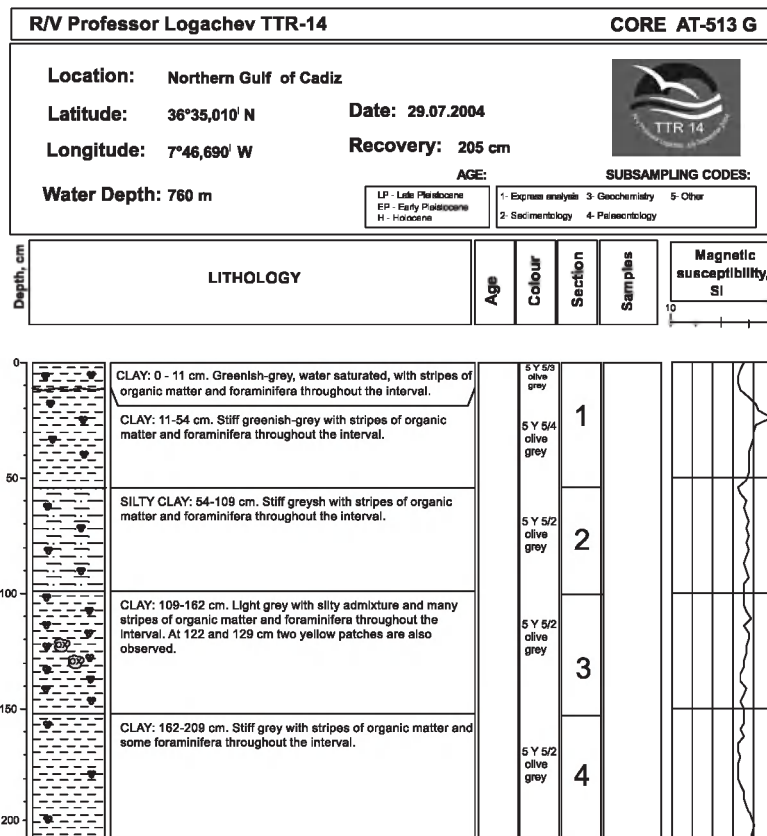


Core log TTR-14-AT-511G

ANNEX I. CORE LOGS (LEG 1, Gulf of Cadiz)

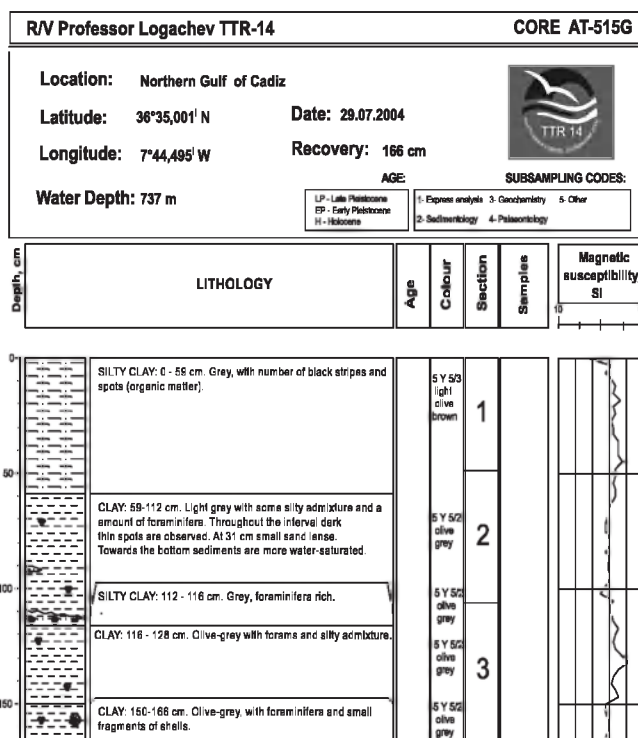


Core log TTR-14-AT-512G

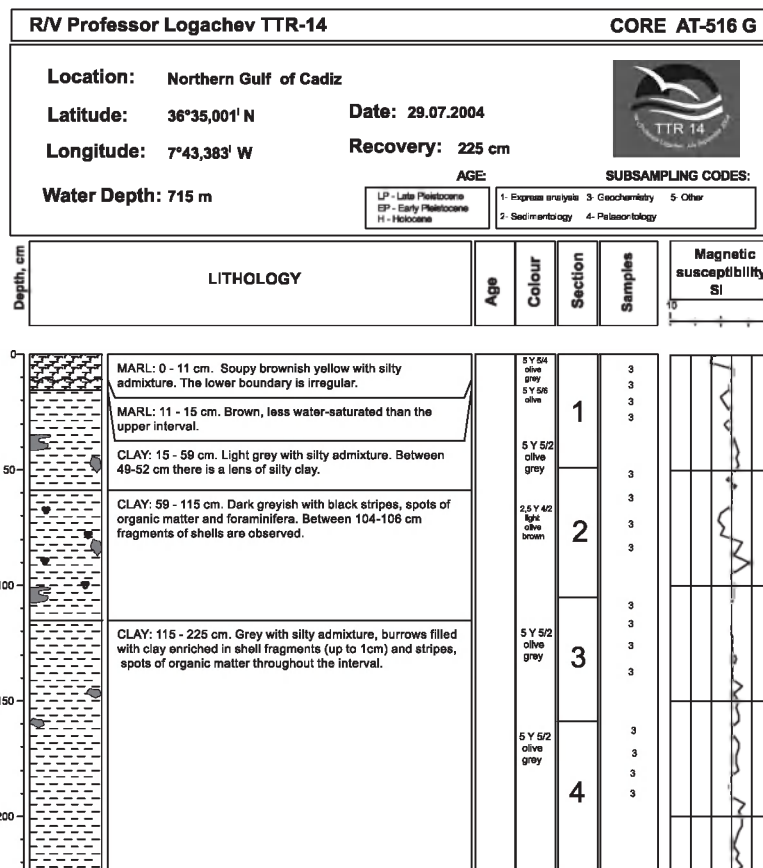


Core log TTR-14-AT-513G

ANNEX I. CORE LOGS (LEG 1, Gulf of Cadiz)

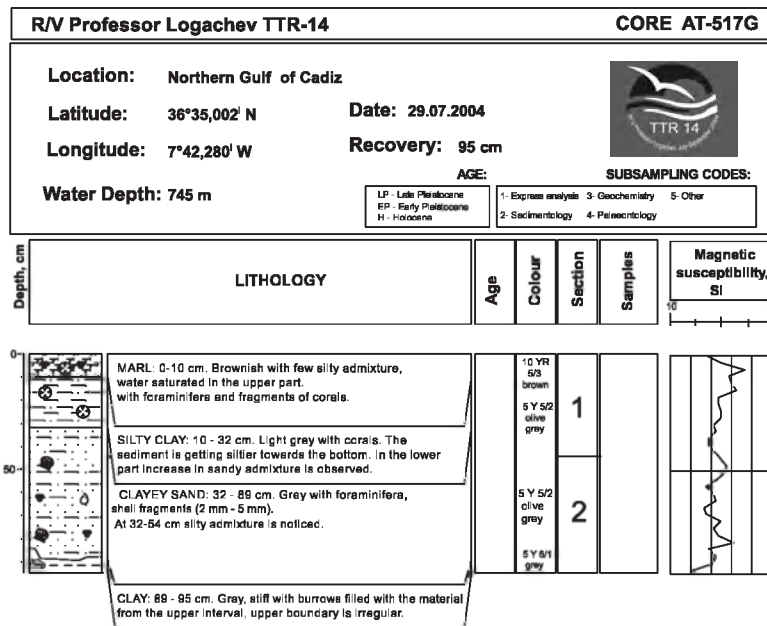


Core log TTR-14-AT-515G

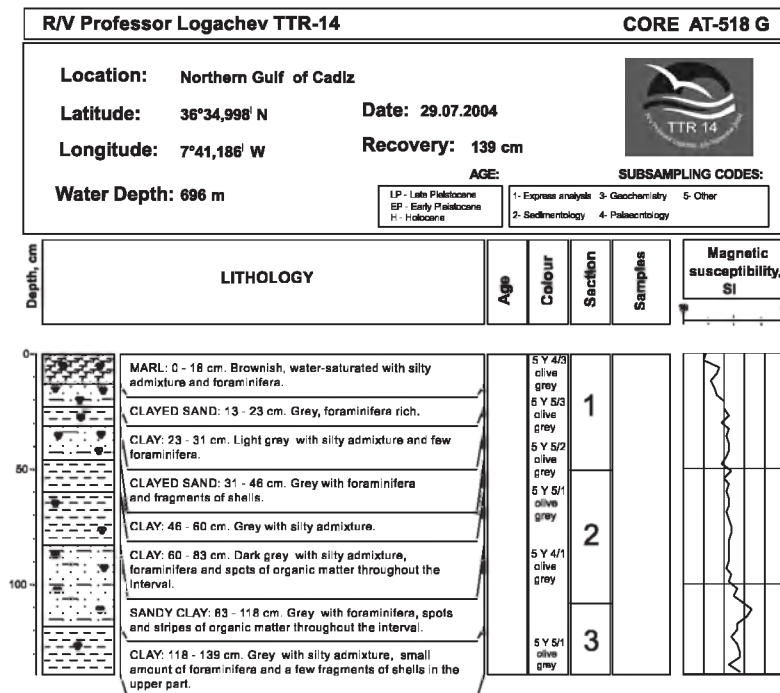


Core log TTR-14-AT-516G

ANNEX I. CORE LOGS (LEG 1, Gulf of Cadiz)

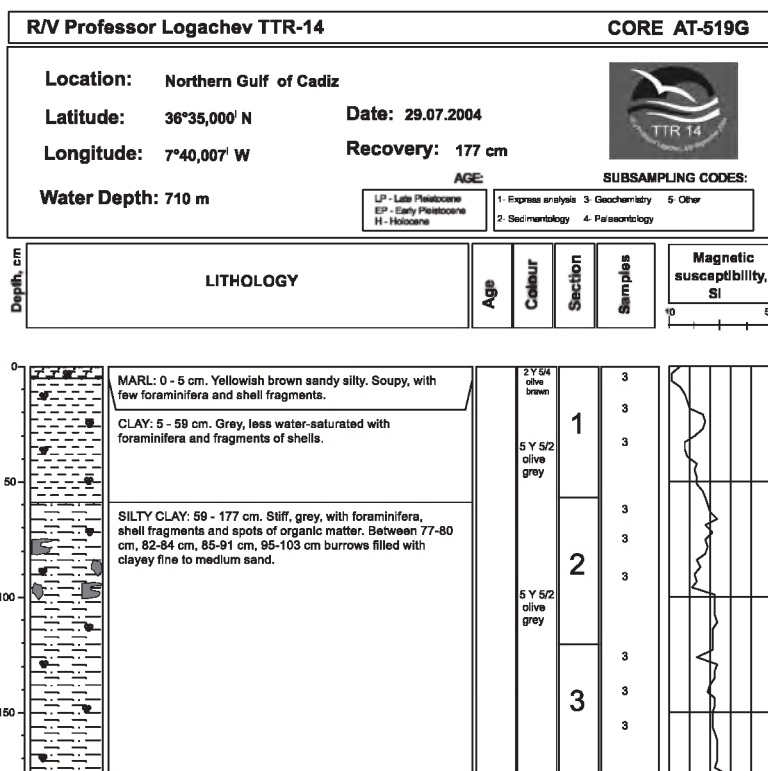


Core log TTR-14-AT-517G

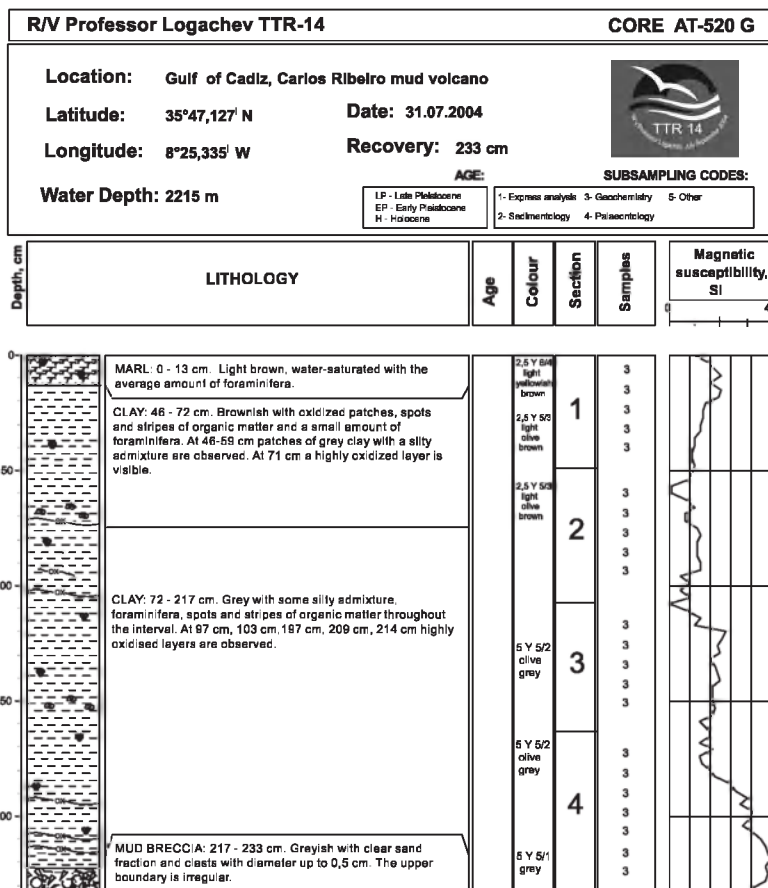


Core log TTR-14-AT-518G

ANNEX I. CORE LOGS (LEG 1, Gulf of Cadiz)

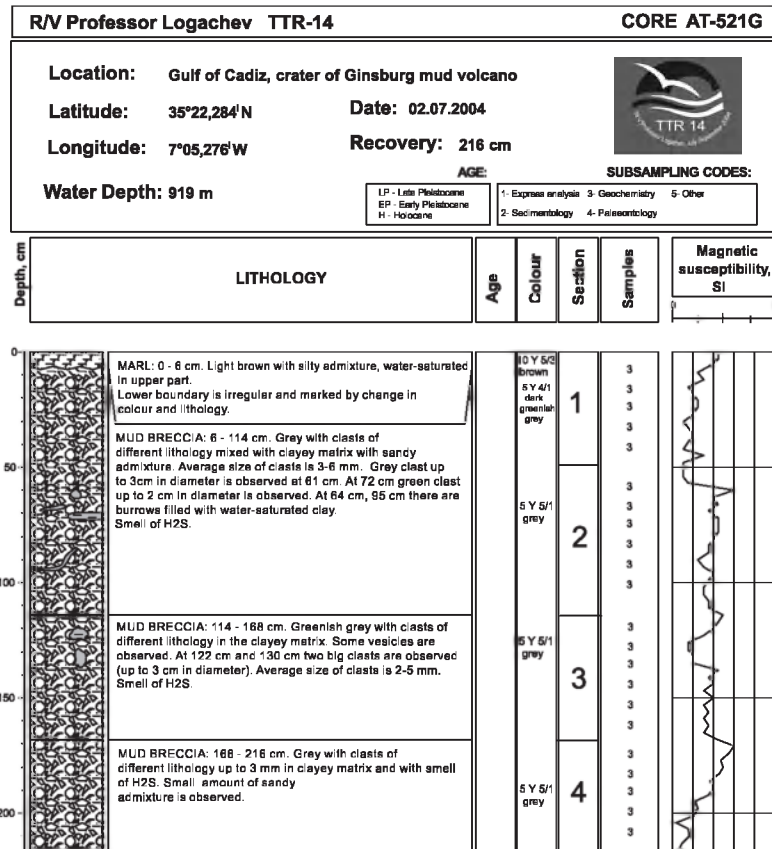


Core log TTR-14-AT-519G

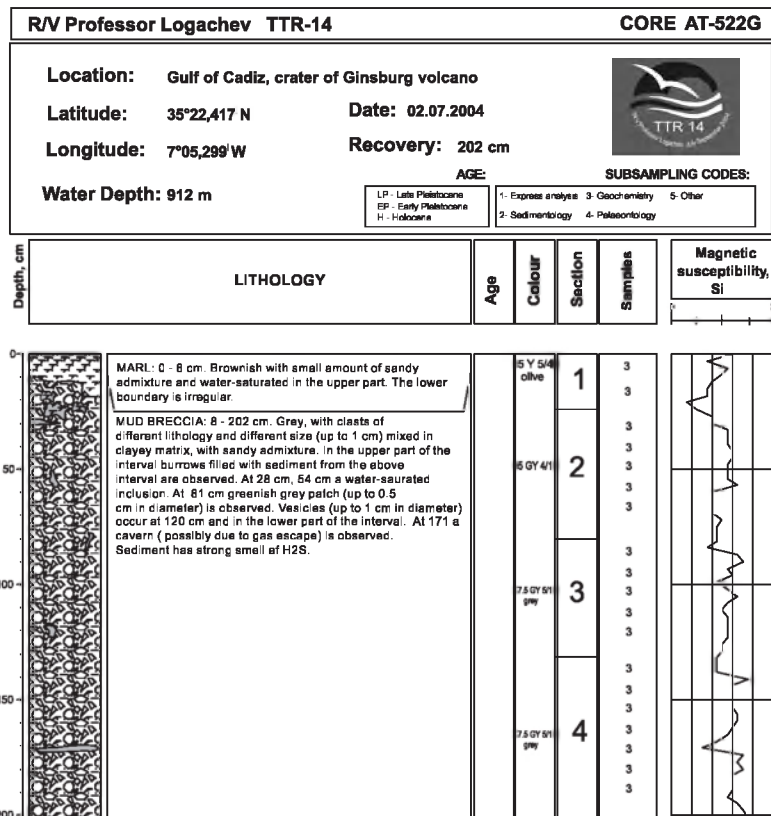


Core log TTR-14-AT-520G

ANNEX I. CORE LOGS (LEG 1, Gulf of Cadiz)

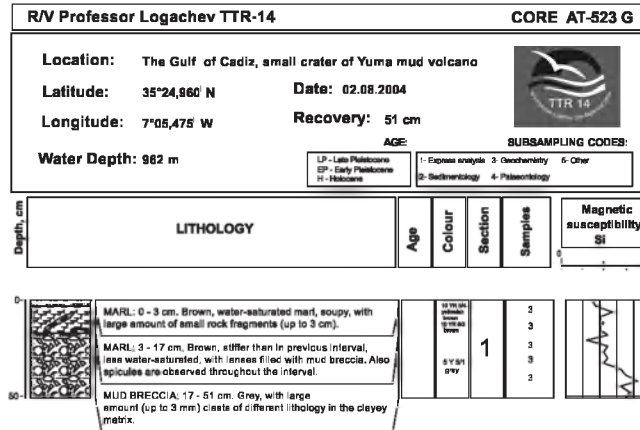


Core log TTR-14-AT-521G

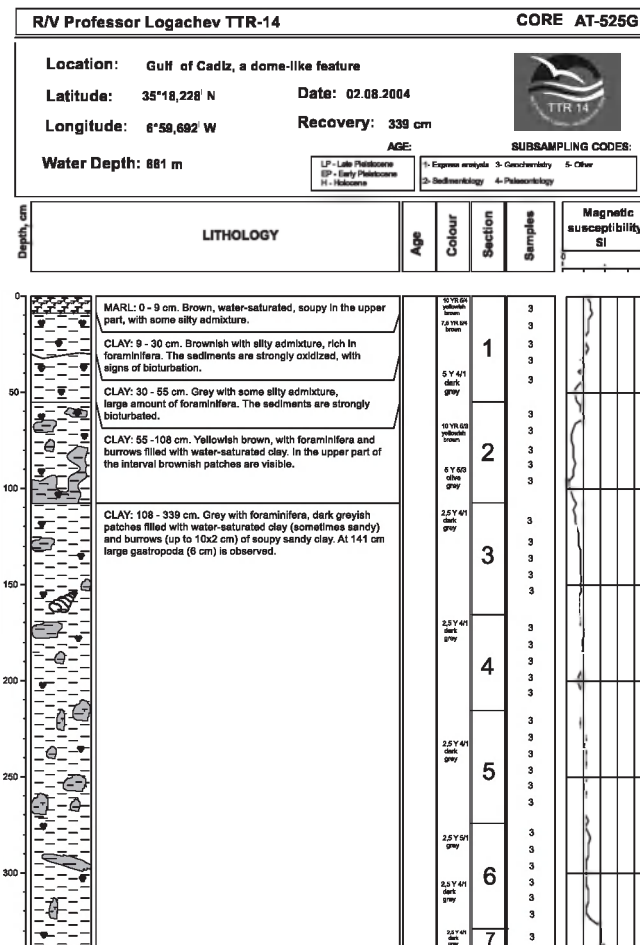


Core log TTR-14-AT-522G

ANNEX I. CORE LOGS (LEG 1, Gulf of Cadiz)




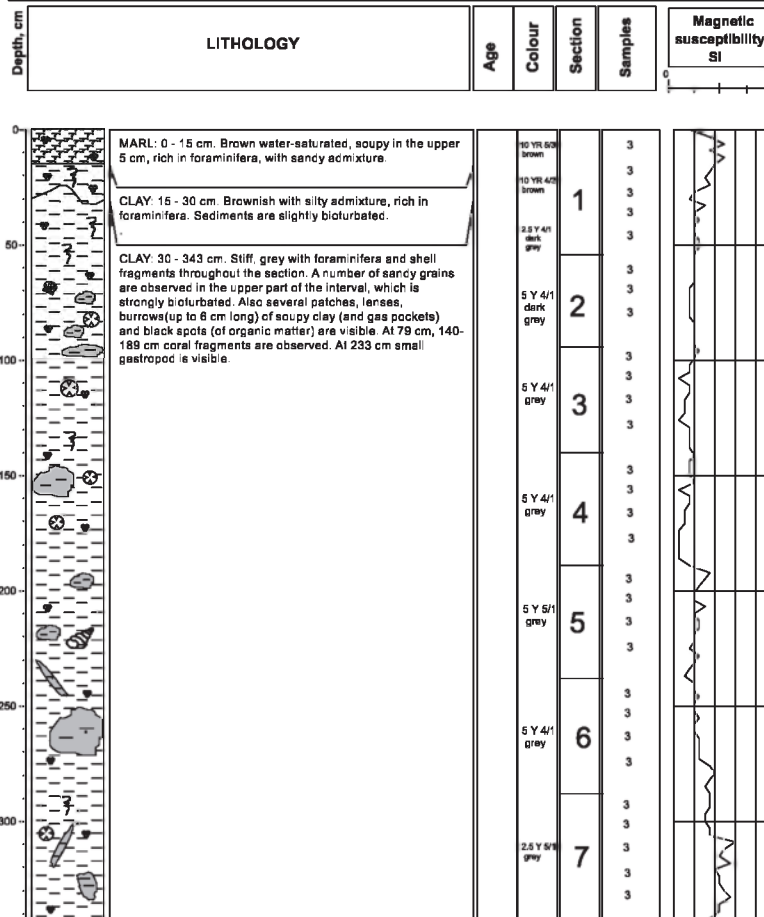
Core log TTR-14-AT-523G




Core log TTR-14-AT-525G

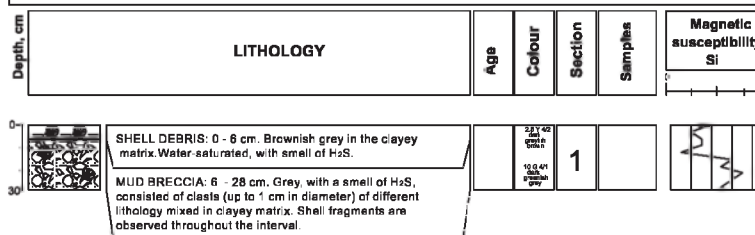
ANNEX I. CORE LOGS (LEG 1, Gulf of Cadiz)

R/V Professor Logachev TTR-14		CORE AT-526 G	
Location: Gulf of Cadiz, a dome-like feature			
Latitude: 36°18,135' N	Date: 02.08.2004		
Longitude: 6°59,693' W	Recovery: 343 cm		
Water Depth: 862 m		AGE:	
<small>LP - Late Pleistocene EP - Early Pleistocene H - Holocene</small>		<small>1- Express analysis 3- Geochemistry 5- Other 2- Sedimentology 4- Paleontology</small>	



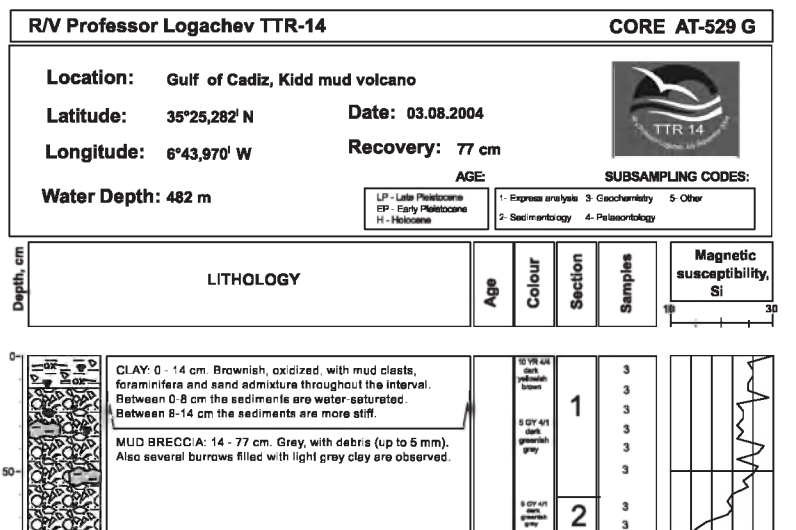
Core log TTR-14-AT-526G

R/V Professor Logachev TTR-14		CORE AT-527 G	
Location: Gulf of Cadiz, Kidd mud volcano			
Latitude: 35°25,281' N	Date: 03.08.2004		
Longitude: 6°43,970' W	Recovery: 28 cm		
Water Depth: 482 m		AGE:	
<small>LP - Late Pleistocene EP - Early Pleistocene H - Holocene</small>		<small>1- Express analysis 3- Geochemistry 5- Other 2- Sedimentology 4- Paleontology</small>	

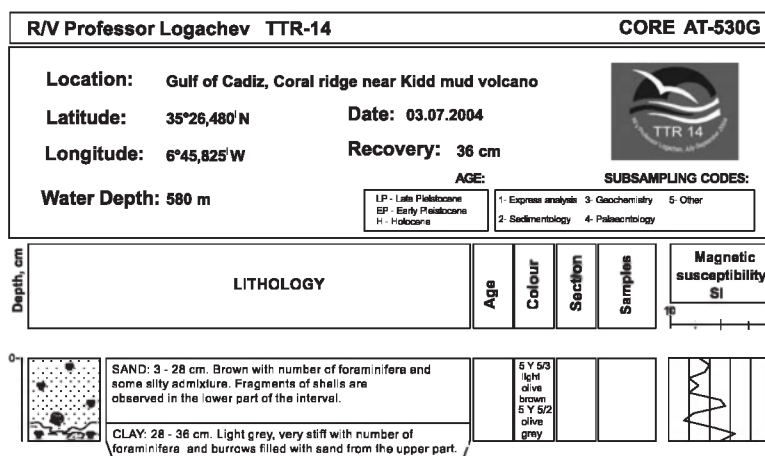


Core log TTR-14-AT-527G

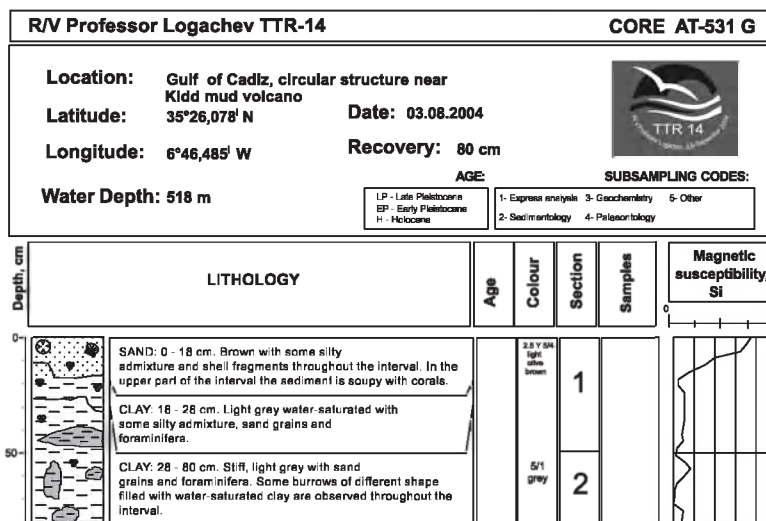
ANNEX I. CORE LOGS (LEG 1, Gulf of Cadiz)



Core log TTR-14-AT-529G

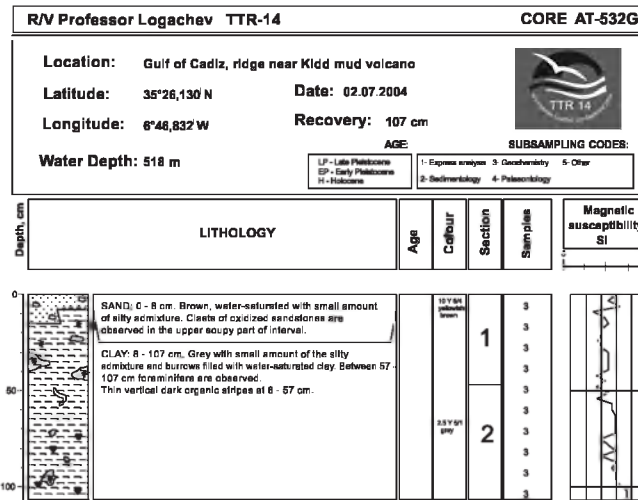


Core log TTR-14-AT-530G

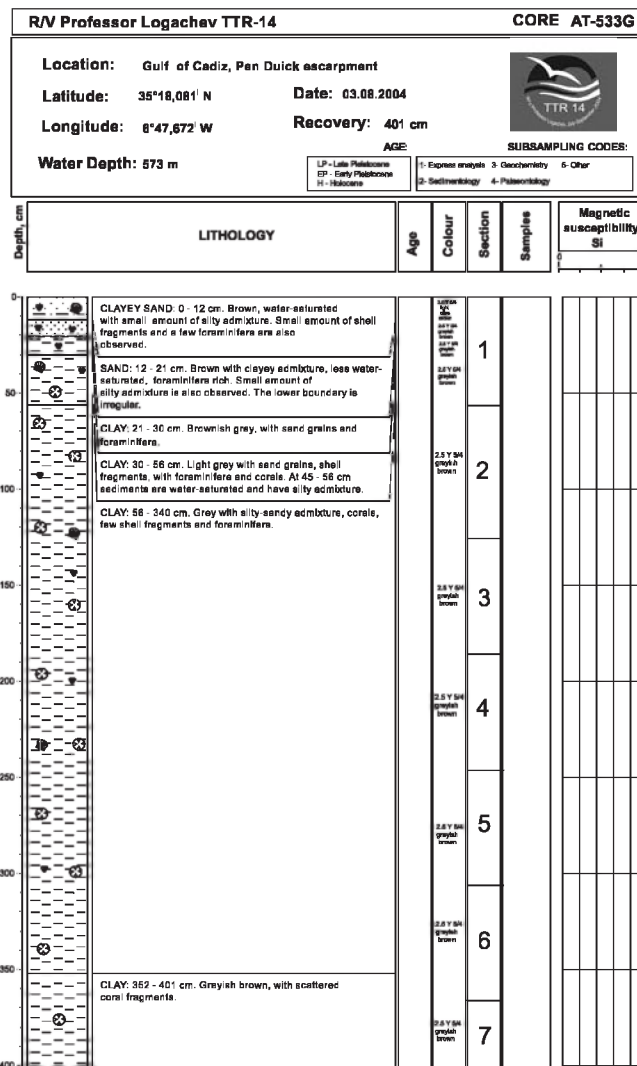


Core log TTR-14-AT-531G

ANNEX I. CORE LOGS (LEG 1, Gulf of Cadiz)

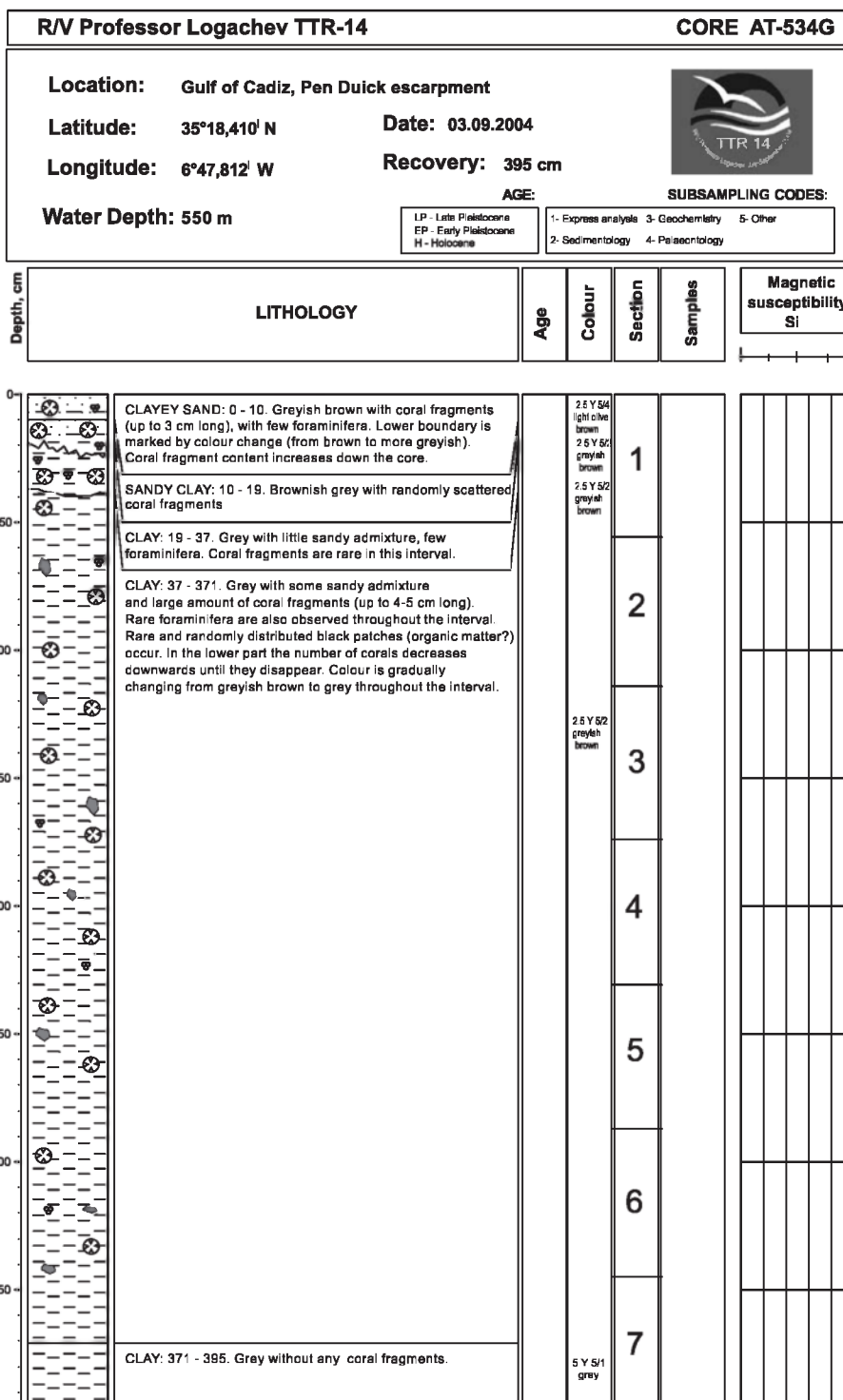


Core log TTR-14-AT-532G



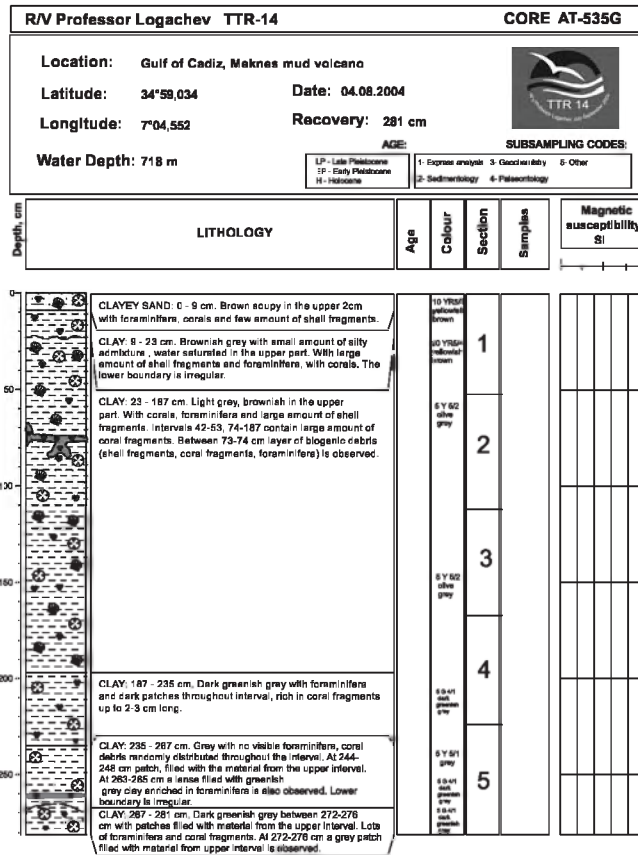
Core log TTR-14-AT-533G

ANNEX I. CORE LOGS (LEG 1, Gulf of Cadiz)

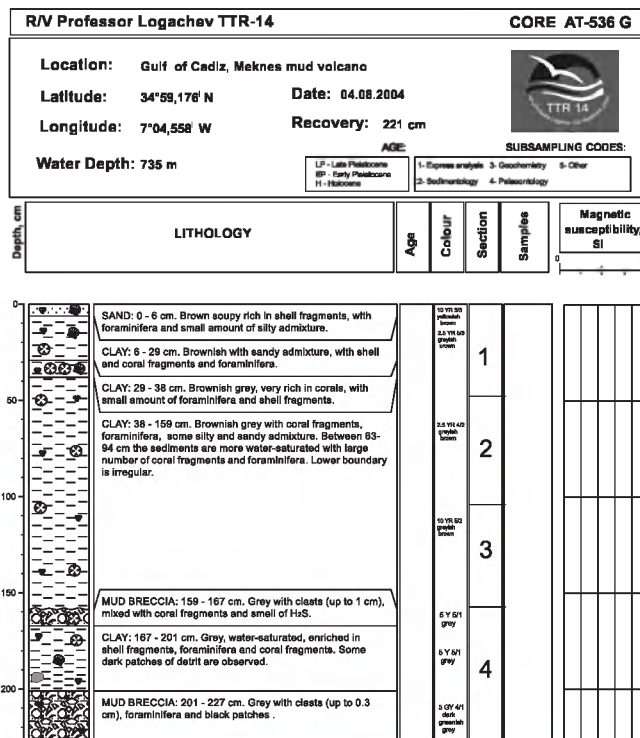


Core log TTR-14-AT-534G

ANNEX I. CORE LOGS (LEG 1, Gulf of Cadiz)

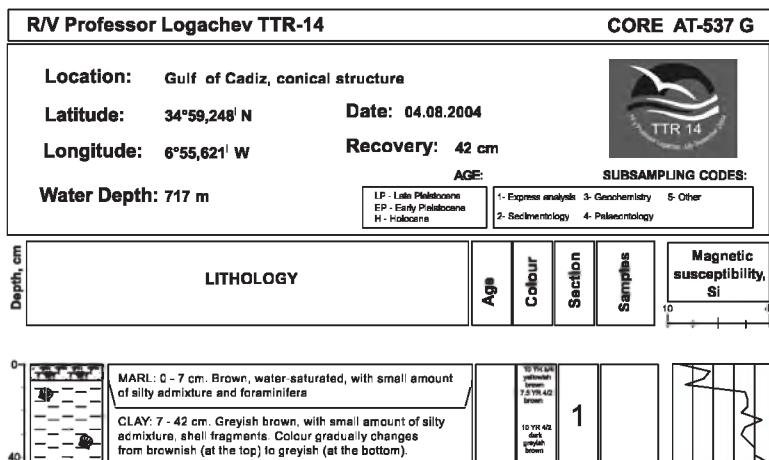


Core log TTR-14-AT-535G

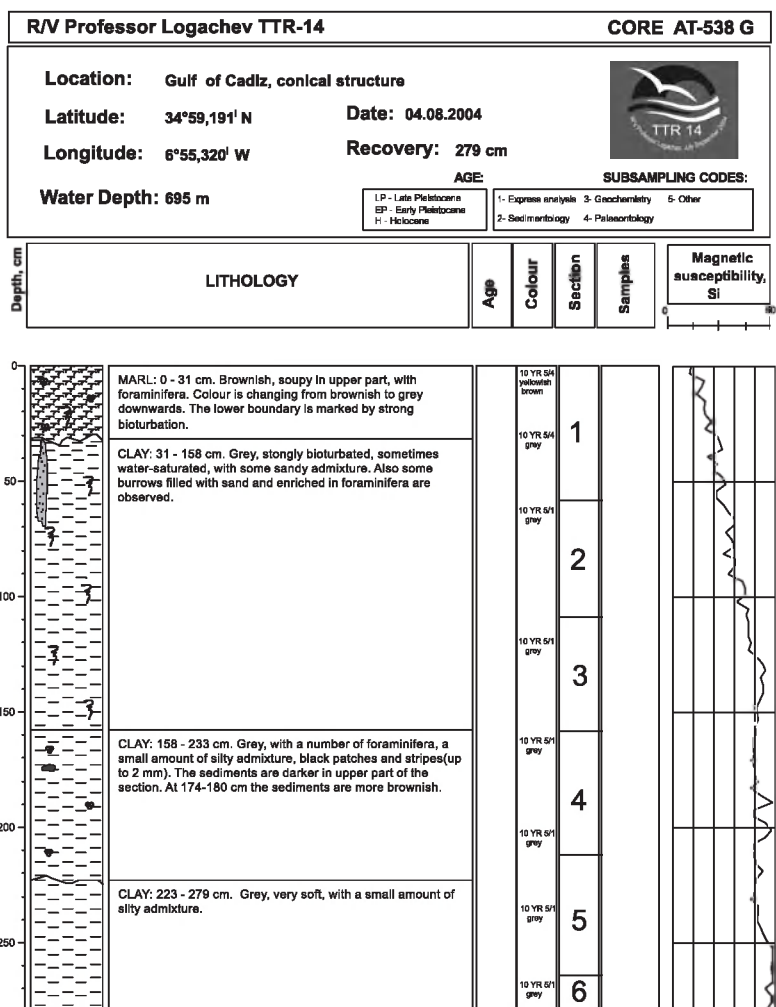


Core log TTR-14-AT-536G

ANNEX I. CORE LOGS (LEG 1, Gulf of Cadiz)

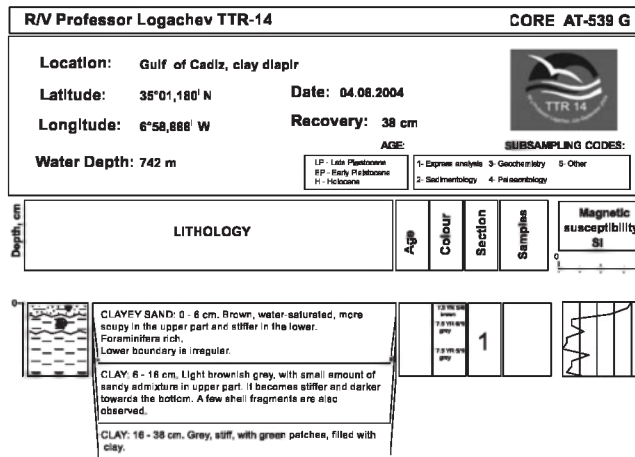


Core log TTR-14-AT-537G

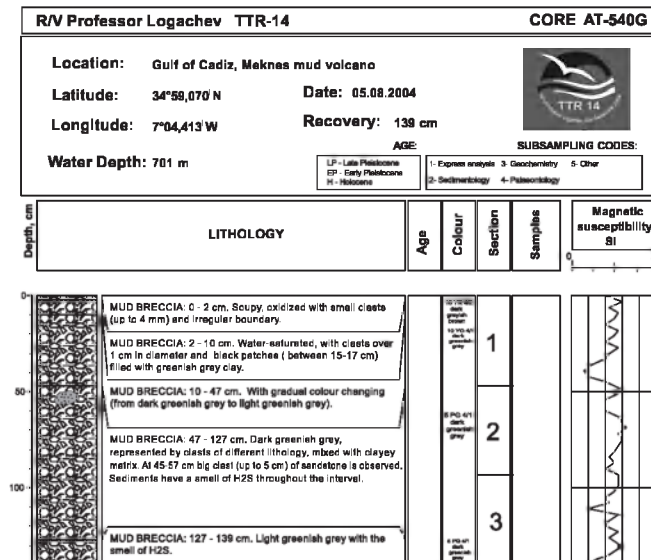


Core log TTR-14-AT-538G

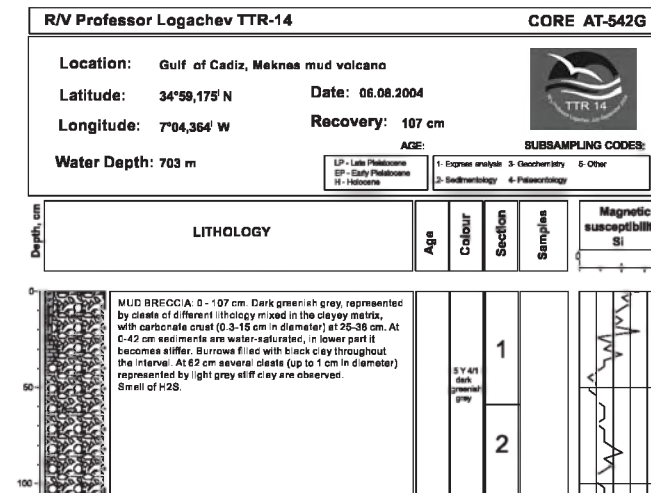
ANNEX I. CORE LOGS (LEG 1, Gulf of Cadiz)



Core log TTR-14-AT-539G

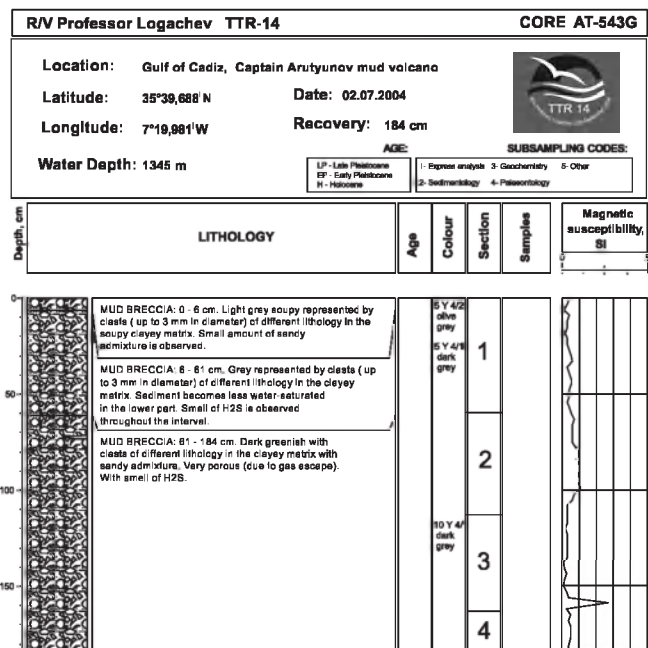


Core log TTR-14-AT-540G

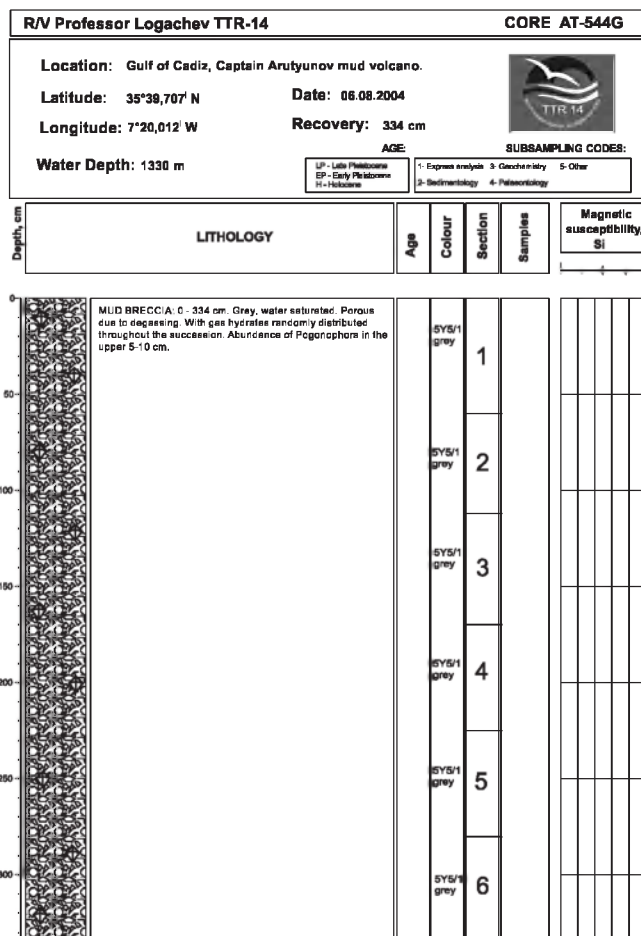


Core log TTR-14-AT-542G

ANNEX I. CORE LOGS (LEG 1, Gulf of Cadiz)

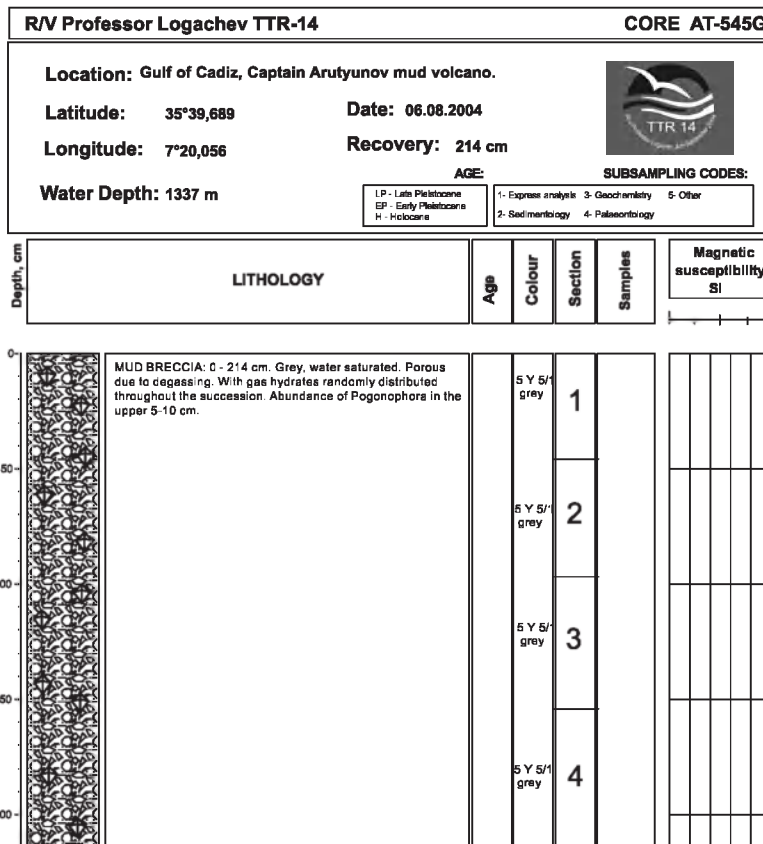


Core log TTR-14-AT-543G

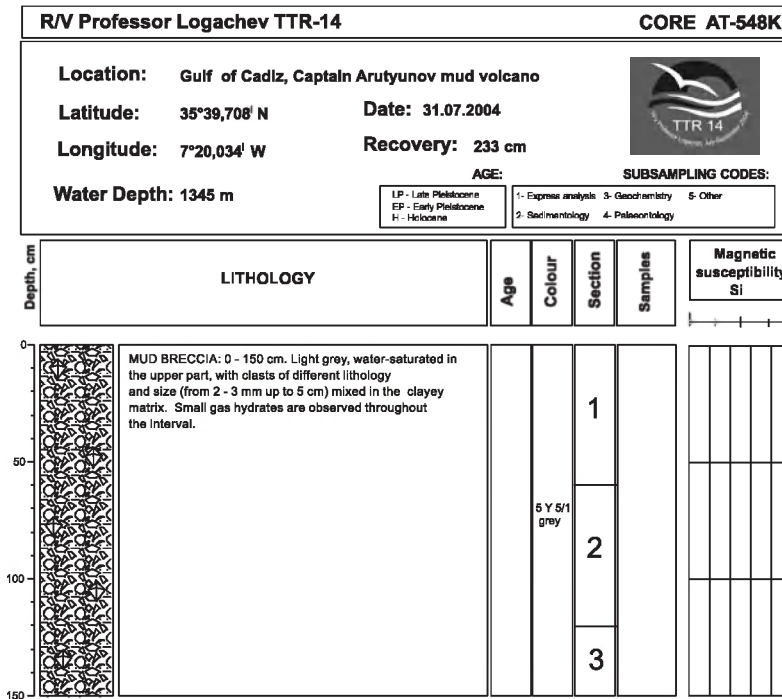


Core log TTR-14-AT-544G

ANNEX I. CORE LOGS (LEG 1, Gulf of Cadiz)

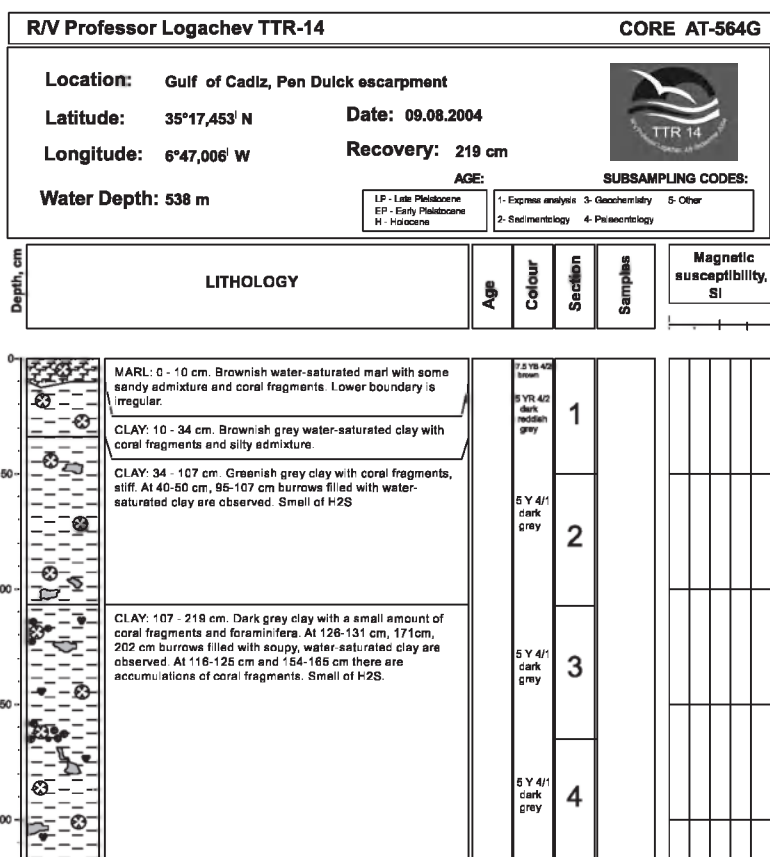


Core log TTR-14-AT-545G




Core log TTR-14-AT-548K

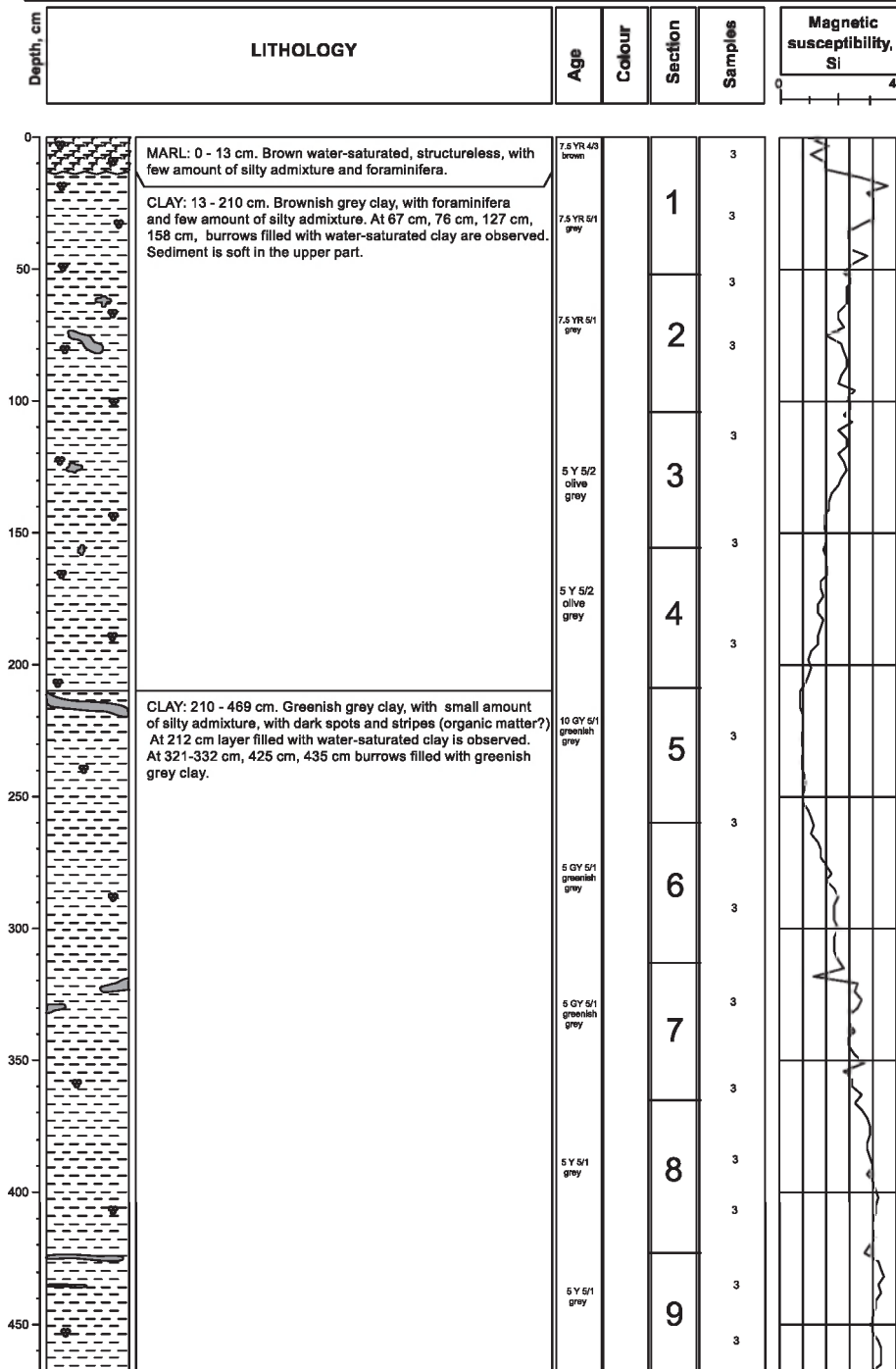
ANNEX I. CORE LOGS (LEG 1, Gulf of Cadiz)



Core log TTR-14-AT-564G

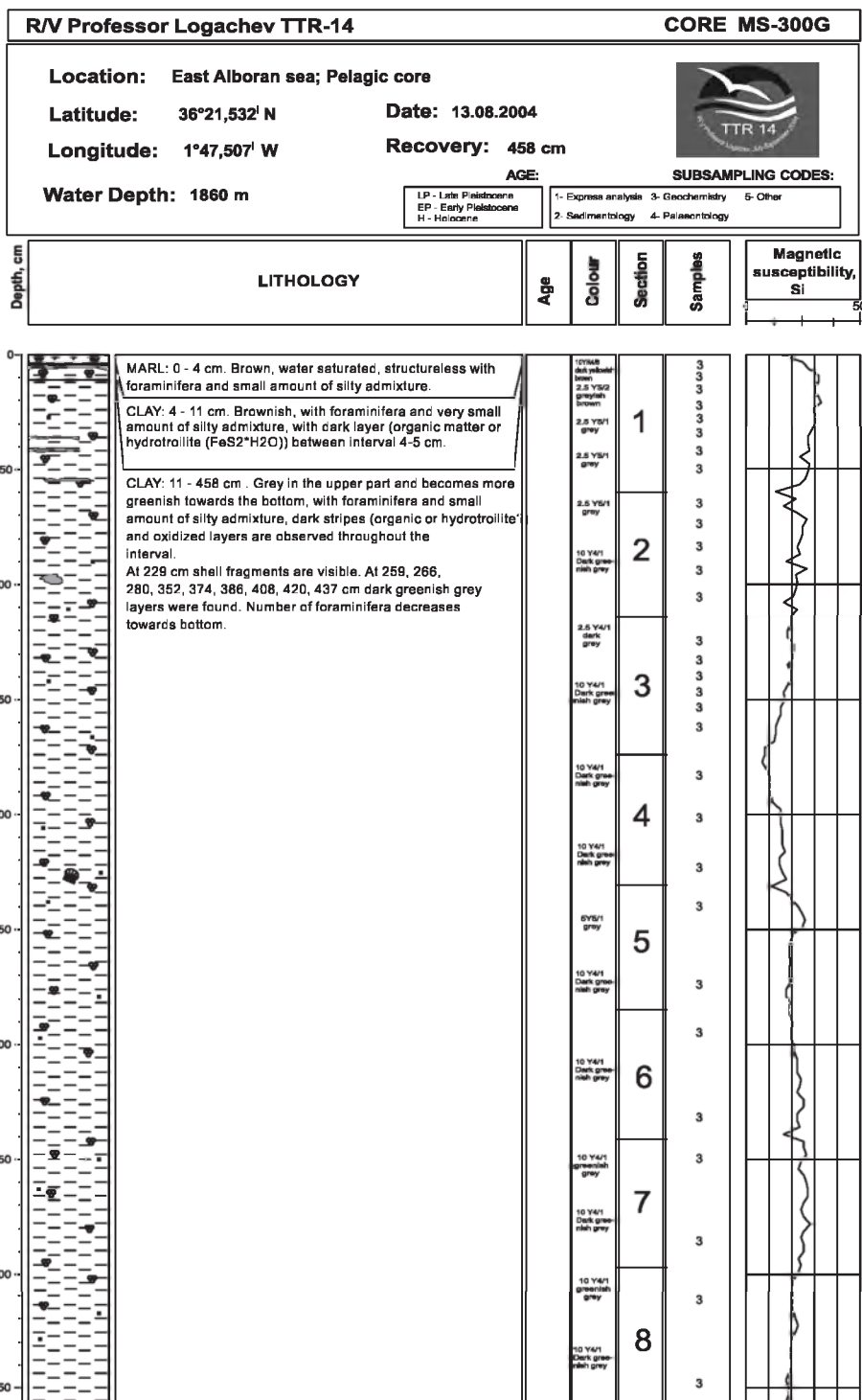
ANNEX I. CORE LOGS (LEG 2, Alboran Sea)

R/V Professor Logachev TTR-14		CORE MS-299G												
Location: East Alboran sea; Pelagic core														
Latitude: 36°13,897' N	Date: 13.08.2004													
Longitude: 2°03,350' W	Recovery: 469 cm													
Water Depth: 1938 m	AGE:	SUBSAMPLING CODES:												
	<table border="1" style="font-size: small;"> <tr> <td>LP - Late Pleistocene</td> <td>1- Express analysis</td> <td>3- Geochemistry</td> <td>5- Other</td> </tr> <tr> <td>EP - Early Pleistocene</td> <td>2- Sedimentology</td> <td>4- Palaeontology</td> <td></td> </tr> <tr> <td>H - Holocene</td> <td></td> <td></td> <td></td> </tr> </table>	LP - Late Pleistocene	1- Express analysis	3- Geochemistry	5- Other	EP - Early Pleistocene	2- Sedimentology	4- Palaeontology		H - Holocene				
LP - Late Pleistocene	1- Express analysis	3- Geochemistry	5- Other											
EP - Early Pleistocene	2- Sedimentology	4- Palaeontology												
H - Holocene														



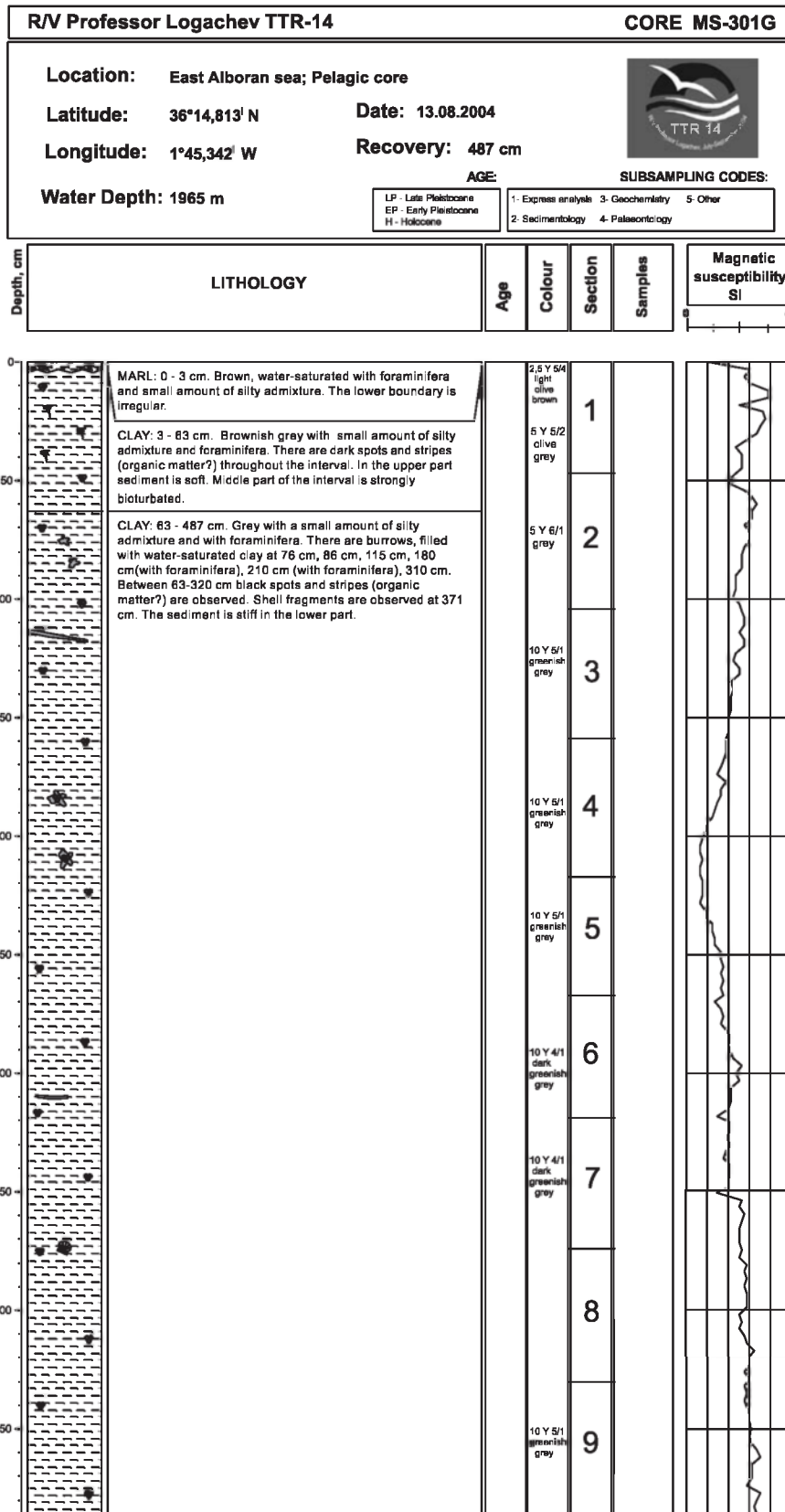
Core log TTR-14-MS-299G

ANNEX I. CORE LOGS (LEG 2, Alboran Sea)



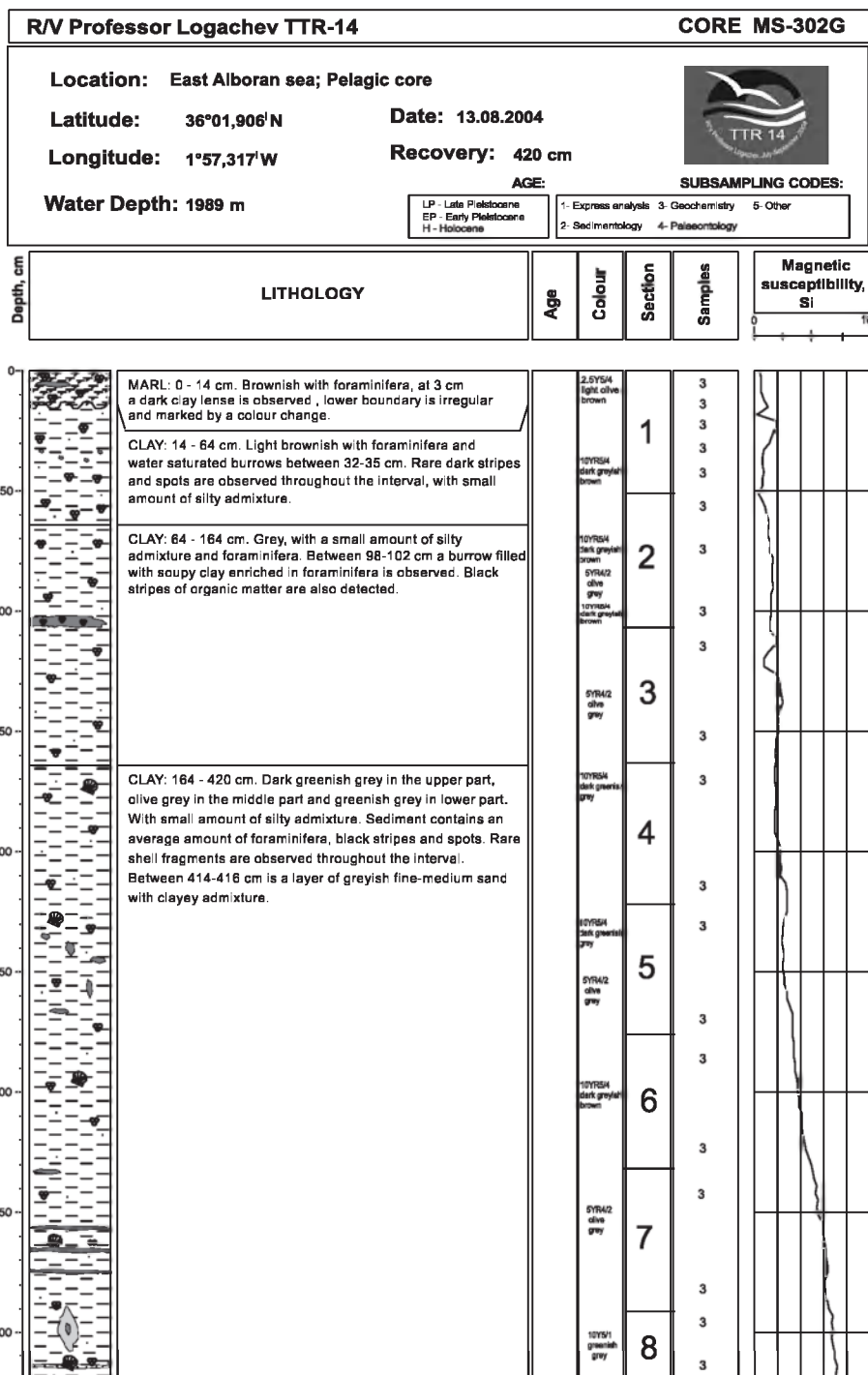
Core log TTR-14-MS-300G

ANNEX I. CORE LOGS (LEG 2, Alboran Sea)




Core log TTR-14-MS-301G

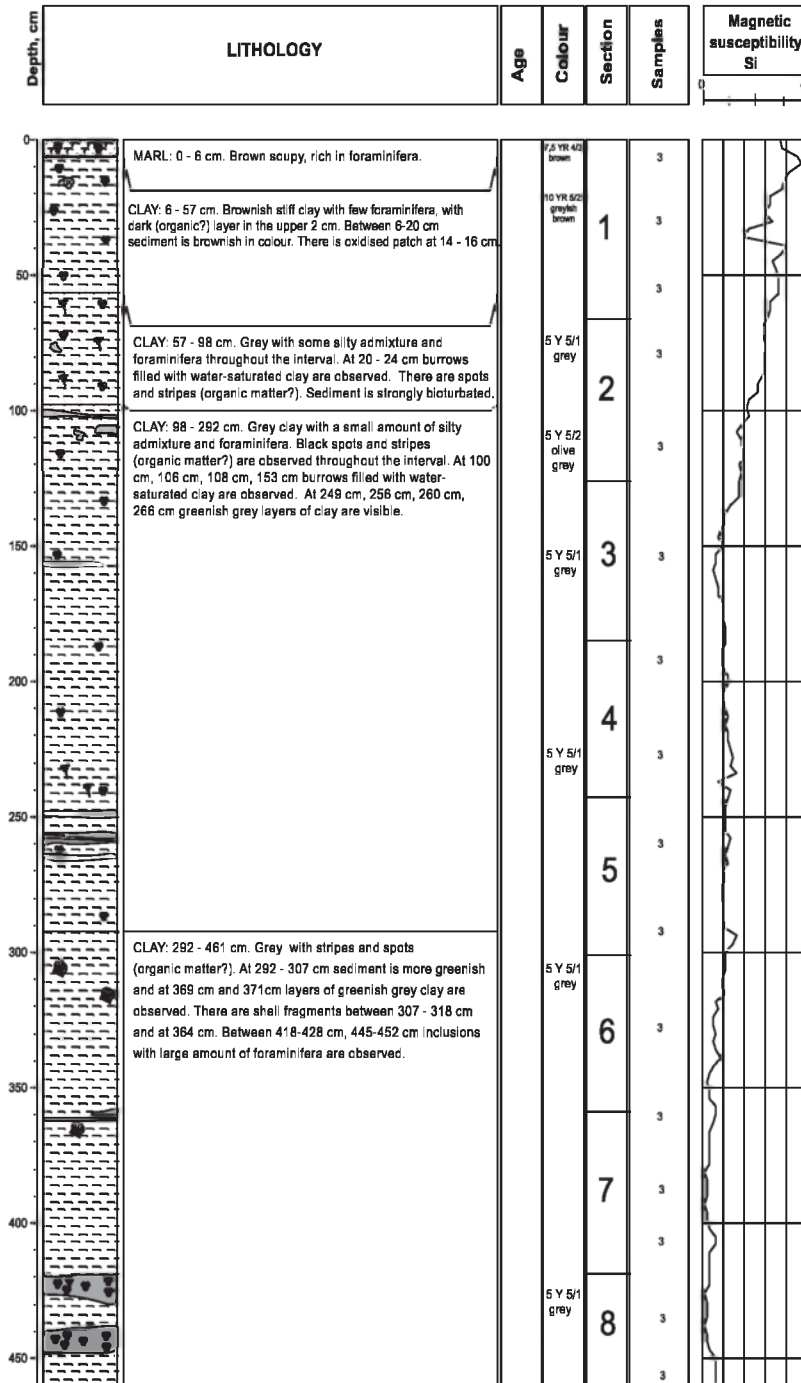
ANNEX I. CORE LOGS (LEG 2, Alboran Sea)



Core log TTR-14-MS-302G

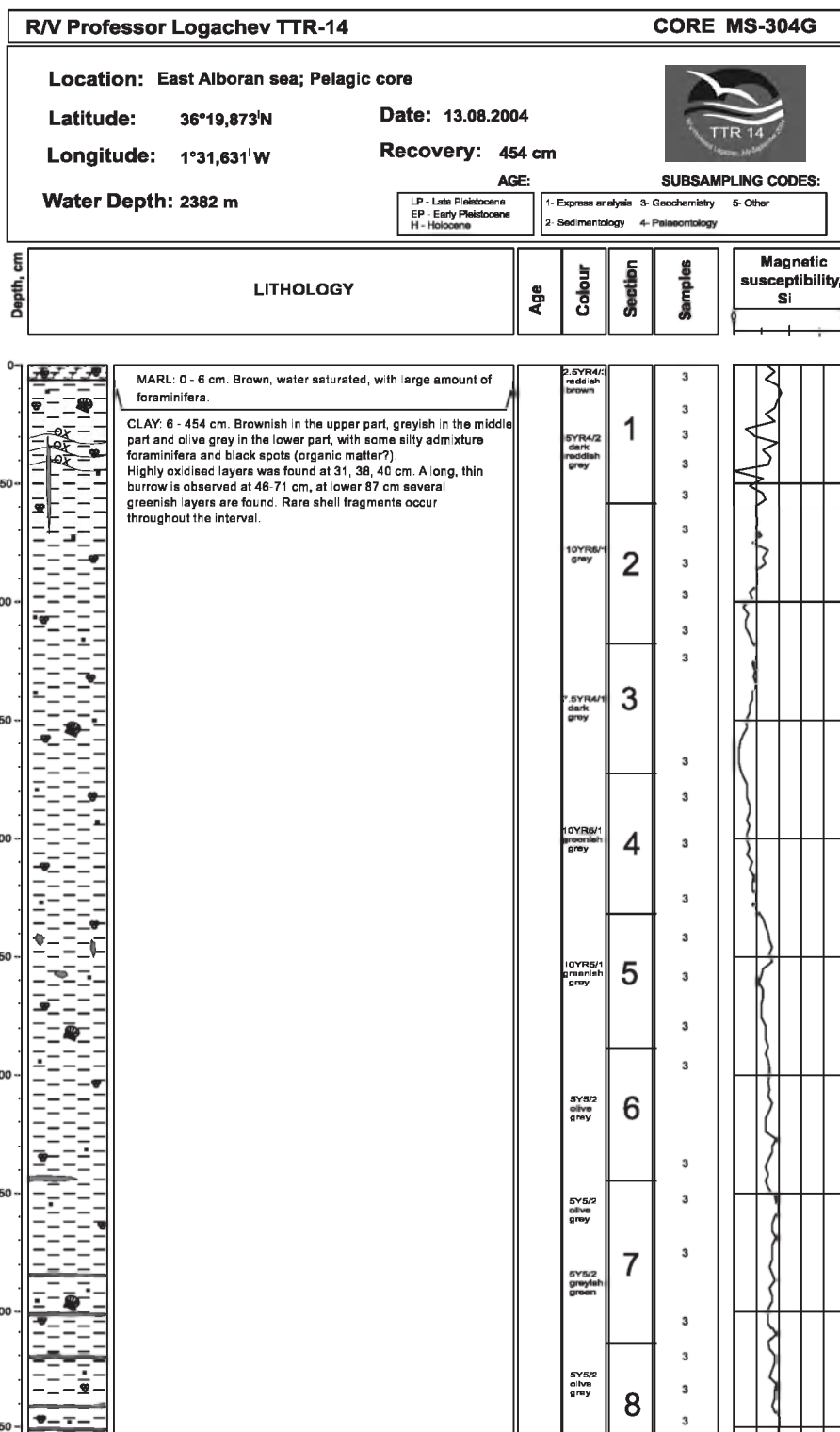
ANNEX I. CORE LOGS (LEG 2, Alboran Sea)

R/V Professor Logachev TTR-14		CORE MS-303G												
Location: East Alboran sea; Pelagic core														
Latitude: 36°17,429' N	Date: 13.08.2004													
Longitude: 1°37,380' W	Recovery: 461 cm													
Water Depth: 2094 m	AGE:	SUBSAMPLING CODES:												
	<table border="1" style="font-size: small;"> <tr> <td>LP - Late Pleistocene</td> <td>1: Express analysis</td> <td>3: Geochemistry</td> <td>5: Other</td> </tr> <tr> <td>EP - Early Pleistocene</td> <td>2: Sedimentology</td> <td>4: Paleontology</td> <td></td> </tr> <tr> <td>H - Holocene</td> <td></td> <td></td> <td></td> </tr> </table>	LP - Late Pleistocene	1: Express analysis	3: Geochemistry	5: Other	EP - Early Pleistocene	2: Sedimentology	4: Paleontology		H - Holocene				
LP - Late Pleistocene	1: Express analysis	3: Geochemistry	5: Other											
EP - Early Pleistocene	2: Sedimentology	4: Paleontology												
H - Holocene														



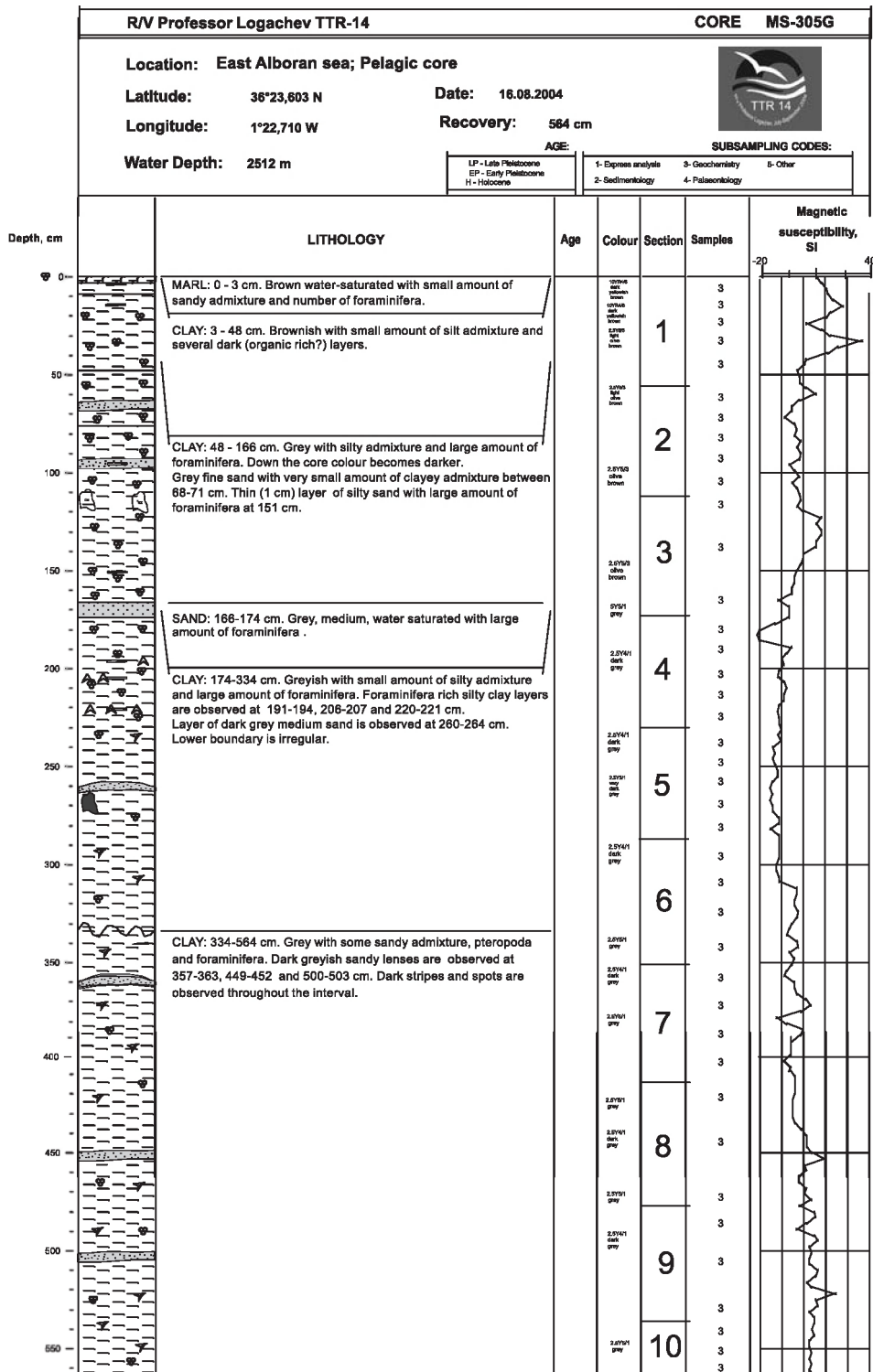
Core log TTR-14-MS-303G

ANNEX I. CORE LOGS (LEG 2, Alboran Sea)




Core log TTR-14-MS-304G

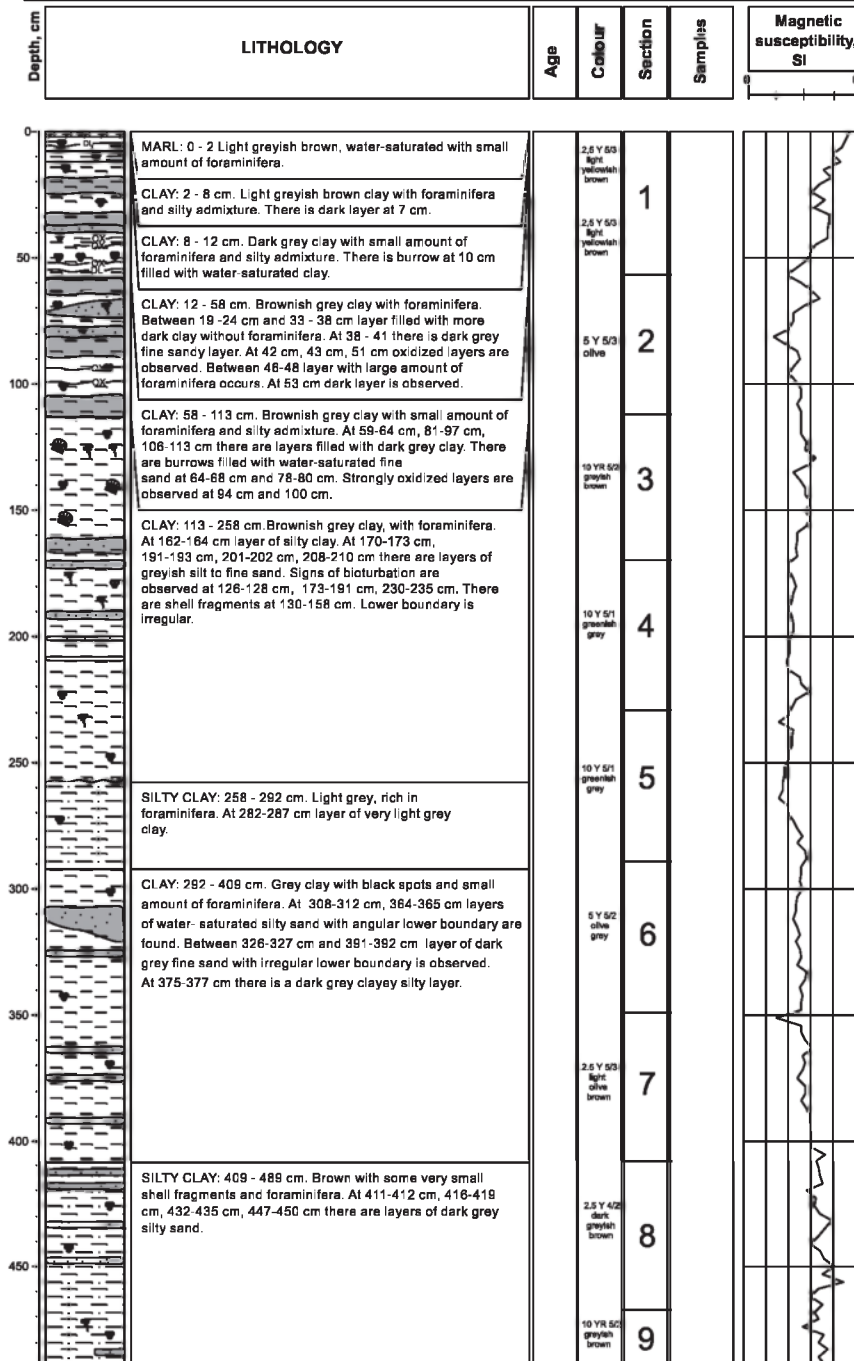
ANNEX I. CORE LOGS (LEG 2, Alboran Sea)



Core log TTR-14-MS-305G

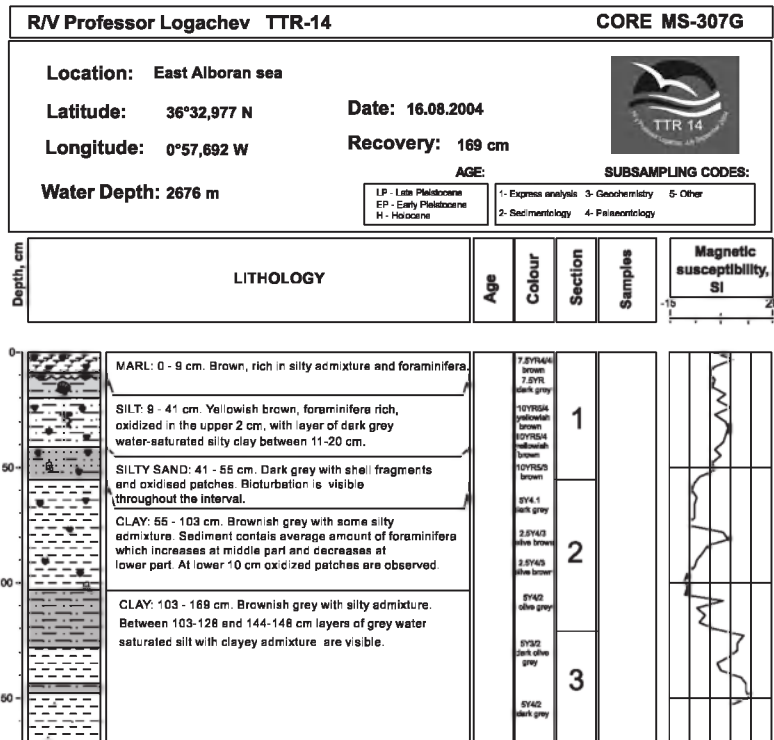
ANNEX I. CORE LOGS (LEG 2, Alboran Sea)

R/V Professor Logachev TTR-14		CORE MS-306G
<p>Location: East Alboran sea; Pelagic core</p> <p>Latitude: 36°27,846' N Date: 16.08.2004</p> <p>Longitude: 1°11,166' W Recovery: 489 cm</p>		
<p>Water Depth: 2574 m</p>		
<p>AGE:</p> <p>LP - Late Pleistocene EP - Early Pleistocene H - Holocene</p>		<p>SUBSAMPLING CODES:</p> <p>1- Express analysis 3- Geochemistry 5- Other 2- Sedimentology 4- Paleontology</p>

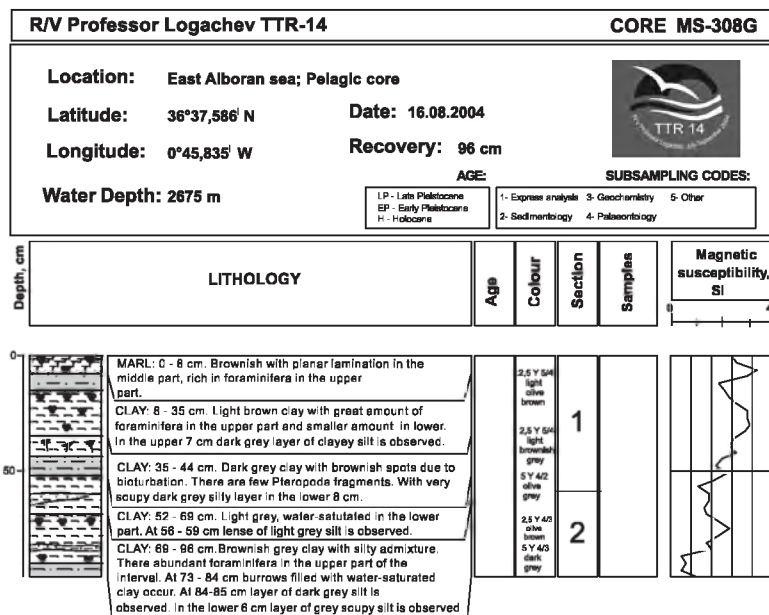


Core log TTR-14-MS-306G

ANNEX I. CORE LOGS (LEG 2, Alboran Sea)

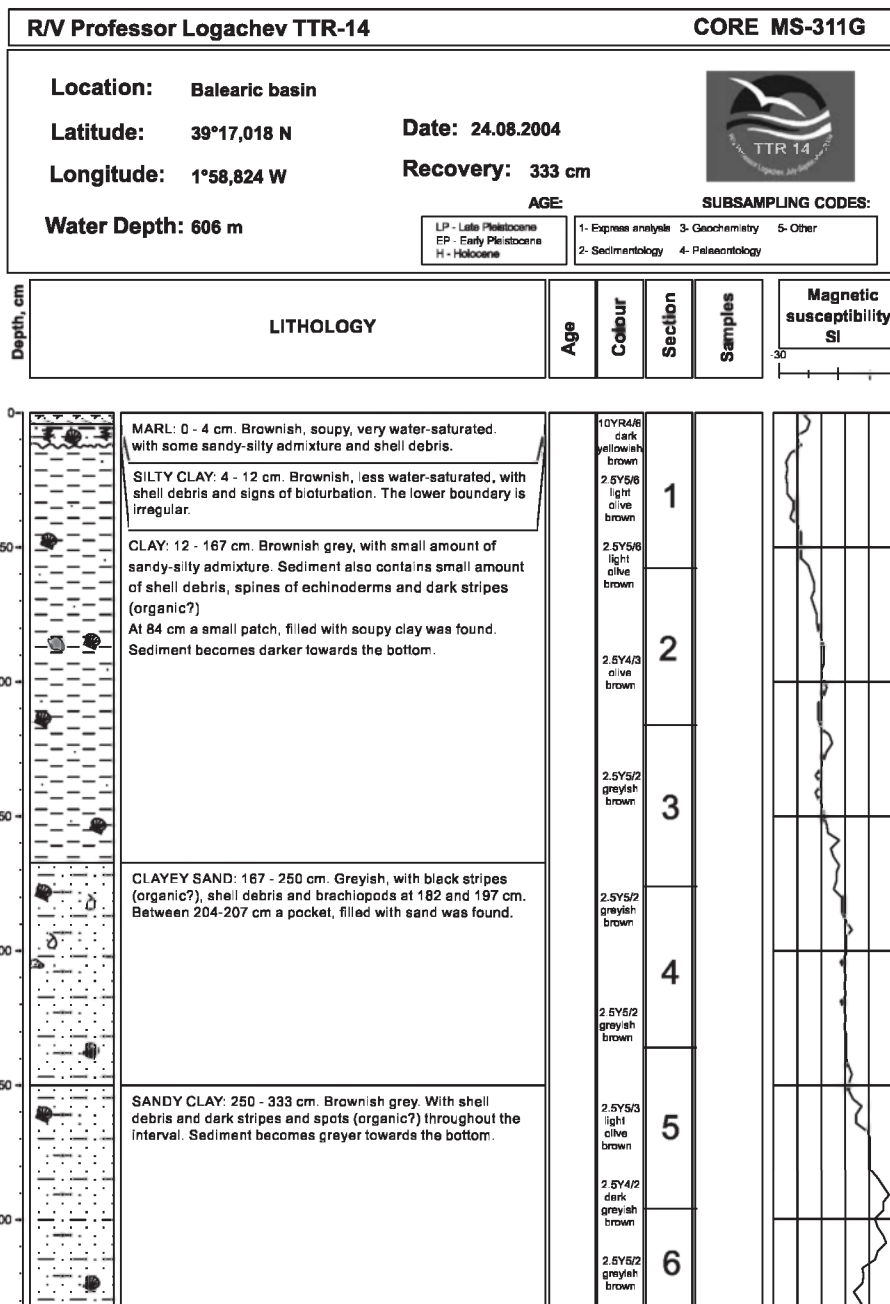


Core log TTR-14-MS-307G



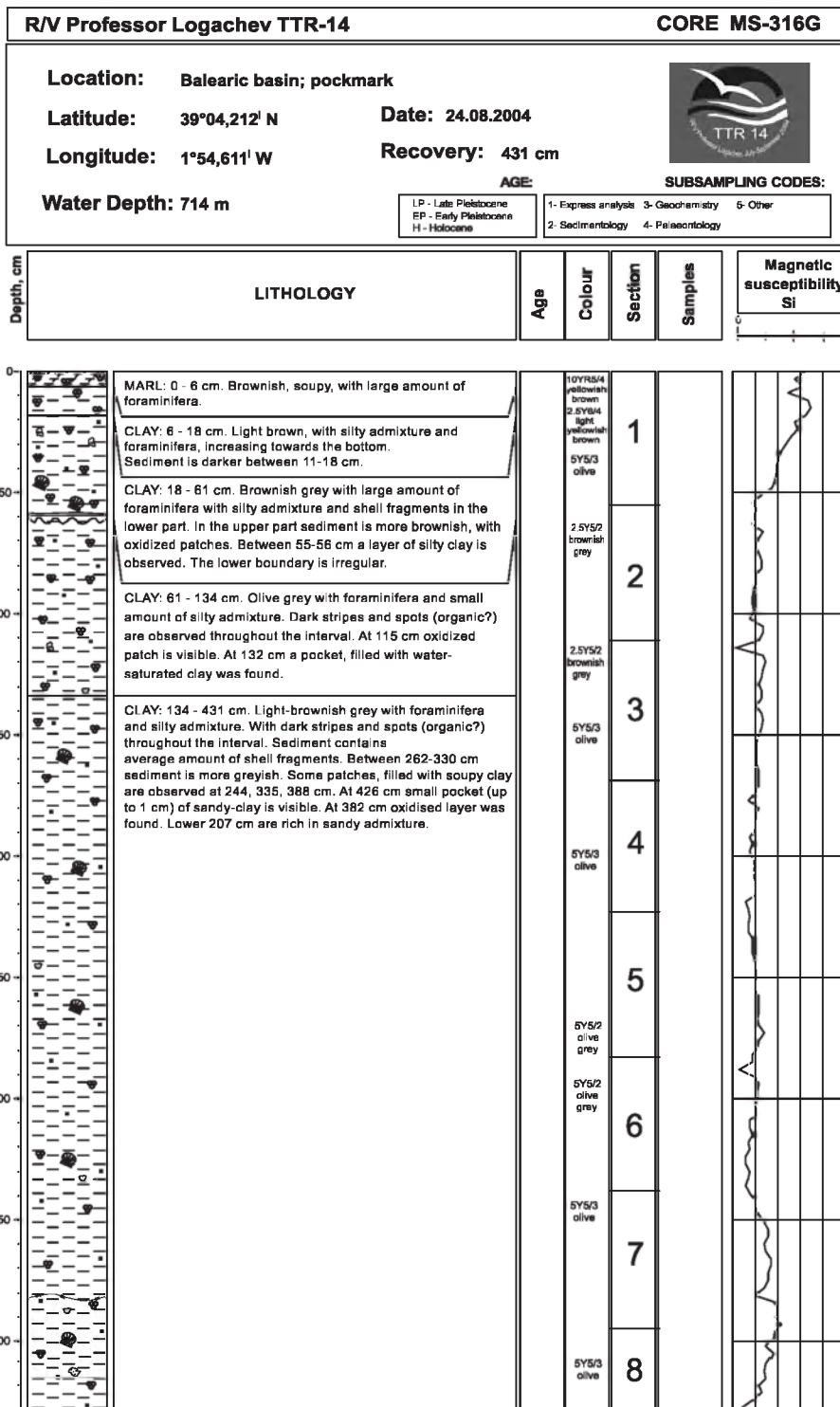
Core log TTR-14-MS-308G

ANNEX I. CORE LOGS (LEG 3, Balearic Basin)



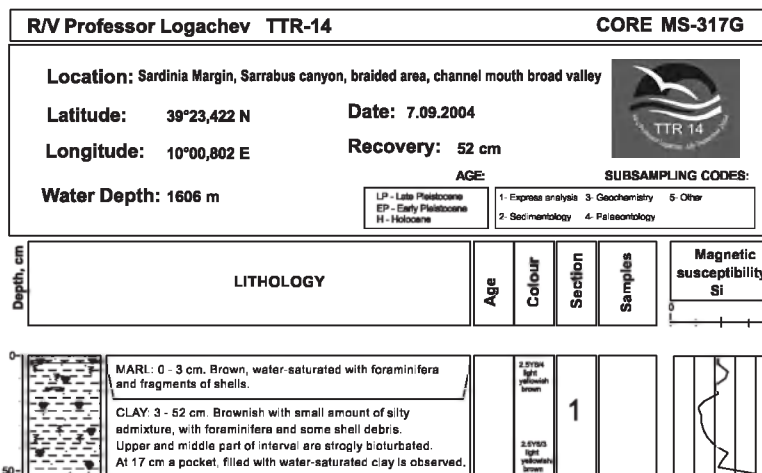
Core log TTR-14-MS-311G

ANNEX I. CORE LOGS (LEG 3, Balearic Basin)

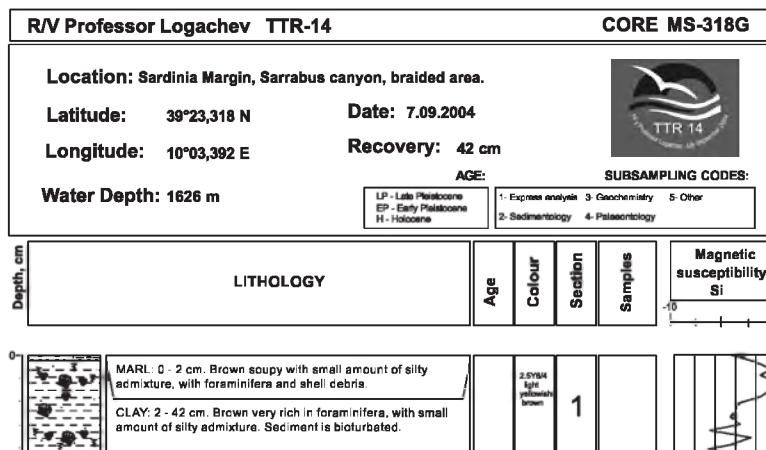


Core log TTR-14-MS-316G

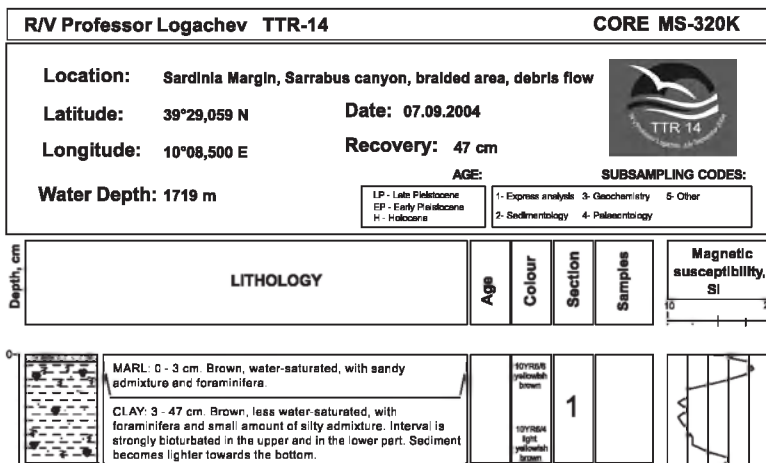
ANNEX I. CORE LOGS (LEG 4, Tyrrhenian Sea)



Core log TTR-14-MS-317G

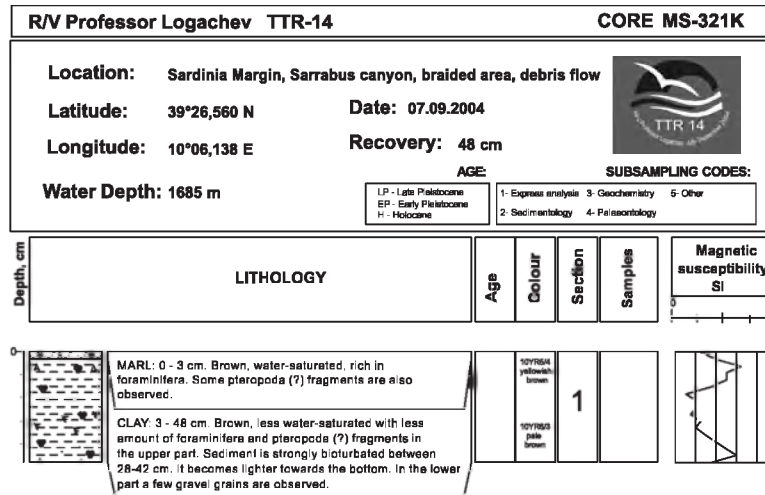


Core log TTR-14-MS-318G

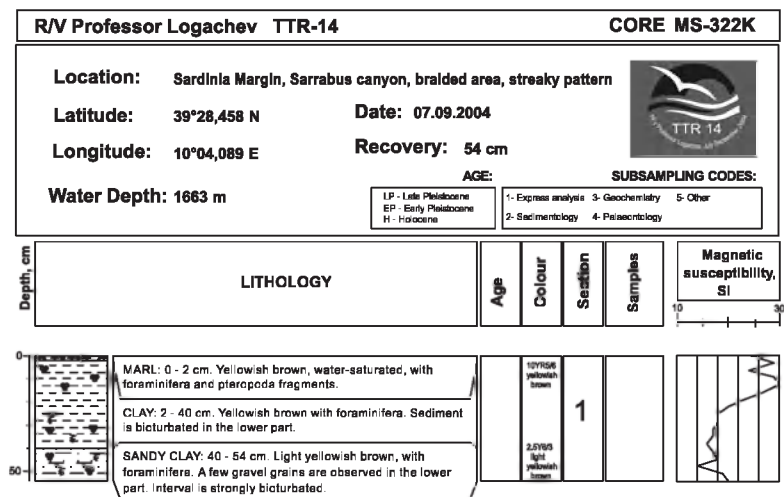


Core log TTR-14-MS-320K

ANNEX I. CORE LOGS (LEG 4, Tyrrhenian Sea)

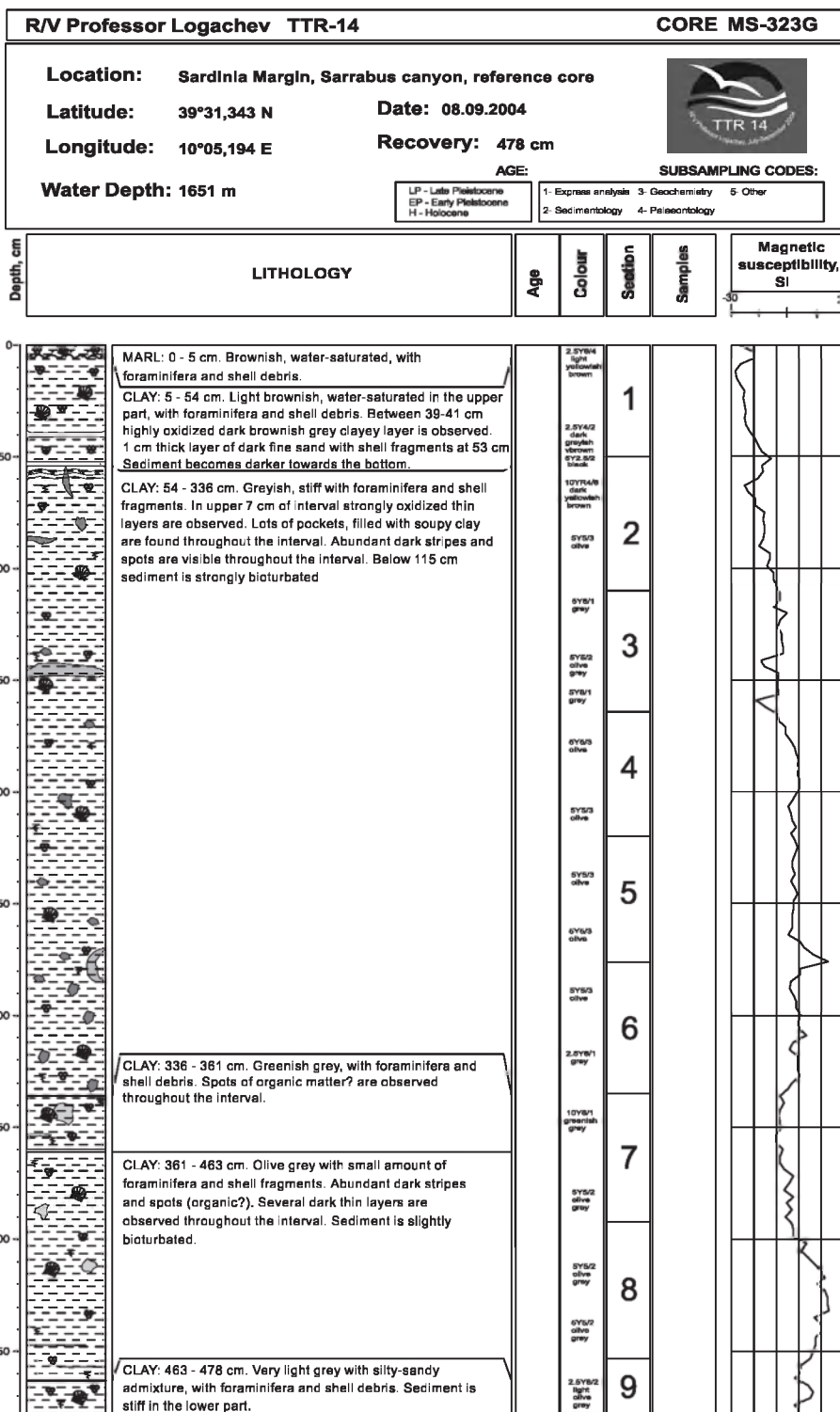


Core log TTR-14-MS-321K



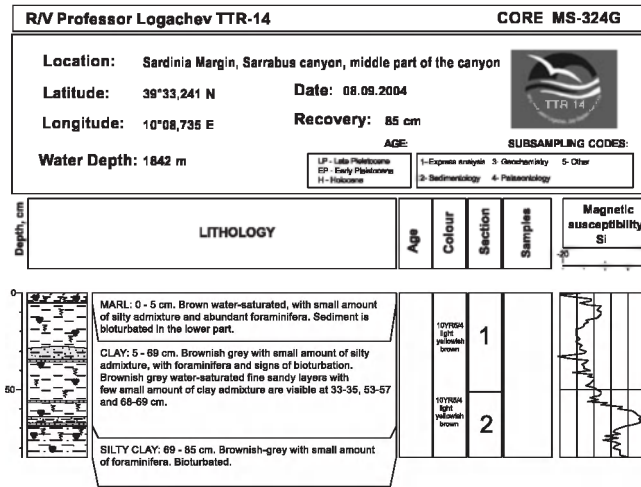
Core log TTR-14-MS-322K

ANNEX I. CORE LOGS (LEG 4, Tyrrhenian Sea)

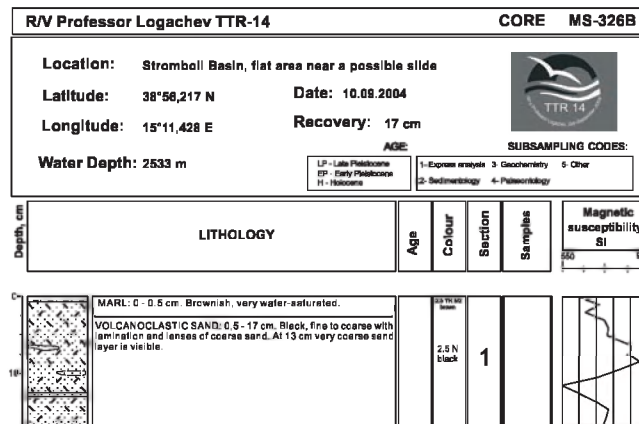


Core log TTR-14-MS-323G

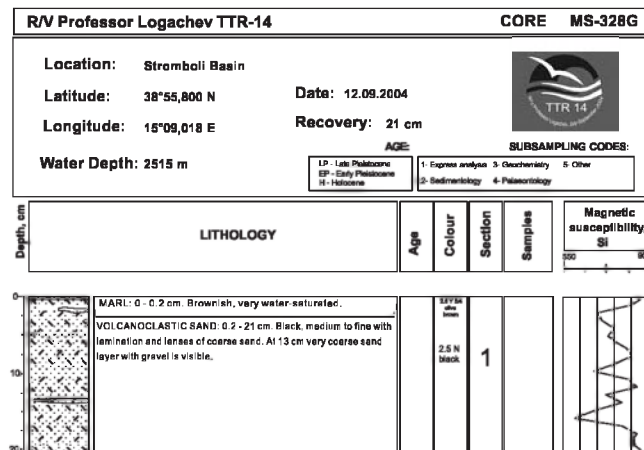
ANNEX I. CORE LOGS (LEG 4, Tyrrhenian Sea)



Core log TTR-14-MS-324G

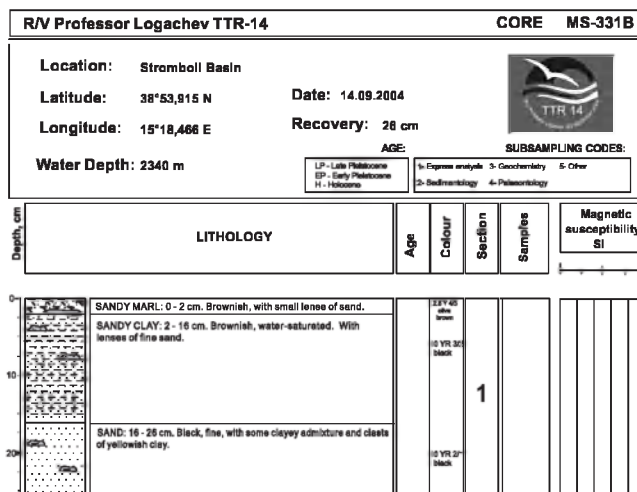


Core log TTR-14-MS-326B

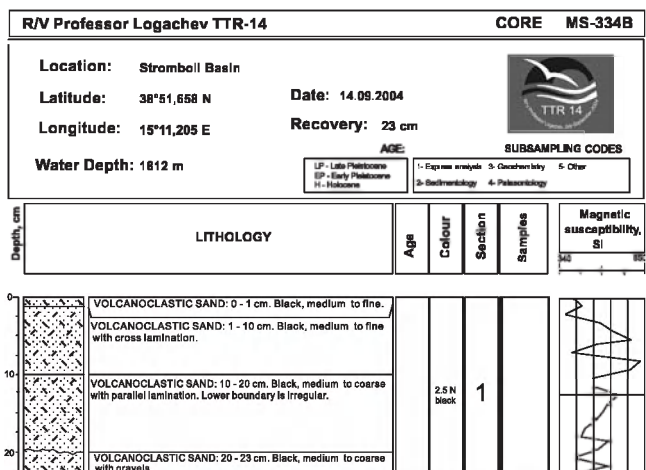


Core log TTR-14-MS-328B

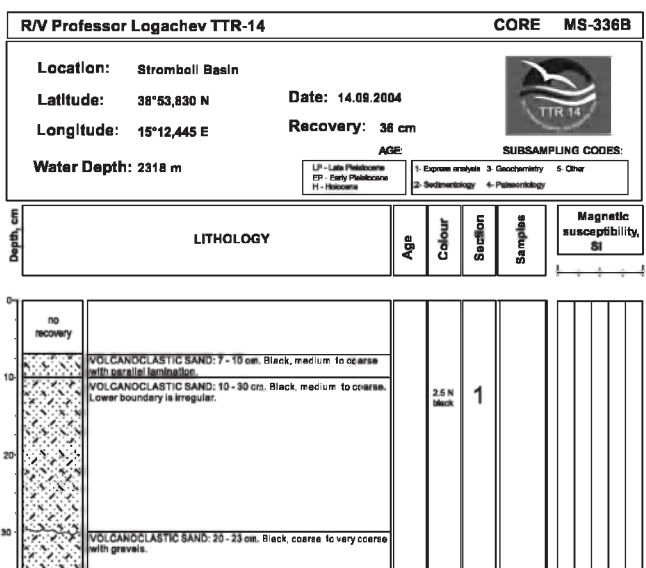
ANNEX I. CORE LOGS (LEG 4, Tyrrhenian Sea)



Core log TTR-14-MS-331B

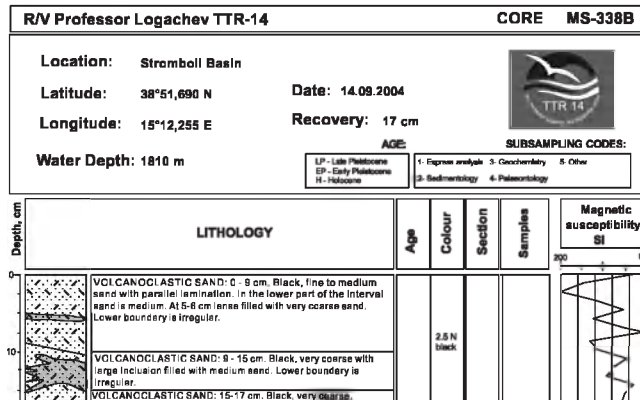


Core log TTR-14-MS-334B

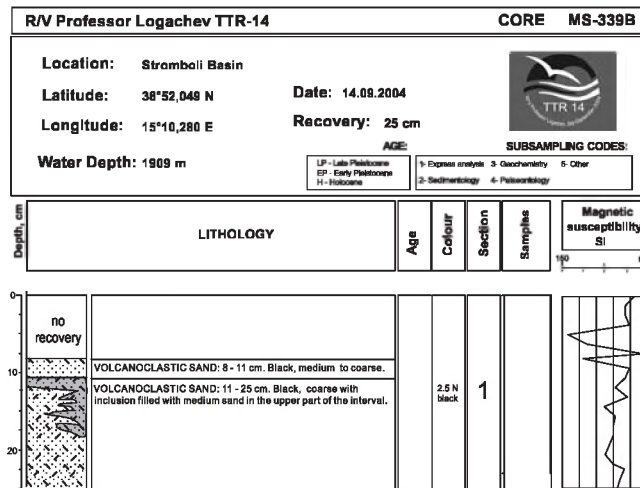


Core log TTR-14-MS-336B

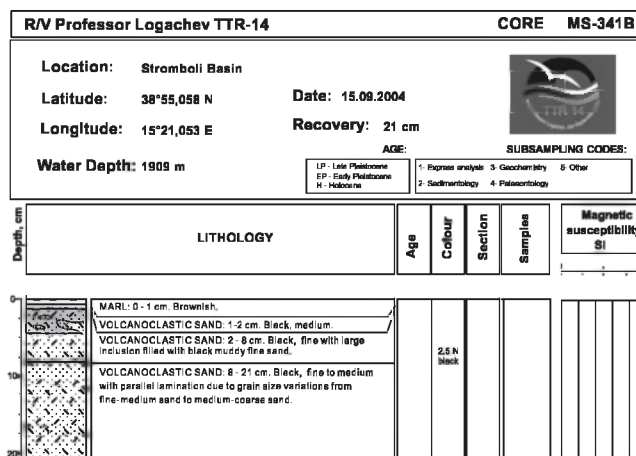
ANNEX I. CORE LOGS (LEG 4, Tyrrhenian Sea)



Core log TTR-14-MS-338B



Core log TTR-14-MS-339B



Core log TTR-14-MS-341B

ANNEX II. LIST OF TTR-RELATED REPORTS

- Limonov, A.F., Woodside, J.M. and Ivanov, M.K. (eds.), 1992. Geological and geophysical investigations in the Mediterranean and Black Seas. Initial results of the "Training through Research" Cruise of R/V *Gelendzhik* in the Eastern Mediterranean and the Black Sea (June-July 1991). UNESCO Reports in Marine Science, 56, 208 pp.
- Limonov, A.F., Woodside, J.M. and Ivanov, M.K. (eds.), 1993. Geological and geophysical investigations of the deep-sea fans of the Western Mediterranean Sea. Preliminary report of the 2nd cruise of the R/V *Gelendzhik* in the Western Mediterranean Sea, June-July, 1992. UNESCO Reports in Marine Science, 62, 148 pp.
- "Training-Through-Research" Opportunities Through the UNESCO/TREDMAR Programme. Report of the first post-cruise meeting of TREDMAR students. Moscow State University, 22-30 January, 1993. MARINF, 91, UNESCO, 1993.
- Limonov, A.F., Woodside, J.M. and Ivanov, M.K. (eds.), 1994. Mud volcanism in the Mediterranean and Black Seas and Shallow Structure of the Eratosthenes Seamount. Initial results of the geological and geophysical investigations during the Third UNESCO-ESF "Training-through-Research" Cruise of R/V *Gelendzhik* (June-July 1993). UNESCO Reports in Marine Science, 64, 173 pp.
- Recent Marine Geological Research in the Mediterranean and Black Seas through the UNESCO/TREDMAR programme and its "Floating University" project, Free University, Amsterdam, 31 January-4 February 1994. Abstracts. MARINF, 94, UNESCO, 1994.
- Limonov, A.F., Kenyon, N.H., Ivanov, M.K. and Woodside J.M. (eds.), 1995. Deep sea depositional systems of the Western Mediterranean and mud volcanism on the Mediterranean Ridge. Initial results of geological and geophysical investigations during the Fourth UNESCO-ESF "Training through Research" Cruise of R/V *Gelendzhik* (June-July 1994). UNESCO Reports in Marine Science, 67, 171 pp.
- Deep-sea depositional systems and mud volcanism in the Mediterranean and Black Seas. 3rd post-cruise meeting, Cardiff, 30 January - 3 February 1995. Abstracts. MARINF, 99, UNESCO, 1995.
- Ivanov, M.K., Limonov, A.F. and Cronin, B.T. (eds.), 1996. Mud volcanism and fluid venting in the eastern part of the Mediterranean Ridge. Initial results of geological, geophysical and geochemical investigations during the 5th Training-through-Research Cruise of R/V *Professor Logachev* (July-September 1995). UNESCO Reports in Marine Science, 68, 127pp.
- Sedimentary basins of the Mediterranean and Black Seas. 4th Post-Cruise Meeting, Training-through-research Programme. Moscow and Zvenigorod, Russia, 29 January-3 February. Abstracts. MARINF, 100, UNESCO, 1996.
- Woodside, J.M., Ivanov, M.K. and Limonov, A.F. (eds.), 1997. Neotectonics and Fluid Flow through Seafloor Sediments in the Eastern Mediterranean and Black Seas. Preliminary results of geological and geophysical investigations during the ANAXIPROBE/TTR-6 cruise of R/V *Gelendzhik*, July-August 1996. Vols. 1, 2. IOC Technical Series, 48, UNESCO, 226 pp.
- Gas and Fluids in Marine Sediments: Gas Hydrates, Mud Volcanoes, Tectonics, Sedimentology and Geochemistry in Mediterranean and Black Seas. Fifth Post-cruise Meeting of the Training-through-research Programme and International Congress, Amsterdam, The Netherlands, 27-29 January 1997. IOC Workshop Reports, 129, UNESCO, 1997.
- Geosphere-biosphere coupling: Carbonate Mud Mounds and Cold Water Reefs. International Conference and Sixth Post-Cruise Meeting of the Training-through-Research Programme, Gent, Belgium, 7-11 February 1998. IOC Workshop Reports, 143, UNESCO, 1998.
- Kenyon, N.H., Ivanov, M.K. and Akhmetzhanov, A.M. (eds.), 1998. Cold water carbonate mounds and sediment transport on the Northeast Atlantic Margin. IOC Technical Series, 52, UNESCO, 178 pp.
- Kenyon, N.H., Ivanov, M.K. and Akhmetzhanov, A.M. (eds.), 1999. Geological Processes on the Northeast Atlantic Margin. IOC Technical Series, 54, UNESCO, 141 pp.
- Geological Processes on European Continental Margins. International Conference and Eighth Post-cruise Meeting of the Training-Through-Research Programme, University of Granada, Spain, 31 January - 3 February 2000. IOC Workshop Reports, 168, UNESCO, 2000.

Kenyon, N.H., Ivanov, M.K., Akhmetzhanov, A.M. and Akhmanov, G.G., (eds.), 2000. Multidisciplinary study of geological processes on the Northeast Atlantic and Western Mediterranean margins. IOC Technical Series, 56, UNESCO, 119 pp.

Geological processes on deep-sea European margins. International Conference and Ninth Post-Cruise Meeting of the Training-through-Research Programme. Moscow/Mozhenka, Russia, 28 January - 3 February 2001. IOC Workshop Reports, 175. UNESCO, 2001, 76 pp.

Kenyon, N.H., Ivanov, M. K., Akhmetzhanov, A. and Akhmanov, G. G. (eds), 2001. Interdisciplinary Approaches to Geoscience on the North East Atlantic Margin and Mid-Atlantic Ridge. IOC Technical Series, 60, UNESCO, 134 pp.

Geosphere/Biosphere/Hydrosphere Coupling Processes, Fluid Escape Structures and Tectonics at Continental Margins and Ocean Ridges. International Conference and Tenth Post-Cruise Meeting of the Training-through-Research Programme. Aveiro, Portugal, 30 January - 2 February 2002. IOC Workshop Reports, 183. UNESCO, 2002, 50 pp.

Kenyon, N.H., Ivanov, M. K., Akhmetzhanov, A. and Akhmanov, G. G. (eds.), 2002. Interdisciplinary studies of geological processes in the Mediterranean and Black Seas and North East Atlantic. IOC Technical Series, 62, UNESCO, 134 pp.

Geological and biological processes at deep-sea European margins and oceanic basins. International Conference and Eleventh Post-Cruise Meeting of the Training-through-Research Programme. Bologna, Italy, February 2-6, 2003. IOC Workshop Reports, 187. UNESCO, 2003, 32 pp.

Kenyon, N.H., Ivanov, M. K., Akhmetzhanov, A. and Akhmanov, G. G. (eds.), 2003. Interdisciplinary geoscience research on the North East Atlantic margin, Mediterranean Sea and Mid-Atlantic Ridge. IOC Technical Series, 67, UNESCO, 152 pp.

North Atlantic and Labrador Sea Margin architecture and sedimentary processes. International Conference and Twelfth Post-Cruise Meeting of the Training-through-Research Programme. Copenhagen, Denmark, January 29-31, 2004. IOC Workshop Reports, 191. UNESCO, 2004, 47 pp.

Kenyon, N.H., Ivanov, M.K., Akhmetzhanov, A.M., Kozlova, E.V. and Mazzini, A. (eds.), 2004. Interdisciplinary studies of North Atlantic and Labrador Sea Margin Architecture and Sedimentary Processes. Preliminary results of investigations during the TTR-13 cruise of RV Professor Logachev, July-September, 2003, Intergovernmental Oceanographic Commission technical series, 68 , 92 pp & annexes.

Geosphere-Biosphere coupling processes: the TTR interdisciplinary approach towards studies of the European and North African margins International Conference and Post-Cruise Meeting of the Training-Through-Research Programme, Marrakech, Morocco, 2 - 5 February 2005. IOC Workshop Report, 197, UNESCO 2005, 71 pp.

